CRANFIELD INSTITUTE OF TECHNOLOGY

C. L. D. ARAUJO

A Study of Coarse Grain Heat Affected Zone of Accelerated Cooled Structural Steels

School of Industrial Science

PhD Thesis

CRANFIELD INSTITUTE OF TECHNOLOGY

SCHOOL OF INDUSTRIAL SCIENCE

PhD THESIS

Academic year 1990-91

C. L. D. ARAUJO

A Study of Coarse Grain Heat Affected Zone of Accelerated Cooled Structural Steels

Supervisor: R. L. Apps

November 1990

This thesis is submitted in partial submission for the degree of

PhD

To Ângela, Célia and Rita

ABSTRACT

Modern structural steels have significantly different (generally leaner) compositions than equivalent conventional steels developed over 20 years ago. To compensate for the lower carbon and alloy content more sophisticated thermomechanical treatments have been introduced to give very fine ferrite grain size and hence good strength, ductility and fracture toughness. Despite the fact that these changes were largely introduced to improve weldability, the modern structural steels have given problems of heat affected zone (HAZ) hydrogen induced cold cracking leading to considerable debate over the causes of this apparently increased susceptibility.

The present work aimed to provide the basis for a better understanding of the metallurgical behaviour of the HAZ of these new modern steels. This was accomplished by employing three low carbon (C<0.15%) low sulphur (S<0.005%) content steels produced by the OLAC process which combines controlled rolling with accelerated cooling. A normalized low carbon (0.12%C) higher sulphur (0.031%S) steel was also included in the present project for comparison purposes. The starting point was to determine the transformation temperatures of the various microconstituents in the HAZ's by 'In Situ' thermal analysis. A new approach was developed in which thermal data obtained from real weld thermal cycle measurements were employed in the thermal analysis. The steels studied were analyzed in the light of the results of transformation temperatures, microstructural examinations and hardness measurements in the coarse grained region of the HAZ. This approach offers much greater accuracy and consistency than previous methods of determining thermal cycles and HAZ transformation temperatures, giving a better opportunity for studying the anomalous HAZ behaviour of modern steels

Between the OLAC steels, two steels presented very low hardness (<300HV5) within the entire range of heat inputs used (0.8-3.5kJ/mm), whereas the other gave hardnesses higher than those of the normalized steel. Higher carbon (0.13%C) and a poorly balanced alloy content was considered to be an explanation for the HAZ behaviour of this steel. An investigation on the accuracy of current carbon equivalent in predicting hardenability and hardness formulae was carried out but none of the

existing formulae were completely satisfactory in indicating the trend in hardenability found in all the steels. An alternative formula for predicting the variation of hardness based on one put forward by Yurioka was developed, which proved to be suitable for three of the steels studied. However, the restricted nature of all empirical carbon equivalent formulae is demonstrated and the need to limit any such formula to a restricted range of steels is re-emphasized.

ACKNOWLEDGEMENTS

The author wishes to express his gratitude to his supervisor Professor R. L. Apps, Cranfield Institute of Technology, for his guidance, support and encouragement throughout the research project.

The financial support from Conselho Nacional de Desenvolvimento Científico e Tecnológico (CNPq) is acknowledged.

I would like to thank the following people for all their friendly support and help for the production of my thesis: Messrs. J. Basset, D. Woolnough, J. Savill, P. Middleton, J. Holmes and A. Nelson.

Special thanks are addressed to Mr. J. Norrish for his assistance and fruitful discussions during the development of the thermal cycle measurement system.

The author is indebted to Mr. J. Nixon for his support in building the interface amplifier, important equipment in my experimental temperature measurements.

I would like to thank Mrs. Rita Bastos for her support in the final stage of my work and her help in the presentation of the thesis.

Finally, the author would like to express sincere gratitude to his friends and colleagues Daming Wang, Ronaldo Paranhos, Américo Scott and Sebastiãao da Costa for their support and encouragement during some difficult moments of this research work. Special thanks are addressed to Paulo Modenesi and Sadeck Alfaro the 'three amigos' for their invaluable assistance and friendly guidance.

CONTENTS

CHAPTER 1 INTRODUCTION

The composition and quality of structural steels have changed significantly over the last two decades owing to higher requirements brought about by heavy constructions in severe environments such as Arctic regions and submarine areas (North Sea). The size and service loading of these structures have stimulated steel industries also to improve the thermomechanical processes necessary to develop materials capable of meeting the proposed 480/550 N/mm^2 strength level and brittle fracture resistance at -62°C whilst maintaining or improving weldability and formability.

About 20-25 years ago, requirements for improved weldability in structural steels resulted in a drive to reduce carbon and carbon equivalent (CE) values. However this approach also led to lower strength levels which this was unacceptable. The solution lay in the introduction of thermomechanical processes to refine grain size and maintain good strength levels. Of these techniques controlled rolling (CR), in which a low finish rolling temperature was implemented proved the most effective. During this time carbon levels were reduced from approximately 0.2% to 0.15% or even lower and IIWCE values from 0.46 to 0.41 or less, and this trend has continued to the present. This approach (i.e. lower C and IIWCE plus CR) brought an improvement in weldability in particular to less risk of heat affected zone (HAZ) hydrogen cracking.

Apart from the properties mentioned above, toughness through the plate thickness had also to be improved. Problems related to lamellar tearing in the steels were associated with the high level of aligned inclusions, principally manganese sulphide (MnS) and these were frequently reported by the fabricators during the fabrication of the earliest off-shore structures for the North Sea. This problem was addressed by the steel producers which required some investments on the steelmaking plant to improve their deoxidation and desulphurisation processes. Oxygen levels as low as 10ppm became commercially available and **sulphur** reached **very low** levels no higher than 0.008%. Although such 'Z quality' steels were specially produced at higher cost for weld designs which could give susceptibility to lamellar tearing, the improved processes did lead to general improvements in all structural steels. Now

%S is rarely above 0.015% and C above 0.15%.

The developments described above culminated with a new thermomechanical process which combine the benefits of the controlled rolling with an accelerated cooling of the plate from temperatures just above A_{r3} (start temperature of the decomposition of austenite). Developed by the Japanese in the early 80's the **OLAC** (**O**n-**L**ine **A**ccelerated **C**ooling) method as it became known, is to achieve a further grain refinement of general microstructure by thermomechanical treatment of lean alloy steels. The **OLAC** process also marked the beginning of a more rationally balanced chemical composition where lower carbon was virtually essential to guarantee good weldability. This is reflected in their basic chemical composition being carbon-manganese for steels with 50kgf/mm^2 tensile strength grade and toughness requirements at -60°C. In critical applications where higher toughness is required this can be achieved by additional reductions in carbon and a balanced increase of Mn combined with additions of Ni and Cu to avoid any significant reduction in tensile properties.

Despite low carbon content and reduced CE values, the modern steels appeared to exhibit an increased susceptibility to HAZ hydrogen cracking (Smith and Bagnall, 1968 and Hart, 1978). The increased susceptibility was related to the very low S contents necessary to avoid lamellar tearing but the exact cause has remained a matter of controversy (see Chapter 2). Although the reports mentioned above may be sure evidence of problems, no investigation has been done to analyze in depth the various microstructural aspects in the coarse grained region and their implication for hardness of the HAZ of these modern steels. The studies carried out up to the present work, have attempted to find explanations for reported increases in hardenability on the basis of variations occurred in IIWCE and/or P_{cm} but this has not led to any conclusive evidence of increased hardenability in these steels. This is a strong indicator that, in fact, these new modern steels require a different approach which cannot be conducted on the basis of factors (IIWCE and P_{cm}) developed for the 'old' generation of steels.

The present investigation attempts to establish the basis for a more **realistic** and **fundamental** approach in the thermal analysis of these low carbon and low sulphur structural steels. It was accomplished by studying the coarse grained region (near to the fusion line) of the HAZ's

of three OLAC steels in attempt to understand the mechanisms which govern the weldability of these high strength low sulphur steels. A more traditionally produced steel (higher sulphur and normalizing heat treatment) was also included in this research work with the intention of obtaining some basis for comparison and understanding of the mechanisms which govern the weldability of these high strength low sulphur steels. The starting point in the study of the HAZ was the determination of the transformation temperatures of the microstructures produced in the coarse grained region by the weld thermal cycle. This was done on the basis of real welds by employing 'In Situ' thermal analysis. The decision for using real welds rather than simulation was that little evidence was available to assure that the latter can reproduce thoroughly the actual thermal history of a particular point in the plate under a real weld thermal cycle. In fact significant criticisms of the simulation have been advanced in recent years [Tecco, 1985]. Although recent techniques were available to apply the 'In Situ' thermal analysis (the latest was developed in Cranfield Institute of Technology) [Tecco, 1985]), it was established that there was a lack of accuracy intrinsic to those measurements owing to the experimental procedure adopted. In these past analyses, analogue recorders were employed which have very limited flexibility and accuracy if transformation temperatures are to be determined with the support of computers. On this basis, a data gathering system was developed which employed a modern **digital** unit. Computer software routines were designed to provide relevant information regarding the thermal characteristics of each thermal cycle measured. Software routines were also developed to assist the 'In Situ' thermal analysis. The transformation temperatures of the microstructures produced in the coarse grained region of the HAZ's of the steels under investigation were determined by a statistical method.

The test welds consisted of a series of bead on plate welds within the range of heat inputs of 0.8-3.5kJ/mm which are typical for the manual metal arc and submerged arc welding of structural steels. A considerable number of thermal cycles was measured. The reproducibility of the experiments was analyzed on the basis of the cooling time through 800-500°C (Δt_{8-5}) and 800-300°C (Δt_{8-3}). The various Δt_{8-5} times measured were compared with theoretical predictions. The various microstructural features in the coarse grained region of the steels under study were analyzed by means of quantitative and

qualitative optical metallography. The identification of the transformation temperatures shown by the 'In Situ' thermal analysis was supported by the metallography examination. Hardness measurements were also carried out in the plates welded. The variations in the measurements have been discussed in the light of the thermal characteristics of the weld thermal cycles and metallographic examination. Attempts were made to investigate the hardenability of the steels by using some carbon equivalent formulae found in the current literature. In the same manner, the variation in the maximum hardness with the increase of heat input was evaluated. Owing to the poor correlation shown by these formulae, a new formula was developed a by employing multiple correlation analysis, which gave a rather more satisfactory correlation with the steels investigated in the present work.

This thesis is presented in ten Chapters with a literature survey of the main subjects investigated in the present work following this introduction. The programme of work is presented in Chapter 3 and a technical description of the equipment and materials employed in the experimental work is in Chapter 4. Chapter 5 describes the technique used in the thermal cycle measurements and the results are also included in this Chapter. The technique employed for the 'In Situ' thermal analysis is presented in Chapter 6 where a discussion about the limitations gathered during the determination of the transformation temperatures is also given. The transformation temperatures were determined by the development of a statistical approach fully described in Chapter 7. The techniques used for metallographic examination and hardness measurements are reported in Chapter 8 as well as the results. The overall situation established in the present work is discussed in Chapter 9 where an attempt is made to develop a general explanation of the response of the steels studied to welding. Finally, specific conclusions are presented in Chapter 10.

CHAPTER 2 LITERATURE SURVEY

2.1 Structural Steels

2.1.1 Introduction

In this section will be presented a general description of the development of steel making process, hot rolling, chemical composition, and mechanical properties of the structural steels produced in the last three decades. As part of this, the high strength low alloy steels or HSLA steels as they became known, will be reviewed. It is worth however, presenting the definition of HSLA steels adopted in the description of the development of these steels. A high strength steel is regarded as one presenting a yield stress of at least 300N/mm^2 [Preston, 1976]. Elements such as Nb, Ti, V, Al, Ta and Zn, which are strong carbide, nitride or carbonitride formers, when added up to 0.15%, are defined as microalloying elements [IIW, 1971].

2.1.2 Development

In the early sixties, virtually all structural steels were hot-rolled, ranging in yield strength from 280-480MPa. The majority were carbon manganese (C-Mn) steels (0.15 to 0.25%C) modified by small additions of niobium (Nb), vanadium (V) or titanium (Ti). Their toughness and formability were limited and plagued by a high degree of directionality. Although 480MPa was believed to be the upper limit for ferrite-pearlite steels, for many engineering applications a satisfactory balance of properties could only be achieved at a 345MPa yield strength level [Korchynsky, 1985]. In processing these steels, the hot-rolling process step was regarded as a means for an economical and accurate change in the geometry, from slab to plate or strip. In the area of metallurgical implications of hot-rolling, the benefits of a low finishing temperatures were well recognized, triggering the development of low temperature controlled rolling practice for plates.

The hot-rolling process had then gradually become a much more closely-controlled operation. As part of this, the concept of controlled rolling emerged where the various stages of rolling were temperature-controlled, the amount of reduction in each pass was predetermined and

the finishing temperature was more precisely defined. From this stage, advances included full deoxidation and use of controlled rolling to achieve small ferrite grain sizes, e.g. use of low finishing temperatures and reductions greater than 30% below 950°C [Andrade,1985]. For instance, Figure 2.1 taken from Cohen et al [1985] shows a schematic temperature/time profile for controlled rolling of 19mm thick steel plate. The process starts from slabs 150 to 250mm thick reheated to temperatures in the range of 1100 to 1250°C. The rolling operation itself generally involves two distinct stages, i.e. high-temperature rolling or 'roughing' and a lower-temperature series of deformation steps designated as 'finishing'. If the roughing and finishing operations are continuous, the process is termed *hot rolling*, while if there is a delay between the two stages, as shown in Figure 2.1, the process is referred to as *controlled rolling*. After rolling, the plate is usually air cooled.

In metallurgical terms, the purpose of the controlled-rolling operation in HSLA steels is first to refine the relatively coarse, as-reheated austenitic microstructures by a series of high-temperature rolling/recrystallization steps, and then to impose a moderate to heavy reduction in a temperature regime where austenite recrystallization is inhibited between rolling passes (below the T_R temperature indicated in Figure 2.1) such that the plastically deformed austenite grains remain 'pancaked'. Subsequent transformation after rolling into ferritic microstructures results in the desired fine grain size and associated mechanical properties.

Developments in structural steels have tended to follow the development of steel for linepipe since 1965. With the increase in demand for energy in the 1970's, natural gas and petroleum resources were exploited increasingly in severe environments as Arctic regions (i.e. Alaska and Siberia) and submarine areas (North Sea). Consequently, a large demand was created for steel with outstanding strength and toughness that could be applied to facilities and equipment related to energy development, such as pipelines, off-shore structures, and storage vessels. This has stimulated further development in materials to meet the proposed 480/550 N/mm^2 strength level and brittle fracture immunity at -62°C. In this manner, the starting point for a rational alloy design of ferrite-pearlite HSLA steels containing microalloy elements was provided by the methodology developed by Pickering and collaborators [Korchynsky, 1985]. Starting with the Petch equation,

relating yield strength to grain size, they expanded the friction stress term to include the effect of two other strengthening mechanisms: solid solution and volume fraction of pearlite. By means of quantitative metallography and multiple regression analysis, the strength increments attributed to solutes, pearlite, and grain size could now be quantified. The fourth major strengthening mechanisms: precipitation hardening was estimated as the difference between the measured and calculated yield strength values. By evaluating the effect of various strengthening mechanisms on properties, a new alloy design concept evolved. The best balance of properties was achieved by maximizing grain refinement, increased by a judiciously selected amount of precipitation strengthening.

The importance of grain refinement became clear, since it produced the extremely useful combination of an increase in strength and an improved reduction in the Charpy impact transition temperature. The special controlled rolling process developed to replace normalising or quench and tempered treatments. This new concept reduced many of the shortcomings of HSLA steels strengthened by carbon and solid solution, i.e. by means of high carbon equivalent. In this respect, Nb and/or V have been the most commonly used microalloying elements added to HSLA steels. The controlled rolling routine was by low finishing temperatures and deformation as high as 70% below 840°C, with resulting very fine microstructure [Andrade, 1985]. Although these steels have enjoyed an increased production from the mid 70's, there is controversy on the beneficial effect of the microalloy elements principally Nb and V added to HSLA steels which are to be welded. This is due to the loss of their grain pinning capability the moment they go into solution, and the austenite at the border with the fusion line will coarsen. For instance, Perdigao [1978] carried out an extensive research project using an HSLA microalloyed quenched and tempered steel containing 0.15%C, 1,44%Mn, 0.06%Nb and 0.03%V in which he found that over the peak temperature (simulation) range of 1150-1400°C (equivalent to the coarse grained HAZ region), a strong deterioration in toughness was observed relative to that of the base metal, the maximum embrittlement occurring at about 1250°C. Furthermore, the decrease in toughness over this range was attributed to the microalloys which might have dissolved into the austenite, allowing grain coarsening. The use of Ti in controlled rolling HSLA steels has also been reported [Andrade, 1985]. According to him very low C

microalloyed steels containing Ti are effective in restricting HAZ austenite grain growth.

The development of a rational alloy design of ferrite-pearlite HSLA steels had to be followed by changes in steelmaking processes to match the mechanical properties required by heavy constructions combined with the adverse climatic conditions of working sites. For instance, the European Steel Industry was less than ideally placed to produce the bulk tonnages of quality structural steel plates that were to be required for the construction of the massive steel jacket production platforms that have become a common place feature over the past decade [Walker, 1988]. Structural steels were still rolled from ingots cast from open hearth steel and the move to higher quality plate products was being achieved through the rapid introduction of basic oxygen steel making (BOS) and through the limited use of electric arc steelmaking capacity. Consequently, to respond to the quality challenge investments had to be made in new plant and facilities to modify the process route in steelmaking processes. This was summarized by Walker [1988] as follows:

1. The bulk supply of desulphurized iron from large closely controlled blast furnaces;

2. The almost exclusive use of basic oxygen steelmaking;

3. The widespread use of continuous casting of thick slab for rolling to plate, accounting for between 80/90% of plate production up to a thickness of 75mm;

4. The development and exploitation of thick plate products directly rolled from ingot stock;

5. The widespread introduction and use of ladle and ladle arc steelmaking procedures including in particular vacuum arc degassing (VAD), vacuum degassing, argon stirring and injection techniques.

With the implementation of these routes it was expected to achieve suitable chemical compositions in which the steels would possess the mechanical properties required. As far as the quality of the welded

joints are concerned they would be free from lamellar tearing (as a consequence of a much cleaner steel), preheat temperatures would be reduced as a result of the reduction in HAZ hardness, and the toughness of the HAZ would be improved. In this respect, it is interesting to compare, for instance, the BS4360: Grade 50D 1969 standard specification governing the composition of typical structural steels produced in the early 1970's and those presently being produced to meet the requirements of the users and fabricators of modern off-shore structures. Such a comparison is provided in Figure 2.2 [Walker, 1988], from which it can be noted that the need to improve weldability has resulted in a noticeable reduction in carbon, whilst the need to improve the resistance to lamellar tearing and impact toughness has brought about a most remarkable reduction in the sulphur. Although, the reduction in sulphur to below 0.008% would reduce the risk in lamellar tearing , this could also be achieved by the modification of the sulphide shape [Stuart, 1985]. The reduction in carbon and carbon equivalent would reflect on the improvement in weldability with less risk of hydrogen cracking and, consequently lower pre-heat temperatures or even complete avoidance for it [Dolby,1984]. The carbon level has dropped from about 0.2% to an average not much greater than 0.1% and the maximum carbon equivalent (IIWCE) has been reduced from as high as 0.46 to 0.41 or even lower. This reduction of carbon in some steels (e.g. normalized steels) has been compensated for by an increase in solid solution hardening elements such as manganese, silicon, nickel and copper and possibly additions of niobium and/or vanadium.

Another important aspect which is related to the various changes in steel making processes already mentioned is the internal quality of the plates. Although improvements were brought about by continuous casting, giving better production efficiency, surface quality and flatness of the products, internal quality has been reported [Walker, 1988] as a potential problem regarding segregation. The extent of segregation can be affected by the degree of ladle superheat, base composition and the condition of the continuous casting machine. The apparent feature of this segregation would be what often is described as a dark line at about mid-plate thickness. This is considered very undesirable and techniques have been developed in order to redistribute the segregation band in the plate. The steelmakers are now concentrating upon the minimization of the use of those elements known to segregate more readily during solidification, such as carbon, manganese, sulphur and

phosphorus and to make more effort to maintain control over secondary vessel steelmaking and the maintenance of the continuous casting machines.

2.1.3 Structural OLAC Steels

It was in 1980 when a new method launched by the Japanese [Nippon Kokan, 1982], became available on an industrial scale for making high-grade steel plate. The concept of this method is to combine the **controlled rolling** process with an **O-Line Accelerated Cooling** (**OLAC**) zone installed behind the finishing mill for plate rolling. That is, the OLAC method is to submit the plate, immediately after controlled rolling (CR), to an accelerated cooling condition within the range of temperatures of the decomposition of the austenite (Figure 2.3). This route brings an improvement to the properties of the plates already achieved by the grain refinement of microstructures promoted by the controlled rolling.

The OLAC method is characterized in general in three main stages: First, steel plate immediately after being rolled is subjected to controlled water cooling (the upper side being cooled by a laminar flow cooling system and lower side by a spray cooling system) over a particular temperature range, in general within 800-500°C, and at a cooling rate between 3°C/sec to 15°C/sec. This range of cooling rate has been demonstrated [Kozasu, 1983] to increase strength without deterioration of the fracture appearance transition temperature (FATT) of either Si-Mn or HSLA steels (Figure 2.4). Secondly,after being water-cooled to the required temperature (between 500 and 600°C), the plate is air-cooled. Thirdly, steel plate is finished for flatness and smoothness by means of flatness control system.

The steps described above give properties which are superior in comparison to conventional methods. In this respect, the OLAC steels producers claim the following improvements achieved in comparison with steels produced by the conventional method.(Although the conventional method is not mentioned by the Nippon Kokan report [1982] it is assumed by the author this refers to controlled rolling)

(i) superior in strength and low temperature toughness due to grain refinement promoted by the combination of controlled

rolling and accelerated cooling;

(ii) for steels with equivalent strength, the OLAC steel has superior weldability and formability because it can be produced with low alloying elements or carbon equivalent;

(iii) on the basis of strength OLAC steel is superior in ductility;

(iv) superiority in toughness in the thickness direction, since the separation characteristic of the fracture surface in Charpy test due to controlled rolling occurs less frequently as the banded pearlite microstructure and crystallography texture are eliminated due to the OLAC method;

(v) OLAC steel can be produced without being passed through the normalizing heat treatment required by the conventional method, resulting in a significant energy saving.

In general, the mechanical properties of a predominantly ferritic structural steel (Tensile Strength (TS) $\approx$ 50kG/mm^2) can be improved by the general refinement of the microstructures, in particular by the refinement of ferrite grain size. This improvement can be achieved in principal on the basis of three major metallurgical factors, i.e. alloy elements, accelerated cooling or controlled rolling, or by their combination [Kozasu, 1985]. Figure 2.5 presents schematically the various mechanisms of ferrite grain refinement. Alloy elements such Mn and Ni lower the gamma (γ) to alpha (α) transformation temperature (A_{r3}). The decreased A_{r3} promotes an increase in ferrite nucleation rate with a decrease in ferrite growth rate to result in refined ferrite grain size and this has been incorporated in the alloy design of high strength steels. Accelerated cooling from above A_{r3} through the transformation temperature range also lowers A_{r3} and produces ferrite grain refinement by a mechanism similar to that by alloying. However, general experience, shows that these two measures are limited in the extent of ferrite grain refinement in the case of transformation from equiaxed austenite, and excessive action in these directions always results in undesirable coarse bainitic structures. This originates from the fact that only preferential sites on austenite grain boundaries are able to nucleate ferrite [Kozasu, 1985]. The accelerated cooling after controlled rolling

exerts more attraction because it produces industrially more significant effects than the case of accelerated cooling from equiaxed austenite by providing more nucleation sites. It has been claimed [Kozasu, 1985] that for identical controlled rolling conditions, accelerated cooling exerts much greater ferrite refinement capability than alloying elements (Ni) compared at identical A_{r3}temperatures.

In summary, the accelerated cooling (ACC) promotes an additional increase in tensile strength (TS) without deterioration of toughness (FATT) which is mainly determined by controlled rolling (ICR). This strengthening effect is believed to be derived from refinement of ferrite grain size, substructure strengthening of ferrite, increased fraction of the second phase (bainite) and enhanced precipitation hardening in the case of microalloyed steels. Figure 2.6 taken from Kozasu [1987] illustrates schematically the influence of cooling variables on properties. According to this author, T_S should be above A_{r3} to fully exploit the accelerated cooling effect. Though the optimum cooling rate may vary according to alloy system, it should be chosen so as to obtain the maximum strengthening, but not to an extent to deteriorate FATT due to excessive fractions of bainite and to minimize the through-thickness variation of properties due to difference of cooling rate. T_F below about 450° usually gives rise to a large strengthening accompanied by noticeable deterioration in FATT because of the presence of large amounts of various low temperature transformation products. Therefore, T_F above 500°C is preferred in practice. For low carbon steels such as pearlite-free steel (PFS), the limitations on cooling rate and T_F are relaxed to some extent as shown in Figure 2.6.

The contribution of the alloying elements to the lowering of A_{r3} during controlled rolling has been expressed in the following equation developed by Ouchi et al [1982].

$$A_{r3}(°C) = 910 - 310C - 80Mn - 20Cu - 15Cr - 55Ni - 80Mo \quad [2.1]$$

This equation indicates that C has the major effect on the transformation temperature. However, an increased C level is undesirable from a toughness/weldability viewpoint. The favourable elements to replace carbon are the elements that cause the maximum A_{r3} decrease with the minimum increase in CE(IIW). For structural

steels produced by the OLAC method such elements are Mn and Ni, and Cu is also preferred from a cost viewpoint. According to Kozasu [1987] a typical alloy system may be low C (<0.10), Mn (1.2-1.5), Ni(<0.5) and Cu (<0.5).

2.1.4 Implications of Low Sulphur Content on HAZ

In spite of the 'boast' of the Japanese in having developed steels with high mechanical properties (high toughness and strength) with very low risk of both **lamellar tearing**, by lowering sulphur content to less than 0.008%, and **hydrogen cracking** owing to low carbon equivalent (CE< 0.37), problems have been reported due to an increase in susceptibility of hydrogen cracking when welding low sulphur C-Mn steels [Hewitt et al, 1968 and Hart, 1978]. According to Smith and Bagnall [1968], the increased incidence of cracking at low sulphur levels is a result of an effective increase in the interstitial hydrogen content arising from a reduction in the number of manganese sulphide (MnS) inclusions which are believed to act as *sinks* and *traps* for hydrogen. As reported by them, manganese sulphide has a coefficient of thermal expansion greater than steel matrix, thus in cooling from forging or normalising temperature, shrinkage cavities can form at the MnS/metal interfaces. This is in contrast to oxides and silicates which have lower expansion coefficients than the steel and which can be expected to maintain close contact with the matrix. In addition to the mechanical occlusion of hydrogen in voids, it is possible that 'solution' occurs in the sulphides, thereby increasing their effectiveness as hydrogen sinks [Boniszewski et al, 1967].

In order to verify the effectiveness of the MnS inclusions on preventing hydrogen cracking, Hart [1978] carried out extensive work on the basis of a series of Implant cracking tests and CTS tests. The results showed that low sulphur steels (0.005%) were consistently found to have a higher risk of HAZ hydrogen cracking than higher sulphur steels (0.033%). This was qualitatively verified by Implant cracking tests and quantitatively confirmed by CTS tests. Examination carried out on the HAZ of the Implant cracking tests indicated a higher proportion of high temperature transformation product in the high sulphur steels than in the low sulphur steels for the same cooling time, and this difference produced higher hardness of the low sulphur level. This was attributed to MnS and Silicate inclusions acting apparently as nucleation sites for

proeutectoid ferrite and bainitic ferrite and, in effect, producing a decrease in hardenability. He pointed out that one aspect of this important observation was that inclusions other than MnS could nucleate ferrite and hence produce a decrease in hardenability. With regards to the CTS, tests the results confirmed the dependence of critical hardness on the CE and showed that for effective CE's as low as 0.3 the critical hardness fell to values around 300Hv. It was assumed by him that the immediate practical importance of this was that the degree of improvement in weldability with reduction in CE is not as great as could be anticipated. He suggested that the reason for the higher risk of cracking was primarily associated with an enhanced hardenability and not a change in hydrogen diffusivity. According to him, the hardenability and hence risk of cracking of the steels is strongly influenced by their total inclusion content since it was observed that inclusions could nucleate ferrite during the austenite transformation. Consequently, low inclusion contents increased the hardenability. It is worth mentioning that in his experiments special steels were employed with different base compositions produced under different processes of deoxidation. Semi-killed steels were produced with 0.2%C and 1.4%Mn, sulphur contents ranged from 0.006 to 0.033%. For Al-treated steels a lower carbon (0.12%) level with 1.5%Mn had sulphur contents ranging from 0.005 to 0.023%.

McKeown et al [1983] pointed out that changes in steelmaking practice to improve cleanliness of structural steels can cause side effects due to the reduction of sulphur (< 0.006%) and oxygen (< 20ppm). For instance, further desulphurisation is adopted by Nippon Kokan [1983] to give a greater decrease in MnS inclusion. Due to rigorous deoxidation to achieve low sulphur content, this can cause hydrogen and nitrogen pick up and the extent to which they remain in the liquid steel will depend on the oxygen content. Consequently, with low sulphur and low oxygen content there is an increase in hydrogen content which cannot be trapped by the reduced number of inclusions. In respect to nitrogen, it can increase up to 80ppm when processing steels to achieve sulphur level down to 0.002%. This would promote an increase in the typical final steel of 20-30ppm. According to them, although nitrogen has not yet been incorporated into any carbon equivalent calculation, it is an interstitial hardening element of at least the potency of carbon so that even small amounts may be significant at low carbon contents.

Hart [1985] conducting a survey on published references found that the majority (80%) of eighteen publications reported an increased risk of HAZ hydrogen cracking caused by a reduction in parent steel sulphur level. However, only one of the reports was of fabrication experience, all remaining reports being of laboratory investigations. The lack of published reports on actual fabrication problems is not really an indication that no problem exists. Few fabricators are prepared to publicise their failures and discussions with practising welding engineers indicate that the problems do exist. In Hart's [1985] survey, two main factors were considered to be causing the increased risk; an increased hardenability and an increased hydrogen diffusivity. Some 80% of the investigations examining hardenability found it to increase with reduced sulphur level while only 60% of those examining hydrogen diffusivity found an increase. Finally, he pointed out that a decrease in sulphur from 0.025% to 0.005% may be equivalent to an increase in carbon equivalent of about 0.03%, which in turn could lead to increase preheat levels of between 50-100°C. Thus, the effect of cleanliness on HAZ hardenability may be important for fabrications which have maximum HAZ hardness requirements even when the risk of hydrogen cracking is low.

The evidence above presented does not necessarily imply that HAZ hydrogen cracking incidents have increased with the lowering of sulphur content. This finds support in recent publications [Boothby and Rodgerson, 1984 and Kirkwood, 1987] where there is no evidence that could link any noted variation in hardenability with measured variations in overall cleanliness, sulphur level and/or oxygen level. Further possible mechanisms for the role of sulphur have been reported [Yurioka, 1990]. As described by Yurioka [1990], sulphide inclusions are mostly MnS precipitates around which a manganese depleted zone results during the precipitation process. The lack of manganese facilitates carbon diffusion around the sulphide precipitates, thereby enhancing ferrite nucleation. In this respect, it was mentioned that HAZ hardenability was increased by reducing the sulphur content from 0.030 to 0.001% in a C-Mn steel, but hardenability was increased in a niobium bearing steel. New steelmaking processes where rare-earth metals (REM), oxysulphide, calcium oxide and titanium oxide are used, have been claimed [Yurioka, 1990] to influence ferrite nucleation in HAZ where HAZ hardness reduction by oxides is expected.

What has become marked in respect to analyses of these modern steels is that IIWCE as well as P_{cm} have been used as an indicator for their hardenability and the potential risk that they might present regarding hydrogen cracking. However, these carbon equivalent formulae were developed on the basis of a previous generation of steels where possibly other metallurgical factors (sulphur and oxygen level) were unimportant compared to carbon. For instance, Boothby [1984] analyzing HAZ hydrogen cracking of a different steel generation concluded that carbon equivalent (CE), whether expressed as IIWCE, IIWCE+Si/6 or P_{cm} was a poor indicator of hardenability. Actually, attempts have been made to develop new formulae which could describe more realistically the consequences of these new factors in terms of hardenability. This involves predicting HAZ maximum hardness on the basis of a method of calculation which links the carbon equivalent to the cooling time through 800-500°C (Δt_{8-5}) [Düren, 1990]. For instance, Cottrell [1984] developed a formula to predict maximum hardness in which sulphur content is included. However, there is no evidence of the success of this development. Yurioka et al [1981], developed a formula to predict hardness in which two carbon equivalent are used. This, is justified by the authors because it is not possible for a simple formula of carbon equivalents to describe overall the susceptibility of steels to cold cracking if their carbon contents range widely. Furthermore, they claim that this new formula is suitable for modern low carbon steels. These new attempts are a clear sign of the complexity brought by the new developments which needs further investigation.

2.2 Weld Thermal Cycle

The temperature gradients generated by a very intense, moving heat source applied to the workpiece are described in arc welding processes by the term **weld thermal cycle**. The thermal cycle has a major influence on the metallurgical structure and properties of welded joints, on the tendency to cracking and on the degree of distortion. The difficulty in analyzing the heat flow in the molten weld pool has been reported before [Apps et al, 1963 and Easterling, 1983]. Experimentally, it is laborious to locate a thermocouple precisely and theoretically there are difficulties in allocating values of the thermal properties because of turbulence in the weld pool whilst the heat source can scarcely be regarded as a point or line source. Several brief mentions have been made of weld pool temperatures, however, and a wide range of

temperatures have been quoted, many of them many hundreds of degrees above the melting temperature. Interpretation of slag-metal partition data in steel have inferred weld pool temperatures of 1800-2200°C [Mat. No.69, 1986]. With respect to the determination of the weld thermal cycles in the parent plate (heat affected zone, HAZ) these can made by either theoretical calculations based on heat flow equations or local thermal cycles measurement by means of thermocouples embedded in the plate to be welded. Even in the HAZ however, difficulties can occur: in calculations by variation of thermal properties with temperature and latent heat effects, in practice by local disturbance of heat flow by the insertion of thermocouple and the need for the rapid response of recording instruments.

2.2.1 Theoretical Determination

The theoretical determinations of the weld thermal cycles in the parent plate are based on heat flow theory, in a manner similar to that described by Rosenthal [1941]. He found it necessary to make the following assumptions:

- the physical properties of the metal are independent of the temperature and physical state of the metal;
- constancy of thermal properties;
- the heat source can be approximated to either a point, a line or a plane;
- the workpiece geometry is such that the dimensions are infinite;
- heat diisipation by conduction through the plate.

For the case where a point heat source is travelling on the surface of a very thick plate, Rosenthal's [1946] solution is:

$$T - T_o = \frac{q}{2\pi kR} .\exp[-v(R + x)/2\alpha] \qquad [2.2a]$$

and for a linear heat source moving in a plate of thickness h, i.e. 2 dimensional (2D) heat flow, the solution is:

$$T - T_o = \frac{q}{2\pi kh} .\exp(-vx/2\alpha)K_o(vr/2\alpha) \qquad [2.2b]$$

where T is the temperature at point (x,y,z),
T_o is the plate initial temperature,
$\alpha = k/\sigma c$ is the thermal diffusivity,
$q = {}_n VI$ is the arc effective heat input,
$R = (x^2 + y^2 + z^2)^{1/2}$,
$r = (x^2 + y^2)^{1/2}$,
v is the speed of the heat source and
K_o is the modified Bessel function of zero order.

Rosenthal's analytical solutions have been modified and extended by several workers. For instance, Wells [1952] predicted the weld bead width by simplifying the equation [2.2b]. In 1955 Apps and Milner [1955] characterized the heat input in autogenous TIG welding as a function of arc length, welding current and the nature of the parent metal from calorimetric measurements Al, Cu, Pb, Ni and mild steel specimens. Further experimentation involving the welding of thin sheets of those material showed that actual pool lengths were much longer than predicted, leading those authors to propose a parameter to account for latent heat effects. Adams [1958] calculated the cooling rate and the peak temperature distribution in the workpiece. Nunes [1983] introduced the concept of thermal dipoles to account for heat liberated by phase transformations. The validity of Rosenthal's model was investigated by Christensen et al [1965] by changing the equations [2.2a] and [2.2b] to dimensionless equations and comparing the theoretical bead area, width and penetration with a large number of experimental results. Moore et al [1985] compared the cooling times from Rosenthal's model against results of a finite element model. It has been shown that Rosenthal's model predicts adequately the temperatures and cooling rates at some distance from the weld pool, and the cross-sectional areas of the fusion zone (autogenous welding) and the heat affected zone, provided the welding speed is sufficiently slow [Kovitya et al, 1986]. The heat flow equation has also been solved numerically by different authors in an attempt to reduce the simplifications necessary for an analytical solution, for instance, Ushio et al [1977], [Kou and Lee, 1983], Kovitya et al [1986], and Tekrival and Mazumder [1986].

The criticism against Rosenthal's based equations is based on the assumptions made by him to help simplify the mathematics involved. This is summarized by Kou [1987] as follows. First, the peak

temperature calculated at the weld centreline approaches infinity even though the power of the heat source is finite. This unrealistically high peak temperature is due to the singularity problem of Rosenthal's solutions, which is caused by the point heat source assumptions. Secondly, thermal properties of most materials are not constant but tend to vary with temperature significantly. Thirdly, considerable errors can be caused by neglecting the latent heat of fusion either in 2D or 3D heat flow.

Most of these theoretical equations have not given satisfactory results to be employed in thermal cycle measurement in the coarse grained HAZ. Mathematical solutions have been mainly concentrated on weld bead shape [Barlow, 1982a]. This could be attributed to difficulties in choosing values for thermal properties (as mentioned above) which seem to pose a major drawback. In addition, there is difficulty in determining the effect on the thermal cycle due to the latent heat of transformation of the various microconstituents developed in the coarse grained region HAZ as a result of the decomposition of the austenite.

In the present work, the following equations described by Barlow [1982b], which derived from the work of Kohno and Jones [1978] and Christensen [1965] for 3-dimensional (3D) and 2-dimensional (2D) respectively, were employed to calculated the cooling time through 800-500°C ($\Delta t_{8\text{-}5}$). Comparisons were made with experimental measurements in the present work (see Chapter 5).

For 3D heat flow, cooling time (Δt) is

$$\Delta t_{\theta 1\text{-}\theta 2}\ (\text{sec}) = \frac{10^4}{2\pi\lambda}\, nQ_e \left[\frac{1}{(\Theta_2-\Theta_o)} - \frac{1}{(\Theta_1-\Theta_o)} \right] \qquad [2.3a]$$

and for 2D heat flow, cooling time (Δt) is

$$\Delta t_{\theta 1\text{-}\theta 2}\ (\text{sec}) = \frac{10^6}{4\pi\lambda C\rho}\, \frac{(nQ_e)^2}{h^2} \left[\frac{1}{(\Theta_2-\Theta_o)^2} - \frac{1}{(\Theta_1-\Theta_o)^2} \right] \qquad [2.3b]$$

where:

λ = thermal conductivity, J/cm/sec/°C,
C = specific heat capacity, J/g/°C,
ρ = density, 7.622 g/cm^3 for steel,
n = arc efficiency, (assessed to be 0.95 for submerged arc welding),
Q_e = nominal energy input, kJ/mm,
h = plate thickness, mm,
Θ_o = initial plate temperature, °C,
Θ_1 = upper temperature in cooling range, °C,
Θ_2 = lower temperature in cooling range, °C.

The critical plate thickness (h_c) [Barlow, 1982b] determining the flow pattern is given by:

$$h_c = \sqrt{nQe \frac{1}{2C\rho} \left[\frac{1}{(\Theta_2-\Theta_o)} + \frac{1}{(\Theta_1-\Theta_o)} \right]} \qquad 2.4$$

where a plate thickness greater than h_c indicates 3D heat flow.

The formula [2.3] can be simplified by applying the following values (supplied by the same author) for the parameters given above:

C = 0.8106 J/g/°C at 650°C,
Θ_o = 25°C,
Θ_1 = 800°C,
Θ_2 = 500°C,
ρ = 7.622 g/cm^3 for steel at 650°C.

Therefore, the critical thickness can be re-written as:

$$h_c = 16.34 \times \sqrt{(Qe)} \qquad [2.5]$$

For the calculations of the cooling time through 800-500°C, λ can be taken as 0.3276 J/cm/sec/°C, although the reservations mentioned above still apply.

2.2.2 Experimental Determination of Weld Thermal Cycle

The only really effective sensor system available for actual weld thermal cycle measurements in the HAZ has been the thermocouple. Infrared pyrometry has been used but it was considered unsatisfactory

[Barlow,1982a]. The type of thermocouple varies according to the level of temperatures involved in the experiment. For instance, where temperatures reach 1400°C or higher, thermocouples of Platinum (Pt) and Platinum-Rhodium (Rh) have been widely used. The most suitable thermocouple for measurement around the fusion line has been claimed to be Pt/Pt-13%Rh [Barlow, 1982a,]. However, the output of this thermocouple is very low and problems related to electrical background noise have been reported [Araujo, 1989] during thermal cycle measurements due to the high amplification needed to improve resolution. It can measure temperatures from below those of molten steel to room temperature. On the other hand, this thermocouple is best replace by Tungsten/Tungsten 26% Rhenium for measurements in the weld pool [Barlow, 1982a] considering the high temperatures encountered and the length of time that the thermocouple have to spend in the weld metal. Techniques have been developed in order to improve the placement of the thermocouple either in the weld metal [Pedder, 1973] or the heat affected zone (HAZ) [Barlow, 1982a].

2.2.2.1 Thermal Cycle Measurement in the HAZ

The most widely used technique for temperature measurement in the HAZ in particular the **coarse grained region**, is the drilled hole technique [Aronson, 1966, Apps et al, 1967, Kohno and Jones, 1978, Barlow, 1982a and Tecco, 1985]. In this technique measurement is accomplished by insertion of the thermocouple inside a hole drilled in the reverse side of the plate to be welded. For this, the position of interest relative to the weld fusion line must be known beforehand so that, the thermocouple can be positioned accurately at this point before the welding operation. This is obtained by carrying out trials employing the welding parameters envisaged for the actual experiment. Transverse cuts to the weld bead are then made for observation of the weld bead profile. More than one transverse section is usually observed due to variations of the welding bead profile in particular the penetration along the weld run. These variations are expected to occur owing to the inherent nature of arc welding. The success of an experiment, i.e. to measure the weld thermal cycle at the point of interest depends on taking into consideration these variations. In this manner, it has become a common practise to employ more than one thermocouple which are positioned at different distances from the fusion line. This is usually accomplished by drilling holes with different depths in respect to the

surface of the plate to be welded.

In the drilled hole technique, disturbance to the heat flow (in the region where the hole is drilled) is possible due to the presence of a hole in the plate. Hole diameter can also affect arc stability. Tecco [1985] investigating the influence of different hole diameters verified that the reproducibility and arc stability tended to improve with decreasing hole diameter. It has also been reported that the influence on heat flow can be minimized by placing the thermocouple normal to the fusion line [Barlow, 1982a]. Kohno and Jones [1978] found no significant disturbance to the heat flow in the region of the hole, positioned near to the fusion line at the root of the weld bead. Hole diameters vary usually from 4 to 1.7mm. Limitations in using diameters smaller than 1.7mm are usually posed by the diameters of ceramic insulators (used to protect the thermocouple in the hole) of corresponding size not being available [Apps and Coward, 1967 and Tecco, 1985]. Coating the wires with a refractory mixture may eliminate the need for ceramic insulators [Barlow, 1982a] but this technique has not been used widely.

The thermocouple diameter also varies in the range of 0.13-0.5mm. However, some reasons have been given to use thermocouple wires as fine as possible [Apps and Coward, 1967]. First, to produce a hot junction as small as possible in order to minimize the temperature gradient across the globule, i.e. to minimize the region of the heat affected zone whose thermal cycle is to be measured, secondly, to minimize conduction of heat from the solid and the error due to a temperature gradient along the wires and thirdly, to keep the response time of the thermocouples to a minimum. The fabrication of the hot junction is usually obtained by twisting the ends of the bare wires together and welding them using either a carbon arc or TIG welding. For the last process welding currents, not much higher than 50A have been reported to be able to produce a very small globule [Tecco, 1985]. The most popular process used for the attachment of the thermocouple hot junction to the bottom of the hole has been spot welding by means of a capacitor discharge unit. In this respect the cleanliness of the hole is essential for a successful attachment. It must be free from any dirt or grease. Due to the high cost of platinum type thermocouples, compensating cables are normally used to link the thermocouple cold junction to the recording instruments. In addition, the use of

compensating cables prevent the recording instrument from remaining too close to the experimentation area which sometimes can represent a real danger for delicate recording instruments. Compensating cables have the same thermo-electric properties as the thermocouple materials they are matched for, although they are often made of materials differing from the associated thermocouple [Humphries, 1973]. For instance, copper/copper-nickel compensating cables are usually used with Pt/Pt-Rd thermocouple. Nickel-chromium/nickel-aluminium compensating cables are appropriate for chromel/alumel thermocouples. The most suitable technique for linking the thermocouple wires to the compensating cables has been soldering [Tecco, 1985 and Andrade, 1985]. This technique according to these authors provides adequate electrical contact between both and assures satisfactory mechanical strength.

The implant technique has been also employed in studies involving temperature measurements in the HAZ [Granjon, 1967, Perdigao, 1980 and Andrade, 1985]. This technique as described by Granjon [1967] consists of inserting a steel plug containing a hole- which is drilled beforehand for subsequent attachment of the thermocouple- in a steel plate of the appropriate thickness. This technique, although useful in situations where the amount of material available is very little has been highly criticized because possible distortions may be caused by the assembly of the plug in the plate. Tecco [1985] believed that abnormalities in the heat flow under situations where differential contraction of the implant occurs relative to the rest of the plate, could result in the formation of a gap between the two. Granjon [1969] did not note differences when analysis was carried out in order to verify the influence in the cooling time through 800-500°C by both the fitting of the implant (freely or tightly in the hole) and the reproducibility of the thermal cycle regarding the conditions found with integral testpieces. This, however, was not shared by Tecco [1985] who found differences in cooling times (cooling times longer than expected) more noticeable when welds were performed at heat inputs higher than 2.0kJ/mm. According to him, the small heat inputs (HI≤2.0kJ/mm) employed by Granjon [1969] (cooling times through 800-500°C of less than 6s) did not provoke significant detachment of the implant from the testpiece.

In the present work, the measurements of the thermal cycle at the root of the weld bead in the coarse grained region of the HAZ was by

the insertion of thermocouple twin bore ceramic shielded into holes drilled perpendicular to the surface of the test plate followed by capacitor discharge welding. This technique was preferred as opposed to the implant on the basis of the range of heat inputs (0.8-3.5kJ/mm) to be employed in the test welds.

2.2.2.2 Recording Instruments

Some of the various instruments employed in studies of actual thermal cycle measurements are described briefly in this section. It is not intend to consider their electronic circuits in detail due to their complexity.

By definition, recorders are instruments that provide a graphical record of the history of the measurement of some physical event [Jones and Chin, 1983]. In particular, chart recorders or as they are also known, strip-chart recorders, are devices for producing a permanent record, in **analogue** form the change of a variable y against time t(whether this be continuous or intermittent).

In weld thermal cycle measurement one of the most important technical attraction of a recording instrument is the capability of giving fast response to the very steep temperature gradients developed in the workpiece. That is, a particular point under study is submitted to a fast heating and cooling cycle within a short length of time during the welding operation. The level of response achieved by the electrically actuated recorders justifies their frequent employment in measurements of weld thermal cycle. These recorders can be categorised into two basis types: galvanometric and potentiometric.

A galvanometric recorder consists of a moving coil suspended either on pivots or a taut ligament. The coil is then able to rotate in the field produced by a permanent magnet. When a small current is applied to the coil a field is created which reacts with that of the permanent magnet and the coil rotates which is shown by the deflection of a pointer. In practice this principle is applied in several ways. In direct-writing moving-coil instruments, an arm with a pen attached, which is fed from an ink reservoir, is directly connected to the moving coil. The pen then writes in sympathy with the coil movement on a chart, which may be either in strip form or circular. On the other hand, the self-

balancing potentiometer type of instruments consists of a bridge circuit. Across one arm of the bridge is a reference voltage, and across the other arm is a feedback network (Figure 2.7). Initially, the bridge is adjusted so that the servo-amplifier and its motor are in balance and stationary. When a signal is fed to the amplifier the output causes the servo-motor to drive a balancing potentiometer, which in turn refers a feedback voltage to the amplifier input. When the two signals are equal and opposite the system balances and the servomotor stops. If a pen unit is attached to the motor-potentiometer mechanised drive, at the point of the balance, the pen will show the proportional value of the input signal. As with galvanometric instruments this principle may be applied in various ways.

In addition to these types of electrical recorders, oscillographs and photoelectric potentiometers were employed in the initial studies of the weld thermal cycle [Rosenthal and Schmerber, 1938 and Hess et al, 1943]. More recently the ultraviolet (a galvanometric type) recorder has largely been employed in actual thermal cycle measurements [Kohno and Jones 1978, Rodrigues, 1978, Tecco and Andrade, 1985]. This type of recorder can have frequency responses up to about 10kHz [Thomas, 1972] and are suitable to record signals in the frequency range from 125Hz to a few thousand hertz [Jones et al, 1983].

Although the electrically actuated recording instruments mentioned above can be reliably employed in studies which involve analysis of the thermal history of weldments, the hard copy traces of the outputs of the thermocouple cannot be directly employed. They have to be converted to temperature/time plots on the basis of calibration tables according to the type of thermocouple used. This operation can be very time consuming, principally in measurements in the HAZ where two or more thermocouples are normally used.(The use of two or more thermocouples in this type of measurements is to increase the chances of success considering the difficulty in precisely positioning the thermocouple in the region of the HAZ of a particular interest. The inherent small variations of the bead penetration along the weld can change the dimensions of the HAZ to an extent that the point of interest can be missed and the experiment might be considered unsuccessful.)

In view of the limitations posed by the plots supplied by the electrical recorders, data acquisition systems have been employed in

measurements of the thermal cycle of the HAZ [Barlow, 1982a]. One of the greatest attraction of these equipments is the possibility of storing a number of simultaneously recorded thermal cycles in a computer file for future analysis. These units employ techniques similar to those used in computers to store parameter information. Analogue input data is fed into the unit where it is converted, at a specified rate, into digital code words and these are stored in a region of computer memory. These units are categorised as analog/digital converters (A/D converters). Owing to the rate at which data is captured by these units discontinuities are inherent to the data, i.e. numbers change in steps. On the other hand, analog variables, by their very nature, are capable of a continuous variation. There is no lower limit to the smallest change possible in an analog variable. It follows that there is a limit to the precision (a resolution limit) with which an analog magnitude can be prescribed numerically. Whenever a numerical measure of magnitude is assigned to an analog variable there is an element of uncertainty even though the measurement system is ideal. An A/D converter produces a binary number which represents the magnitude of an analog input signal. There is inevitably an element of uncertainty in the binary number. Analog values which lie in the uncertainty range all give rise to the same number and are not resolved as different. The resolution of an n-bit binary A/D converter is variously expressed as one part in 2^n, as a percentage $(1/2^n)$ x 100 per cent or sometimes simply as n bit.

An A/D converter was chosen in the present work in order to optimize and to improve the accuracy of the processing of the thermal data for its use in future analyses. An 8 bit A/D converter was then chosen with a resolution of less than approximately 1% of the full scale. In respect the range of 200-1530°C envisaged for the measurements of the thermal cycle in the HAZ an accuracy of the approximately 6°C was expected.

2.2.2.3 Remarks

In view of the review presented in this section, it can be noted that a large number of theoretical equations predicting thermal cycle in the HAZ can be found in the literature. Many experimenters have made comparisons between actual and predicted results. These are normally done on the basis of the cooling time through 800-500°C due to the importance of this range regarding microstructural transformation in the

HAZ. An enlarged range of temperatures (800-300°C) has also been used in order to compare theoretical and actual results [Kohno and Jones, 1978]. However, one point which is important to stress is that the differences found between those results vary in general, from extremely good to very poor agreement and this can be an indication that some important influence in the weld thermal cycle due to the solidification of the weld bead and the microstructural transformations in either weld metal and HAZ have not been totally comprehended or have been neglected in assumptions made in theoretical predictions. For instance, no concrete study has been carried out in the internal stresses generated in the HAZ due to the solidification of the weld bead and its influence on the weld thermal cycle. Attempts have been made to incorporate the effect of the latent heat liberated by microstructural transformation in the theoretical predictions [Nunes, 1983] but these do not seem to be conclusive. Another aspect which has also been mentioned previously is the variation of some thermal properties of the materials. For instance, thermal conductivity varies with temperature, therefore in the use of those formulae to calculate the cooling time through 800-500°C what would be the best value for thermal conductivity? Any fixed value is only an approximation which does not depict the real behaviour of that property of the material. Finally, studies in the HAZ based on simulation of actual weld thermal cycles have been extensively carried out employing equipment which, apart from limitations in achieving the fast heating rates found in actual welding, do not consider the possible influences of stress and directional heat flow.

Contradictions found in theoretical predictions plus discrepancies in respect to microstructures of specimens submitted to simulation compared to those obtained from actual welds, can only be solved on the basis of deeper understanding of actual measurements. As reviewed here, most practical aspects of the conduction of actual measurements seem to be quite well reported in the literature and it can be noted that a good understanding of them has been reached. Although the preparation involved in an actual measurement can be time consuming, this can well be compensated by the use of the modern data gathering systems described above. The flexibility offered by these systems regarding the storing of the data from various measurements is in fact very attractive. Moreover, the possibility of the direct employment of this data without any need for conversions in subsequent analysis is

also pointed out. Finally, the use of computers in this type of studies have in fact made a step forward towards the improvement of the understanding of the weld thermal cycle and its influence in the mechanical and metallurgical properties of a weldment.

2.3 Determination of Transformation Temperatures

Principal techniques employed to determine the transformation temperatures of the microstructures produced under continuous cooling conditions during welding will be reviewed. This will be done with focus on those applied to the HAZ. However, techniques applied for HAZ can be also used in most studies of the transformation temperatures in the weld metal [Akselsen and Simonsen, 1987].

The determination of the transformation temperatures of the products of the decomposition of the austenite during cooling are obtained by either thermal analysis [Granjon et al, 1966 and Phillip, 1983], dilatometry [Watkinson and Beker, 1967] or magnetic analysis [Constant and Murry, 1963]. However, the latter technique is of a very limited use [Akselsen et al, 1987] and will not be considered in this section.

Thermal analysis is based on the principle that the change in lattice from fcc (γ) to the bcc (α products) is accompanied by a reduction in free energy. The enthalpy difference liberated as heat, ΔH_{trans}, results in a slower cooling rate through the range of temperatures where the transformation occurs. The change in lattice involves movement of atoms which results in lattice parameter changes. Consequently, the range of temperatures where volume expansion or contraction takes place is associated with transformation and recorded by **dilatometric methods.** Both techniques can be employed in studies employing small scale laboratory test specimens in weld simulation and also for 'In Situ' measurement, during the actual welding operation.

A variety of methods are employed in thermal analysis and some of them are described below. First the temperature-time method where temperature is plotted against time should detect the reduction in cooling rate caused by the heat liberated during the decomposition of the austenite. The temperature at which the change in the cooling rate takes place (indicated as an inflection in the temperature-time cooling

curve) is considered the start of transformation (T_s). After the end of transformation (T_f), the temperature-time curve recovers its normal curvature but with a displacement Δt with respect to time (Figure 2.8). The location of these temperatures is rather difficult on such a cooling curve [Phillips, 1968 and Akselsen, 1987]. Secondly, the direct rate method can more accurately locate the start of transformation not detected in the first method presented [Phillips, 1968]. In this method successive equal intervals (ΔT) of temperature are plotted against the temperature resulting in an approximately linear plot until transformation occurs. At this temperature a marked deviation from linearity is seen (Figure 2.9). Thirdly,the differential method is considered to be one of the most sensitive methods for recording the temperatures for start of transformation [Akselsen, 1987]. In this method the difference between a reference temperature at a specimen or point which does not undergo transformation and the temperature at a test specimen is plotted against the reference temperature.

Variations of the methods listed above and in particular the first two consist of plotting the first and/or second derivative(s) of the original curve against temperature. In this manner, it has been claimed [Tecco, 1985] that an improvement is obtained in the accuracy of the determination of the transformation temperatures.

Dilatometric analysis has been employed in the determination of transformation temperatures in tests using either simulation specimens [Rothwell et al, 1980] or actual welds [Hofmann and Burat, 1962]. Phillips [1968] comparing the use of various thermal and dilatometric techniques found that for fast cooling, thermal analysis gave the most precise transformation temperatures. At slow cooling the dilatometric technique appeared as the more precise method. According to this author, slower cooling corresponding to $\Delta t_{8\text{-}5}$ longer than 30sec indicates that dilatometric analysis should be applied.

2.3.1 Simulated Specimens

Up to the present work the studies involving microstructural transformation in welding have been based on small scale specimens used in weld simulation and a small amount of examination in actual weld HAZ's. The former approach involves the reproduction of microstructures similar to those found in actual weld HAZ's as first

developed by Nippes and Savage [1949]. They designed an equipment capable of imposing a pre-set thermal cycle which was similar to that experienced by a particular point in a real HAZ on a small scale specimen. This specimen is resistance or induction heated, and the dimensions are usually restricted to a small cross section. Although flexibility, accuracy and convenience are the main advantages of this technique, difficulties in matching the grain size of austenite found in the real HAZ with that of a simulated sample has been a principal limitation. Dolby and Widgery [1970] found that for the same thermal cycle simulated specimens showed coarser grain sizes. The major cause of this discrepancy was the narrow width of the weld HAZ, which restricts grain growth. These discrepancies have also been attributed to different heating rates, the heating rates during simulation being too slow [Phillips, 1983]. Another interesting aspect found by Dolby and Widgery [1970] was that a good agreement was found between the microstructures of simulated specimens and the HAZ when the peak temperature was 1210°C as opposed to peak temperatures higher than 1300°C which are often used [Koso et al, 1981 and Harrison et al,1987]. These authors also pointed out that the discrepancies found might not be dependent significantly on the design of the simulator but a general problem of the technique. Another factor which has been reported [Dolby, 1979] related to the grain size differences is the absence of a steep temperature gradient in the central part of the specimen, unlike the weld situation. In addition, Dolby [1979] reported that several investigations have shown that Charpy V tests on simulated specimens give consistently higher transition temperatures than tests on weld HAZ's, an effect due mainly to the Charpy specimen having a constant yield strength and microstructure across the ligament below the notch, unlike the real weld HAZ specimen.

2.3.2 Actual HAZ Transformations

The limitations presented by simulated specimens have highlighted the importance of performing tests on real weldments to determine transformation temperatures in the HAZ [Phillips, 1983]. The actual determination, or as it is also known the 'In Situ' analysis of the transformation temperatures in the HAZ, was first developed by Granjon et al [1967a and 1967b] in the 60's. In their experiments thermal analysis was employed and the implant technique (refer Section 2.2.2.1.) was used to locate the thermocouple. In order to make more

evident the inflexions originating from transformation, the signal output from the thermocouple was differentiated (dT/dt) by an electronic differentiator. A second differentiation was also used for further improvement in accuracy. The resultant graphical curves of the thermal analysis were recorded by an X-Y recorder. Furthermore, some curves were presented illustrating the interpretation of the results and a variety of CCT curves were also shown. No example of split transformation, i.e. consecutive bainite and martensite reactions are given in the published work. Although electrical background noise is claimed to be the main experimental problem with the electronic differentiation method in thermal analysis [Phillips, 1983], this was not mentioned by Granjon et al [1967a and 1967b].

Modifications have been introduced to the 'In Situ' thermal analysis. For instance, Rodrigues [1978] used an equipment consisting of a transient recorder, an oscilloscope and a paper tape puncher; around 1000 samples could be taken per thermal cycle trace, data processing being made with a computer. Noise problems were mentioned which required the design and incorporation of additional filtering stages. Phillips [1983] developed a technique which consisted of using two thermocouples inserted in the implant and a recording equipment of X-Y and Y-t. The first thermocouple, identified as the test thermocouple was in contact with the material which was expected to undergo transformation, whereas the second, the reference thermocouple, positioned 4mm apart was encased in a stainless steel sheath. The reference thermocouple was to undergo a similar thermal cycle but without recording microstructural transformations owing to the protection of the stainless steel sheath. The thermocouples were positioned in a manner such that the test thermocouple would experience temperature increases first, followed by the reference thermocouple. The X-Y recorder plotted the variation of the difference temperature between the test and reference thermocouple against the temperature at the reference thermocouple. Simultaneously, the temperature-time curve was recorded. In the first trials, the author found noise pick-up problems which he attributed to low frequency electric currents in the thermocouple leads induced by the magnetic effects associated with the welding arc. This was minimized by shielding the X-Y recorder input leads and encasing the thermocouple wires and cold junction box in a soft iron tube. A comparison between the CCT diagram resultant from the thermal analysis of a steel used in the

study and that obtained from simulated tests verified that diagrams were generally similar in form but under simulated welding conditions the whole diagram was depressed to lower temperatures and longer times. Furthermore, the author claimed that the 'In Situ' method can detect almost all phase transformations that occur during cooling with the exception of the martensite which was not detected when present in concentrations less than 8%, at slow cooling rates.

More recently [Tecco, 1985] the two methods, namely temperature/time and temperature/temperature, were further developed to be employed in thermal analysis of the transformation temperatures in the HAZ. The temperature/time method involved digitizing the thermal cycles recorded by an U-V recorder and differentiating (dT/dt) the curve with respect to time. The temperature/temperature method involved plotting the temperature of the point under investigation (test thermocouple) against the temperature of another point of reference (reference thermocouple) on the same body, using an X-Y recorder. The test thermocouple was positioned near to the fusion boundary, while the reference thermocouple was placed at point which would experienced a much lower temperature away from all transformations. The thermocouples were placed in a way that the reference thermocouple would heat first than the test one. In this manner, transformation temperatures could be identified by local deviations in slope (Figure 2.10). In order to avoid interference from microstructural transformation in the weld metal, which could mask the transformation from the HAZ, a nickel filler wire was used in combination with an acid flux in the submerged arc welding (SAW). Difficulties in detecting the temperature of the end of transformation by the temperature-time method was found owing to a much smaller variation in cooling rate compared to high temperatures. Consequently, the end of transformation occurred much more smoothly than the start of transformation. With the temperature/temperature method, the time was indirectly eliminated, which minimized the loss of resolution at lower temperatures. According to the author, unlike simulated welding the 'In Situ' thermal analysis is subject to thermal effects which are originated from arc and pool phenomena. This might mask the thermal effect generated by phase transformation. Nevertheless, the 'In Situ' approach was preferred to simulation techniques as he felt that insufficient evidence was available to support the use of the latter for transformation studies.

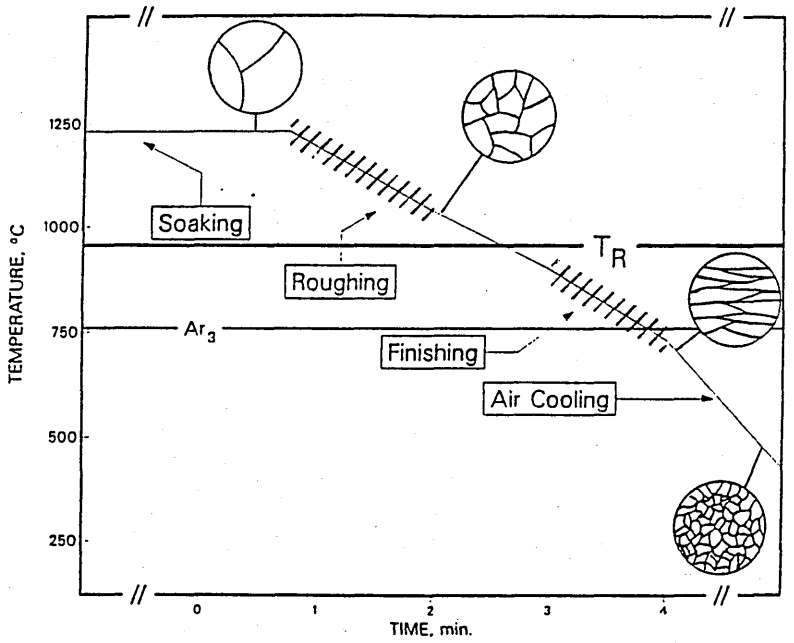

Figure 2.1- Schematic temperature/time for controlled rolling of 19mm steel plate. [Cohen, 1985]

BS 4360 Grade 50D (1969)

C	Si	Mn	S	P	Nb
0.22 max	0.1/0.55	1.6 max	0.05 max	0.05 max	0.1 max

Plate product was Si killed and normalised. Other microalloying elements e.g. V could be added if required.

Typical Supply to Fabricators in 1972/3

C	Si	Mn	S	P	Nb	Al_{sol}
0.17	0.4	1.30	0.20	0.025	0.05	0.028

Si killed, Al treated

Typical Supply to Fabricators in 1986

C	Si	Mn	S	P	Nb	Ni	N_2	Al_{sol}
0.10 0.12 max	0.40	1.50	0.002	0.012	0.03	0.25	0.006 max	0.035

Other alloying elements such as Cu and Cr may be added to maintain yield and tensile strength.

Figure 2.2- Chemical composition of steels used in offshore construction. [Cohen, 1985]

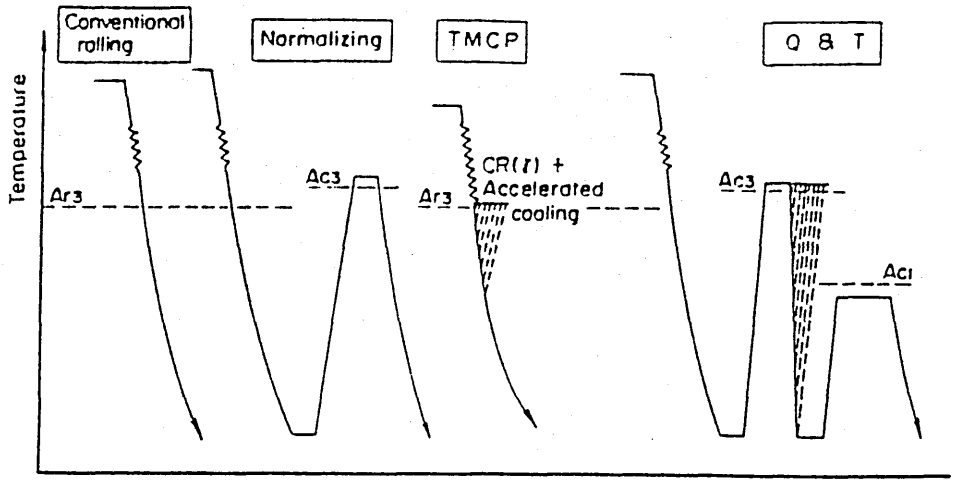

Figure 2.3- Schematic illustration of manufacturing processes. [Kitada, 1986]

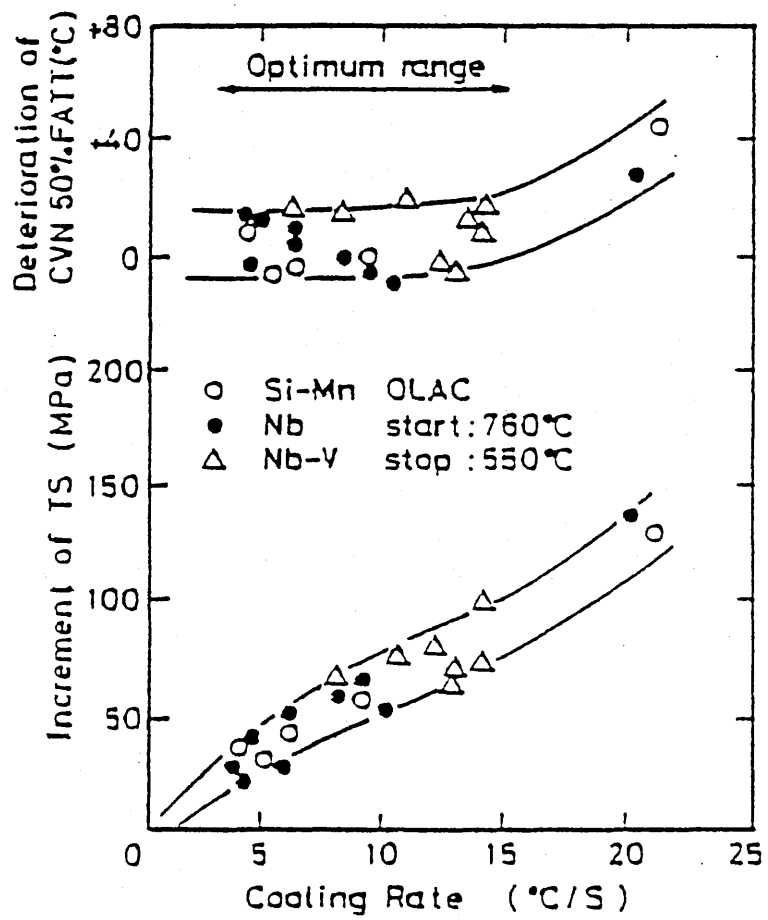

Figure 2.4- Effect of On-Line Accelerated Cooling on TS and FATT. [Kozasu, 1983]

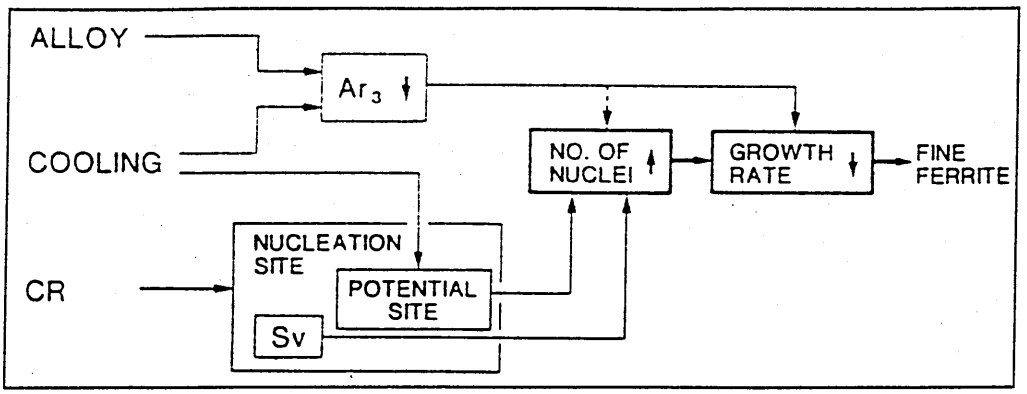

Figure 2.5- Schematic diagram to illustrate various mechanism of ferrite grain refinement.
cooling: accelerated cooling
Sv: effective grain boundary area per unit volume
[Kozasu, 1985]

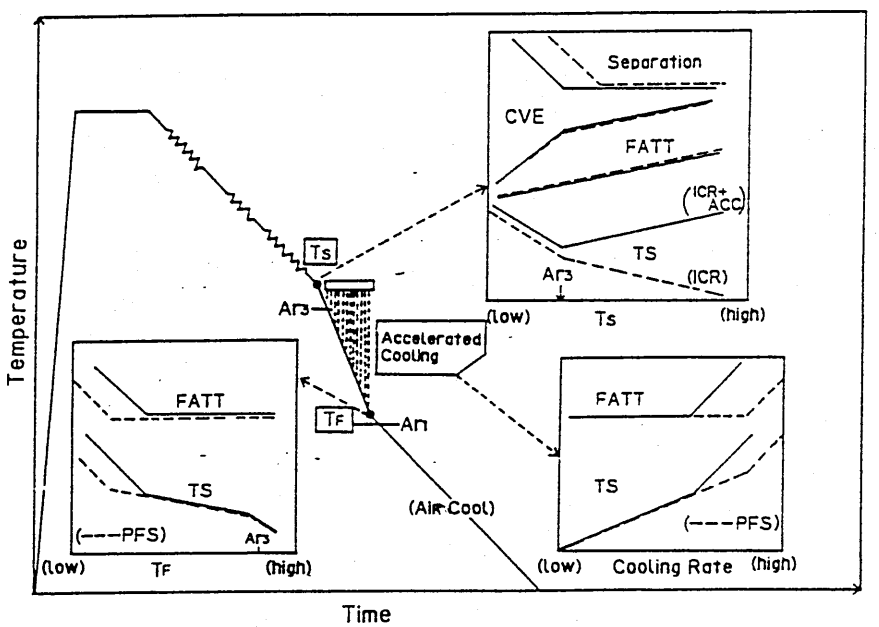

Figure 2.6- Schematic representation of the effect of processing in accelerated cooling.
ICR: intensified controlled rolling
PFS: pearlite free steel
TS and TF: starting and finishing temperature of water cooling
[Kozasu, 1987]

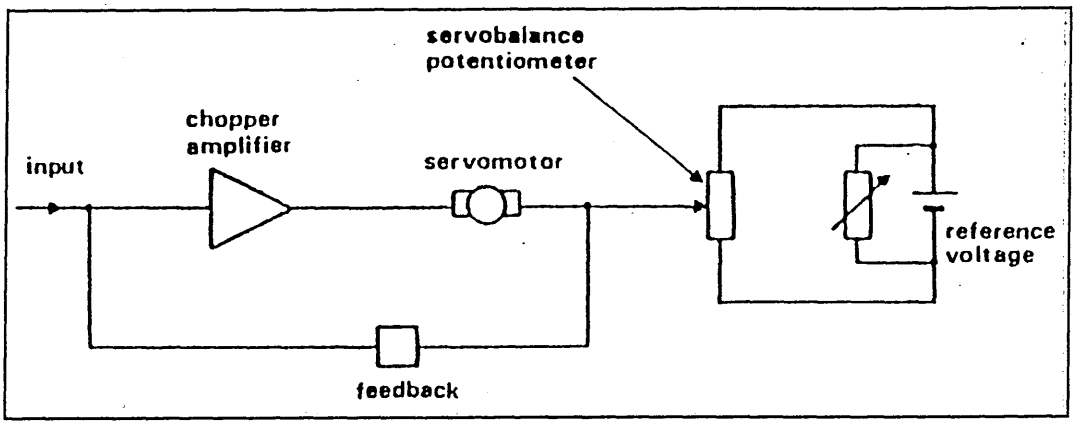

Figure 2.7- Simplified principle of operation of self-balancing potentiometer. [Jones, 1983]

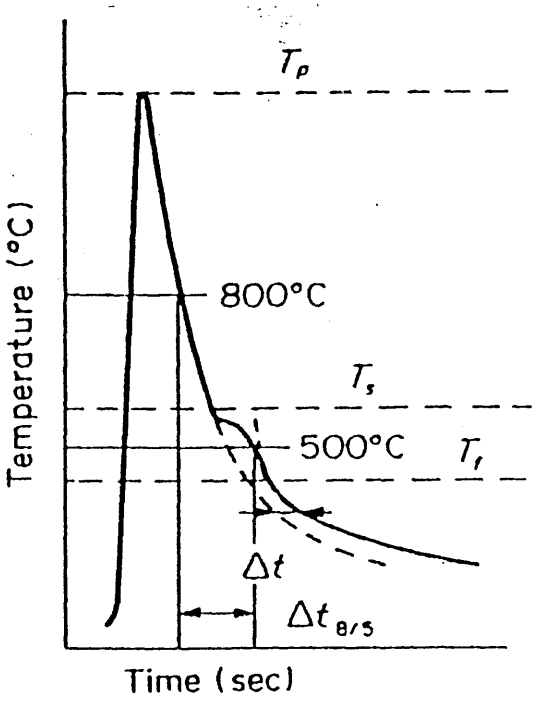

Figure 2.8- Schematical illustration of a cooling curve. [Akselsen, 1987]

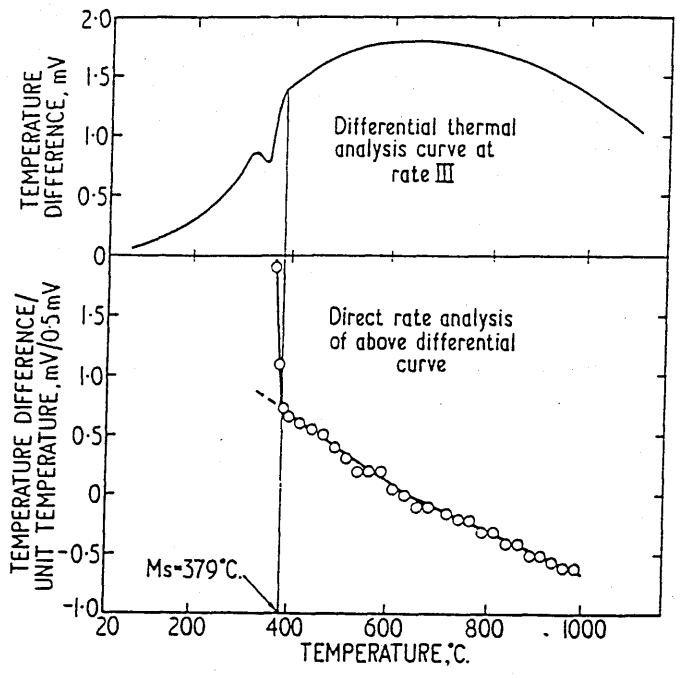

Figure 2.9- Derived differential thermal analysis curve. [Phillips, 1968]

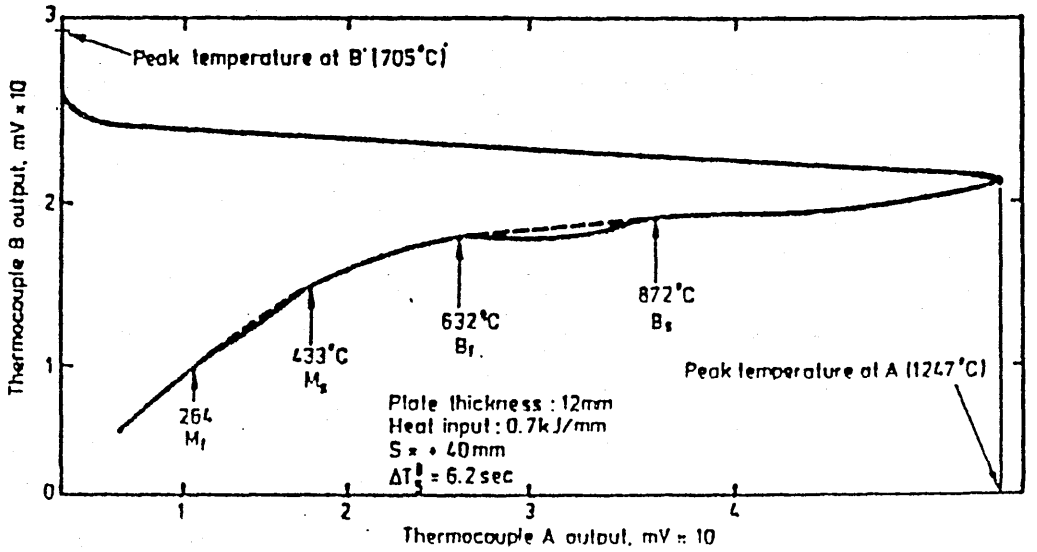

Figure 2.10- Typical temperature/temperature traces showing start and finish of martensitic and bainitic transformations. [Tecco, 1985]

CHAPTER 3 PROGRAMME OF WORK

3.1 Objective

The project was aimed at the study of the real weld HAZ's of one conventional normalized C-Mn steel and three modern 'lean' steels produced by the new OLAC (**O**n-**L**ine **A**ccelerated **C**ooling) process as described in Chapter 2. The study was focused on the coarse grained region of the HAZ near to the fusion boundary. This region, where peak temperatures can reach 1100°C or even higher as a result of the weld thermal cycle, is associated with a coarse austenite grain size. Consequently, the microstructure resultant from the decomposition of the austenite during cooling can lead to embrittlement of the weld joint. Thus for the present work, it was established to investigate the microstructural changes (and hence properties) in the HAZ as a result of the weld thermal cycle. Initially, it was considered that the temperature measurement of the real weld thermal cycle in this region would merely be an application of established technique. However, the state of the art proved inadequate and much more time had to be devoted to the improvement of temperature measurement techniques.

Thus, the first task was to develop a data gathering system capable of measuring real weld thermal cycles in the HAZ. Secondly, was to develop a software programme to handle the thermal data where relevant information regarding each test weld (such as peak temperatures, cooling and heating times) could be obtained and reliably employed in analysis of microstructural changes and properties of the HAZ's of the steels under investigation. Thirdly, was to apply the thermal data (**as measured**) in thermal analysis to determine the transformation temperatures of the microstructures produced in the HAZ's. Fourthly, it was required to identify and quantify the various different microstructural products present in the HAZ in each steel. Finally, the requirement was to analyze the hardenability of each steel on the basis of the results produced in the present research work.

3.2 Limitation of Previous Work

Studies of the decomposition of austenite during cooling in the HAZ can be experimentally approached by weld thermal simulation or actual

welding. Notwithstanding some sophisticated equipment presently available to apply the former technique, it is still a matter of criticism that neither the stress and thermal fields, nor the heating rates typical of actual welds, can be fully reproduced. As a result, simulated and actual welded specimens having identical thermal histories do not give identical microstructure and hardness [Widgery,1972]. These discrepancies prevent simulation techniques from being fully accepted without reservation, by many investigators.

The use of real weld thermal cycle measurement as a means to investigate the microstructural transformations in the HAZ can lead to satisfactory results despite the limitations on methods, i.e. accuracy and experimental difficulties. These limitations are mainly due to the inherent unsteady-state nature of the weld thermal cycle, the development of high gradient temperatures and interactions originating from the microstructural transformations in the weld metal and HAZ. The local change in heat flow due to presence of the thermocouple is also acknowledged. However, improvements in existing methods and the use of microprocessor based instrumentation can minimize the limitations described.

The application of "In Situ" thermal analysis as a means to investigate the microstructural transformation and its implication on mechanical properties of steels (in either weld metal or HAZ) has been a matter of investigation for several years. The combined use of temperature/time with temperature/temperature methods has been claimed [Phillips, 1983 and Tecco, 1985] to be a very useful technique to determine the transformation temperatures occurring in the HAZ of actual welds during cooling. The accuracy and reproducibility of data has left a lot to be desired; some degree of subjectivity is still involved in precisely determining the start and finish of the transformation reaction.

Until the present investigation, the instruments employed, mainly oscilloscopes, in the methods mentioned above had an intrinsic limitation with regards to the format of the data. They had to be submitted to some form of conversion process if they were to be of use in further computer analysis. This process is time consuming and, what is more relevant, is a possible source of error in the data which may lead to misinterpretation of the information obtained by 'In Situ'

thermal analysis. Furthermore, because reliable results are inherently much more difficult to obtain by these methods, considerably less attention has been given to the actual potential that this method offers to the study of microstructural changes in real welds and their effects on mechanical properties.

3.3 Outline Programme

In order to achieve successfully all the proposed objectives, the following programme of experimentation was pursued:

i) Improvements of experimental techniques in measurements of welding HAZ thermal cycles by employing a digital data logger unit;

ii) Measurement of actual HAZ thermal cycles using the drill hole technique in plates welded within a range of heat inputs;

iii) The use of the thermal data gathered during actual temperature measurements in 'In Situ' thermal analysis as a means of determining the transformation temperatures of the various microstructures produced in the HAZ's;

iv) Quantitative and qualitative metallography of samples taken from the welded plates as a means of understanding changes in properties; in addition, to support the identification of the various ranges of transformation temperatures determined by thermal analysis;

v) Hardness measurements in the coarse grained region in order to analyze the influence of the various microstructures produced in this region as a result of actual weld thermal cycle;

vi) Assessment of current empirical techniques available in the literature to analyze the hardenability of the weld HAZ's of the steels under investigation.

From the experimental work,it was then possible to compare the weld HAZ transformation behaviour of three modern structural steels with that of a more conventional one. It was also possible to assess the hardenability of these steels on the basis of carbon equivalent techniques currently found in the literature.

CHAPTER 4 MATERIALS AND EQUIPMENT

4.1 Materials

4.1.1 Parent Plates

A total of four steels were selected for investigation.Three of the steels chosen were manufactured by Nippon Kokan (NKK) using a newly developed process known as the OLAC (**O**n-**L**ine **A**ccelerated **C**ooling) process. The OLAC steels are high strength steels of 50kgf/mm^2 tensile strength grade and designed to be used for Arctic offshore structures where working temperature can be -40°C or even lower, or for ice-breaking vessels [Tsukada et al 1983]. These steels are claimed by their producers [Nippon Kokan, 1983] to obtain their excellent properties through the production process, i.e. the combined application of intensified controlled rolling followed by the OLAC process. According to Nippon Kokan, a very fine ferrite grain size is achieved without recourse to the use of conventional grain refining elements such Nb and/or V and/or Ti. Further they claimed that an improvement in toughness over that achieved by plain Si-Mn steel can be achieved by additions of Cu and Ni. In the current work, a total of three of these steels in the form of 32mm thick plates were identified as steels B,C and D. Their mechanical properties, certified by the producer and their chemical compositions are shown in Tables 4.1 and 4.2, respectively. In Table 4.1, steels B, C and D have very similar tensile properties, whereas D and C have similar impact properties, higher than B. These steels are known by their very lean chemical composition (Table 4.2) in which low sulphur and low carbon are their basic charecteristic. Steels B amd C have a similar chemical composition in which B has higher carbon and lower silicon and manganese than C. On the other hand, steel D has similar Si compared to B and lower than C but it has lower carbon, higher manganese than B and C. Addition of Cu and Ni in proportions of 0.22% and 0.41%, respectively are found in steel D. A more traditionally produced steel, i.e. continuously cast, was also used and the 25mm thick plate was identified as steel 12. This steel was more traditional in composition, being a typical C-Mn steel grained refined by a normalizing heat treatment. The mechanical properties and the chemical composition of this steel is also shown in Tables 4.1 and 4.2. Its tensile properties are

slightly lower than those of steels B, C and D. The impact properties, although only the result at -40°C is presented, does not seem as high as the other steels. As is shown in Table 4.2, steel 12 has carbon content in the same range of the other steels but lower manganese than B and Si slightly lower than C. Sulphur content is markedly higher than that found in steels B, C and D. Additions of Cu and Ni are also found in proportions of 0.25% and 0.10%, respectively.

4.1.2 Welding Consumables

For the Submerged Arc Welding (SAW) an acid fused flux, type Muraflux A50 manufactured by Murex Welding Products Ltd was chosen. The wire was a Ni-base alloy of 1.6mm of diameter. It was manufactured by Henry Wiggin Co. Ltd and was identified as type A61. The nominal composition of 93% min Ni+Co, 0.25% max Cu, 1.0% max Mn, 1.0% max Fe, 0.15% max C, 0.01% max S, 0.75% max Si, 1.5% max Al and 2.0-3.5% Ti corresponded to AWS ERNi-3 classification. This filler was chosen to avoid any complications that could occur in temperature measurement due to solid state transformations in the weld metal. Consequently, any indication of microstructural transformation could only be attributed to the HAZ solid state transformation considering that, in the weld metal no reaction was expected other than the solidification of the Ni-base alloy.

4.2 Equipment

4.2.1 Welding Equipment

Due to the small diameter of filler wire used, a conventional submerged arc welding (SAW) power source was not really suitable. A lower current output power source with a constant voltage characteristic was considered to give better control by means of self-adjustment and a MIG/MAG power source was therefore selected. The Transmig 600, a transformer/rectifier power supply, manufactured by BOC Arc Equipment, was chosen; its welding output range was 60A-600A at 14V-44V. Because of the location of the power source, a remote control was used which enabled arc voltage to be regulated at the site where the welding was done.The wire feed speed was adjusted by a control on the wire feed unit. Welding current was proportional to wire feed speed so that increasing the speed increased the current and vice versa. A

lead to the wire feed unit allowed the start and finish of the welds to be controlled without using the control panel of the wire feed unit. As a result, the experimenter could have better mobility in the area of the welding rig allowing operation of both welding and recording equipment without technician support. The measurements of welding current and arc voltage were made by U-V Recorder,which gave an accuracy of ± 20A and ± 2V for welding current and voltage respectively and permanent recordings of welding parameters. A vertically mounted welding torch was kept stationary whilst the test pieces were traversed beneath it. The table on which the specimens were positioned was driven by a variable speed travel carriage (model GK-171-18, manufactured by GULLCO International Limited) which was calibrated for each welding speed used for the experiments. Its reproducibility was considered satisfactory, with ± 2% of accuracy. A photograph of the welding set-up can be seen from Figure 4.1.

4.2.2 Thermal Cycle Measurement Equipment

Thermal cycle measurements were carried out in the coarse grained region of the HAZ of the steels under study using the drill hole technique. Temperature measurement was by thermocouples and it was essential to select a type and wire diameter suitable for the range of temperature, 200 - 1600°C, of the experiments with the appropriate rapid response. This range of temperature was envisaged on the basis of previous work [Rodrigues, 1978, and Andrade and Tecco 1985] in actual weld thermal cycle measurement. The thermocouple employed was of Pt/Pt-13%Rh,manufactered by Johnson Matthey Metal Limited, type R, 0.25mm thick which could be used for measurements of temperatures up to 1760°C. The thermocouple wires had to be insulated for insertion in the holes drilled in the plates. In this respect, insulation and protection for the thermocouple wires were provided by twin-bore recrystallized alumina tubes with an outside diameter of 2.5mm. The hot junction of the thermocouples, to be positioned at the region of interest in the HAZ for temperature measurements, was carefully produced with a low current (40A) TIG welding power supply. Thermocouples were inserted in drilled holes and spot welded to the bottom of the hole, see 5.2.1.2. The linkage between the thermocouple hot junction and the data gathering system was by appropriate cupro-nickel / copper compensating leads.

The recordings of actual thermal cycles was done by a data gathering system named Databox, manufactured by Data Harvest Group Limited [Data Harvest, 1987]. The Databox was capable of being interfaced with both BBC and IBM compatible personal computers. About the size of a conventional video cassette it could record up to eight channels with eight bit resolution, had a 32 kilobyte memory and was capable of operating independently of a computer once programmed. The Databox was able to perform according to instructions given by the experimenter via a computer software programme, supplied by the manufacturer, named BOX. This enabled the user to set up all the conditions required for each experiment such as number of channels to be recorded, time interval between readings (logging time),and the criterion to initiate and to stop recording.

Owing to the fact that the data logging system accepted analogue voltages in the range of 0 to +2.55V,considerable amplification was required in order to maximize experimental resolution of the output signals from the thermocouple. An interface amplifier capable of converting the output of the thermocouple to a voltage in this range with a known transfer function was constructed. It had eight channels and used discrete IC amplifiers. It was capable of being adjusted to provide full scale amplification of any desired temperature range required for the experiments. The data gathering unit and the interface are shown in Figure 4.1. The electronic circuitry of the interface amplifier can be seen from Figure 4.2.

4.2.3 Optical and Electron Microscopy

Metallographic examination was carried out utilizing a Nikon Metallurgical Microscope OPTIPHOT. The microstructure produced in the HAZ were quantified by means of phase point counting using a Swift Automatic Point Counter, manufactured by James Swift & Son Limited. This stage unit was connected to an electrical counting device which was hand operated by the observer during the entire analysis.

The electron microscopy observations were performed using a Cambridge Stereoscan 600 scanning microscope, at an accelerating voltage of 25kV. An additional X-Ray non-dispersive analyzer by Link Systems was coupled to the scanning microscope.

4.2.4 Hardness

Vickers macrohardness tests were performed on the experimental specimens produced using a Vickers Pyramid Hardness Testing Machine, manufactured by Vickers-Armstrongs Ltd. A 5kg load and a 136 degrees diamond pyramidal indenter was used for all tests.

4.2.5 Computer Hardware

IBM compatible microcomputers were employed for both programming the data logger for test welds and translating the binary data file created by it into an ASCII code version. The analyses of the thermal cycles measured and their thermal characteristics were carried out by utilizing the Cranfield mainframe VAX machine.

Table 4.1 - Mechanical Properties of the Experimental Steels

Steel	Y.S. N/mm (kgf/mm^2)	T.S. N/mm (kgf/mm^2)	Elongation (%)	Impact Test Min-Max / Mean J (-20°C)
B	398 (40.6)	515 (52.5)	34	301.1-319.7 / 311.2
C	404 (41.2)	517 (52.7)	26	390.3-395.2 / 392.3
D	415 (42.3)	506 (51.7)	36	399.1-401.1 / 400.4
12	335 (34.1)	490 (50)	24	69 (-40°C)

Table 4.2 - Chemical Analysis of Experimental Steels

	Chemical Composition (%)												
Steel	C	Si	Mn	P	S	Cr	Mo	Ni	Al	B	Cu	Ceq*	Ceq**
B	0.13	0.32	1.34	0.012	0.005	0.02	<0.03	0.01	0.03	<0.001	<0.01	0.36	0.21
C	0.11	0.38	1.44	0.007	<0.004	0.01	<0.03	0.01	0.08	<0.001	<0.01	0.36	0.20
D	0.08	0.32	1.54	0.004	<0.004	0.02	<0.03	0.41	0.08	<0.001	0.22	0.39	0.19
12	0.12	0.36	1.27	0.013	0.031	0.09	0.04	0.10	0.07	<0.001	0.25	0.38	0.22

Ceq^{*} (IIW) = C+Mn/6+(Cr+Mo+V)/5+(Ni+Cu)/15

Ceq^{**} (P_{CM}) = C+Si/30+Mn/20+Cu/20+Ni/60+Cr/20+Mo/15+V/10

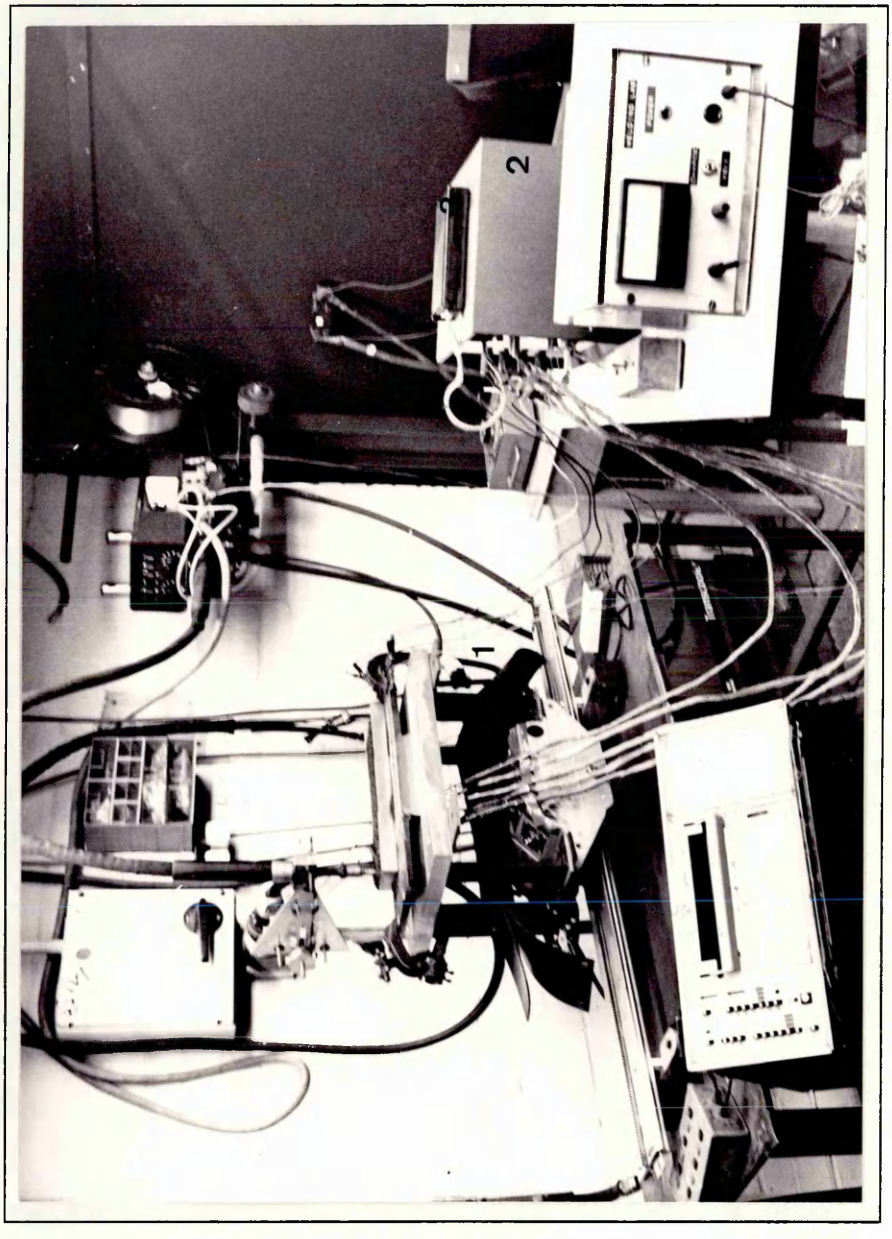

Figure 4.1- Welding set-up for the experimental work.

1) welding assembly
2) interface amplifier
3) data logger unit

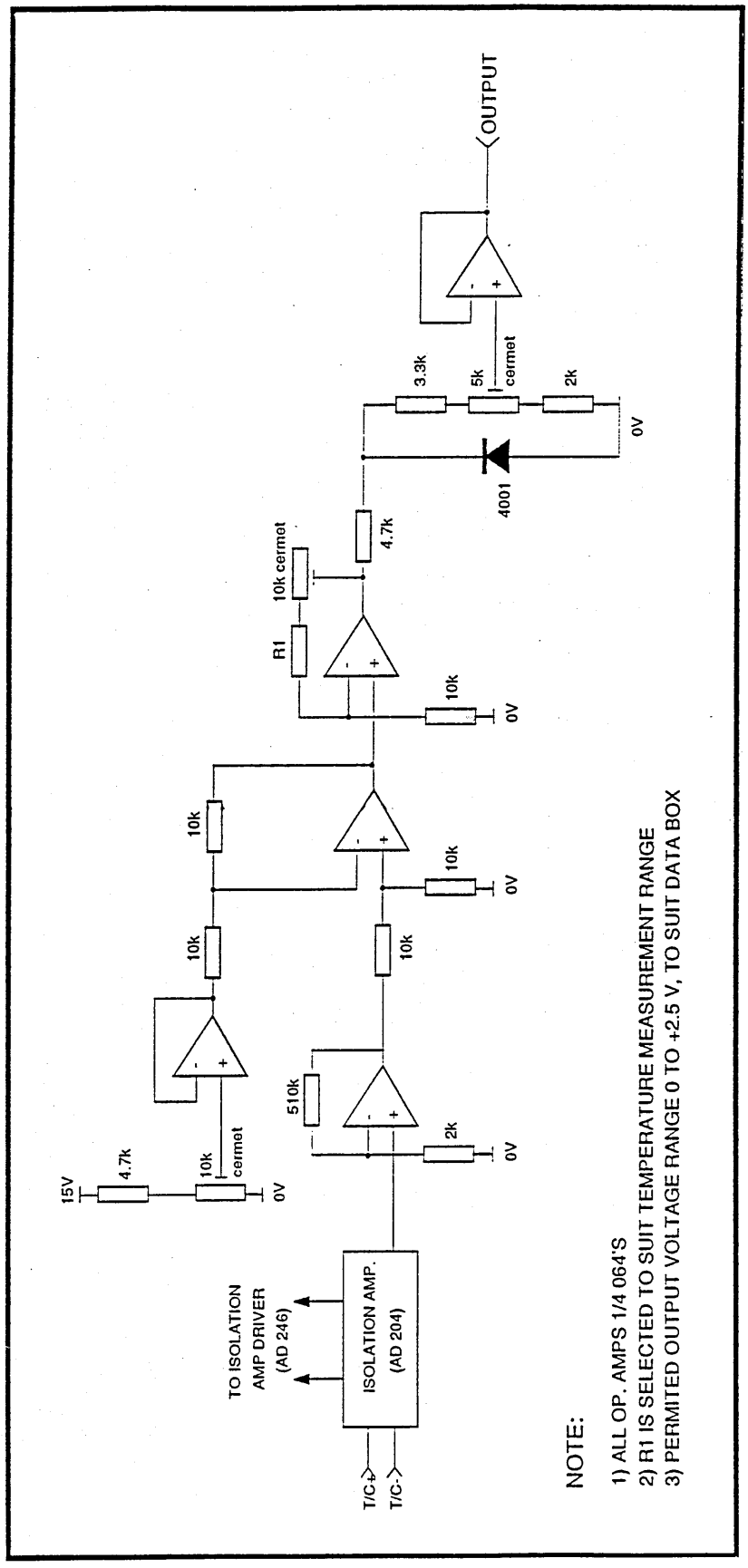

Figure 4.2- Electronic circuitry of the Interface Amplifier.

CHAPTER 5 MEASUREMENT OF WELD THERMAL CYCLES IN THE HAZ

5.1 Welding Procedure

Submerged arc bead on plate welds were performed in the flat position. The welding consumables chosen were a 1.6mm diameter Ni-base filler wire and an acid flux type, Muraflux A50. This choice was made on the basis of a successful work done previously in the Cranfield Institute of Technology [Tecco,1985] in similar experiments which claimed satisfactory reproducibility and arc stability throughout the experiments. The employment of Ni-base wire is justified by the fact that if microstructural transformations were to occur within the weld metal, these would interfere with the identification of the HAZ microstructural transformation temperatures under investigation. The range of heat inputs, from 0.8 to 3.5kJ/mm was chosen as typical arc energies used with these steels in plates to be welded by manual metal arc welding (MMA) or submerged arc welding (SAW). This was achieved by using a stickout of 15mm and keeping constant current and voltage of 300A and 30V respectively. The welding speed was adjusted for each heat input, by a means of stop watch and a ruler. This was carefully done several times just before the start of each experiment. The welding parameters used throughout the present work and the formula used to calculate the nominal heat inputs can be seen from the Table 5.1.

To make the welds, a special jig was built. The need of accessing the parent plates underneath for attachment of the compensating leads to the thermocouples was an important factor in the jig design. This was made possible by attaching a metal structure to the welding tractor of a height of 210mm; this can be seen from Figure 5.1(a). In this Figure, is also seen the table, measuring 460x300x30mmm, where the specimens were placed and clamped. It was made of aluminium to improve the heat dissipation of the specimens. A slot was made in its central part, measuring 290x75mm, which allowed the passage of the thermocouples (Figure 5.1(b)).

5.2 Measurement of Actual Thermal Cycle

5.2.1 Drill Hole Technique

Actual thermal cycle measurements were made by using the drill hole technique where thermocouples are inserted in holes drilled in the reverse side of a plate to be welded. In the present work, thermal cycles were measured in the coarse grained region produced in the HAZ. That is temperature measurements were by thermocouples placed as near as possible to the fusion line. To position the thermocouples accurately in this region, the profile of the bead, in particular the maximum depth of the weld penetration, had to be known beforehand. This was accomplished by carrying out several welding trials employing welding conditions (refer Table 5.1) which were to be used in the actual experiments.

A total of six plates each one corresponding to a particular heat input, namely 0.8, 1.5, 2.0, 2.5, 3.0 and 3.5kJ/mm were examined. The test pieces welded were of identical dimensions of the parent plates under study. Variations of the maximum penetration of the weld beads were expected due to the inherent nature of arc welding. This aspect was analyzed by cutting the plates welded in various transverse sections. The preparation of the surfaces to be examined were by grinding,polishing, and etching using Nital 10%. The penetration of the beads was measured by a magnifying glass and a ruler of 0.5mm of accuracy. A total of 10 measurements of the maximum weld penetration for each test weld were made. Variations up to 0.5mm were found which was taken into account when holes were drilled in the plates for thermocouple insertion in the main experimental welds. These variations were also an important indication of the need for more than one thermocouple in order to achieve successfully the weld thermal cycle measurement in the region of interest. Another aspect which was considered during the observations of the surface of the sections was the influence of the earth lead on the profile of the beads. For all welding trials the earth lead was affixed to the end of the plate from where the welding started. In this respect, the steadiness of the weld beads for this approach was to be found satisfactory and the same position for the earth lead was used during actual experiments.

In the main experimental work, a total of six plates for each of the

four steels studied, measuring 150x180mm, were machine ground on both faces. Their nominal thicknesses of 32mm for steels B,C and D and 25mm for steel 12 were kept unchanged. On the basis of the amount of material available it was decided to make two weld deposits for each test plate in order to save some material for any re-test if necessary. In this manner, two parallel series of five holes, 70mm apart, were drilled perpendicular to the surface of the plate; the positioning of the thermocouple hot junction took place at the root of the bead. The depth of the holes varied in multiples of 0.25mm, the maximum accuracy of the machine used to drill them. The holes were regularly spaced at 20mm from each other. Their diameter was just in excess of the diameter of the alumina tube (2.5mm) used for insulation of the thermocouple wires. The datum for the welding centreline, for every sequence of holes, consisted of two full penetration holes strategically drilled in either plate extremity. These two holes would, therefore, be situated in the same plane as the holes containing the thermocouples for measurements at the weld roots. The layout of the position of the holes can be seen from Figure 5.2.

The depths of the holes varied in multiples of 0.25mm, maximum accuracy of the machine used to drill them. Different depths gave higher probability of success to the experiment and provided data for a range of peak temperatures. Four of the holes were placed as near as possible to the fusion boundary in the coarse grained region of the HAZ. The fifth hole was placed where peak temperature would reach, at the highest, approximately 500°C. This was used in the new temperature/temperature method developed by Tecco[1985] and described in the Chapter 6.

5.2.1.1 Preparation and Positioning of the Thermocouples

The thermocouple hot junction was produced by the TIG welding process. A low welding current of 40A was used in order to obtain globules of the smallest possible size (diameter varied from 0.5 to 1mm)- which would improve heat equalization between the region where the thermocouple was situated and the hot junction. This was accomplished by twisting slightly the wires and advancing them to the arc until a globule of a molten metal was formed.

To avoid contact of the thermocouple wires with the plate in the

hole, a twin bore aluminium insulator of 2.5mm of diameter was used. The thermocouples were spot welded to the bottom of the holes by connecting the plate to one terminal of the capacitor discharge unit and the thermocouples wires to the other. After charging the unit up to 4V, the twin bore aluminium insulator was gently lowered down into the hole. The electrical discharge took place immediately the thermocouple touched the bottom. To produce a satisfactory weld it was essential to ensure that the holes did not contain any dirt or grease. Furthermore, it was necessary to ensure that the small length of thermocouples emerging from the insulator to the hot junction did not touch the walls of the hole during lowering of the thermocouples. Otherwise welding would take place above the base of the hole. As mentioned previously, the diameters of the holes was just in excess of the diameter of the aluminium insulator. This prevented the thermocouples from oscillating excessively during handling operations, which could cause detachment from the bottom of the hole. The firmness of the joint was checked by pulling the wires gently by hand. In Figure 5.3 five thermocouples can be seen attached to a plate to be welded. In order to save thermocouple wires and to prevent the recording unit from being too close to the welding area, compensating cables of copper and copper/nickel were used. Their attachement to the ends of the hot junction was by soldering iron. This brought high electrical contact between the thermocouple wires and the compensating cables and satisfactory mechanical strength to the connection. The compensating cables were shielded by a soft iron tube in order to minimize electrical background noise.

5.2.2 Recording Instrument

The data gathering unit used in the measurements of the welding thermal cycles could only accept signals in the range of 0 to +2.5V. Therefore,the interface amplifier would have to be calibrated in order to make the output signals from the thermocouples, suitable for the gathering of data. The following calibration was set and used for all thermal cycle measurements.

i) Channels 1,2,3 and 4

0V. . . . 1.468mV
2.5V. . . 17.866mV

ii) Channel 5

0V. . . . 0mV
2.5V. . . 5.582mV

The range of temperatures applied in (i) was of 200°C to 1530°C whereas in (ii) it was of 0°C to 600°C. These values were for Pt/Pt-13%Rh, type R thermocouples and were obtained from the table provided by Calex Instrumentation [Calex,1987]. The calibration was by injecting a defined low voltage signal, measured by a high quality digital voltmeter, into the thermocouple input of each channel in turn, to simulate the output of the thermocouple at a defined temperature.

After having assembled the system for measuring the thermal cycles, trials tests were carried out to evaluate its performance. Although the system operated satisfactorily, when a single thermocouple channel was used, highly anomalous behaviour was observed when more than one thermocouple channel was monitored on test plate. It was inferred that when welding was actually in progress, voltages could be generated within the component of a similar magnitude to those generated by the thermocouple. This effect is not observed when using ultraviolet recorders as the various channels are not electrically connected, ensuring that only the voltage difference across the thermocouples is monitored. In order to eliminate this effect, the interface amplifier was modified to incorporate low cost isolation amplifiers. In this form the unit proved reliable and flexible.

With the experimental system prepared, the data gathering unit was programmed. This was done via a user interface software named BOX. A typical table supplied by the programme in which the conditions for each experiment were imputed can be seen from Figure 5.4. In this table the main parameters to be set were:

i) The number of channels to be recorded. Throughout the experiments five channels (from 1 to 5) were selected.

ii) The rate at which data would be collected. The data gathering unit could be programmed within a range of recording intervals. They were chosen on the basis of the heat input to

be used for each test weld. This was made possible by using the information gathered from some trials in previous thermal cycle measurements in the beginning of this project, employing chart recorders. As a result, from a series of logging intervals provided by the Box software, a fast logging was used for test welds with 0.8kJ/mm, reducing as the heat input increased. This can be seen from Table 5.2.

iii) The criterion to initiate and stop the data gathering: Channel 6 was used to trigger the unit. Any signal higher than 1mV would start the recording and smaller than 0.74mV would stop it.

Once programmed, the data logger was detached from the computer and taken to the welding site to be connected to the interface amplifier. The data gathering system was then ready to record the actual thermal cycles.

After finishing the experiment, the data logger could be reconnected to the computer and the thermal cycle graphs displayed on the computer monitor. A typical graph of the thermal cycles given by the BOX software can be seen from Figure 5.5. Although care was taken during the entire preparation and conduction of the actual experiments, some losses of thermocouple readings inevitably occurred. Following the observation of the thermal cycles, the data file was identified and saved on a disk for future data processing. At this stage, it was necessary to identify every file of data in such a way that it would be easy and quick to retrieve any particular thermal cycle data. As a matter of consistency the same type of identification was applied to allow easy recovery of all data related to each welded specimen. The identification adopted was as follows.

T X - Y where,

T= Thermal cycle
X= Steel B,C,D or 12
Y= Heat input from 1 to 6 (in a correspondence with the heat inputs namely 0.8, 1.5, 2.0, 2.5, 3.0 and 3.5kJ/mm respectively)

Finally, an illustrative block diagram of the experimental set up described in this section can be seen from Figure 5.6.

5.2.3 Data Handling

Two pieces of software were developed to assist the data processing. The first was a programme to read the binary data file created by the data logger and to translate it into an ASCII code version. This programme was originally written in Turbo Basic. However, it proved to be slower than considered desirable. As result, a new version was written in 'C', which proved to be ten times as fast. With this programme, it was also possible to select which channel or channels were to be translated. This was useful because a selection could be made when anomalous behaviour was found in a thermal cycle due to breakage or any other problem which prevented appropriate recording. After translating the file in a suitable format, it was saved on a disk to be transferred from an IBM compatible microcomputer to the Cranfield mainframe VAX machine.

The second software programme, written in Fortran (Appendix I) named THERMIC, was designed for use on the mainframe VAX computer. This programme would read the data file and could convert its entries into temperature values. With this programme, it was possible to generate a report containing summarized details of the thermal cycles. The summary included the peak temperatures and the heating and cooling times achieved by the channel representing each thermocouple. A typical print out of the summary can be seen in the Figure 5.7. In this programme, graphical routines were also designed in order to obtain, either on screen or as a hard copy, graphic representation of the thermal cycle measurements. This can be seen from the Figure 5.8.

5.3 Results

A series of thermal cycles in the coarse grained region of the HAZ's of the steels under study were measured by the experimental assembly developed in the current work. The two pieces of software programme designed to handle the data gathered by the recording unit used proved to be capable of reproducing satisfactorily the typical temperature-time diagram, representative of each weld thermal cycle. These can be seen

in Figures 5.9 to 5.20.

Relevant thermal characteristics of each individual thermal cycle measurement were obtained on the basis of summaries similar to that presented in Figure 5.7. This can be seen from the Table 5.3, where the peak temperature, the cooling time between 800-500°C (Δt_{8-5}) and the heating time between 300-1000°C (Δt_{3-10}), measured by each thermocouple (channel) in each test weld, are listed.

The different depths of the holes with respect to the surface of the parent plate - the depths of the holes varied in multiples of 0.25mm - did not provide a wide range of peak temperatures. In most test welds, the peak temperatures ranged between 1300-1500°C. This range of temperature indicates that the thermocouples were placed in the coarse grained region of the HAZ's and very near to the fusion line. This was observed from samples similar to that shown in Figure 5.21 obtained from a test weld using steel 12 and welded at heat input of 0.8kJ/mm. In this Figure, the peak temperatures measured by the thermocouples numbered 2, 3 and 4 were 1489,1194 and 1446°C, respectively.

The cooling times for each test weld were obtained using the summaries supplied by the software programme mentioned above and shown in Figure 5.7. In this respect, the cooling time through 800-500°C (Δt_{8-5}) was calculated by the difference between the cooling time from the peak temperature reached by a particular test weld to temperatures of 500°C and 800°C. Despite the peak temperatures reached, consistent values for Δt_{8-5} were obtained in each test weld. A marked trend towards increasing values of Δt_{8-5}, i.e. slower cooling rates, as a result of a higher heat input employed is indicated. This can be seen in Figure 5.22. Theoretical heat flow equations and predictions of Δt_{8-5} were made by applying the equations proposed by Barlow [1982b] (refer Chapter 2), to the actual welding conditions employed in the experiments. On the basis of the range of heat inputs used in the welding of the steels under investigation and the critical thickness calculated (h_c) (where thickness of a parent plate greater than h_c indicates 3-D heat flow regime), the test weld employing steel 12 (25mm) changes its heat flow regime from 3D to 2D at heat inputs higher than 2.0kJ/mm. On the other hand for test welds with steels B, C, and D the heat flow regime remains constant and equivalent to 3D throughout the range of heat inputs used. This can be seen from the

Table 5.4. Very good agreement was found between theoretical predictions and actual values measured of Δt_{8-5} in the experimental thermal cycles for heat inputs up to 2.0kJ/mm. For higher heat inputs a clear tendency for longer cooling times than those theoretically predicted was verified in all experiments. This can be seen in Figure 5.23.

Due to the scattering in peak temperatures, the time between 300-1000° (Δt_{3-10}) was used to represent the heating time of the experimental thermal cycle. It was found that as the heat input increases there is a clear trend towards higher heating times, i.e slower heating rates. This can be seen in Table 5.3.

Table 5.1- Welding Parameters

Current (A)	**Voltage (V)**	**Travel Speed (mm/sec)**	**Heat Input (kJ/mm)**
300	30	11.3	0.8
300	30	6.0	1.5
300	30	4.5	2.0
300	30	3.6	2.5
300	30	3.0	3.0
300	30	2.6	3.5

$$H.I. = \frac{\text{Arc Voltage} * \text{Weld Current} * 10^{-3}}{\text{Weld Speed (mm/sec)}}$$

Table 5.2- Recording intervals used in the actual thermal cycle measurements

H.I (kJ/mm)	**Recording Interval (ms)**
0.8	31.25
1.5	62.50
2.0	62.50
2.5	125
3.0	125
3.5	125

Table 5.3 - Thermal characteristics of the thermal cycles measured

Test Weld	**Channel**	**Peak Temperature (°C)**	**Δt_{8-5} (s)**	**Δt_{3-10} (s)**
	1	1458	3.3	0.3
T12-1	2	1489	3.2	0.2
	3	1194	3.4	0.3
	4	1446	3.2	0.2
	1	1421	5.9	0.5
T12-2	2	1412	5.7	0.6
	3	1316	5.4	0.6
	1	1381	7.8	0.8
T12-3	2	1404	8.0	0.9
	3	1403	7.9	1.0
	4	1136	7.7	1.2
	1	1408	11.5	1.2
T12-4	2	1378	10.8	1.5
	3	1340	10.2	1.5
	1	1349	14.4	2.8
T12-5	2	1376	14.6	2.4
	3	1360	15.0	2.4
	1	1400	19.5	1.9
T12-6	2	1305	19.4	2.0
	3	1362	18.9	2.3

Table 5.3 - Cont'd

Test Weld	Channel	Peak Temperature (°C)	Δt_{8-5} (s)	Δt_{3-10} (s)
	1	1229	2.9	0.2
TB-1	2	1220	3.0	0.3
	3	1185	3.2	0.2
	1	1372	5.9	0.5
TB-2	2	1352	6.2	0.5
	3	1283	5.9	0.6
	4	1432	5.8	0.6
	1	1427	8.3	0.8
TB-3	2	1397	8.6	0.9
	3	1371	7.8	0.7
	1	1379	11.0	1.3
TB-4	2	1399	10.8	1.3
	3	1328	10.1	1.4
	1	1389	11.7	1.3
TB-5	2	1337	12.8	1.5
	3	1393	12.1	1.7
	4	1350	11.5	1.6
	1	1395	15.2	1.9
TB-6	2	1378	15.5	2.2
	3	1277	14.2	2.4

Table 5.3 - Cont'd

Test Weld	Channel	Peak Temperature (°C)	Δt_{8-5} (s)	Δt_{3-10} (s)
	1	1485	3.2	0.2
TC-1	2	1367	3.7	0.3
	3	1118	3.0	0.3
	1	1416	5.6	0.6
TC-2	2	1332	5.8	0.7
	3	1373	5.6	0.5
	4	1335	5.4	0.5
	1	1431	7.2	0.7
TC-3	2	1357	7.8	0.8
	3	1220	7.5	0.8
	4	1231	7.1	1.0
	1	1412	9.7	1.2
TC-4	2	1387	10.1	1.3
	3	1260	9.7	1.5
	1	1384	12.9	1.5
TC-5	2	1383	13.8	1.7
	3	1342	13.5	1.7
	4	1361	12.9	2.0
	1	1369	16.6	2.0
TC-6	2	1335	17.6	2.5
	3	1227	17.4	2.6
	4	1164	16.6	3.0

Table 5.3 - Cont'd

Test Weld	Channel	Peak Temperature (°C)	Δt_{8-5} (s)	Δt_{3-10} (s)
	1	1446	3.9	0.2
TD-1	2	1386	3.7	0.2
	3	1022	3.6	0.4
	1	1434	5.9	0.6
TD-2	2	1371	6.2	0.7
	3	1224	6.0	0.8
	1	1356	7.6	0.8
TD-3	2	1463	8.4	0.8
	3	1452	7.9	0.9
	4	1268	7.6	1.1
	1	1397	10.6	1.2
TD-4	2	1375	11.2	1.5
	3	1429	10.7	1.2
	1	1398	12.4	1.4
TD-5	2	1398	13.1	1.5
	3	1372	12.6	2.0
	4	1370	11.8	1.6
	1	1385	14.7	1.6
TD-6	2	1404	15.4	2.1
	3	1367	15.6	2.4
	4	1365	14.9	1.3

Table 5.4 - Theoretical estimates for heat flow regime- after Barlow's [1982].

H.I	**hc***	**Heat Flow Regime (D-Dimentional)**	
(kJ/mm)	**(mm)**	**25mm**	**32mm**
0.8	14.6	3-D	3-D
1.5	20.0	3-D	3-D
2.0	23.1	3-D	3-D
2.5	25.8	2-D	3-D
3.0	28.3	2-D	3-D
3.5	30.6	2-D	3-D

$$\mathbf{hc^*} = 16.34 \times \sqrt{(H.I)}$$

Table 5.5 - Theoretical predictions of the $\Delta t_{8\text{-}5}$- after Barlow's [1982].

H.I	**Steel B,C and D** $\Delta t_{8\text{-}5}$	**Steel 12** $\Delta t_{8\text{-}5}$
(kJ/mm)	**(s)**	**(s)**
0.8	3.0	3.0
1.5	5.6	5.6
2.0	7.4	7.4
2.5	9.3	9.6
3.0	11.1	13.8
3.5	12.9	18.8

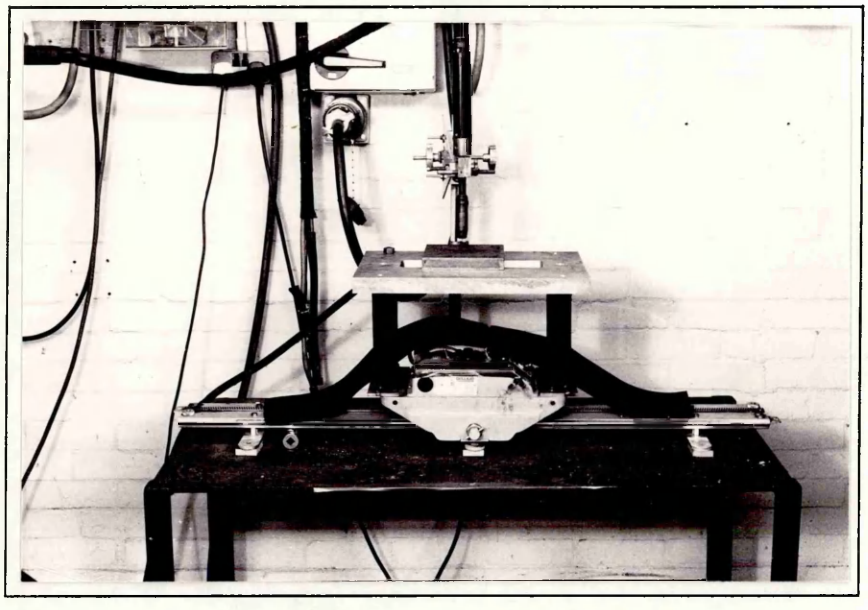

(a)

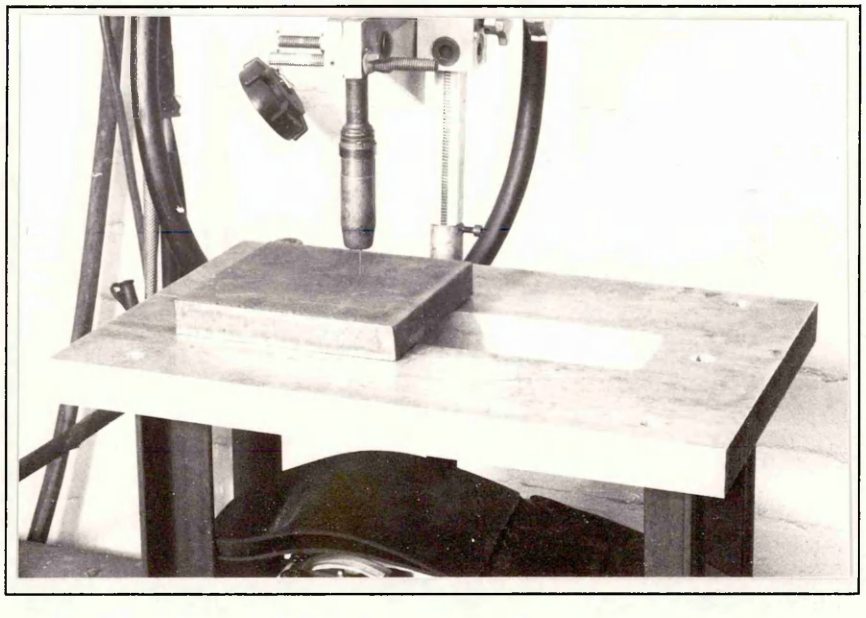

(b)

Figure 5.1- (a) Welding jig for the experimental work.
(b) Slot in the plate for the passage of the thermocouple.

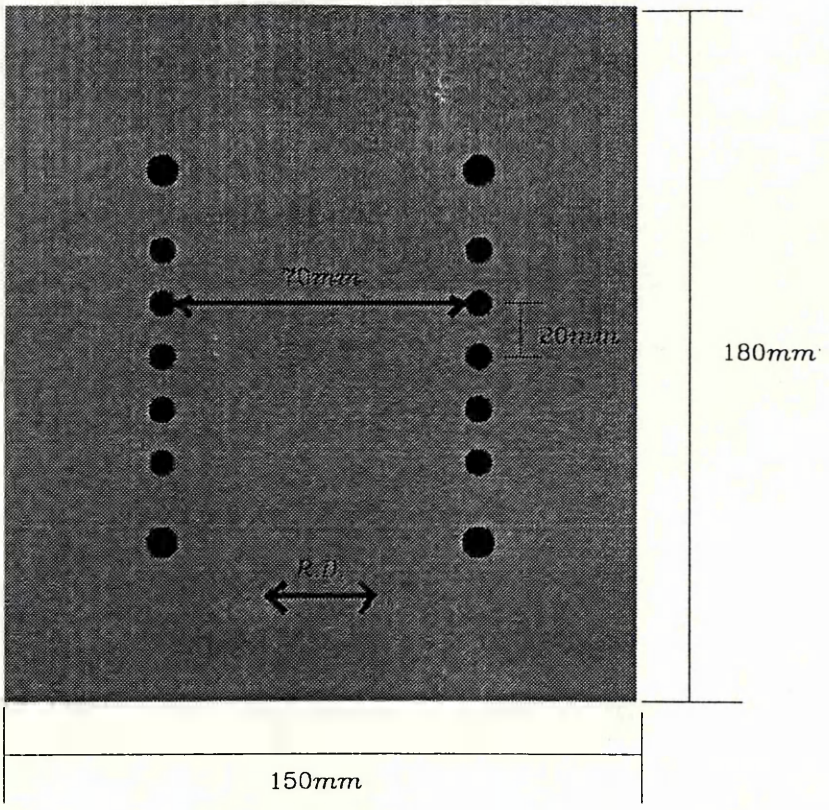

Figure 5.2- Layout of the position of the holes drilled for the insertion of the thermocouples.

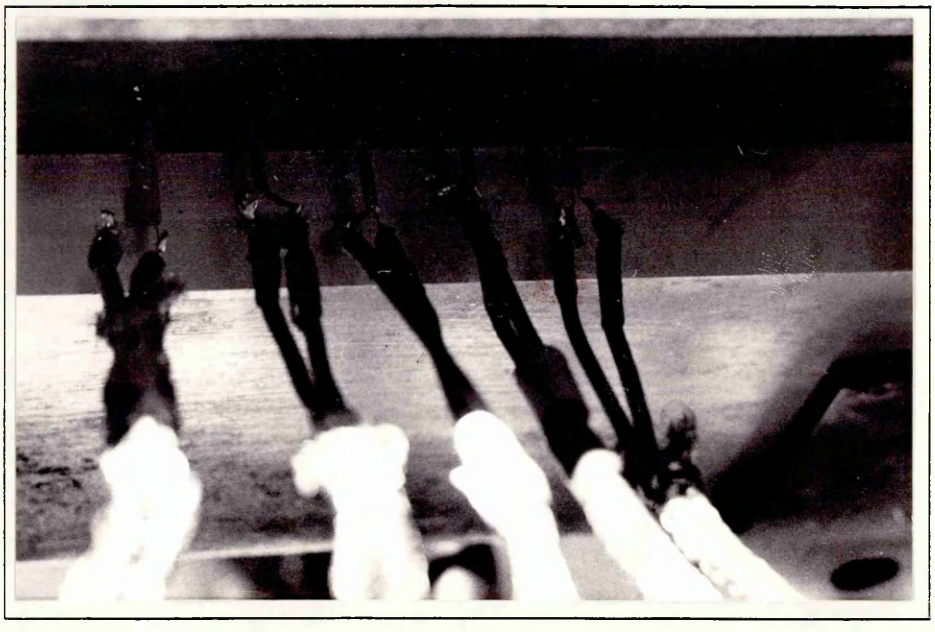

Figure 5.3- Five thermocouples attached to a plate to be welded.

Time:	Date:	Channels: 1
Log: 1 secs	Test: none	Repeat: Off
Status - Databox busy or not connected.		
Next wake up	Elapsed time	
Experiments	Room left bytes	Battery volts
Start:	Stop:	
Breakpoints:		
Channel 1 2 3 4 5 6 7 8		
Reading		

Figure 5.4- Typical table provided by the software BOX to set up the conditions for thermal cycle measurements.

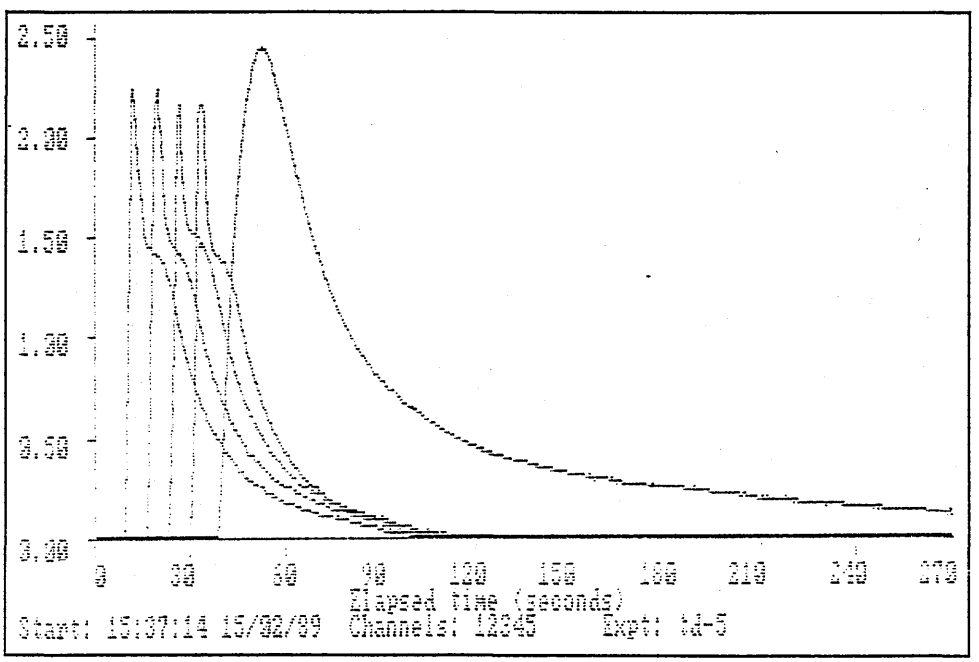

Figure 5.5- Typical plot provided by the software BOX of a thermal cycle measurement.

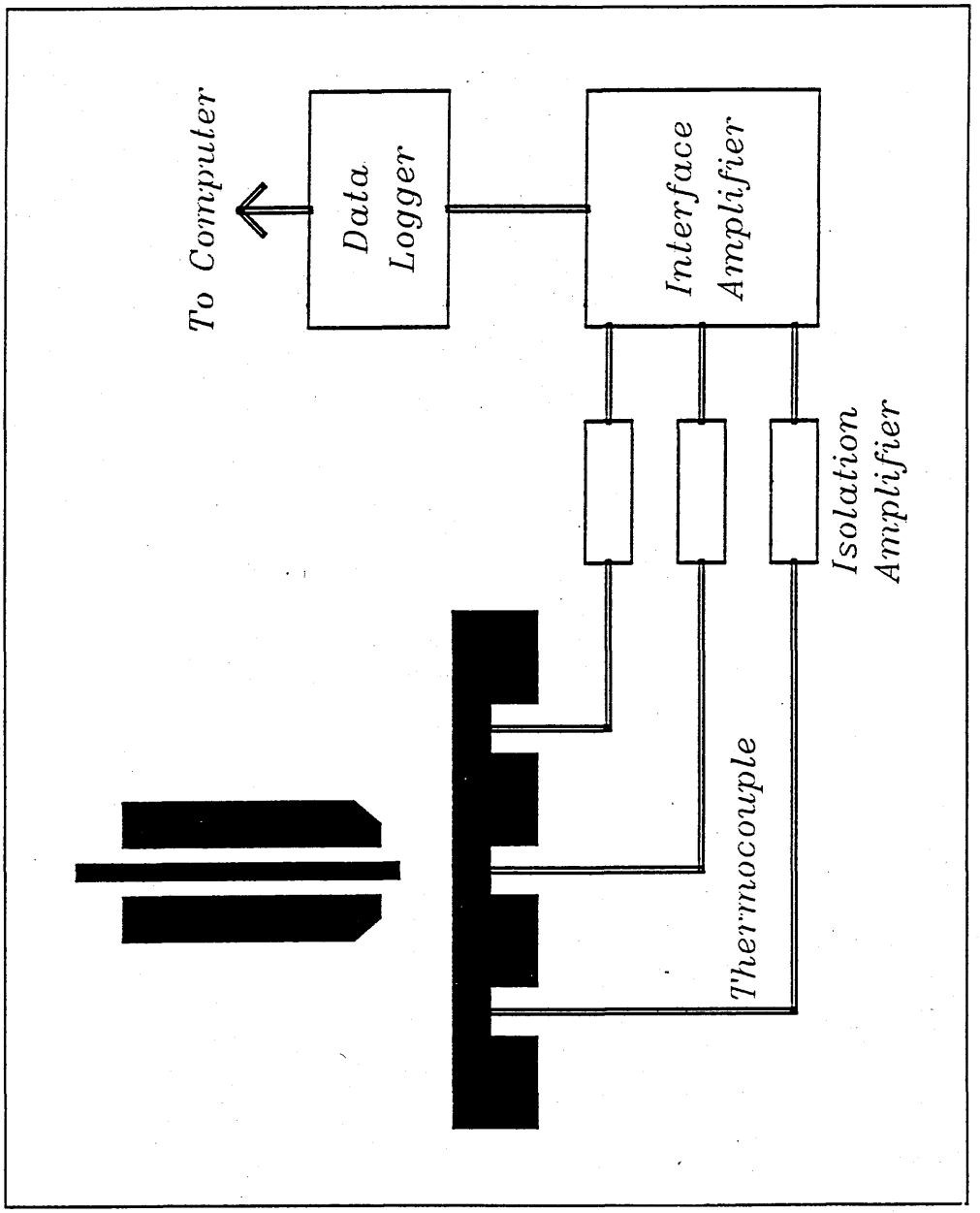

Figure 5.6- Block diagram of the experimental set-up of the thermal cycle measurement.

****

DATA FILE: [.th_cycle]td-3

****

CHANNEL NUMBER: 1
FILTER FACTOR: 4

PEAK TEMPERATURE(C) : 1356.094
THERMAL CYCLE STARTING POINT: 118
PEAK POINT: 142

TEMPERATURE	HEATING TIME(s)	COOLING TIME(s)
300	1.3	30.2
400	1.2	21.7
500	1.0	16.8
600	0.8	13.6
700	0.8	11.1
800	0.6	9.2
900	0.6	7.6
1000	0.5	4.6
1100	0.4	1.6
1200	0.4	0.8
1300	0.2	0.3

Figure 5.7- A typical summary provided by the software programme THERMIC of thermal cycles measured in plate D at a heat input of 2.0kJ/mm.

****

CHANNEL NUMBER: 2
FILTER FACTOR: 4

PEAK TEMPERATURE(C) : 1463.129
THERMAL CYCLE STARTING POINT: 192
PEAK POINT: 213

TEMPERATURE	HEATING TIME(s)	COOLING TIME(s)
300	1.2	32.3
400	1.0	22.5
500	0.8	17.2
600	0.7	13.6
700	0.6	10.9
800	0.5	8.8
900	0.4	6.6
1000	0.4	2.5
1100	0.3	1.7
1200	0.3	1.3
1300	0.2	1.2
1400	0.1	1.0

Figure 5.7- Cont'd

****

CHANNEL NUMBER: 3
FILTER FACTOR: 4

PEAK TEMPERATURE(°C) : 1451.781
THERMAL CYCLE STARTING POINT: 267
PEAK POINT: 290

TEMPERATURE	HEATING TIME(s)	COOLING TIME(s)
300	1.3	31.2
400	1.1	22.0
500	0.9	17.1
600	0.8	13.6
700	0.6	11.1
800	0.5	9.2
900	0.4	7.4
1000	0.4	4.0
1100	0.3	1.7
1200	0.3	1.2
1300	0.2	0.8
1400	0.1	0.2

Figure 5.7- Cont'd

****

CHANNEL NUMBER: 4
FILTER FACTOR: 4

PEAK TEMPERATURE(C) : 1267.588
THERMAL CYCLE STARTING POINT: 342
PEAK POINT: 376

TEMPERATURE	HEATING TIME(s)	COOLING TIME(s)
300	2.0	28.8
400	1.8	20.4
500	1.6	15.9
600	1.5	12.5
700	1.3	10.2
800	1.2	8.3
900	1.1	6.5
1000	0.9	3.5
1100	0.8	1.3
1200	0.6	0.8

Figure 5.7- Cont'd

****

CHANNEL NUMBER: 5
FILTER FACTOR: 4

PEAK TEMPERATURE(C) : 517.815
THERMAL CYCLE STARTING POINT: 468
PEAK POINT: 579

TEMPERATURE	HEATING TIME(s)	COOLING TIME(s)
300	6.5	15.0
400	4.8	8.8
500	1.7	2.8

Figure 5.7- Cont'd

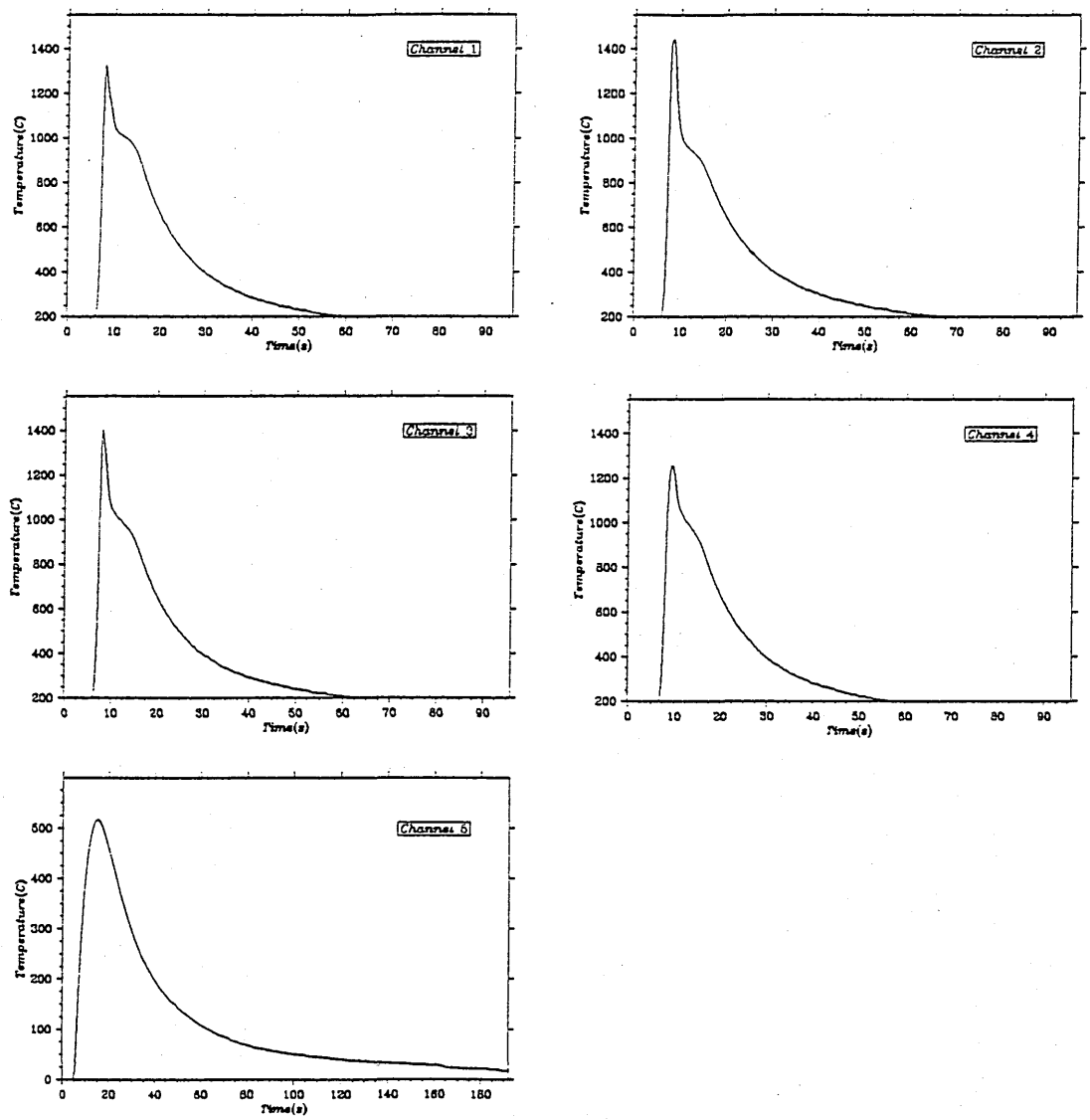

Figure 5.8- A typical print out provided by the sofware programme THERMIC of thermal cycles measured in plate D at a heat input of 2.0kJ/mm.

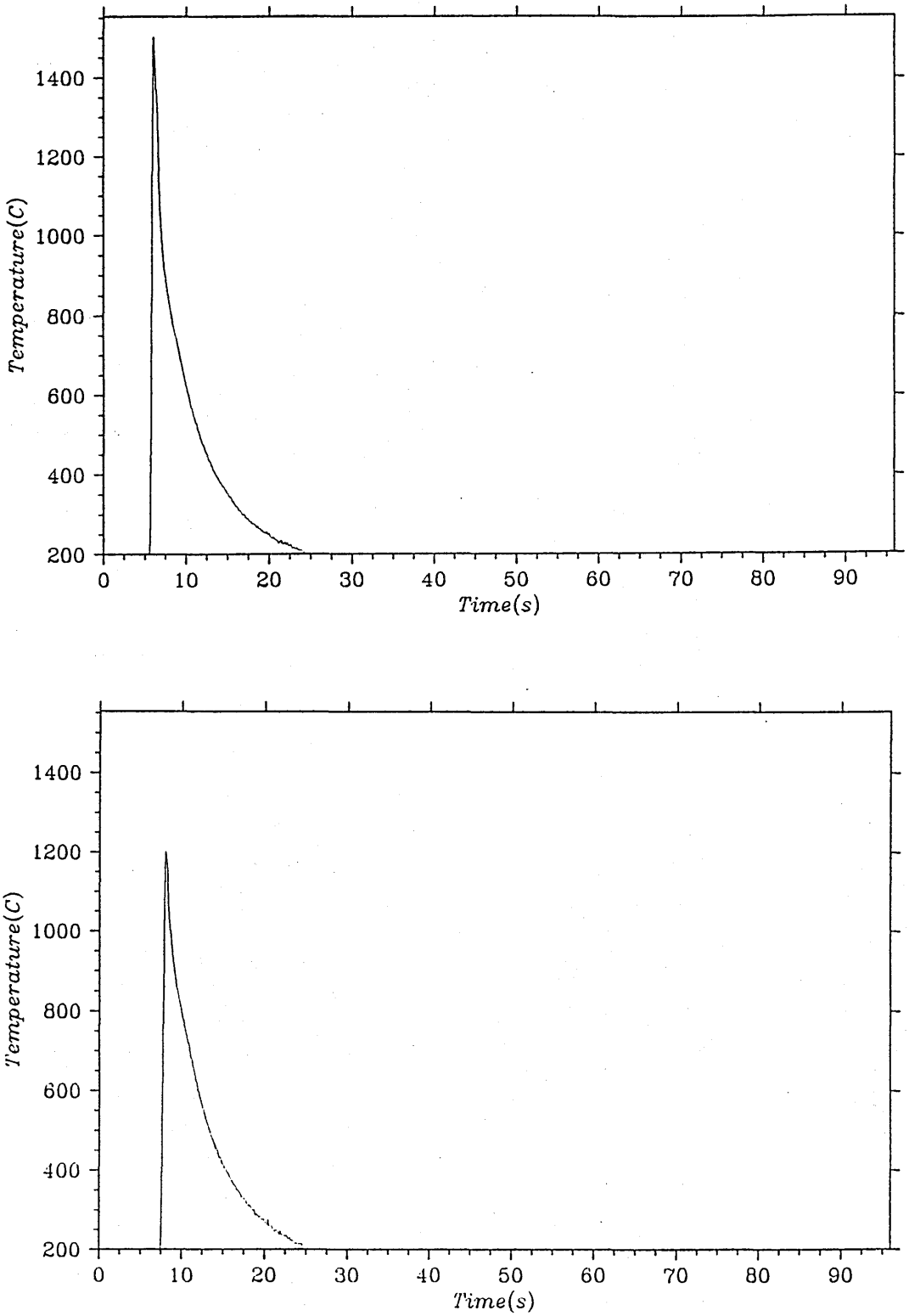

Figure 5.9- Thermal cycles measured in the plate 12 welded at a heat input of 0.8kJ/mm (test weld T12-1).

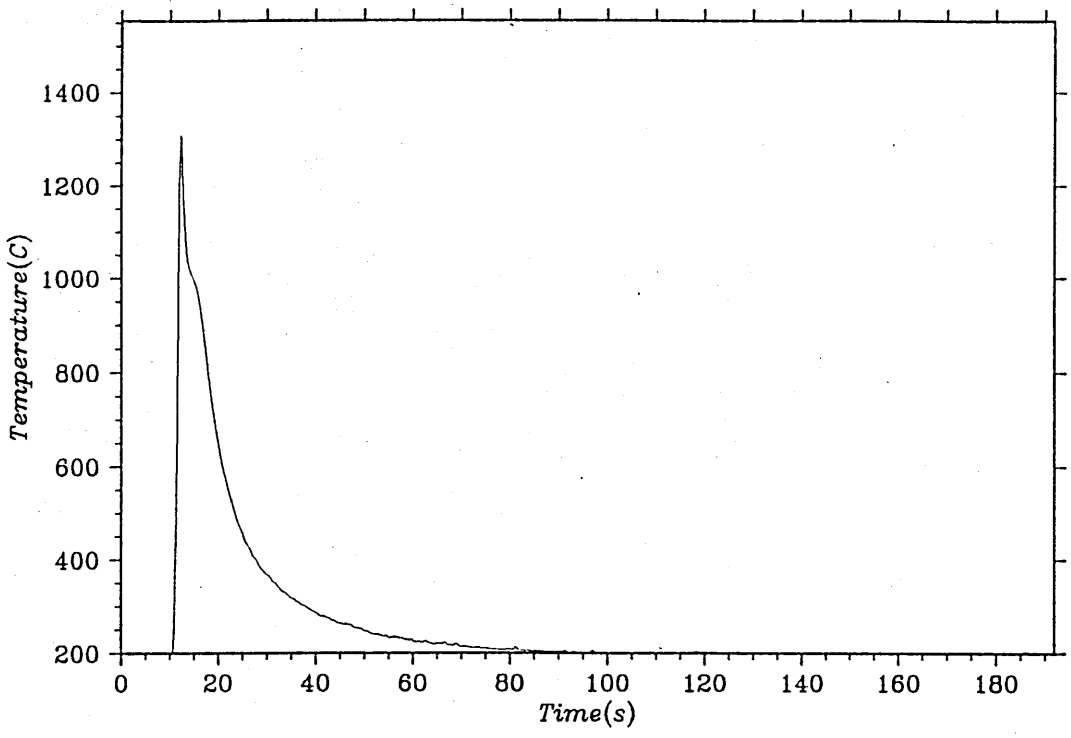

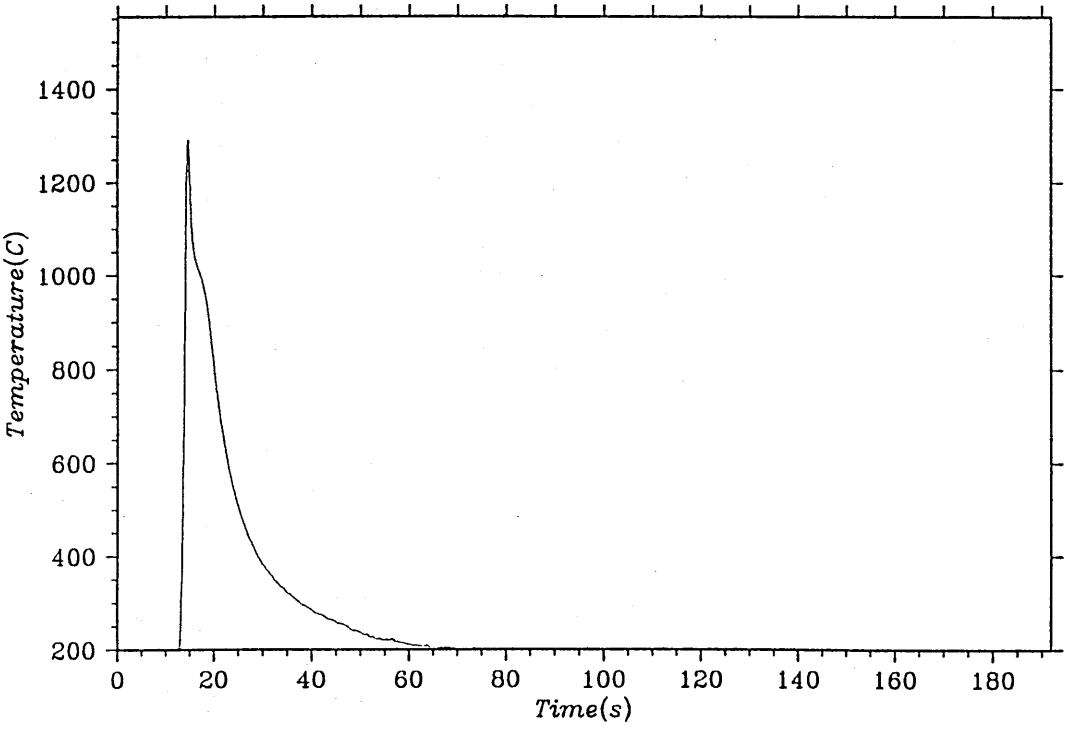

Figure 5.10- Thermal cycles measured in the plate 12 at a heat input of 2.5kJ/mm (test weld T12-4).

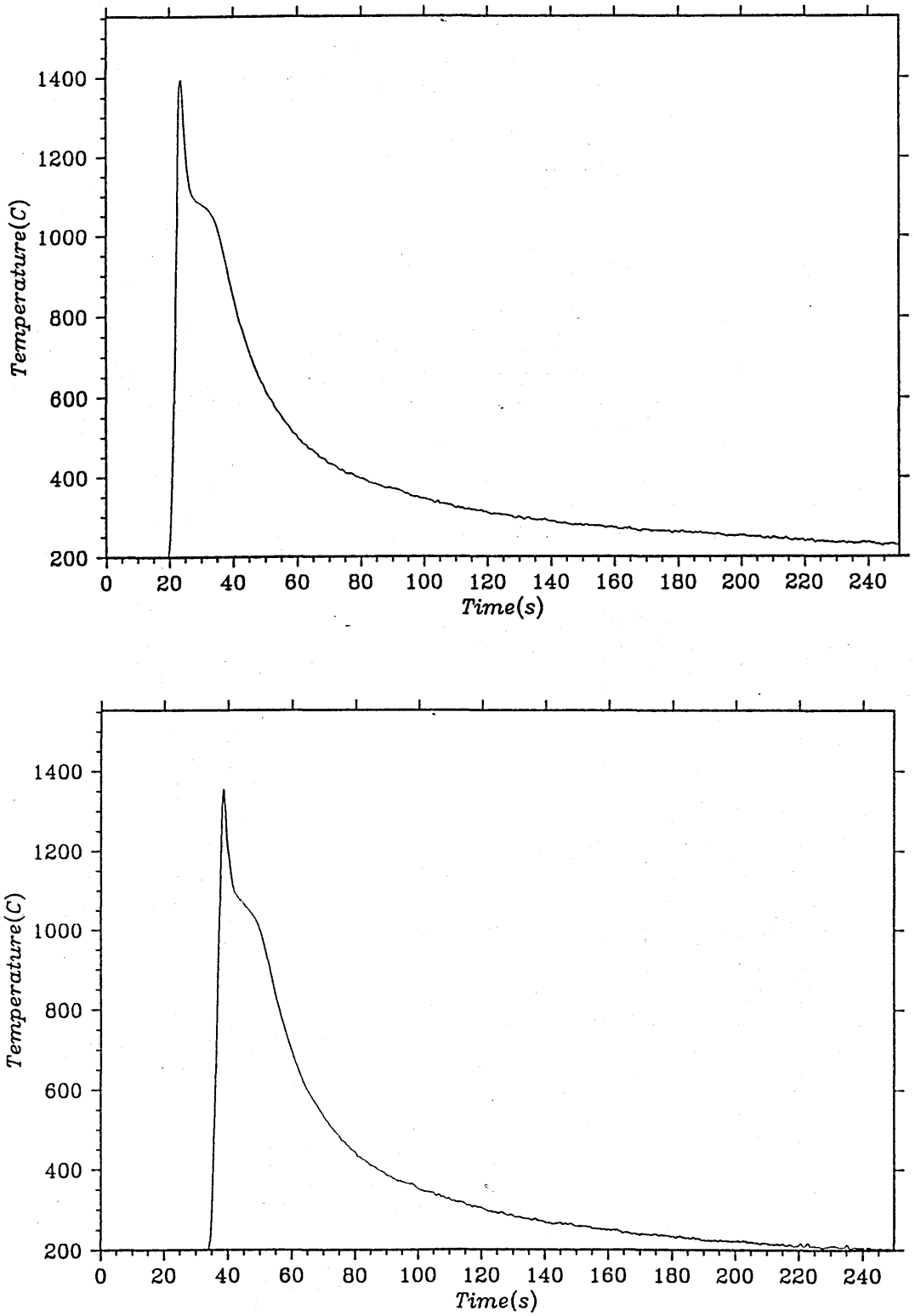

Figure 5.11- Thermal cycles measured in the plate 12 at a heat input of 3.5kJ/mm (test weld T12-6).

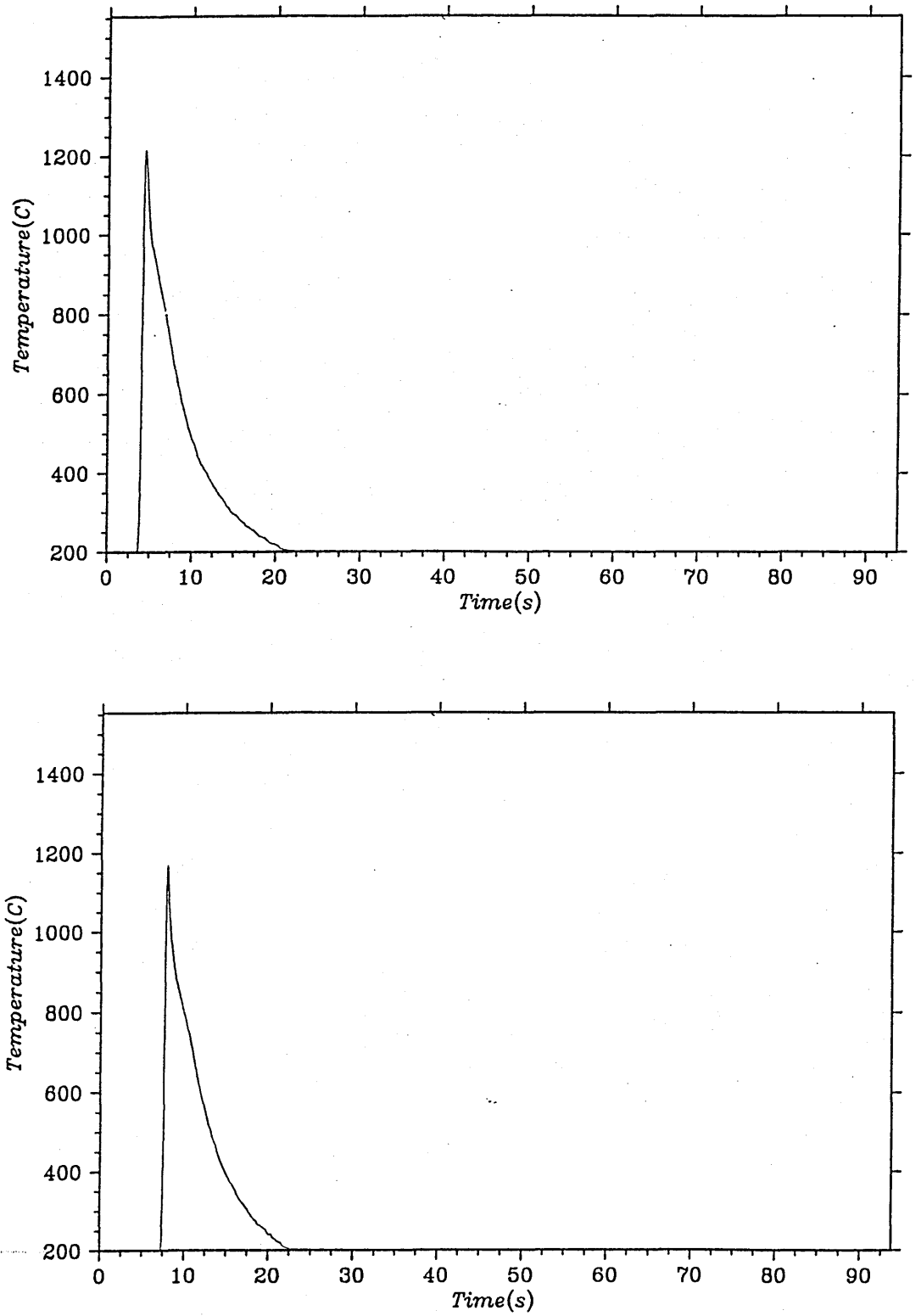

Figure 5.12- Thermal cycles measured in the plate B at a heat input of 0.8kJ/mm (test weld TB-1).

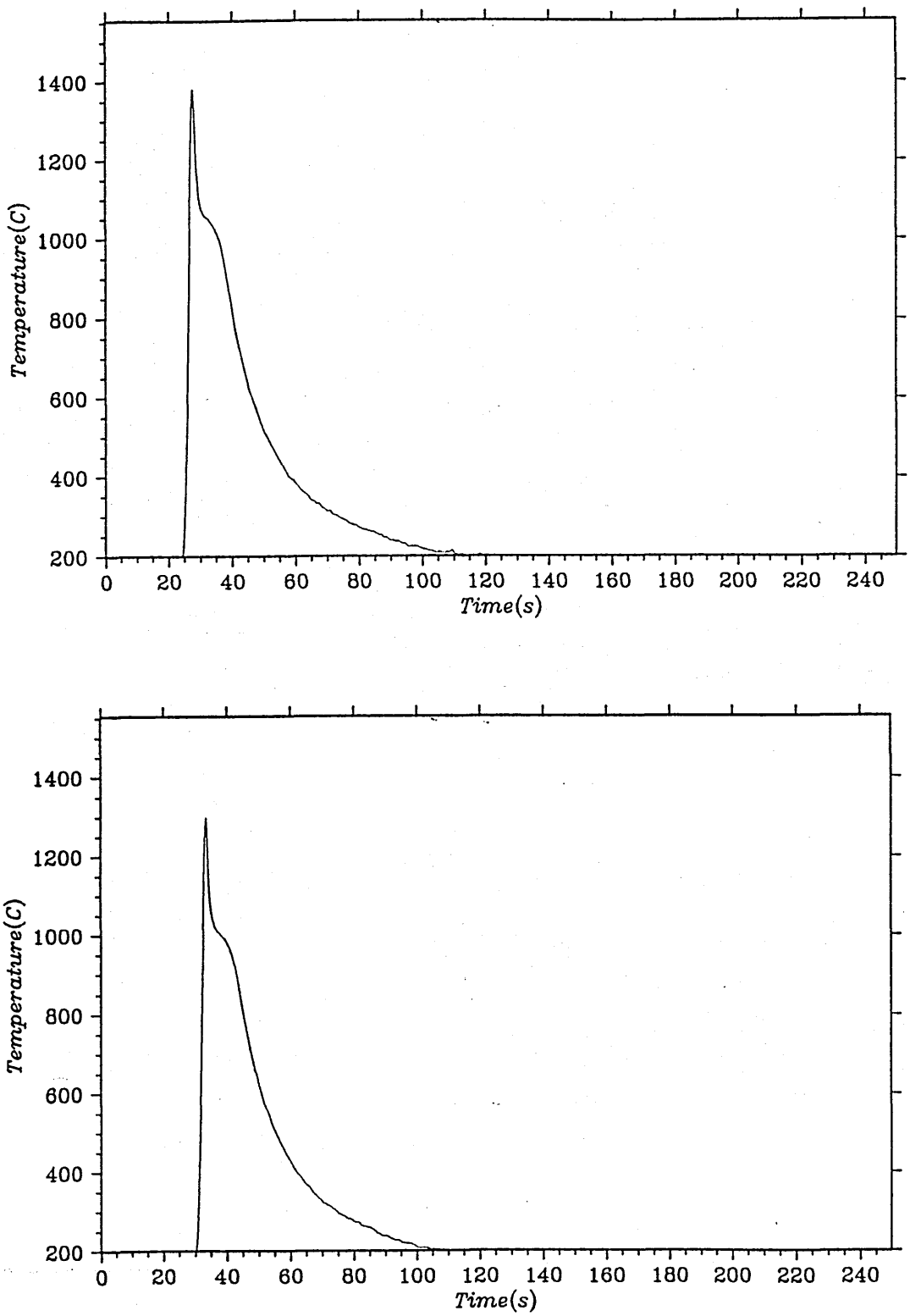

Figure 5.13- Thermal cycles measured in the plate B at a heat input of 2.5kJ/mm (test weld TB-4).

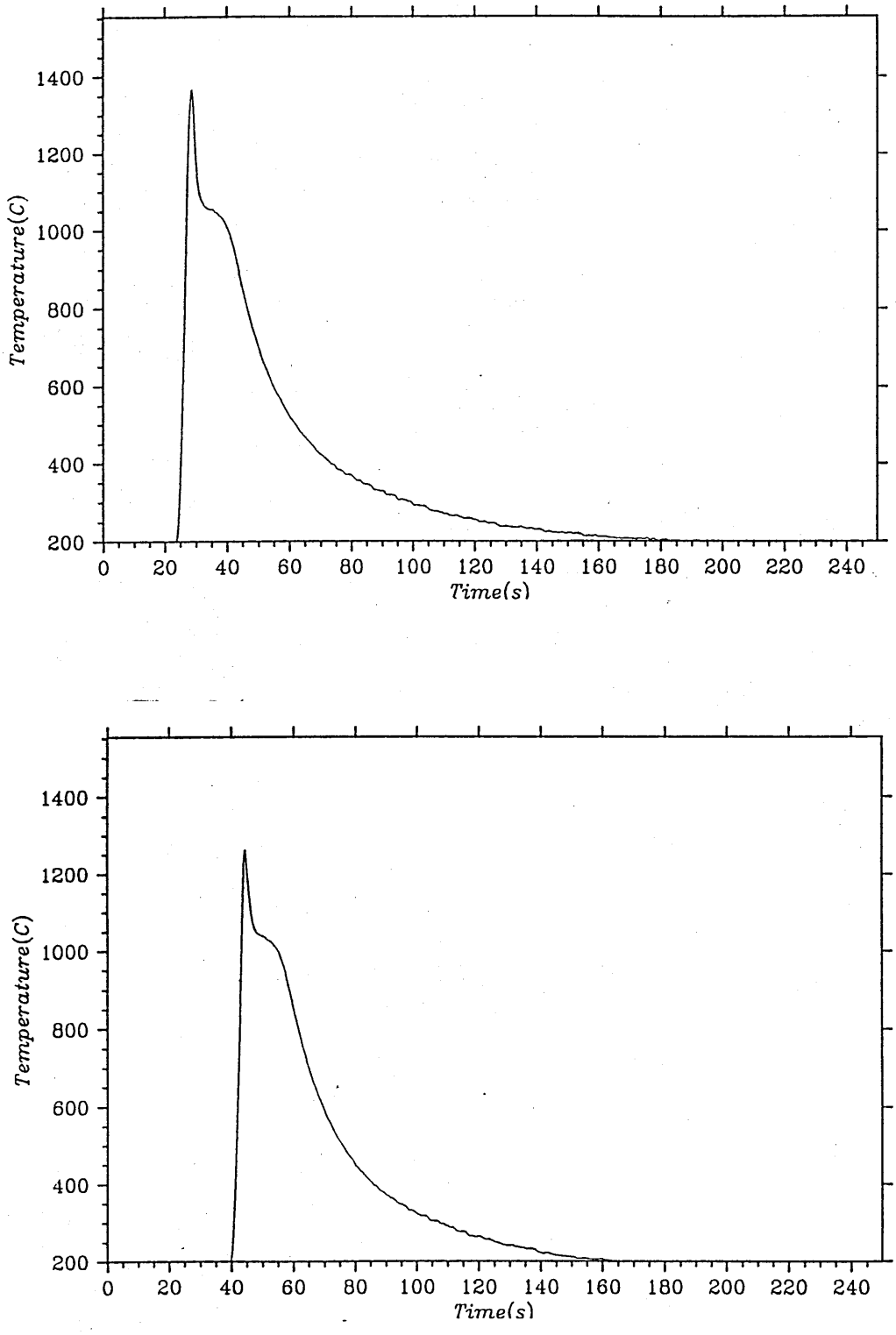

Figure 5.14- Thermal cycles measured in the plate B at a heat input of 3.5kJ/mm (test weld TB-6).

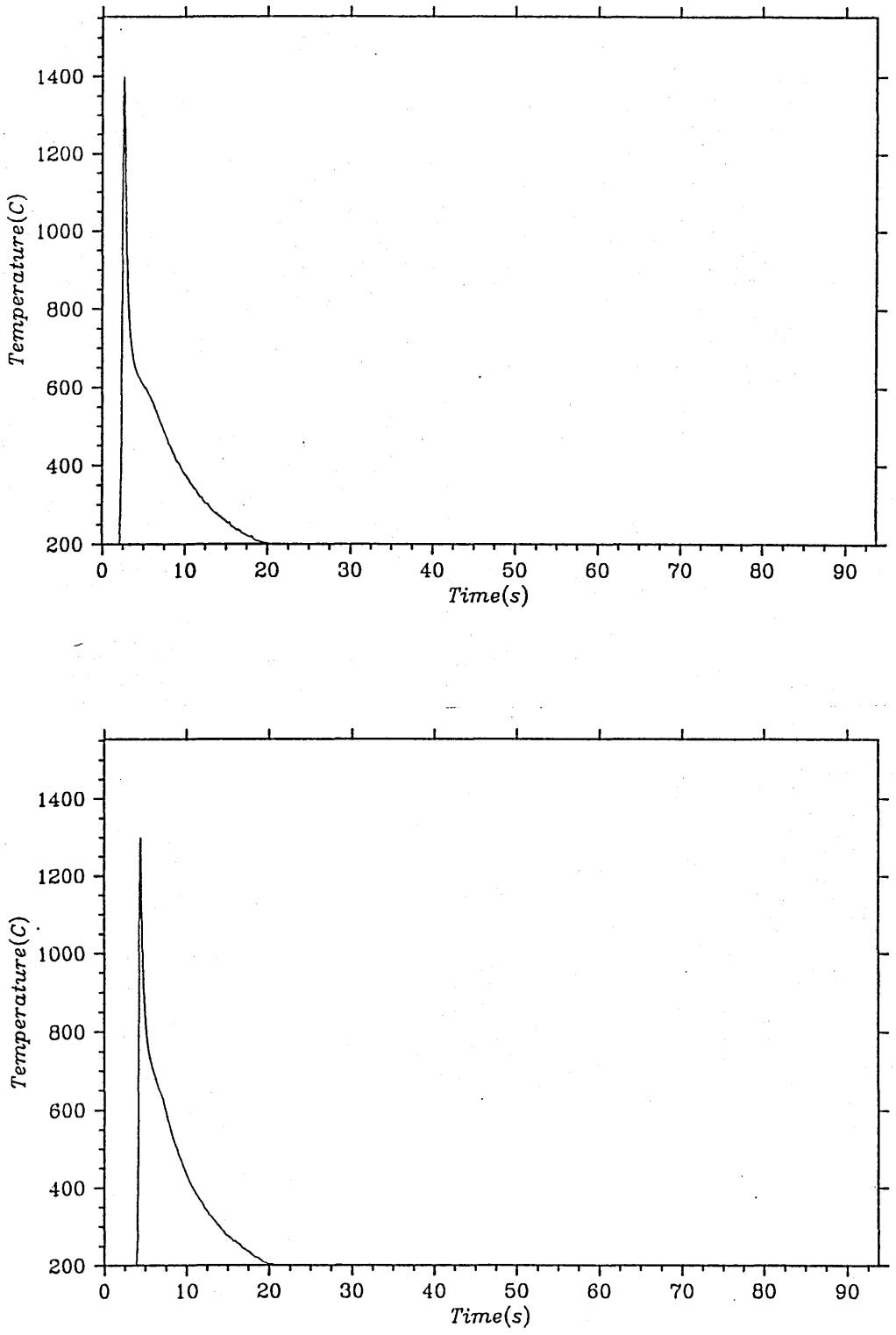

Figure 5.15- Thermal cycles measured in the plate C at a heat input of 0.8kJ/mm (test weld TC-1).

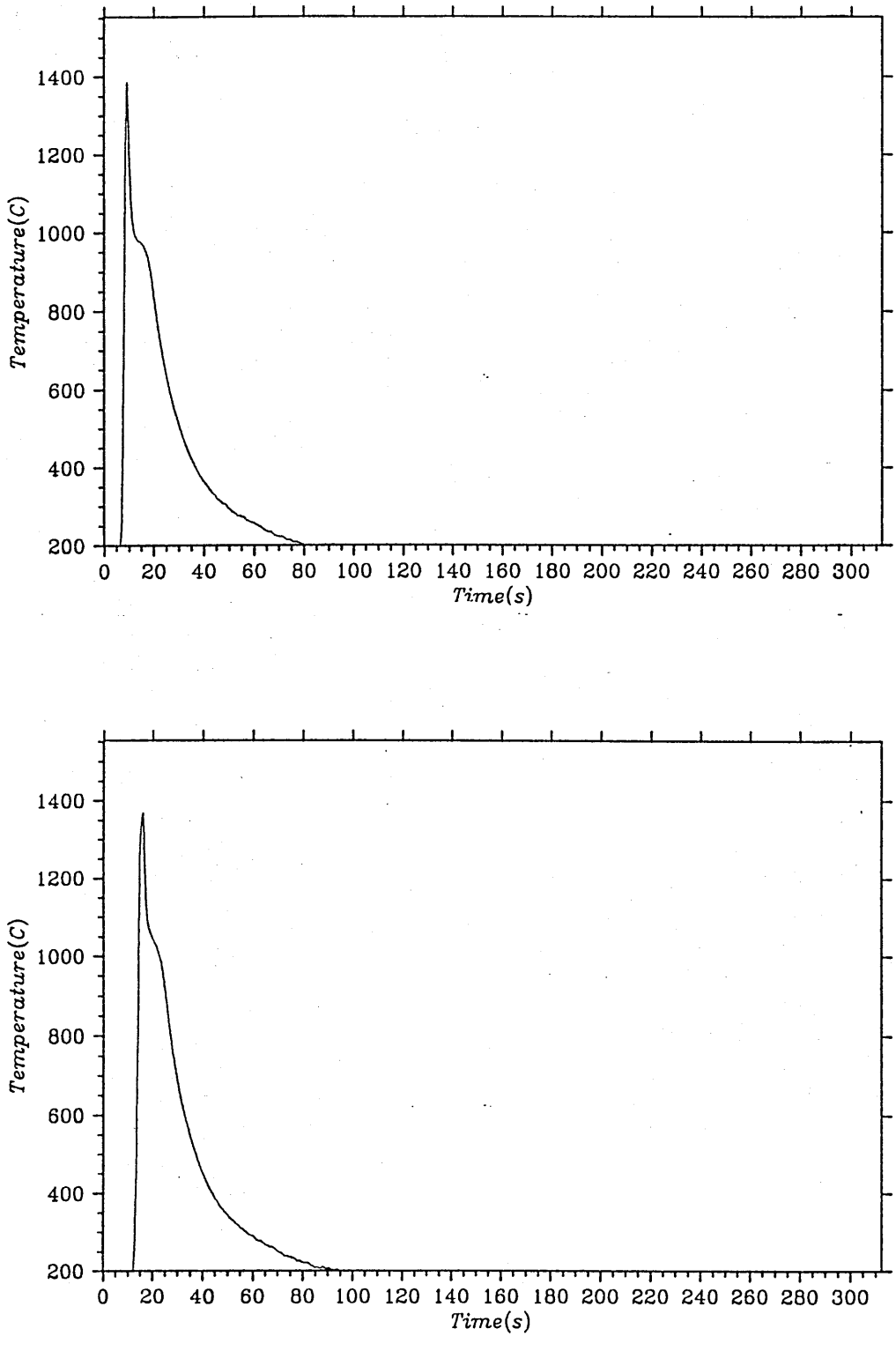

Figure 5.16- Thermal cycles measured in the plate C at a heat input of 2.5kJ/mm (test weld TC-4).

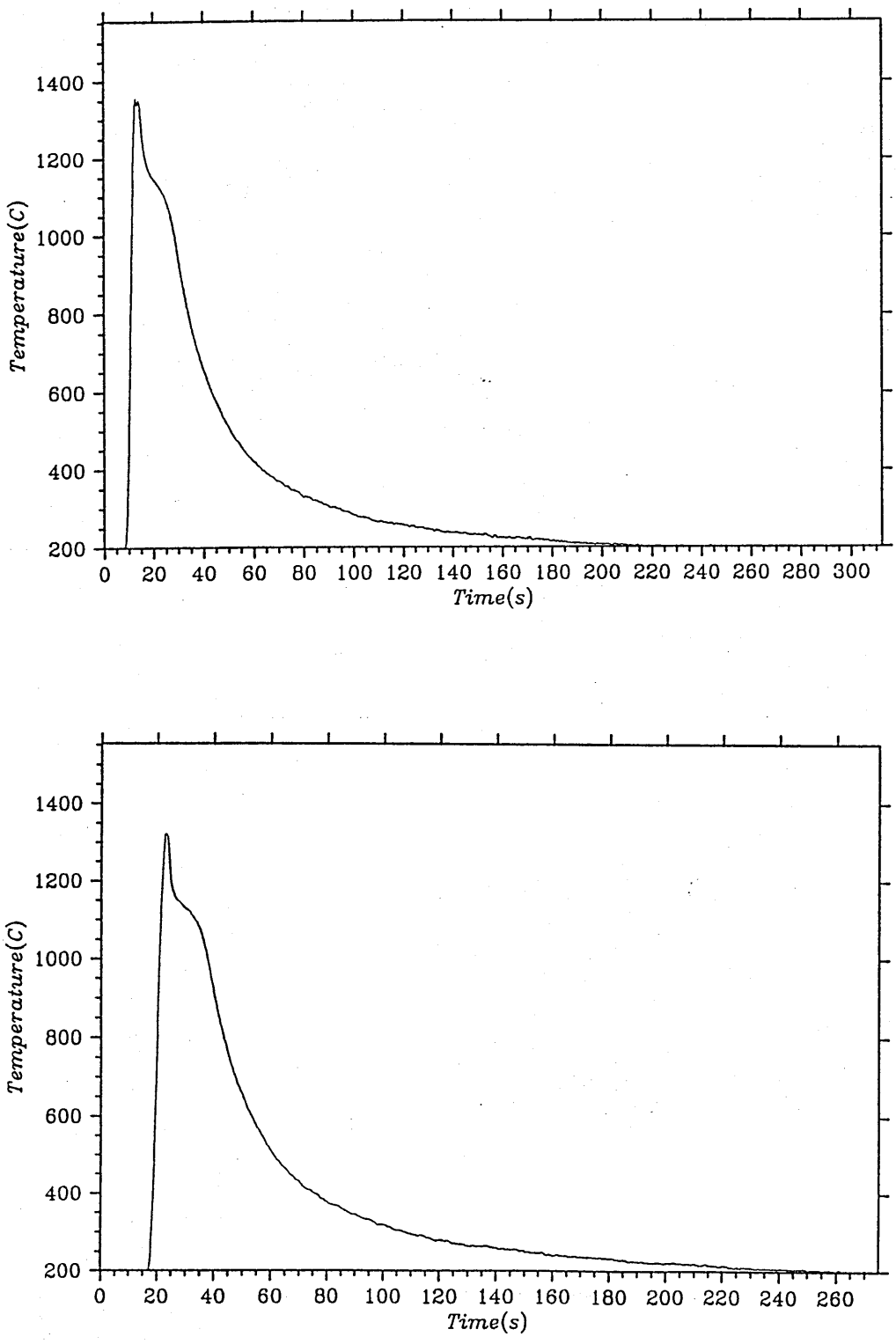

Figure 5.17- Thermal cycles measured in the plate C at a heat input of 3.5kJ/mm (test weld TC-6).

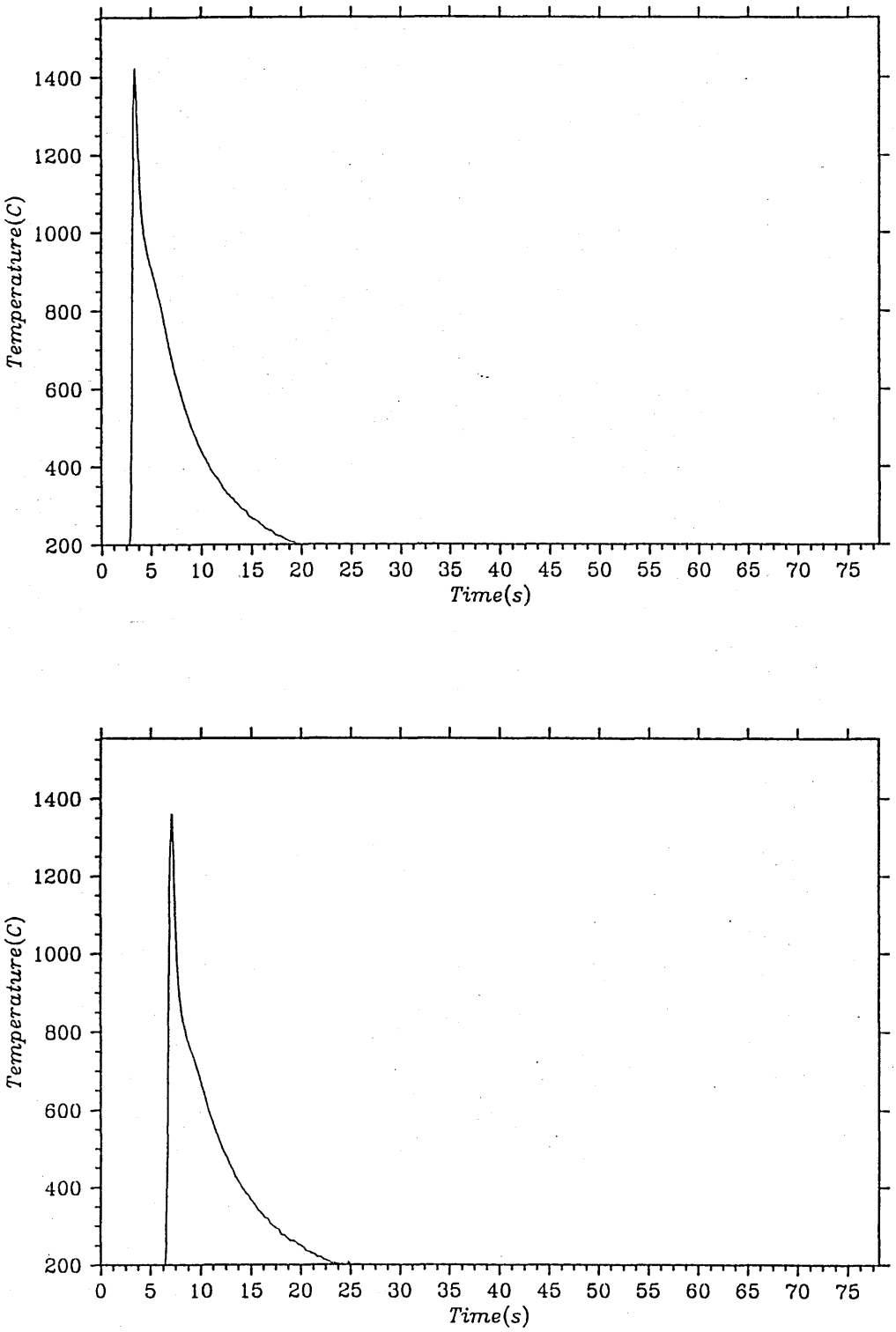

Figure 5.18- Thermal cycles measured in the plate D at a heat input of 0.8kJ/mm (test weld TD-1).

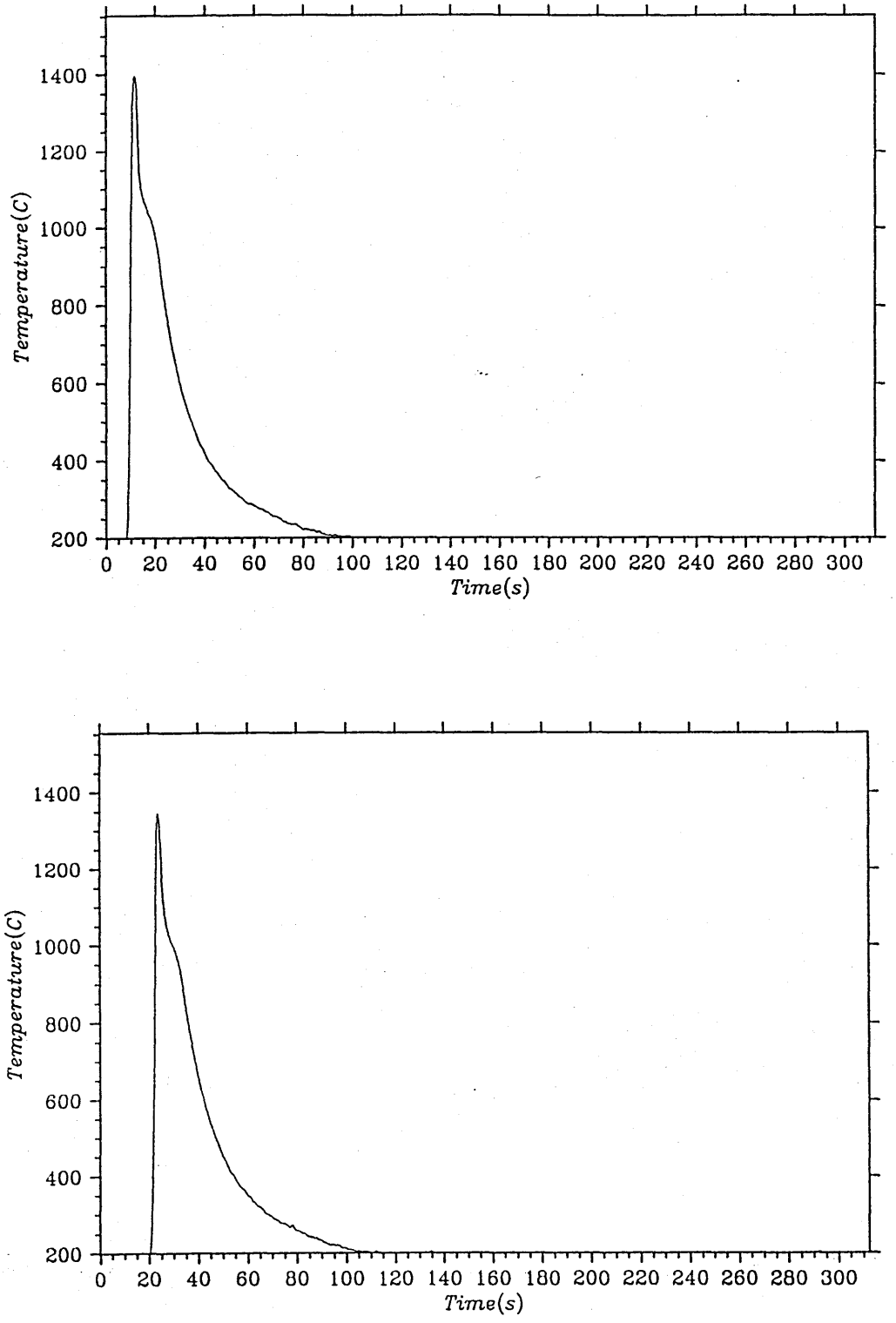

Figure 5.19- Thermal cycles measured in the plate D at a heat input of 2.5kJ/mm (test weld TD-4).

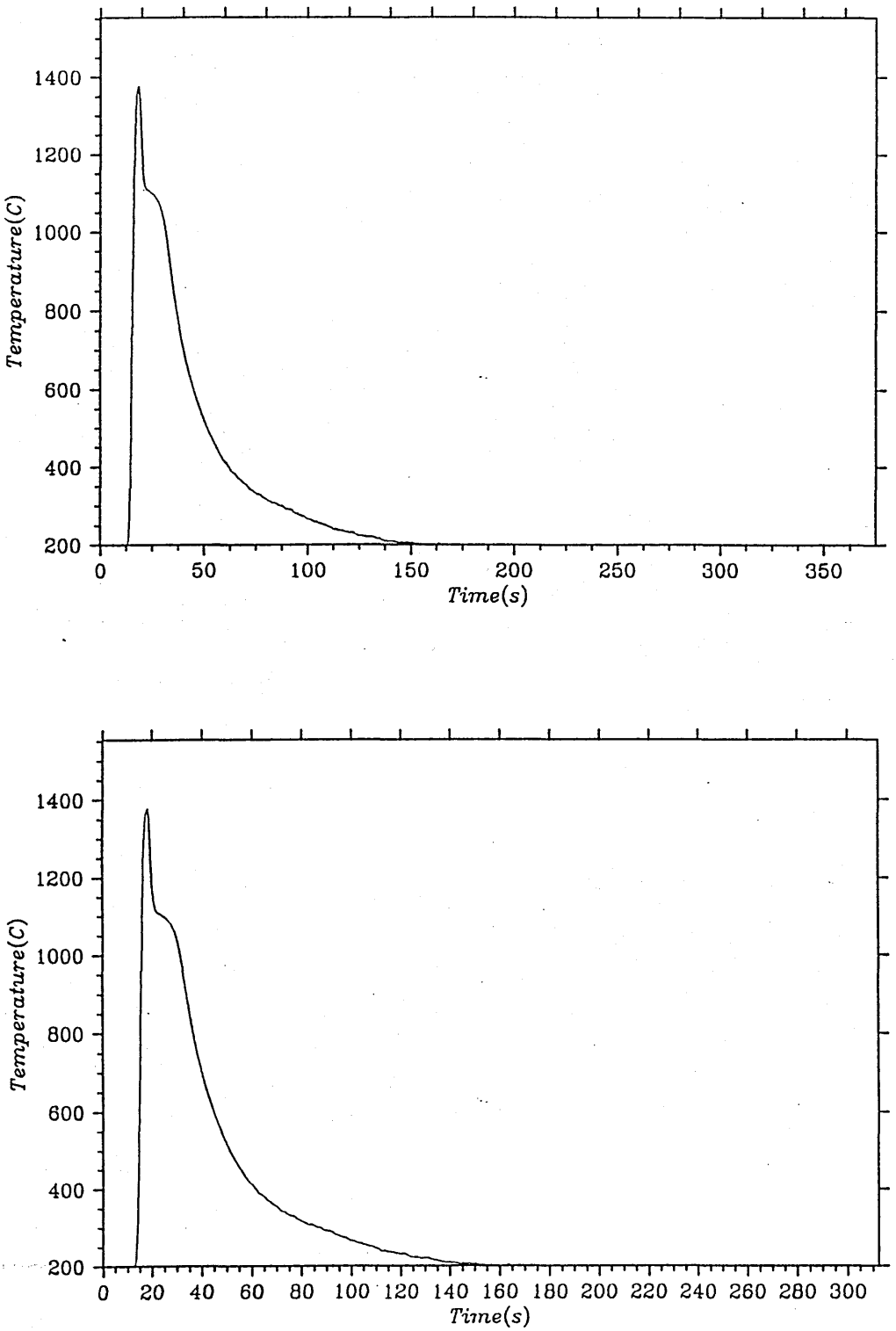

Figure 5.20- Thermal cycles measured in the plate D at a heat input of 3.5kJ/mm (test weld TD-6).

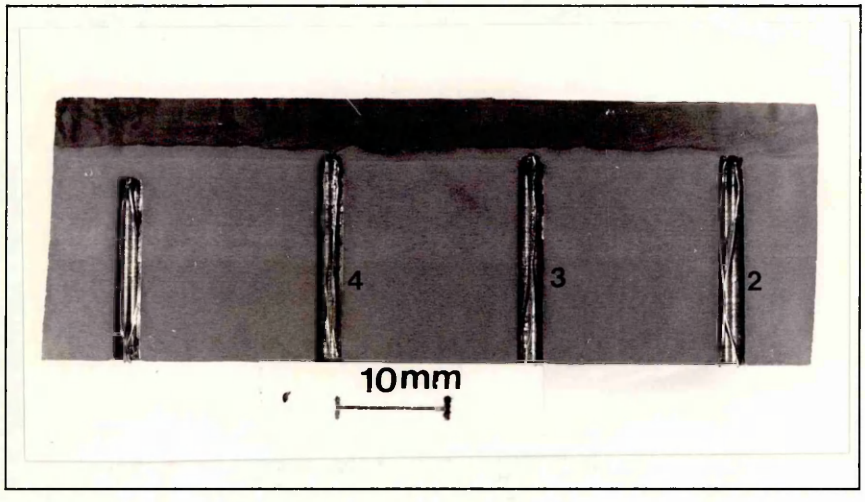

Figure 5.21- Longitudinal section of the test weld T12-1. The peak temperatures reached by thermocouples 2, 3, and 4 were 1489,1194 and 1446°C, respectively.

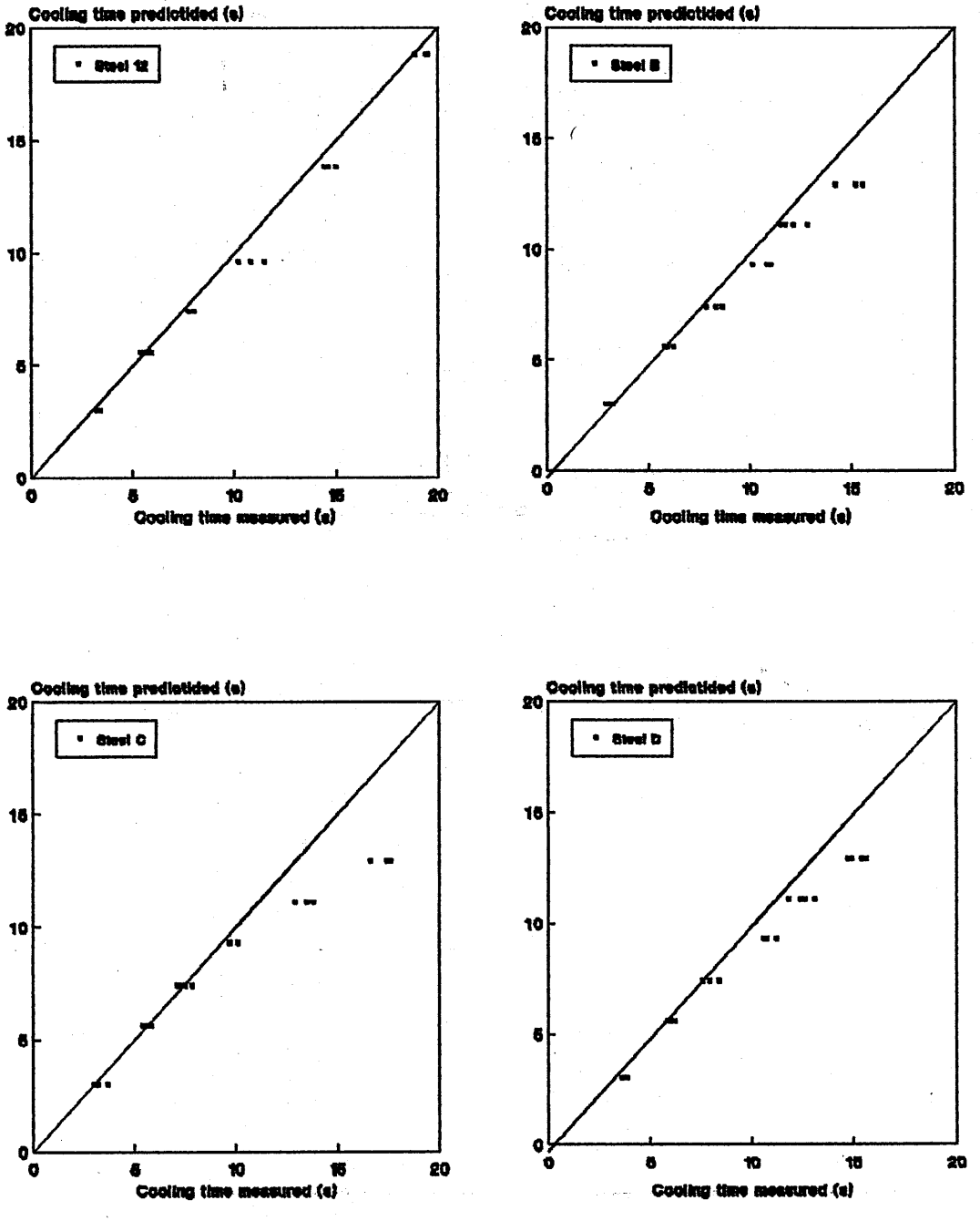

Figure 5.22- Variation of $\Delta t_{8\text{-}5}$(s) with respect to heat input H.I.(kJ/mm) in the test welds with steels 12, B, C and D.

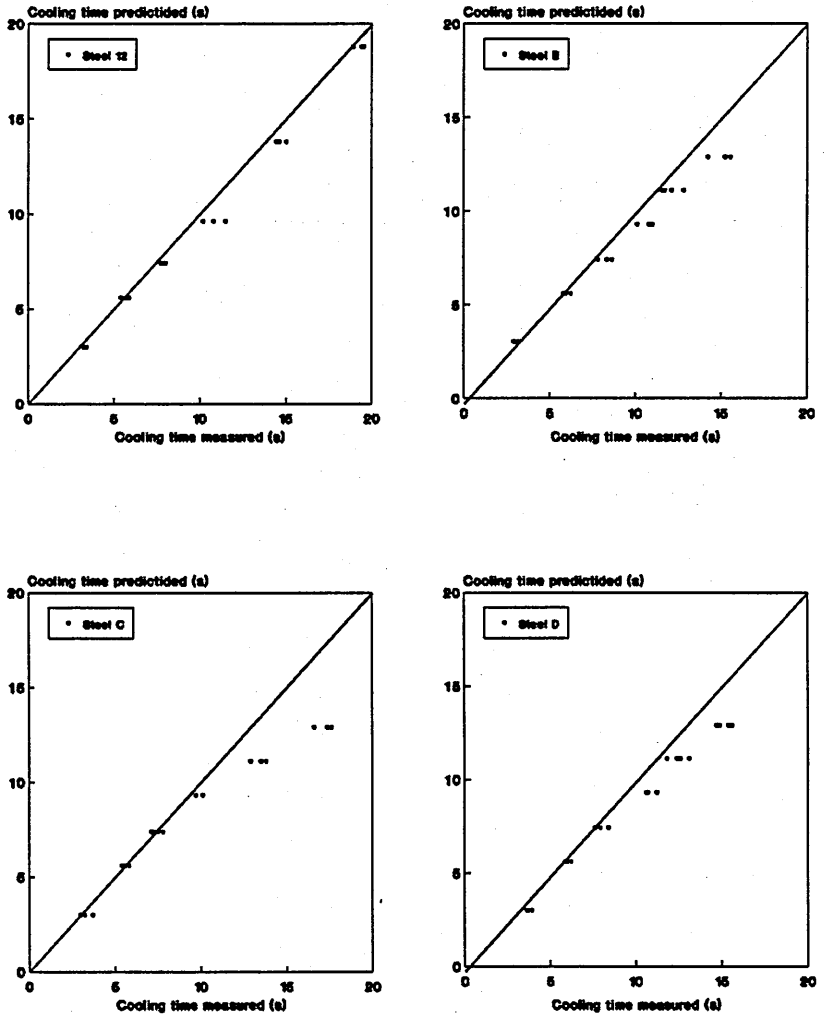

Figure 5.23- Theoretical predictions of Δt_{8-5} compared with the values measured in test welds.

CHAPTER 6 DETERMINATION OF TRANSFORMATION TEMPERATURES IN THE HAZ

6.1 Introduction

The determination of the transformation temperatures in the coarse grained region of the HAZ of the steels under study, was by 'In Situ' thermal analysis. This analysis is based on the principle that the change in lattice from austenite (**fcc**) to ferritic (**bcc**) products is accompanied by a reduction in free energy. That is, the decomposition of the austenite, during cooling, is always exothermic. Consequently, heat is liberated as a result of the solid state transformation. On this basis, at the temperature where transformation occurs the cooling cycle is altered and delay is caused in the cooling. The transformation temperatures are then determine by thermal analysis of the resulting cooling curve. Careful analytical techniques are essential to identify the start and finish temperatures for transformation if any reasonable degree of accuracy is to be attained. In the present work the 'In Situ' thermal analysis was applied by the temperature/time and temperature/temperature methods. The reason for utilizing these methods, was on the basis of successful work developed in the Cranfield Institute of Technology [Tecco, 1985] upon a similar subject.

6.2 Description of the 'In Situ' Thermal Analysis

'In Situ' thermal analysis was applied by a computer software programme named THERMIC, written in Fortran and included in Appendix I. The development of this programme made possible the use of the thermal data (**as measured**) obtained from real thermal cycle measurements in the thermal analysis. In this manner, specific routines were written in the programme in order to apply the temperature/time and temperature/temperature methods. The first method was based on the differentiation (dT/dt) of the variation of temperature with respect to time. With this technique microstructural transformations not detectable in a typical temperature/time, curve would appear in the dT/dt curve as an inflexion owing to the change in cooling rate caused by transformations. On the other hand, the temperature/temperature method involved plotting the temperature of a point of a plate under investigation (test thermocouple) against the temperature of another

point of reference (reference thermocouple) on the same plate. In this respect, the temperature measurement of the reference thermocouple would be registered on the Y axis, whereas the test thermocouple would be registered on the X axis. In the present work the temperature of the reference thermocouple was chosen to be little higher than 500°C.

6.2.1 Temperature/time Method

In the initial graphs produced by the temperature/time method, it was demonstrated that a great amount of background noise was contained in the data, mainly at temperatures below 500°C. Figure 6.1 shows the graphical representation of the temperature/time method applied to a test weld using a heat input of 3.0kJ/mm. As is shown, no realistic analyses could be carried out in order to detect the transformation temperatures. This electrical background noise could have been gathered from the arc or even from the power supply. However, it is worth pointing out that the electrical background noise did not interfere markedly in the determination of the temperature-time curve of the same test weld as is shown in Figure 6.2.

In order to reduce the influence of the background noise present in the data, this had to be filtered by suitable software routine before being analyzed by the programme. A method was applied [Modenise, 1990] in which each data item was substituted by the weighted mean of this data and the number of data items (nf) of its right and left neighbours. In this respect, nf was considered the filter factor, i.e. number of points desired to be filter from neighbours (on the right and left) of a given data:

$$yf_i = p_o.yi + \sum_{j=1}^{nf} [\, p_j.y_{i+j} + p_j.y_{i-j} \,] \qquad [6.1]$$

where yf_i is the filtered data item,
y_i is the unfiltered data,
p_o, ... , p_{nf} are the weighting factors, and
nf is the filter factor.

The weighting factor p_j was calculated from the expression below:

$$p_j = (nf - j + 1) / [(nf + 1)^2] \qquad [6.2]$$

By applying the filtering routine to the thermal data measured in the test welds it was possible to detect transformation temperatures by the temperature/time method. Figure 6.3 shows transformation temperatures at ranges of 640-540°C and 450-360°C, approximately in which the data employed was that used in Figure 6.1, but filtered.

6.2.2 Temperature/temperature Method

The initial graphs produced using the temperature/temperature method, as described, were considered to be unsatisfactory. Although the software programme developed was capable of reproducing the type of results achieved previously (refer Figure 2.10) by Tecco [1985] the transformation temperatures could not be detected as clearly as claimed by the cited author. Figure 6.4 shows the graphical representation of the temperature/temperature method similar to that developed by Tecco [1985] where on the Y axis the peak temperature of the reference thermocouple was 525°C approximately and on the X axis for the test thermocouple was 1350°C.

In order to improve the accuracy of the temperature/temperature method, a new approach was developed which used a synthetic thermal cycle, having the same role as if it was the reference thermocouple. The development of the synthetic thermal cycle was accomplished by employing Rosenthal's equation as described in Section 2.2.1. In this manner, considering that most of the welding conditions used in the present work can be assumed as three dimensional heat flow condition, Rosenthal's equation for thick plate weld thermal cycles was adopted:

$$T = (q/2\pi kr) \exp[-v(r-x)/2\alpha] \qquad [6.3]$$

Where T is the temperature,

$q = \eta VI$,

$r = (x^2 + y^2 + z^2)^{0.5}$,

k is the thermal conductivity,

v is the welding speed, and

α is the thermal diffusivity.

For weld thermal cycles in the heat affected zone, i.e., close to the weld centre line, the following is considered:

$y = 0$, $z = 0$, $x > 0$, and therefore, $r = x$. Then:

$$T = q/2\pi kx \qquad [6.4]$$

But $x = -vt + x_o$
and:

$$T = q/2\pi k(x_o - vt) = q/(-2\pi kx_o + 2\pi kvt) \qquad [6.5]$$

or

$$T = 1/(A + B/E\ t) \qquad [6.6]$$

Where $A = -2\pi kx_o/q$,
$B = 2\pi k$, and
$E = nVI/v$ is the heat input

The equation described above was adopted to artificially reproduce the cooling part of the weld thermal cycles (TC) in the programme THERMIC. In order to quantify the A and B parameters in the synthetic TC equation [6.6], an actual thermal cycle measured in a plate welded with a heat input of 1.5kJ/mm in the experimental work was used. Taking the inverse of the equation [6.6]:

$$1/T = A + B/E\ t$$

The A term can be considered to be the inverse of the temperature at initial time t_o:

$$1/T - 1/T_o = B/E\ t$$

In the computer programme, T_o was arbitrarily assumed to be 1000°C and, therefore, $A = 1 \times 10^{-3}$. Linear regression analysis was used to calculate an estimate of B for 5 selected thermal cycles from the

experimental data. The simple regression model:

$$y = bx$$

was used, where

$y = 1/T - 1/T_o$, and

$x = t/E$

A value for B of 1.342×10^{-4} was obtained by this technique.

By employing the synthetic thermal cycle in the temperature/temperature method it was possible to differentiate the curve obtained by the temperature/temperature method. As a result, it was confirmed that the transformation temperatures would be more directly detected. In addition, the filtering routine could also be employed to minimize the electrical background noise. The improvement in accuracy can be seen in Figure 6.5, where (a) is the previous aspect of the temperature/temperature method (already shown in the Figure 6.4), (b) is the graphical representation of the new temperature/temperature method developed,and (c) is its differentiation. In (c), the indication of transformation temperatures is marked by dashed lines.

The use of the filtering routine brought significant improvements to 'In Situ' thermal analysis. With regards to the temperature/temperature method, better accuracy was certainly achieved by the new development. This can be seen in Figures 6.6(a) (this has been shown in Figure 6.3) and (b) where transformation temperatures could be detected between 640-540°C and 450-360°C, indicated by dashed lines, in both methods. This was obtained by using the same data of the Figure 6.1, but filtered.

After an extensive production of graphs, it was verified that only 40% of a total of 24 test welds could be reliably considered for analysis of the transformation temperatures without misleading indications caused by perturbations in the curves, due to the background noise. For the rest, even increasing the filter factor did not present a standard considered satisfactory to be included in the analysis. Figures 6.7(a) and

(b) shows the temperature/time and temperature/temperature methods respectively which were applied to a thermal cycle measured in a test weld using at a heat input of 2.0kJ/mm. As is shown the use of the filtering routine did not in fact improve the results enough to detect the transformation temperatures owing to excessive interference in the curves.

6.2.3 Remarks

At this stage, some explanations other than the author's inexperience emerged to delineate the limitations encountered in detecting the transformation temperatures by the direct representation of the 'In Situ' thermal analysis using the software programme THERMIC.

Although precautions were taken to minimize the background noise during the thermal cycle measurements such as the shielding of each compensating cables by a soft iron tube and the earthing of each of them, it did not seem to be enough to prevent the acquisition of a large amount of background noise in the data. This could be explained by the great deal of amplification needed to make the output signals of the thermocouple suitable to be gathered by the data logger unit. Though the Pt/Pt-13%Rh thermocouple is the type of thermocouple most suitable for actual thermal cycle measurement in the coarse grained region of the HAZ (peak temperatures in the order of 1400°C or higher), its signal can be considered very low. For comparison purposes, a Chromel-Alumel thermocouple has output signals four times as high in the same range of temperatures up to 1370°C. Although no investigation was carried out in order to measure the magnitude of the background noise, it was assumed that the amplification needed to achieve satisfactory resolution in the thermal cycle measurements, might have amplified the background noise. Consequently, the inflexions expected as indications of the temperatures of microstructural transformation were masked by the interference generated by the electrical background noise.

The introduction of the filtering routine,indeed brought considerable improvement to data which made it possible to read off directly the ranges of temperatures where microstructural transformations occurred. However, during the stage of producing the graphs generated by the 'In Situ' thermal analysis, it was verified by the author that no systematic

number of points could be defined to be filtered. That had to be done by increasing progressively the number of data items to be filtered until a satisfactory shape of curve was achieved. This proved to be very time consuming and an inadequate filter factor could suppress an indication of transformation. For instance, Figure 6.8 shows a range of transformation temperature at 550C-460°C detected from a thermal cycle measured in channel 3 using a filter factor of 24. By increasing this factor to 35, using the same data the previous range of temperature was virtually suppressed as shown in Figure 6.9.

Apart from the improvement in accuracy achieved by the new approach developed for the temperature/temperature method, it was also capable of detecting transformations even at high temperatures (T> 500°C). As it was previously developed this method was claimed [Tecco,1985] to have its best efficiency to detect transformation at low temperatures (T<500°C). The capability of the new temperature/temperature method in detecting transformation at high temperatures is shown in Figure 6.6. However, the electrical background noise , once again, did not allow it to be used extensively, in the experimental work.

Another aspect which could be pondered on the limitations found during the development of this graphical representation of the 'In Situ' thermal analysis was the nature of the data gathered, i.e. digital. With the unit used in the current work, the output signals of the thermocouple were fed into the data logger and they were converted, at a specified rate, into digital information. Consequently, there is always an interval of time between each point gathered. Although not forecasted, by differentiating the data those intervals between points were also amplified which gave some difficulty in detecting the transformation temperatures.

On the basis of what has been discussed in this Chapter the necessity of developing an approach capable of displaying, graphically, the transformation temperatures gathered by the 'In Situ' thermal analysis was verified. In this manner, the thermal data generated by the 'In Situ' thermal analysis were submitted to statistical calculations in order to minimize the interference caused by electrical background noise and the interval between data item. The development of the statistical calculations employed in the present work is extensively

described in Chapter 7.

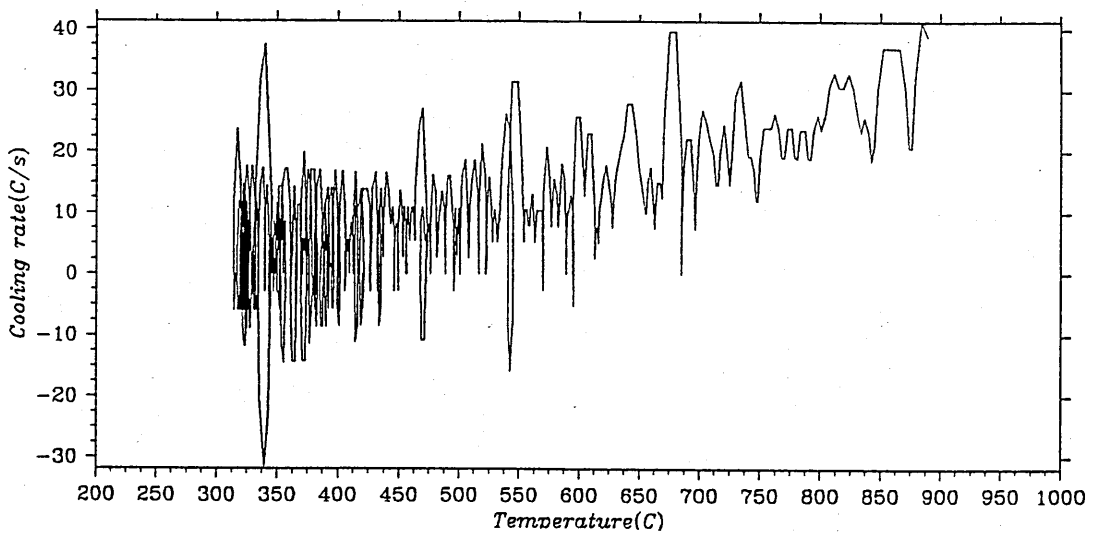

Figure 6.1- Graphical representation of the temperature/time method containing electrical background noise.

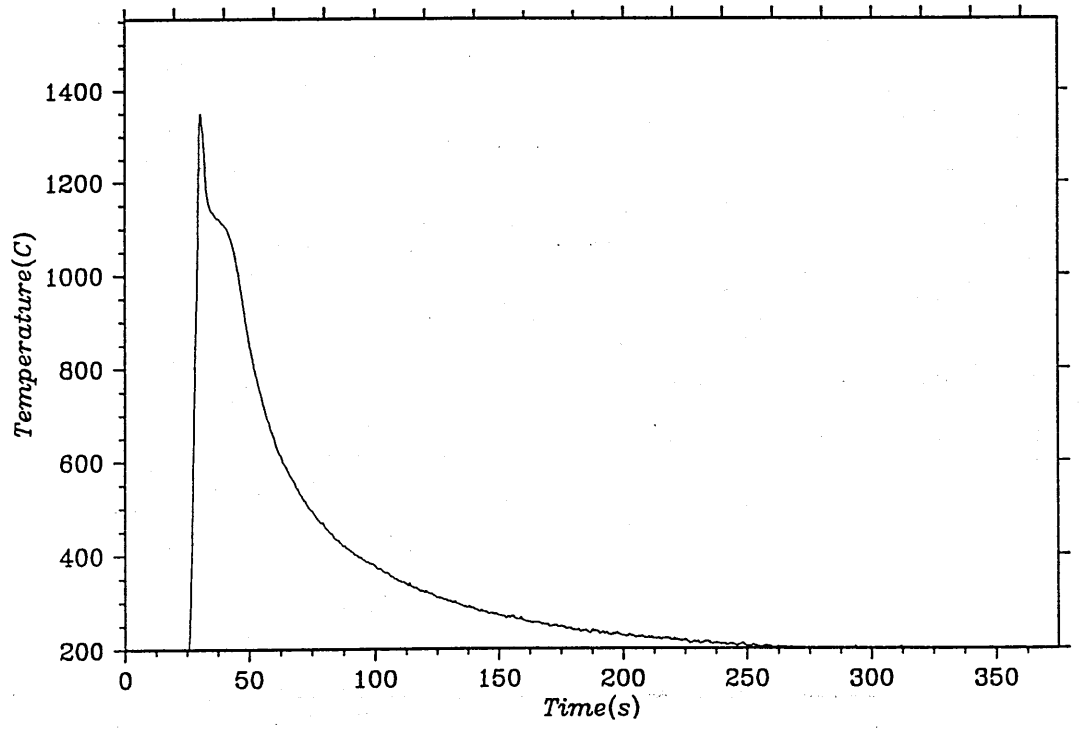

Figure 6.2- Thermal cycle measurement used in Figure 6.1.

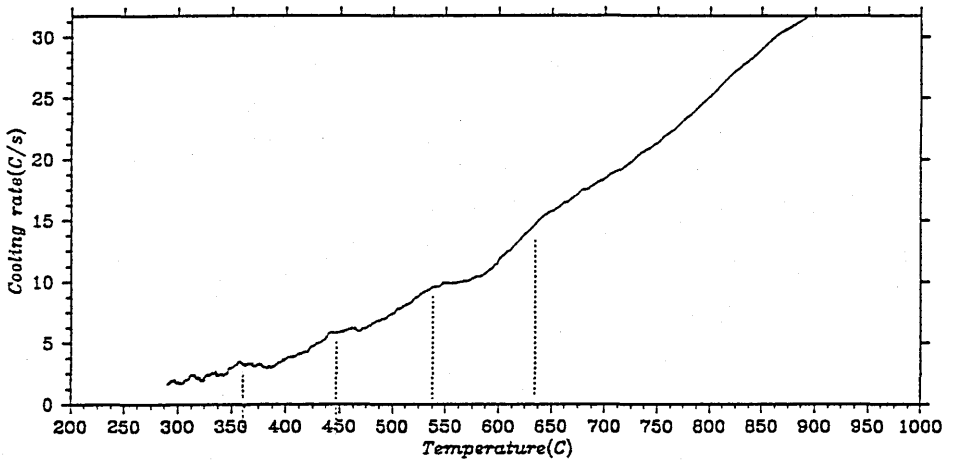

Figure 6.3- Graphical representation of the temperature/time method using the filtering routine.

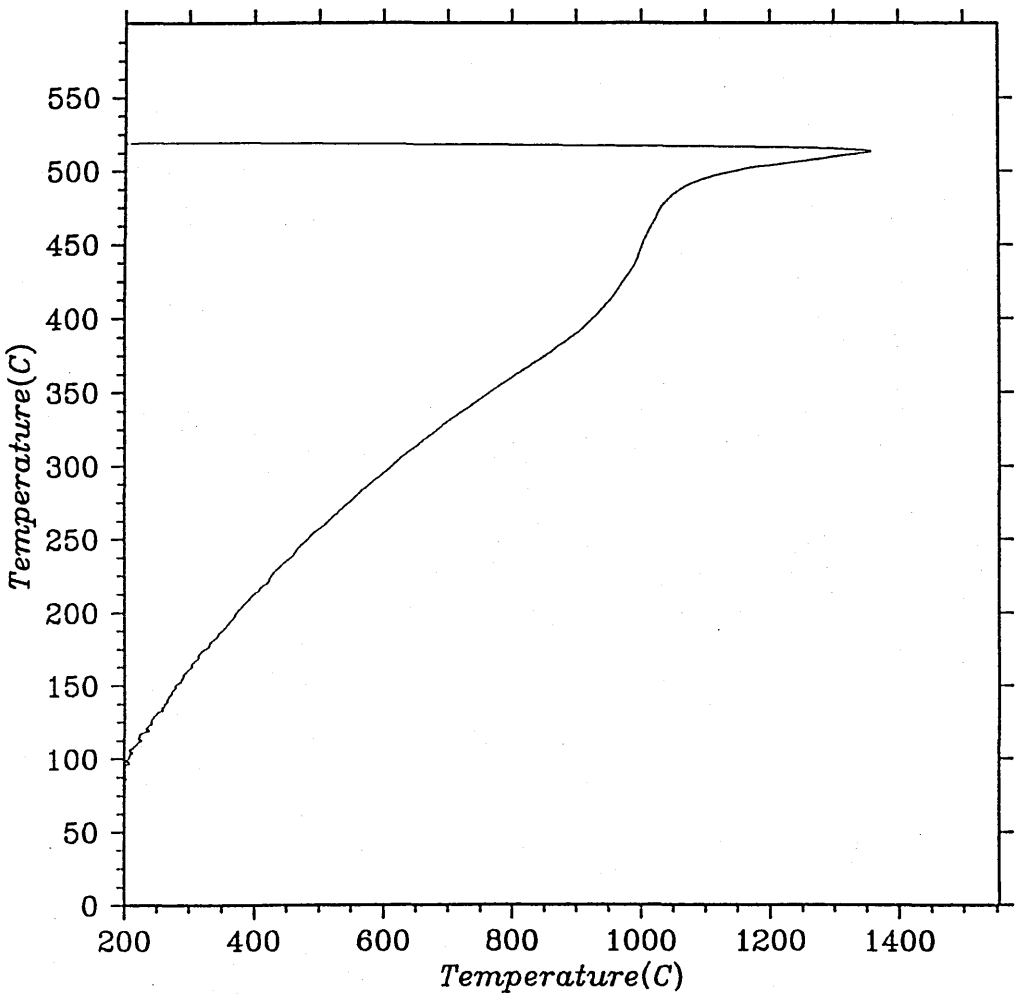

Figure 6.4- Temperature/temperature method as developed by Tecco [1985] and obtained in the present work.

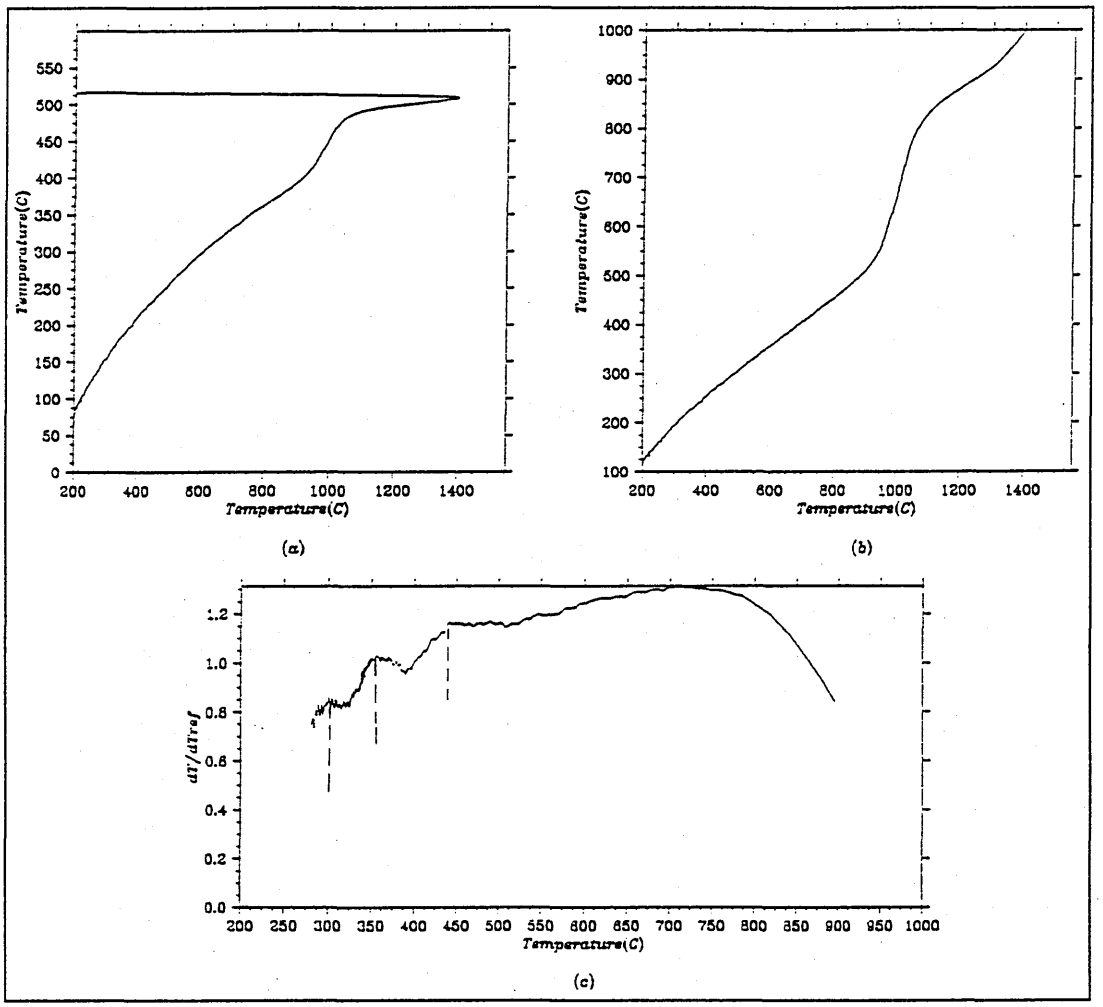

Figure 6.5- (a) Temperature/temperature curve as shown in Figure 6.4.

(b) Temperature/temperature curve using the synthetical thermal cycle.

(c) Differentiation of the curve in (b) indicating ranges of transformation temperatures.

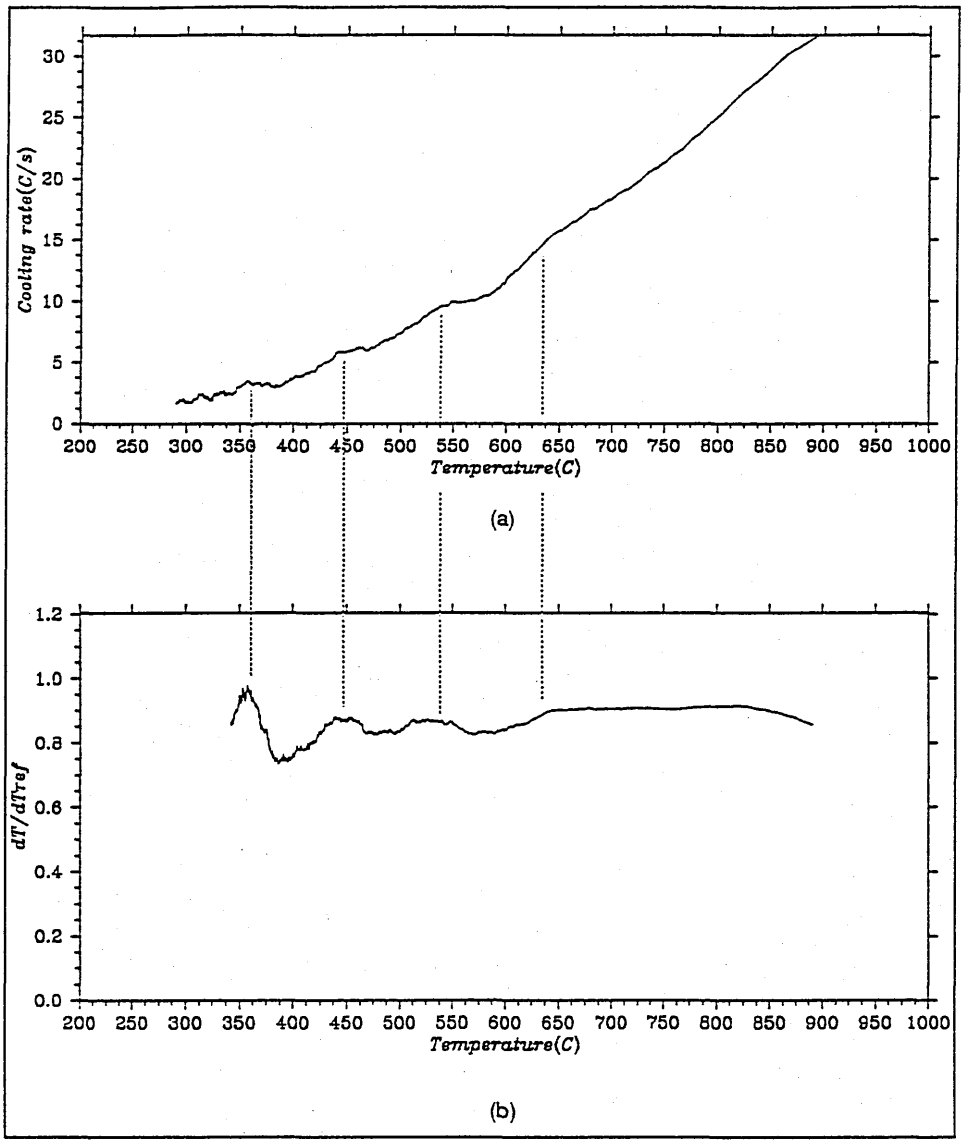

Figure 6.6- Transformation temperatures indicated by both methods: temperature/time and temperature/temperature, (a) and (b) respectively.

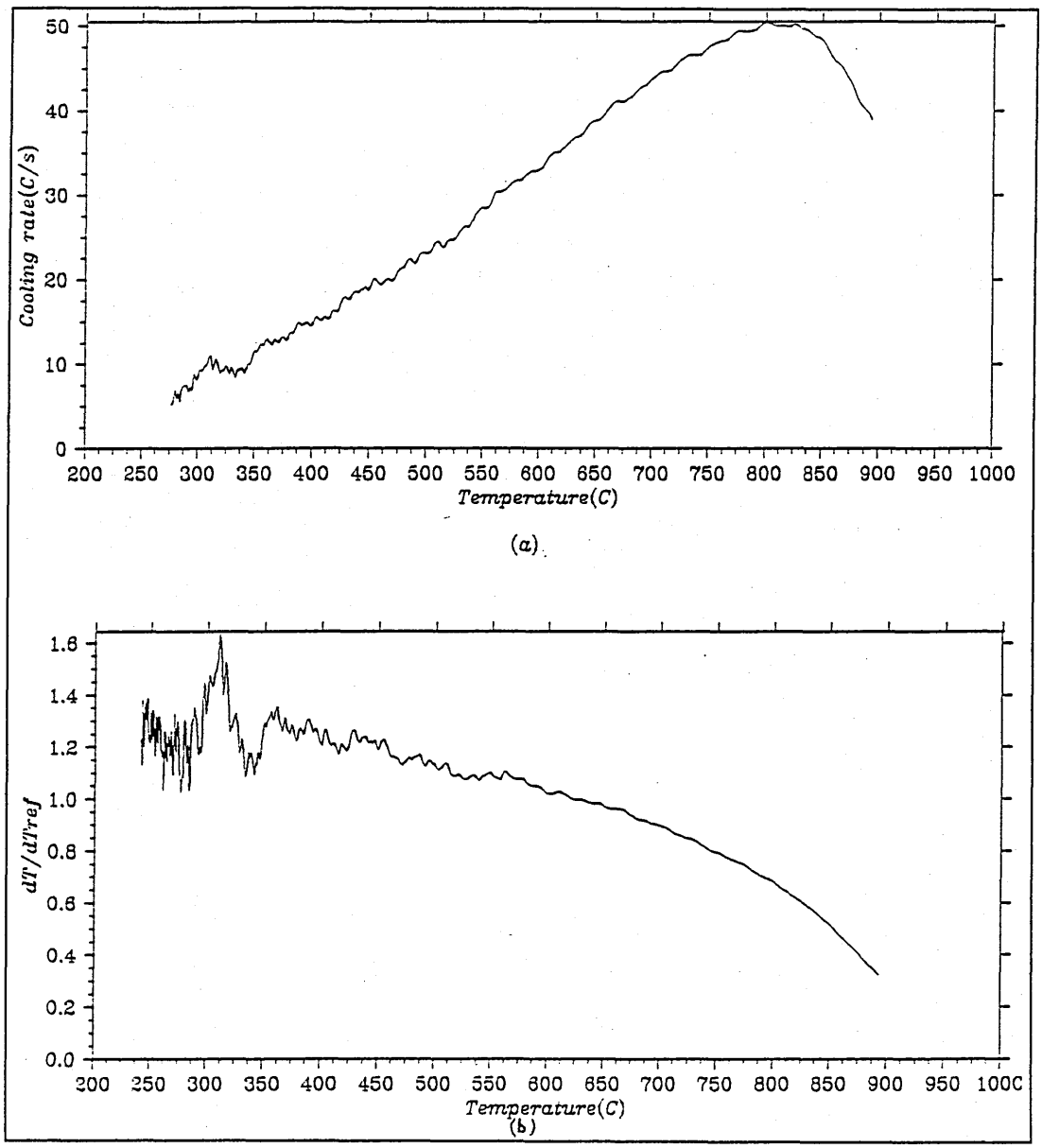

Figure 6.7- Graphical representation of the temperature/time and temperature/temperature methods (a) and (b) respectively of a filtered data.

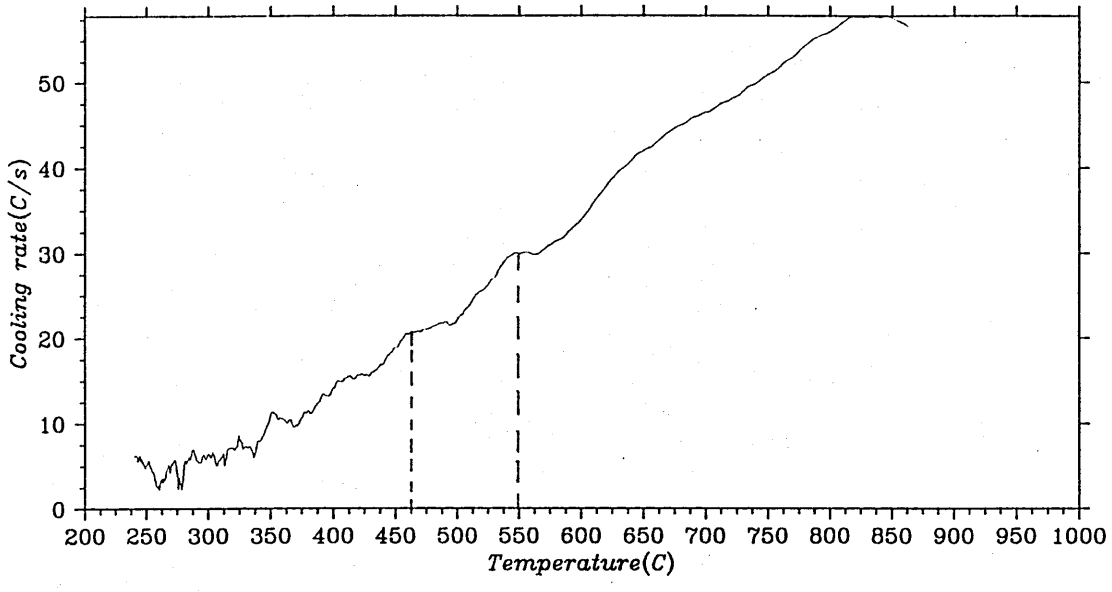

Figure 6.8- Transformation temperatures detected by the temperature/time method using a filter factor of 24.

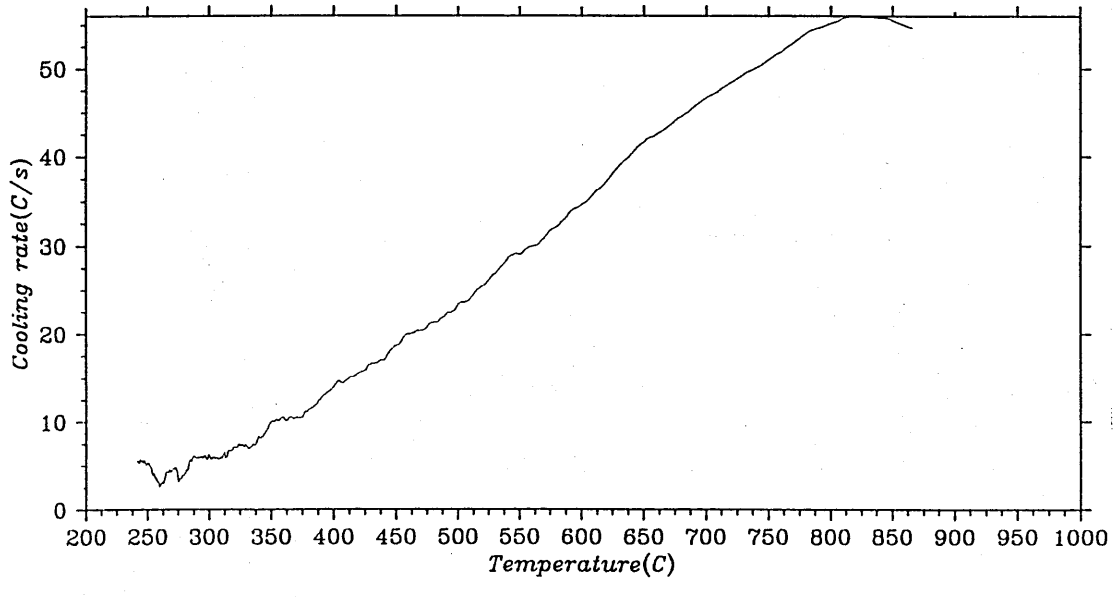

Figure 6.9- Temperature/time method applied to the same thermal data of Figure 6.8 but using a filter factor of 35.

CHAPTER 7 STATISTICAL CALCULATIONS FOR THE 'IN SITU' THERMAL ANALYSIS

7.1 Introduction

It became clear after a series of tests carried out applying the 'In Situ' thermal analysis that the electrical background noise present in the data as well as the interval of time in which the data was gathered, prevented detection of the transformation temperatures by the point-wise analysis (refer Chapter 6). As a result, the transformation temperatures indicated by the temperature/time and temperature/temperature methods could not be clearly detected. The statistical approach arose as a means of bringing the thermal data generated in the current work into a suitable format, capable of displaying graphically the transformation temperatures of the microstructures produced in the coarse grained region of the HAZ's of the steels studied.

In order to minimize the influence of the electrical background noise and the interval between each data item gathered, it was decided to represent the curves of the 'In Situ' thermal analysis by the smallest possible segments of straight line without changing the original thermal characteristic of the curves. This was accomplished by calculating the 'best - fit' segments, employing the method of the least square [Chatfield, 1983], using the data generated by the 'In Situ' thermal analysis. This was supported by the SPSS^x [SPSS^x, 1983], statistical package available on the mainframe VAX.

7.2 Bar Chart Representation of the Statistical Approach

A bar chart was originally chosen as a means of representing the various procedures adopted following the segmentation of the curves. It was envisaged that this graphical representation would be able to indicate changes in the trend of the thermal curves, followed by the segments, due to microstructural transformation.

The application of statistical methods requires a certain amount of data in order to make any approach suitably reliable. As an example, for a small sample the minimum of 15 elements is recommended in

order to apply statistical methods [Chatfield, 1983]. Initial studies, supported by the SPSS^x, revealed that 50°C was the most suitable approximate interval of temperature by which the thermal curves generated in the current work should be segmented. This implied meeting the minimum possible points according to statistical requirements for a small sample.

The initial step taken was to evaluate the response of the segmentation to a cooling curve obtained from actual weld thermal cycle measurements. This was accomplished by using two thermal cycles measured in the current work. For both cooling curves the inclination of the segments was plotted, identified as B Values in each interval of 50°C within the range of 725-275°C. It can be seen in Figure 7.1 that the inclination of the segments represented by the height of the bars decreased as the temperature decreased for both cooling curves. This trend reproduced that obtained by a cooling curve of an actual weld thermal cycle (refer Chapter 5). With regards to transformation, no indication was obtained. This could be anticipated, considering that in the 'In Situ' thermal analysis, the temperature/time method consists of employing the differentiation (dT/dt) of the cooling curve in order to improve the indication of the transformation temperatures not clearly shown in cooling curves. Nevertheless, the validity of using a cooling curve at this initial stage of the approach remained important because it gave an indication that the variation of the inclination of the segments could indeed represent the cooling curve of an actual weld thermal cycle measurement. These cooling curves were then submitted to the temperature/time method and the inclination of the various segments of the resultant curves were calculated. Figure 7.2 shows that the variations of the height of the bars, which represent the inclination of the segments, clearly showed out of trend variations indicating transformations. This was found at temperatures of 625 and 525°C in the thermal cycle measured by channel 3. Although some indications of microstructural transformation could be detected, it was not possible to precisely define the temperatures of start and end of transformation.

One important aspect which could have strongly interfered with the lack of accuracy mentioned above was the electrical background noise. It was clearly shown in Figure 6.1 that the electrical background appeared to be of similar intensity to the signals of the thermocouples. In the point-wise approach (refer Chapter 6), the software filtering routine

developed indeed brought an improvement and some indications of transformation temperatures could be detected. However, that filtering could not be applied in the current approach. This is because the filtering routine developed was based on calculating mean values for a group of data item. Consequently, by using the filtering routine during the statistical approach, the statistical requirements would not be met. To minimize the effect of the background noise, the possibility of calculating an average thermal curve for the thermal cycles gathered in same test weld was taken into consideration. By doing that, it was expected that the noise signals were likely to be smothered due to their random behaviour. With regards to the signals gathered due to microstructural transformation it became clear that they presented a defined distribution (refer Figure 6.3), as opposed to the random behaviour of the noise signals. Furthermore, similar ranges of transformation temperatures are very likely to be gathered by different thermocouples considering that they were attached to the same plate and welded under the same welding conditions. Consequently, the defined distribution of the signals gathered due to transformation would certainly be preserved in the average thermal curve.

To implement the calculation of the average thermal curve a great deal of additional considerations had to be taken in order to evaluate its validity. Up to the time of this research, no similar approach could be found reported in the technical literature for any experimental work of a similar nature. However, from experimental measurements of weld thermal cycle it had been found that, for a given welding process, weld geometry and material, the cooling-time through the range 800-500°C is constant, at least within the heat affected zone base metal (heated to a peak temperature, T_p>900°C), i.e. $\Delta t_{8\text{-}5}$= const [Easterling, 1983]. In the current work it was found that in a test weld, thermocouples positioned in different points in the HAZ and having reached different peaks of temperatures above 900°C, still had a very similar cooling time through 800-500°C (refer Table 5.3 and Figure 5.21). Another examination carried out was to evaluate the cooling time through 800-300°C. Although this range has not been reported as of particular metallurgical interest it has been used [Kohno and Jones, 1978] to evaluate the reproducibility of real thermal cycle measurements. The reproducibility of actual temperature measurements are considered satisfactory when thermocouples attached to the same plate measure similar cooling time through 800-300°C. Figure 7.3 shows that for each

test weld a very similar cooling time between 800-300°C was measured. The corresponding peak temperatures reached by each test weld can be seen in Table 5.3. In resemblance to what was obtained in the variation of the cooling time through 800-500°C ($\Delta t_{8-5)}$ in the current work (refer Chapter 5), the cooling time through 800-300°C increases as the heat input increased with a very similar pattern. The heat inputs, namely 0.8, 1.0, 1.5, 2.0, 2.5, 3.0 and 3.5kJ/mm are represented by the numbers 1 to 6 respectively, on the horizontal axis (Figure 7.3). A qualitative test was also carried out by superimposing the thermal cycles measured from each experimentation and observing, within the range of 800-300°C, any discrepancies in the shape of the curves which could invalidate the use of an average thermal curve. As expected from the calculations of the cooling times, the curves presented very similar shape and no marked discrepancies in their shape were found. On that basis, the investigation was carried out using an average thermal curve to represent the cooling curves of the thermal cycles measured in each test weld. This was considered valid and the development of the statistical approach was continued by applying it.

To calculate the average thermal curves for each test weld, the thermal cycles measured had to be overlapped due to the fact that they were out of the phase, i.e. there were differences in terms of time amongst them due to progression of the welding torch along the joint. To overlap them, a temperature had to be chosen to be used as an intercept. Although the thermocouples were positioned at different points, they were all placed in the coarse grained region of the HAZ. Consequently, the same range of temperatures were gathered during the measurements. Due to the popular use of Δt_{8-5} in welding circles as an important parameter to describe a given weld, it was decided to intercept the thermal cycles within this range. 800°C was then chosen to be one of the temperatures of intercept. This temperature is important in that in most steels, it represents approximately the A_{r3} (temperature of start of the decomposition of austenite) transformation temperature. However, considering the new approach developed, it was decided to choose another temperature to be used as an intercept, so that the temperature of 500°C was also employed to calculate the average thermal curve. As a result, two average thermal curves were used to represent the thermal cycles measured in each test weld. The decision to use two temperatures separately is based on the fact that by intercepting the thermal cycles at one temperature those cooling times

mentioned above would not be changed. Consequently, the thermal characteristics of each individual thermal cycle would be preserved. On the other hand, if two temperatures were used as intercepts at the same time, it possibly could introduce distortions in the cooling times because in this case the thermal cycles were being 'forced' to be intercepted at two points. Therefore, the average thermal curves for each temperature of interception was calculated by the software programme THERMIC [Appendix I].

The continuation of the development of the statistical approach proceeded by calculating the average thermal curves of the thermal cycles used initially. It can be seen from Figure 7.4 that the response of the average thermal curves to the segmentation presented the same pattern to that obtained for individual channels (refer Figure 7.1). The variation of the inclination of the segments obtained within intervals of 50°C decreased as the temperature decreased.(Note that the notation used in Figure 7.4 to represent the bars representative of each average thermal curve using 800 and 500°C as intercepts was A800 and A500.) This was followed by submitting the average thermal curves to the temperature/time method. Figure 7.5 shows that some indications of transformations were detected at temperatures of 625, 525, 475 and 325°C.(The notation used in Figure 7.5 to represent the bars is A800D and A500D.) In resemblance to what was found in Figure 7.2 for temperatures of 625°C and 525°C, those indications arose out of the trend of the variations of the heights of the bars. Nevertheless, the temperature of start and end of transformation could not be clearly detected.

Although some improvements were gathered by the use of average thermal curves showed in Figure 7.5, the detection of the start and end of transformation had remained unclear. Following the course of pursuing improvement in accurately detecting transformation temperatures, it was decided to introduce some modifications in this last approach in order to improve its accuracy. Since the beginning of the development of the statistical approach, the course adopted was to detect variations in the trend of the inclination of the various segments representative of the curves obtained by the 'In Situ' thermal analysis. On this basis, it was thought to plot not individual values of the inclination of the segments but the difference between each of these values and their former neighbours. It was expected that any significant

perturbation in the trend of the variation of the inclination of the segments would be even more emphasized than what is presented in Figure 7.5. The differences in inclination of the segments shown in Figure 7.5 were plotted and these are shown in Figure 7.6. Indeed, abrupt changes as a result of microstructural transformation could be more easily detected and the range of transformation could be clearly identified as 625-575°C, 475-425°C and 325-275°C. The same procedure was also applied to the curves generated by the temperature/temperature method and similar ranges of temperatures were also suggested as shown in Figure 7.7. It should be noted that A800RD and A500RD were used to represent the variation of the inclination of the segments of the curves generated by the temperature/temperature method applied to the average thermal curves at 800 and 500°C respectively.

The differences in transformations temperatures found in the average thermal curve calculated at 800°C and at 500°C (Figures 7.6 and 7.7) could be explained by examining the distribution of points when the average thermal curve is calculated at these two temperatures. By using the statistical package SPSS^x, it was possible to verify the distribution of points in every 50°C starting from 700 down to 250°C. Table 7.1 shows the number of points measured within each interval of 50°C of the resultant curves obtained from temperature/time and temperature/temperature methods. For temperatures lower than 550°C the distribution of points in A800D is not the same as in A500D for the range of temperature of 500-350°C. This could be accounted for by the accuracy of approximately 6°C of the data logger unit. A degree of uncertanty is expected as a result of this accuracy which can lead a given point to be either in one range of temperature or in another depending on the starting point of the segmentation.

At this stage of the programme, it was considered that although the graphical method used, i.e. bar chart, had in fact been capable of graphically representing the improvements implemented throughout this section, it had not been satisfactory with regards to the definition of the temperatures of the start and end of microstructural transformations. This is explained by the type of data (variation of the inclination of the various segments, identified as B Values) used in the statistical approach. These values may look like discrete data and bar charts are very useful visual aids when analyzing discrete data [Chatfield, 1983],

however, they are still regarded as continuous data because the underlying variate, i.e. temperature, is continuous. On this basis, the type of graphical representation was changed and curves were drawn to better indicate the transformation temperatures.

7.3 X-Y Representation of the Statistical Calculations

The curves were drawn by the Uniras graphical routines available on the mainframe VAX computer. The advantage of utilizing the mainframe to draw the curves was the flexibility available with regards to improving the format of the data during the development of this new graphical representation of the statistical approach. This was achieved by a software programme, written in Fortran [Appendix II], which was interfaced with both, the SPSS[x] and the Uniras.

For this graphical representation of the statistical approach, the same concept adopted for the bar chart was applied; that is, to calculate the variation of the differences in inclination between one segment and its former neighbour. This was applied to the curves generated by the 'In Situ' thermal analysis using the average thermal curves obtained from thermal cycles measured in each test weld. However, the segmentation adopted before this stage of the programme was attached to fixed intervals of temperature of 50°C. To improve the fitness of the segments; that is, to make them more representative of the average thermal curves, it was decided to optimize the criteria adopted for the segmentation without breaking the statistical requirements. On this basis, a study was carried out in order to establish the further segmentation to which the average thermal curves would be submitted. In this manner, the distribution of elements (data item of the curves generated by the "In Situ" thermal analysis) was initially analyzed by the statistical package SPSS[x] in intervals of 50°C. Table 7.1 shows that the amount of points for temperatures as low as 500°C was just in excess to what is recommended for the application of statistical methods. For lower temperatures statistical requirements were largely satisfied. This was followed by the development of a software routine to carry out the new segmentation to be adopted. In this programme [Appendix II], the possibility of imposing either number of elements or range of temperatures, or even both, to segment the curves was introduced. This was adopted due to the differences in amount of points shown in Table 7.1. On this basis, some boundary conditions were

introduced in the programme as part of the new segmentation to be adopted. Therefore to guarantee the minimum number of elements the condition was imposed that the minimum number of points (approximately 15) must be satisfied, whatever range of temperatures was adopted to segment the curves. If not, the segmentation would be done over a wider interval of temperature. On the other hand, for temperatures lower than 500°C it was considered that no conditions were needed due to the large amount of points. Even so, a study was carried out using values fixed for both interval of temperatures and number of points. By doing this, it was intended to analyze the influence of both variables in the statistical approach more consistently. The first test was by fixing the number of 15 elements and an interval of temperature of 20°C. In Figure 7.8 the variation of the inclination of the various segments obtained from the curve generated by the temperature/time method followed an uniform trend with the values of B decreasing as the temperature decreased.(Note that identification adopted for these variation is VARIATION OF B.) However, the differences between each of those values and its former neighbour, identified as FIRST VARIATION OF B, presented an irregular trend, especially at temperatures lower than 400°C. This can be seen from Figure 7.9. This is explained by the large number of points obtained within this range of temperatures. By keeping the same range of temperatures but using a greater amount of points it was verified that an improvement was achieved and some indications of transformations could be gathered within approximately 525-450°C and 420-350°C. This can be seen from Figure 7.10. Another investigation was carried out in order to evaluate the response to an interval of temperature of 50°C and number of points of 15. Figure 7.11 reveals that the amount of segments clearly decreased in the FIRST VARIATION OF B but the ranges of 525-450° and 420-350°C were still detected as in Figure 7.10. The interval of 50°C for temperatures lower than 400°C seemed to eliminate the irregular trend verified in Figure 7.10.

Based on the experience gathered up to this stage of the development of the statistical approach, it seemed that a compromise between statistical requirements and the intervals of temperature to segment the curves needed to be reached. As a result, the following general rule was established to help building the final criterion:

i) For temperatures between 700-500°C, the minimum number of

elements was fixed at 15, to be used to segment the curves regardless the interval of temperature needed to reach these number of points;

ii) For temperatures below 500°C, although preserving 15 elements as the minimum number of elements for each segment, the interval of temperatures to segment the curves was fixed by the need to avoid background noise without suppressing the temperatures of transformation.

For criterion (ii), two ranges of temperatures were considered, i.e. temperatures between 500-350°C and 350-250°C. This was done in order to deal with the large number of elements gathered in this former range of temperature.

Consequently, the following criteria were adopted:

i) To segment the curves within the range of temperatures of 700-500°C, the procedure adopted was as follows:

HI (kJ/mm)	Number of eleements
0.8 - 1.5	15
2.0 - 2.5	18
3.0 - 3.5	21

ii) For temperatures between 500-350°C, the segmentation was based in fixed intervals of temperature of 30°C for the whole range of heat inputs;

iii) For temperatures between 350-250°C, the interval of temperature fixed was of 20°C.

It is worth commenting that the number of elements chosen to segment the curves for each range of heat inputs in (i), was based on

observations in tables similar to Table 7.1. Within the range of temperature of 700°C-500°C, these numbers of elements were, approximately, the available number of elements capable of satisfying the statistical requirements for each range of heat input . However, in (ii) and (iii) the intervals of temperatures chosen to segment the curves represented approximately the mean temperature which contained an adequate number of elements to allow the statistical approach to detect the transformation temperatures below 500°C. This was done in order to prevent the analyses from being affected by the background noise.

7.4 Validation Test

The validation test was carried out in order to substantiate the validity of applying the statistical approach to the curves generated by the 'In Situ' thermal analysis. This gave a means of determining the transformation temperatures in the coarse grained region of the HAZ's of the steels under study. In this manner, the first step taken was to verify how the statistical approach would respond to the 'In Situ' thermal analysis applied to a thermal cycle exempt from microstructural transformation. This was achieved by applying the 'In Situ' thermal analysis to the synthetic thermal cycle developed, which has been described in Chapter 6. For the application of the statistical approach, the curves generated by the 'In Situ' thermal analysis had to be segmented.The criteria adopted for the segmentation was that established for test welds with 1.5kJ/mm. It is worth mentioning that the graphical representation of the synthetic thermal cycle was obtained by employing thermal data gathered during a thermal cycle measurement in a test weld with 1.5kJ/mm (refer Chapter 6).

The variation of the inclination of the segments (VARIATION OF B) of the curve obtained from the temperature/time method, revealed that the inclination of the segments (B Values) decreased gradually as the temperature reduced to approximately 400°C. For temperatures lower than 400°C, an abrupt fall in the rate of variation of the inclination of the segments was observed. This can be seem from Figure 7.12. The profile obtained is in accordance with the profile of the temperature/time curves of the actual thermal cycle measurements, as presented in Chapter 6. A similar pattern was obtained when the differences between the inclination of each segment and its former neighbour was plotted (FIRST VARIATION OF B). This can be seen in

Figure 7.13. The fall indicated for temperatures lower than 400°C was not as marked as in VARIATION OF B. This is explained because when the differences between the inclination of each segment are plotted, what becomes more relevant is the comparison between the magnitude of the variation of the inclination of one segment in respect to the complete trend of the thermal cycle. As a result, the fall noticed in the inclination of the segments for temperatures lower than 400°C is in fact less marked when compared with the trend of the thermal cycle.

The evaluation of how the statistical approach would respond to the 'In Situ' thermal analysis applied to a thermal cycle containing microstructural transformation, was by **simulating** microstructural transformation employing the synthetic thermal cycle. This was accomplished by choosing initially, three ranges of temperatures, 600-570°C,520-465°C and 460-455°C, to represent the simulated microstructural transformations. The choice of the total range of temperature of 600-455°C is justified considering that during welding, an actual microstructural transformation is likely to take place within a similar range of temperatures. With respect to each of the ranges, the idea was to evaluate the response of the statistical approach to different magnitudes of intervals of transformation temperatures found amongst various microstructures.

The introduction of the simulated microstructural transformation in the synthetic thermal cycle was implemented by taking into account the effect of the exothermic characteristic of the decomposition of austenite in the actual weld thermal cycle. That is, the heat liberated as a consequence of the solid transformation results in a slower cooling rate causing a permanent delay in the thermal cycle. This effect was simulated by adding increments to each data item within the ranges of temperatures chosen to represent microstructural transformations. Furthermore, to simulate the permanent delay caused by an actual microstructural transformation, the addition of the increments was carried out accumulatively. As an example, for the simulated transformation within the range of 600-570°C, the increment arbitrarily chosen was of 0.5°C. In this manner, the introduction of the simulated transformation started by adding 0.5°C to the next data item just below 600°C. The next one was then added of 1°C. This procedure was continued until the increment added to each data item reached an accumulative value of 10°C. This implied that 10°C had be added to

each data item from the temperature of 570°C downwards. As a result, the thermal cycle became displaced by 10°C with respect to the original synthetic thermal cycle for temperatures below 570°C. The simulated transformation within the range of 520-465°C was then implemented and the increment was of 0.2°C (once again this increment was arbitrarily chosen) until an accumulative value of 10°C was reached. Consequently, 10°C was added to each data below 465°C. For the last simulated transformation an increment of 0.5°C was applied until the accumulative value of 5°C was obtained. In this manner, 5°C was added to temperatures below 460°C . As a consequence, the thermal cycle containing simulated microstructural transformation was displaced from 460°C downwards, by a total of 25°C with respect to the original synthetic thermal cycle. Once the synthetic thermal cycle containing simulated microstructural transformation was developed, the 'In Situ' thermal analysis was applied in order to detect these simulated ranges of transformation temperatures. The resultant curves generated by the temperature/time and temperature/temperature methods were then submitted to the statistical approach.

The variation of the inclination of the segments (VARIATION OF B) of the curve generated by the temperature/time method revealed an abrupt fall in the inclination of the segments (B Values) within the ranges of temperatures where the simulated transformations were created. These ranges were approximately 630-590°C, 550-510°C and 475-450°C. This can be seen from Figure 7.14. The reproducibility of the temperatures at the start of transformation were +30°C, 0°C and +15°C respectively, whereas for the temperatures of end of transformation, the reproducibility were +20°C, +45°C and +10°C respectively. When the differences between the inclination of each segment and its former neighbour (FIRST VARIATION OF B) was plotted, a criterion had to be laid down in order to analyze the ranges of transformation temperatures. It was established that the start of transformation would be characterized by the first point out of the trend of the curve. Conversely, the end of the transformation would be considered to be the first point to return to the trend of the curve. On this basis, the ranges of transformation temperatures were approximately 610-575°C, 530-495°C and 460-430°C. This can be seen from Figure 7.15. The temperatures of start of transformation presented a reproducibility of +10°C, -20°C and 0°C respectively. On the other hand, for the temperatures of end of transformation the reproducibility were +5°C,

+30°C and -25°C.

The variation of the inclination of the segments (VARIATION OF B) of the curve obtained from the temperature/temperature method, presented abrupt changes in the inclination of the segments (B Values) within the ranges of temperatures of approximately 630-585°C, 550-505°C and 475-450°C (Figure 7.16). The reproducibility obtained compared to the range of temperatures of the simulated transformations were: +30°C, 0° and +15°C respectively. These applied to the start of transformation, whereas for the end of transformation the reproducibility was +15°C, +35°C and -5°C respectively. With regards to the FIRST VARIATION OF B the same criteria to determine the transformation temperatures described above, was employed. The range of transformations were approximately 610-570°C, 530-495°C and 465-430°C. This can be seen from Figure 7.17. The reproducibility gathered for the temperatures of start of transformation were +10°C, -20°C and +5°C respectively. For the temperatures of end of transformation the reproducibility were of 0°C, +25°C and -25°C respectively.

From the results presented in the Validation Test, it it is demonstrated that very similar ranges of transformation temperatures were gathered by the VARIATION OF B when it was applied to the curves generated by both methods; i.e. temperature/time and temperature/temperature. A similar result was obtained for the FIRST VARIATION OF B. The reproducibility was best achieved by the FIRST VARIATION OF B for both curves generated by the 'In Situ' thermal analysis. The absolute values of the deviation was not higher than 20°C for temperatures of start of transformation and no higher than 30°C for temperatures of end of transformation. Figure 7.18(a) shows the reproducibility of the temperatures of start and end of transformation in the curve VARIATION OF B from the temperature/time method. Figure 7.18(b) shows the reproducibility in the FIRST VARIATION OF B. Both were plotted with respect to the temperatures of the simulated microstructural transformations.

On the basis of the Validation Test carried out, the statistical approach has been shown to be capable of readily detecting transformation temperatures. The reproducibility gathered was considered to be satisfactory. The curve FIRST VARIATION OF B presented the smallest absolute deviation from the ranges of

temperatures of the simulated microstructural transformation, when applied to both types of curve generated by the 'In Situ' thermal analysis. Consequently, the determination of the temperatures of microstructural transformations in the coarse grained region of the HAZ in the current work was done by the statistical approach applied to the curves generated by the 'In Situ' thermal analysis. Moreover, the FIRST VARIATION OF B was employed to determine the actual ranges of transformation temperatures and some of the graphs obtained are shown from Figures 7.19 to 7.36. Note that series of graphs also includes the VARIATION OF B for each of the FIRST VARIATION OF B presented.

7.5 Results

The transformation temperatures in the coarse grained region of the HAZ's were obtained from the curves generated by the statistical approach as described in Section 7.3. Table 7.2 presents the temperatures of start (S) and end (E) of tranformations obtained in the coarse grained region of the HAZ's of the steels under study.

Table 7.1 - Number of elements present in the data generated by the "In Situ" method

	Range of Temperatures (°C*10)								
H.I. = 3.5kJ/mm	70/65	65/60	60/55	55/50	50/45	45/40	40/35	35/30	30/25
A800D	19	19	24	31	36	49	74	110	173
A500D	19	19	24	31	37	48	75	111	173
A800RD	19	19	24	31	36	49	74	110	173
A500RD	19	19	24	31	37	48	75	111	173

Table 7.2- Transformation Temperatures obtained by the Statistical Approach.

Thermal	**Transfomation Temperature** (°C)			
Cycle	**S**	**E**	**S**	**E**
T12-1	600	500	460	420
T12-2	575	475	420	325
T12-3	590	470	440	360
T12-4	600	490	450	375
T12-5	625	548	441	378
T12-6	633	548	438	379

Table 7.2 - Cont'd

Thermal	Transformation Temperature (°C)			
Cycle	**S**	**E**	**S**	**E**
TB-1	530	460	450	365
TB-2	575	515	425	370
TB-3	590	525	430	350
TB-4	570	520	425	350
TB-5	580	530	440	350
TB-6	610	505	425	360

Table 7.2 - Cont'd

Thermal	**Transformation Temperature (oC)**			
Cycle	**S**	**E**	**S**	**E**
TC-1	560	485	450	350
TC-2	600	510	440	370
TC-3	600	515	435	340
TC-4	580	535	430	360
TC-5	600	530	460	435
TC-6	605	525	450	350

Table 7.2 - Cont'd

Thermal	**Transformation Temperature (oC)**			
Cycle	**S**	**E**	**S**	**E**
TD-1	610	525	450	350
TD-2	560	500	450	340
TD-3	605	485	450	360
TD-4	525	470	425	350
TD-5	570	470	425	325
TD-6	560	475	440	350

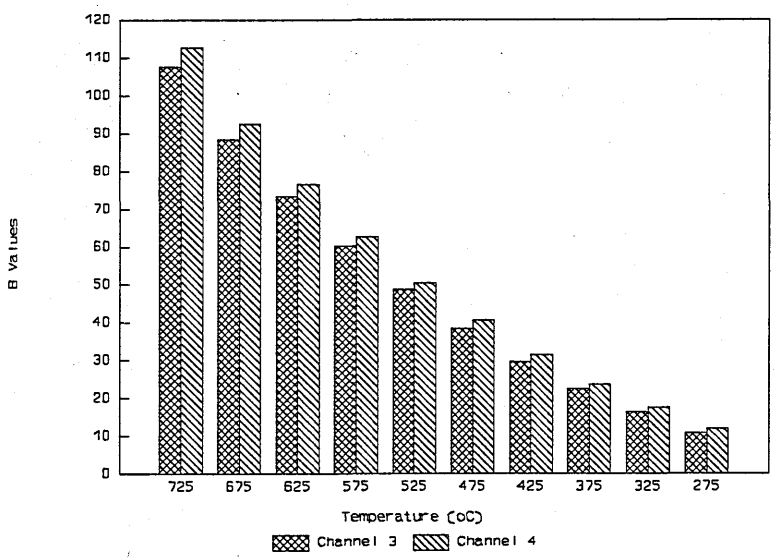

Figure 7.1- Variation of the inclination (B values) of the segments obtained from the segmentation applied to thermal cycles measured.

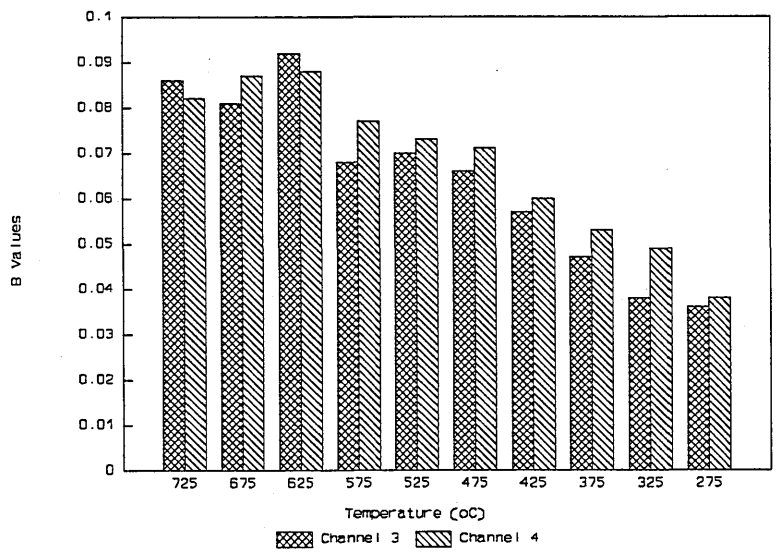

Figure7.2- Variation of B obtained from the segmentation of the curves generated from the temperature/time method applied to thermal cycles used in Figure 7.1.

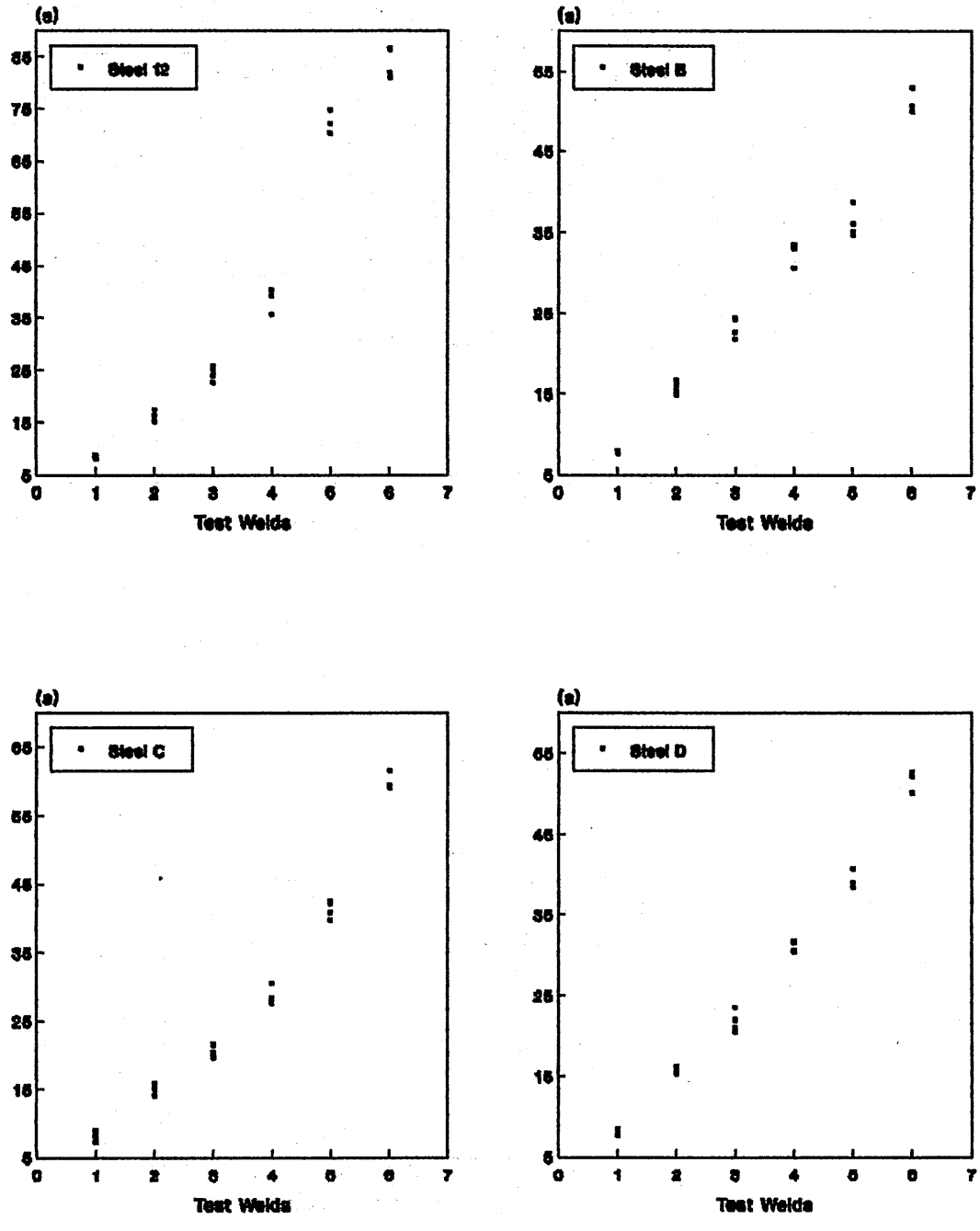

Figure7.3- Variation of the cooling time through 800-300°C in the test welds.

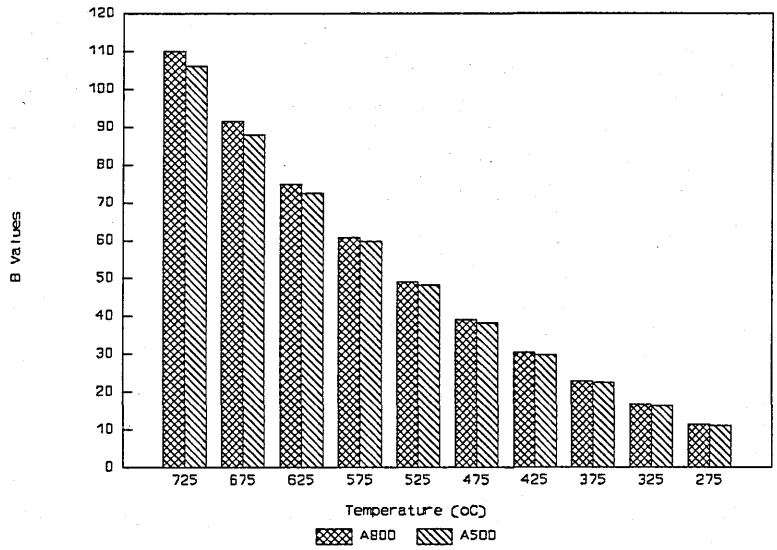

Figure 7.4- Variation of the inclination B obtained from average thermal curves of thermal cycles measured.

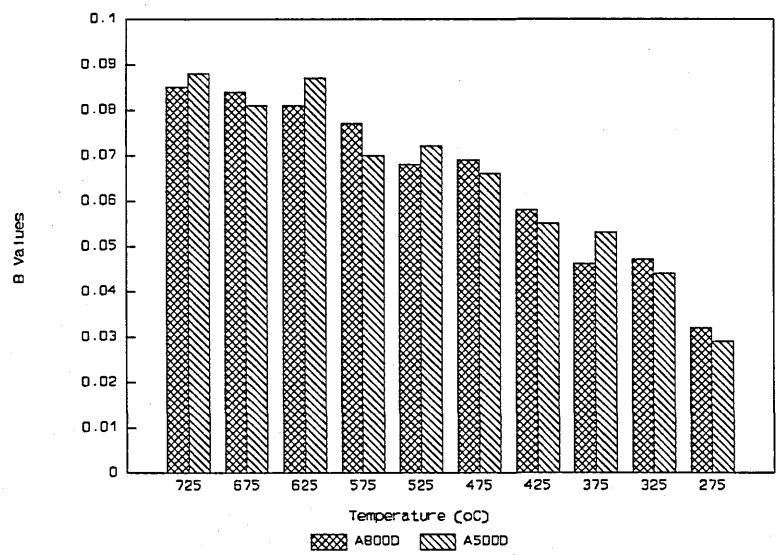

Figure 7.5- Variation of the inclination of the segments obtained from the temperature/time method applied to the average thermal curves used in Figure 7.3.

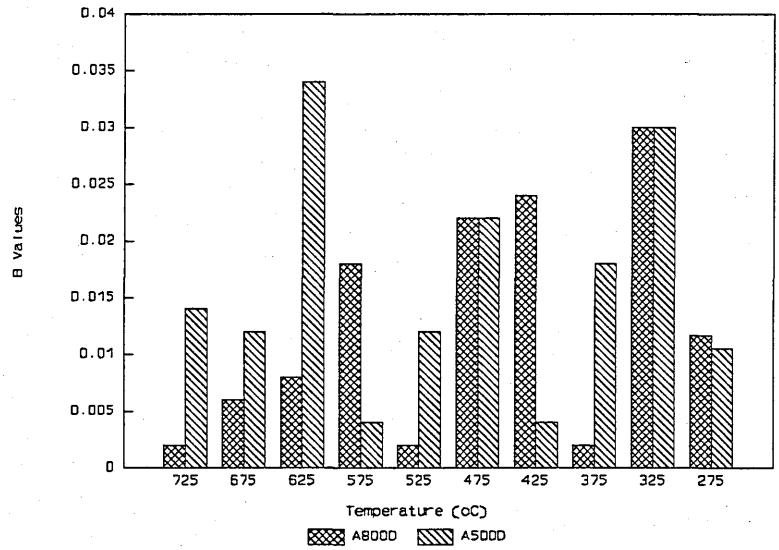

Figure 7.6- Variation of the differences of the inclination of the segments used in Figure 7.5.

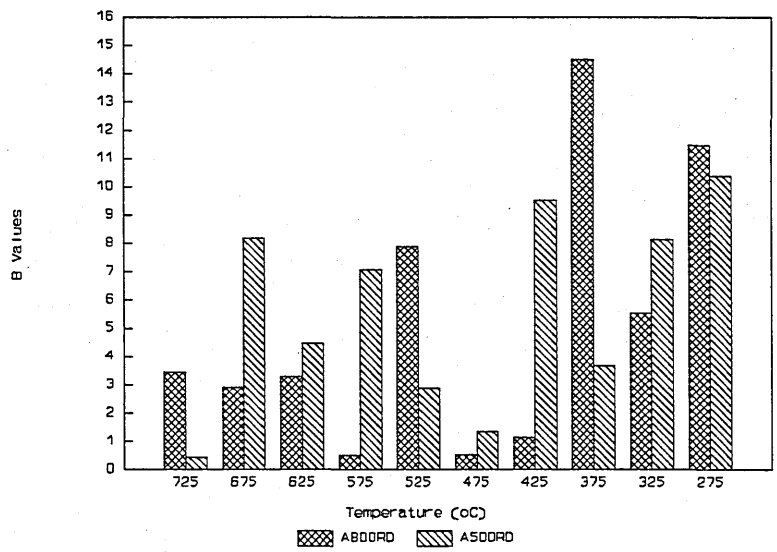

Figure 7.7- Variation of the differences of the inclination of the segments obtained from the temperature/temperature method applied to the average thermal curve.

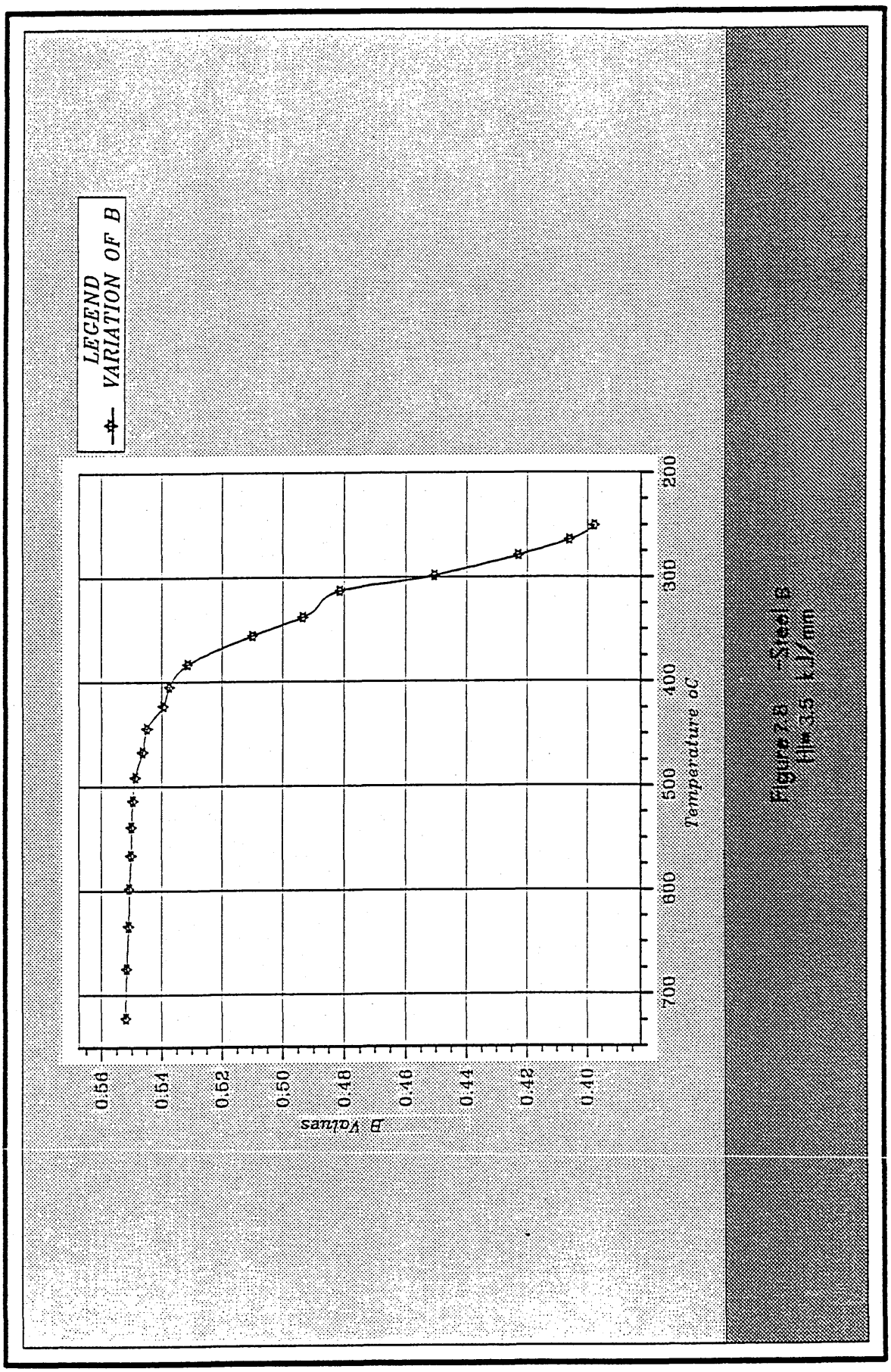

Figure 7.8 -Steel B
Hin 3.5 kJ/mm

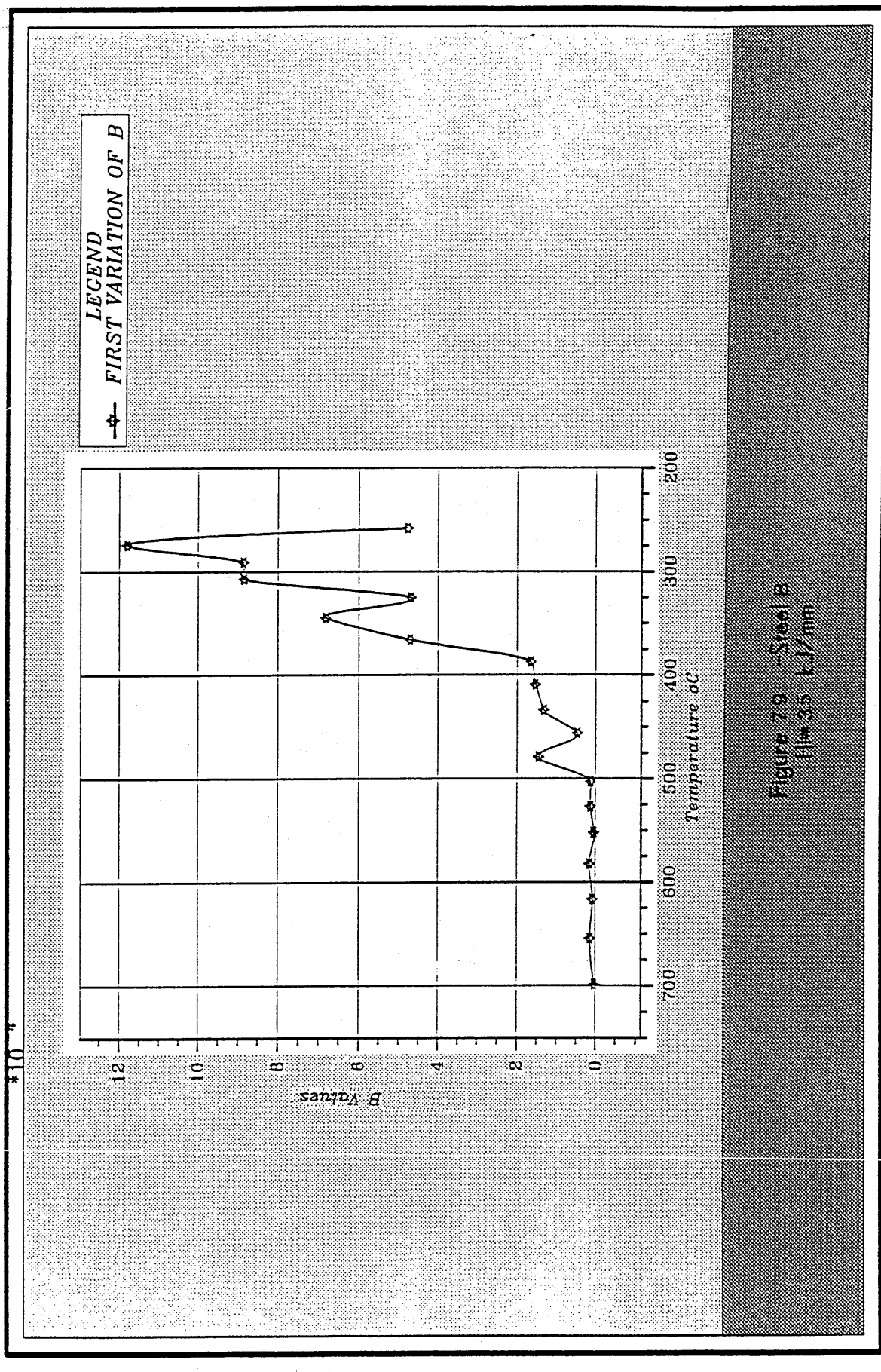

Figure 79 -Steel B
Hin 35 kJ/mm

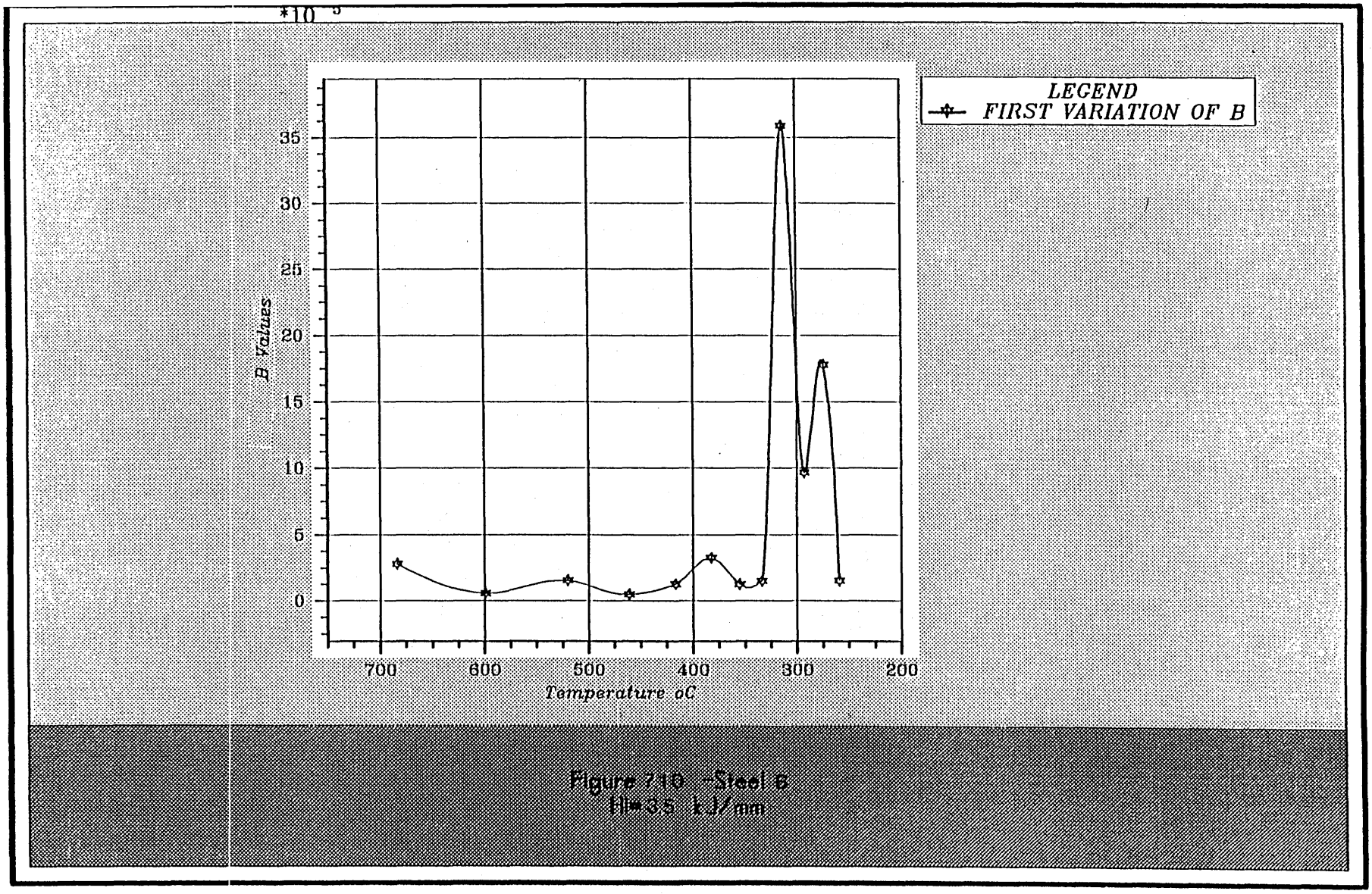

Figure 7.10 -Steel B
H= 3.5 kJ/mm

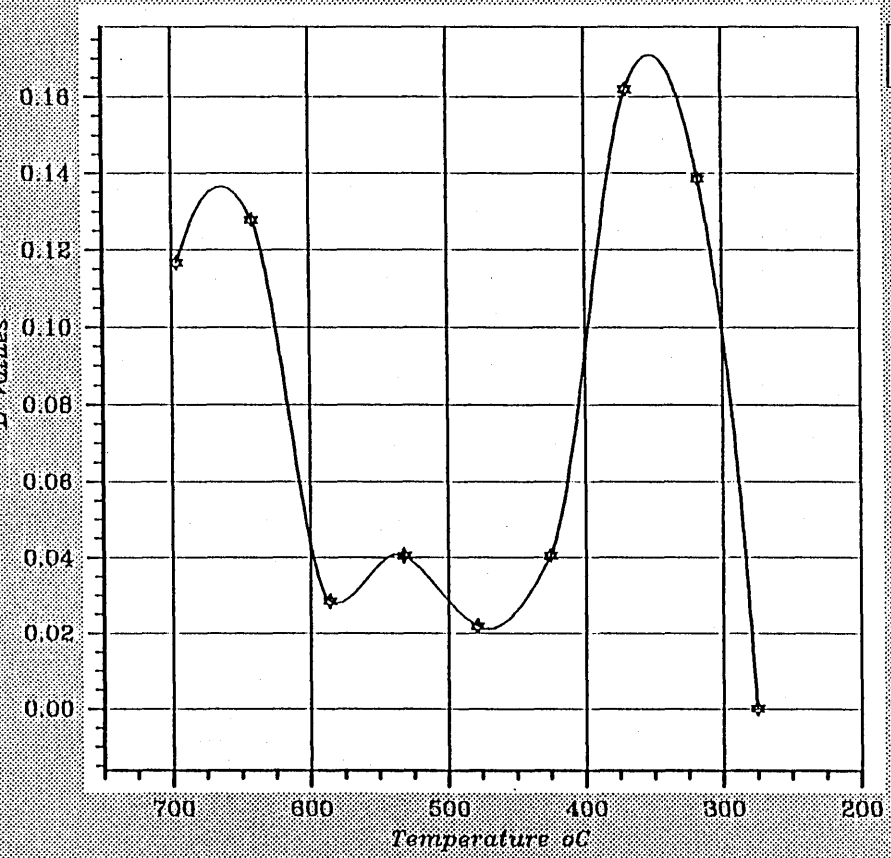

Figure 2.11 -Steel 6
H= 3.5 kJ/mm

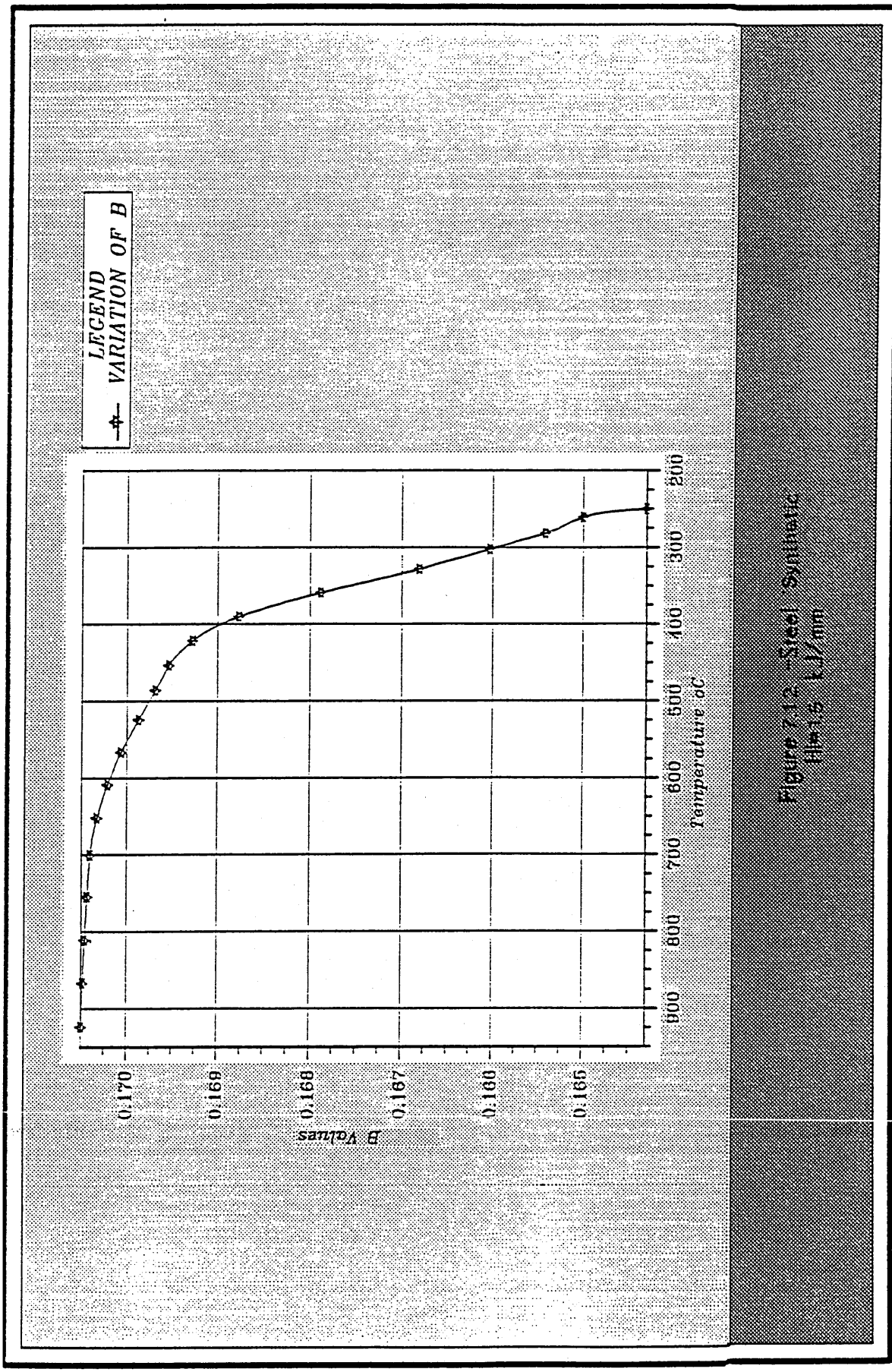

Figure 7.12 -Steel Synthetic
Heat 15 kJ/mm

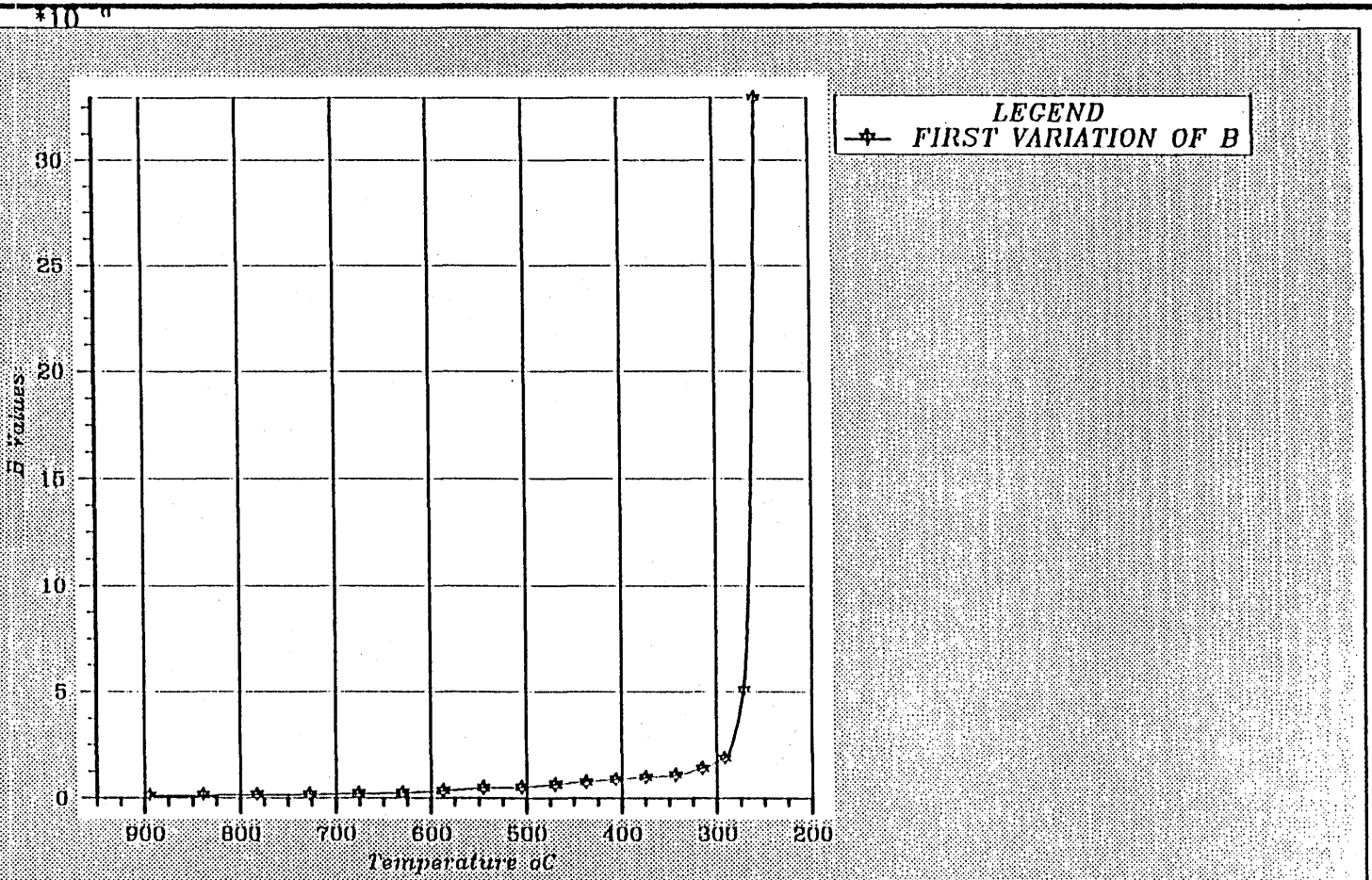

Figure 7.13 -Steel Synthetic
H=1.5 kJ/mm

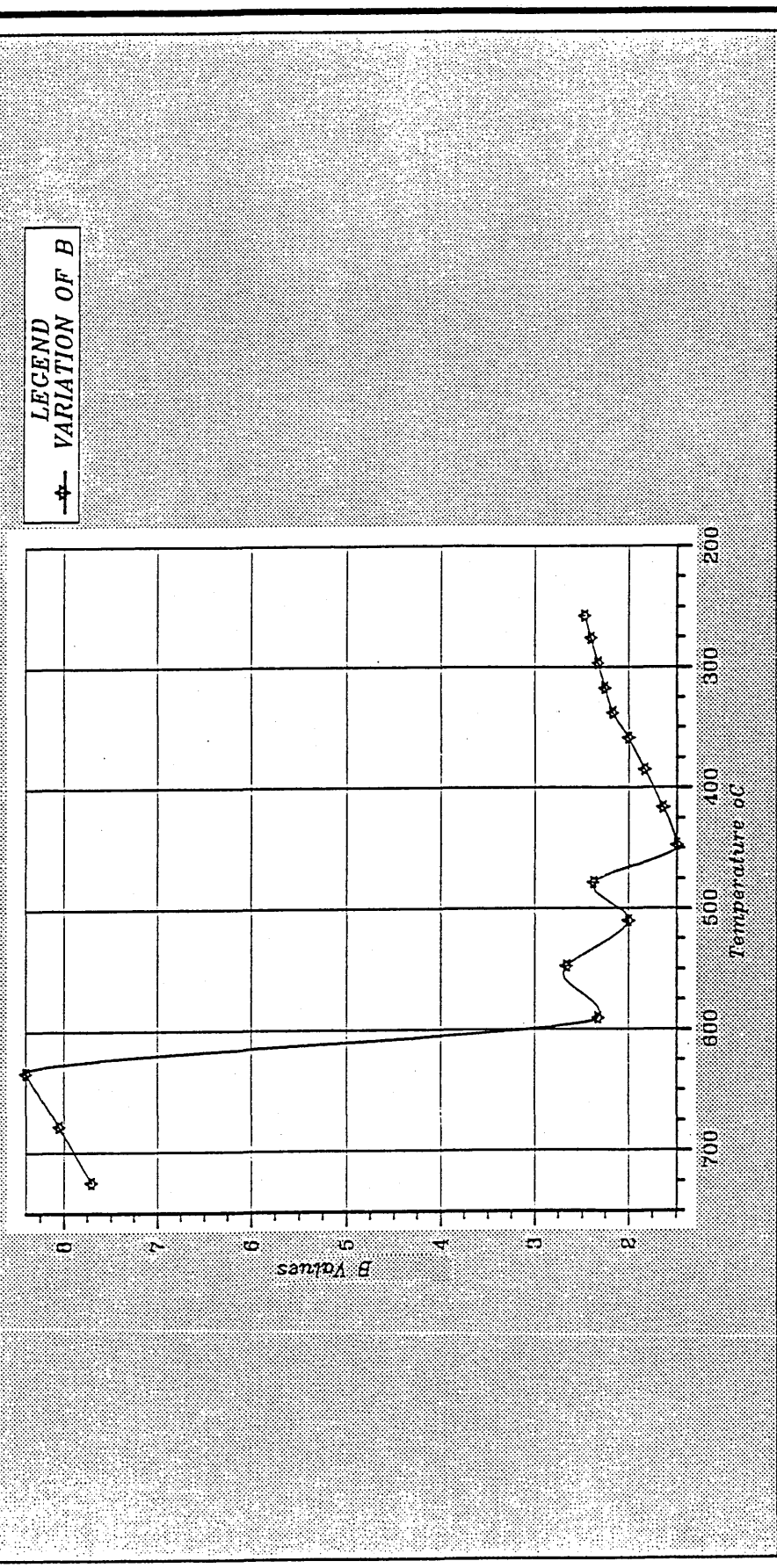

Figure 7.14 -Steel Symbiote
Hi= 1.5 kJ/mm

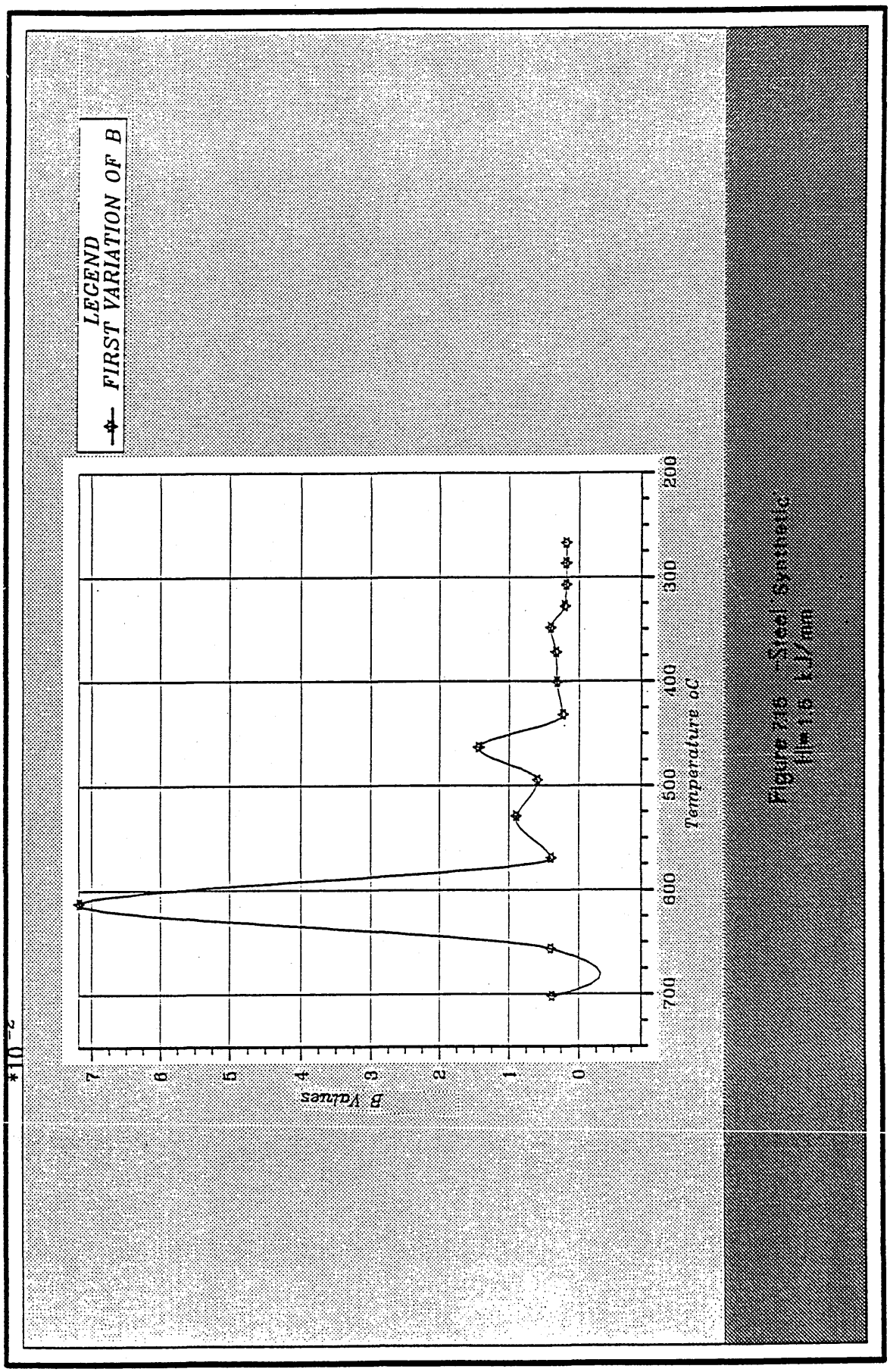

Figure 7.18 -Steel Synthetic
H= 1.6 1.1/mm

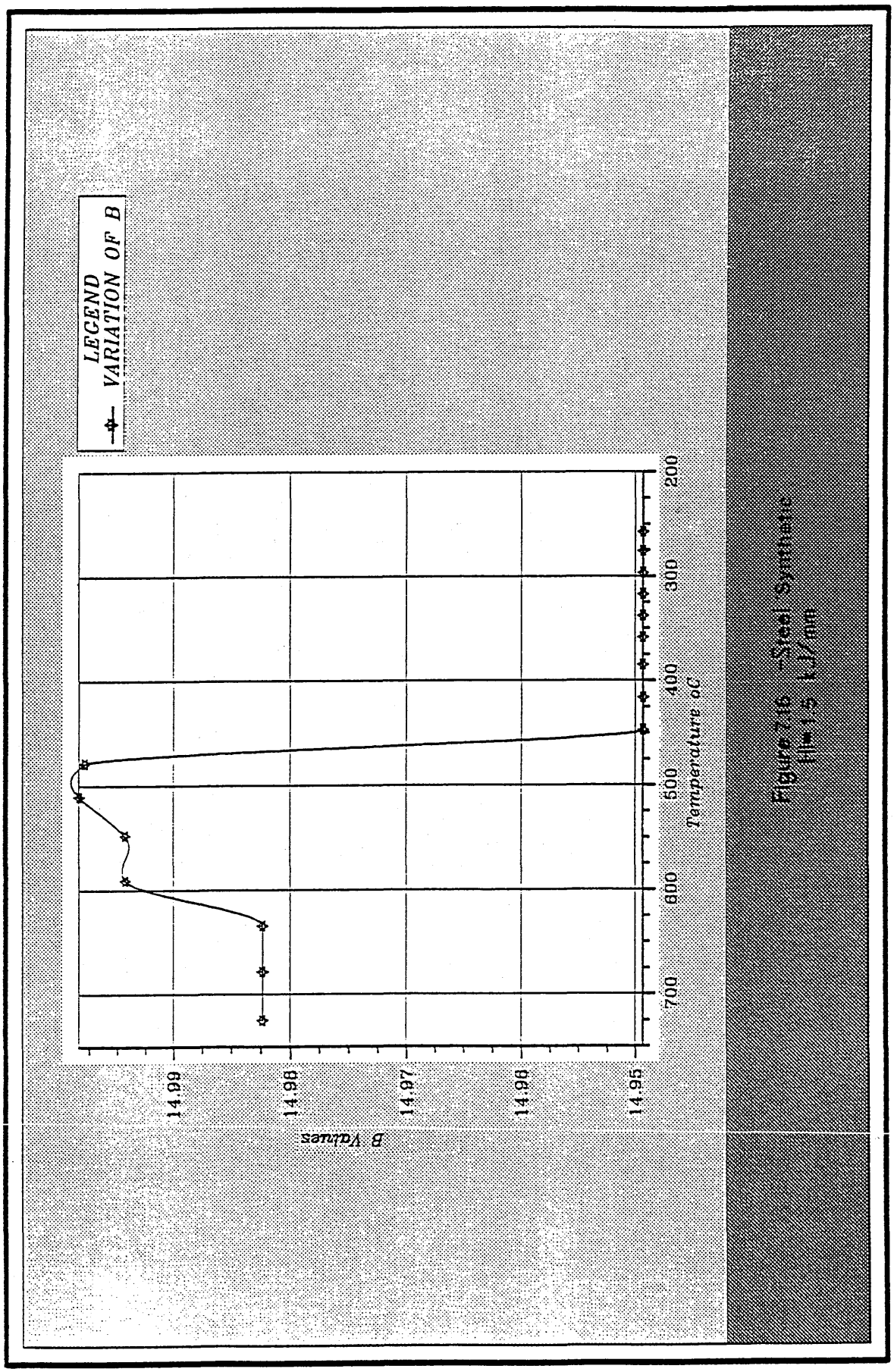

Figure 7.16 -Steel Synthetic
H= 1.5 kJ/mm

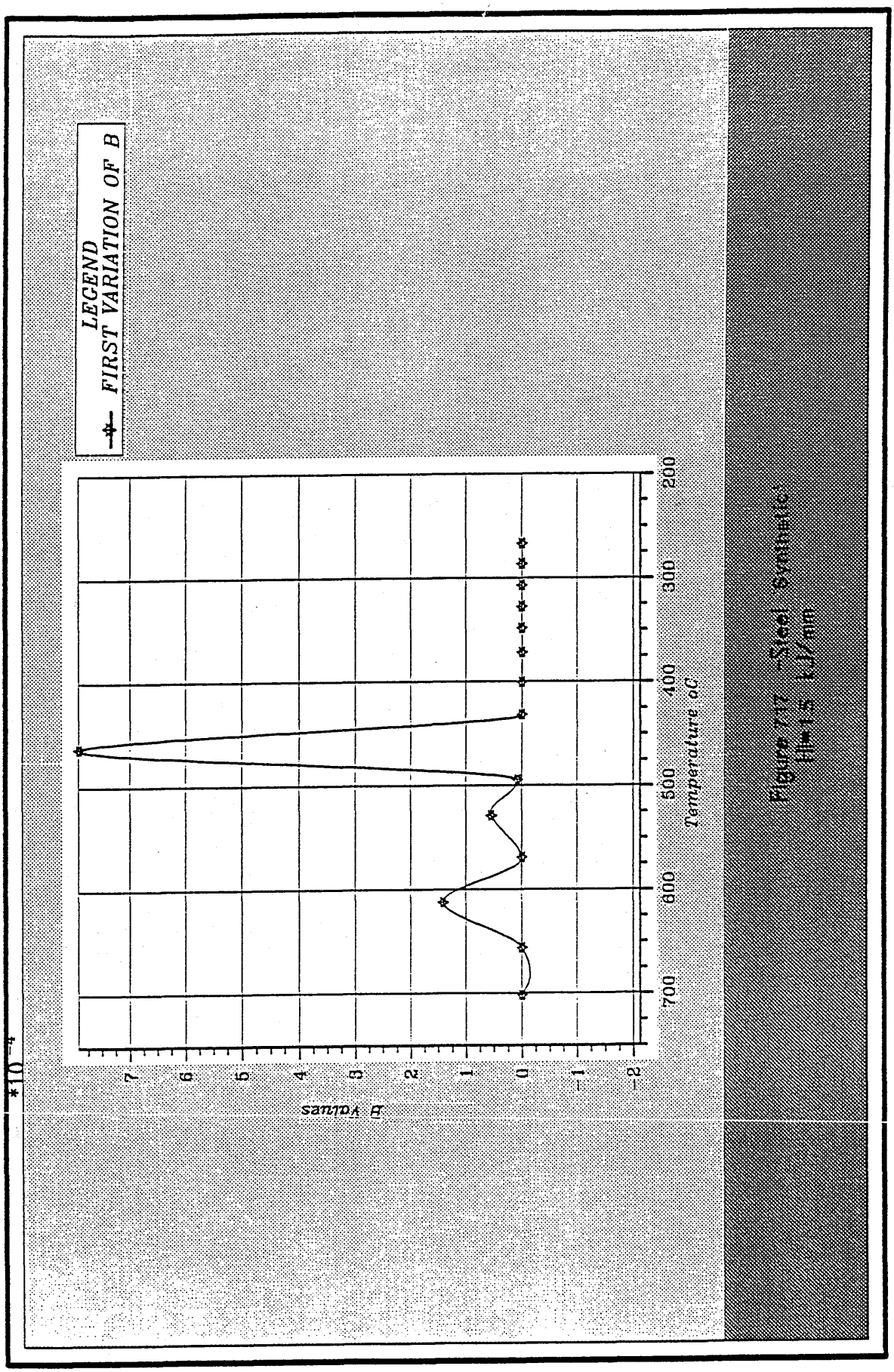

Figure 7.17 -Steel Synthetic-

(a)

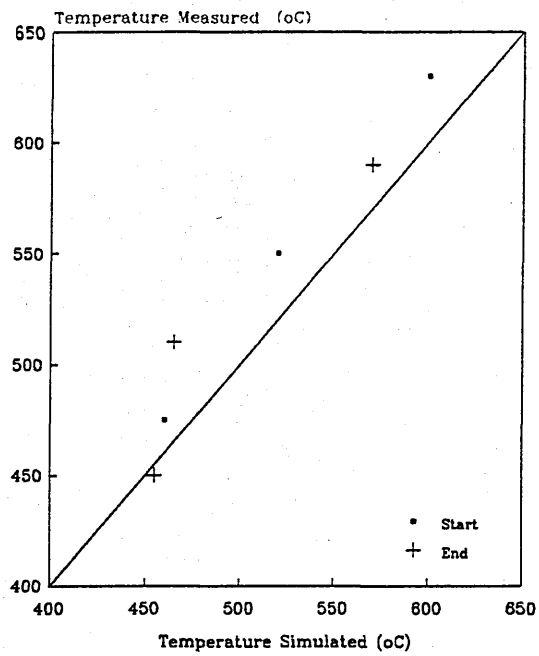

(b)

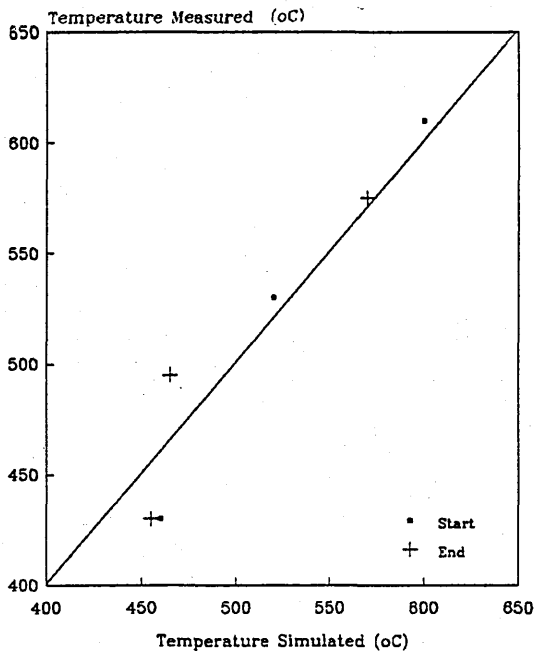

Figure 7.18- (a) Reproducibility of the temperatures of start and end of transformation obtained from the curve VARIATION OF B.

(b) Reproducibility of the temperatures of start an end of transformation from the FIRST VARIATION OF B.

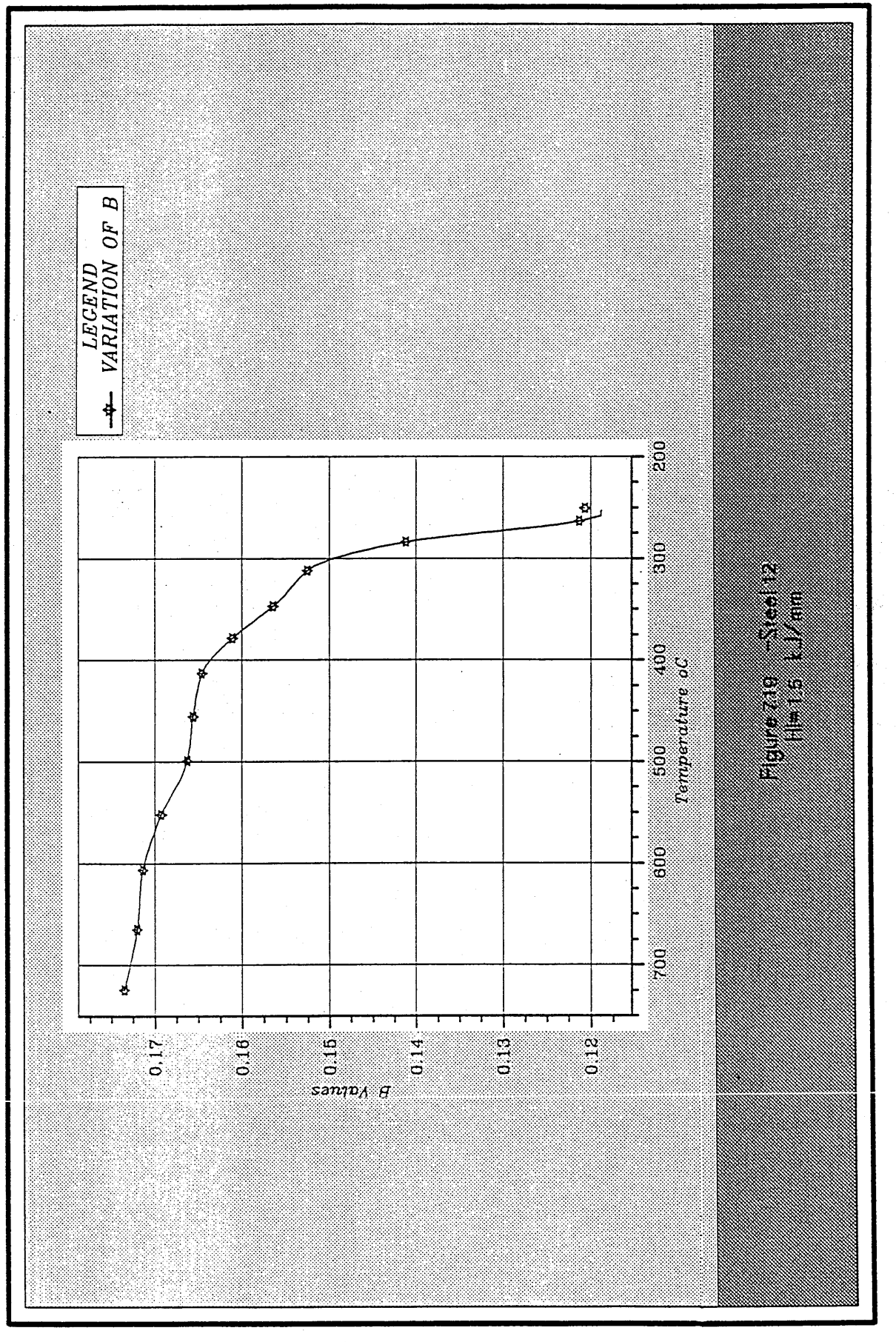

Figure 7.10 -Steel 12
H= 1.5 kJ/mm

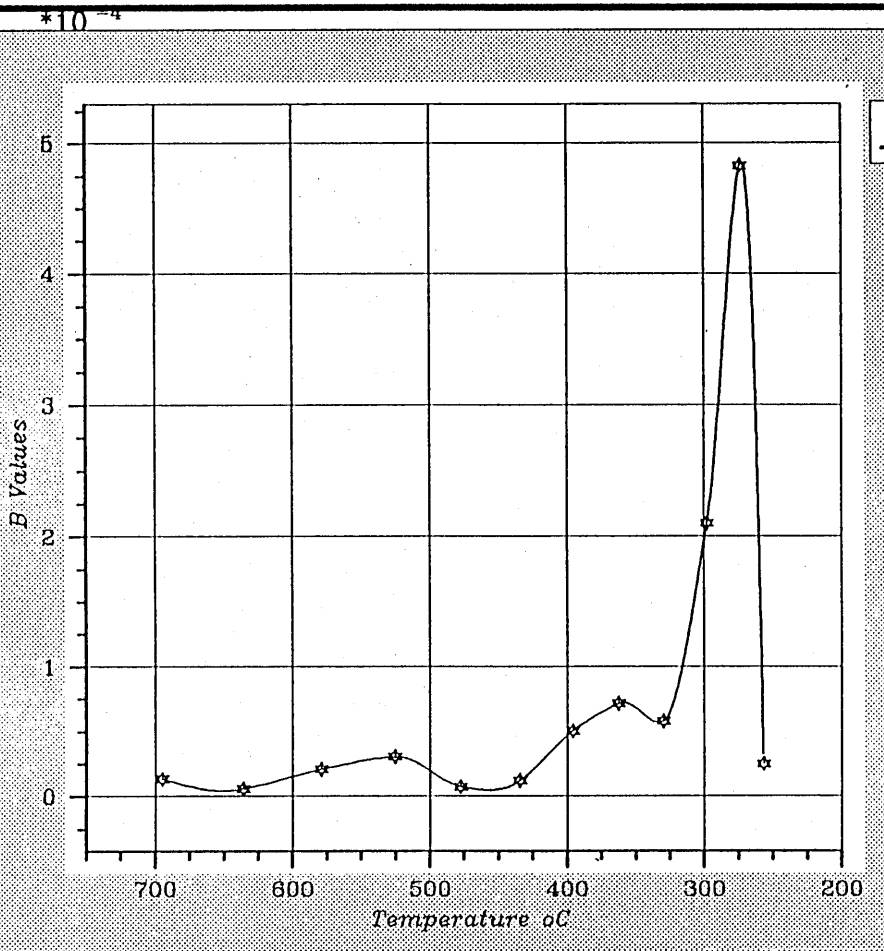

Figure 7.20 -Steel 12
H=1.5 kJ/mm

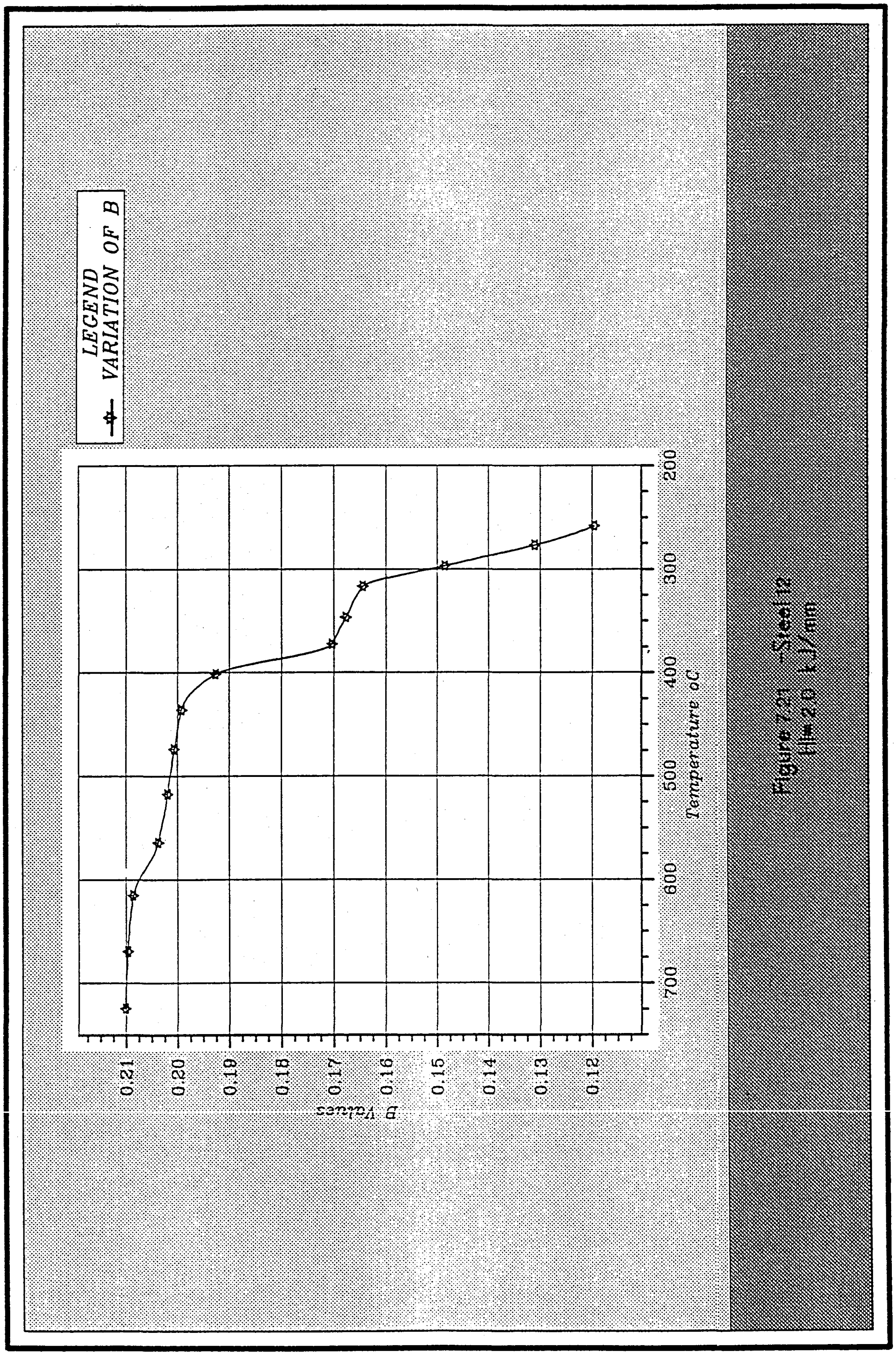

Figure 7.21 -Steel 12
Hi= 2.0 kJ/mm

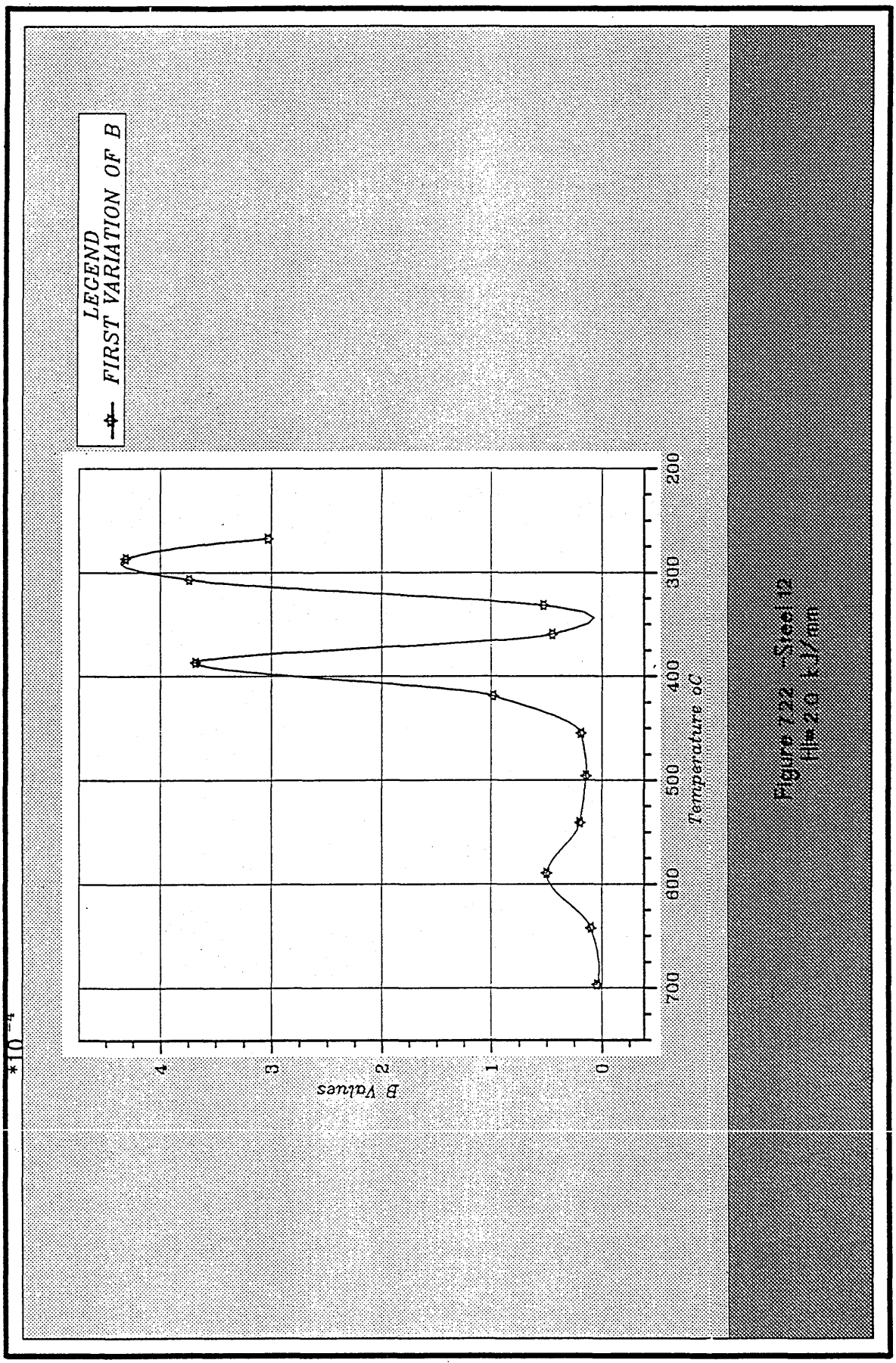

Figure 7.22 -Steel 12
H=2.0 kJ/mm

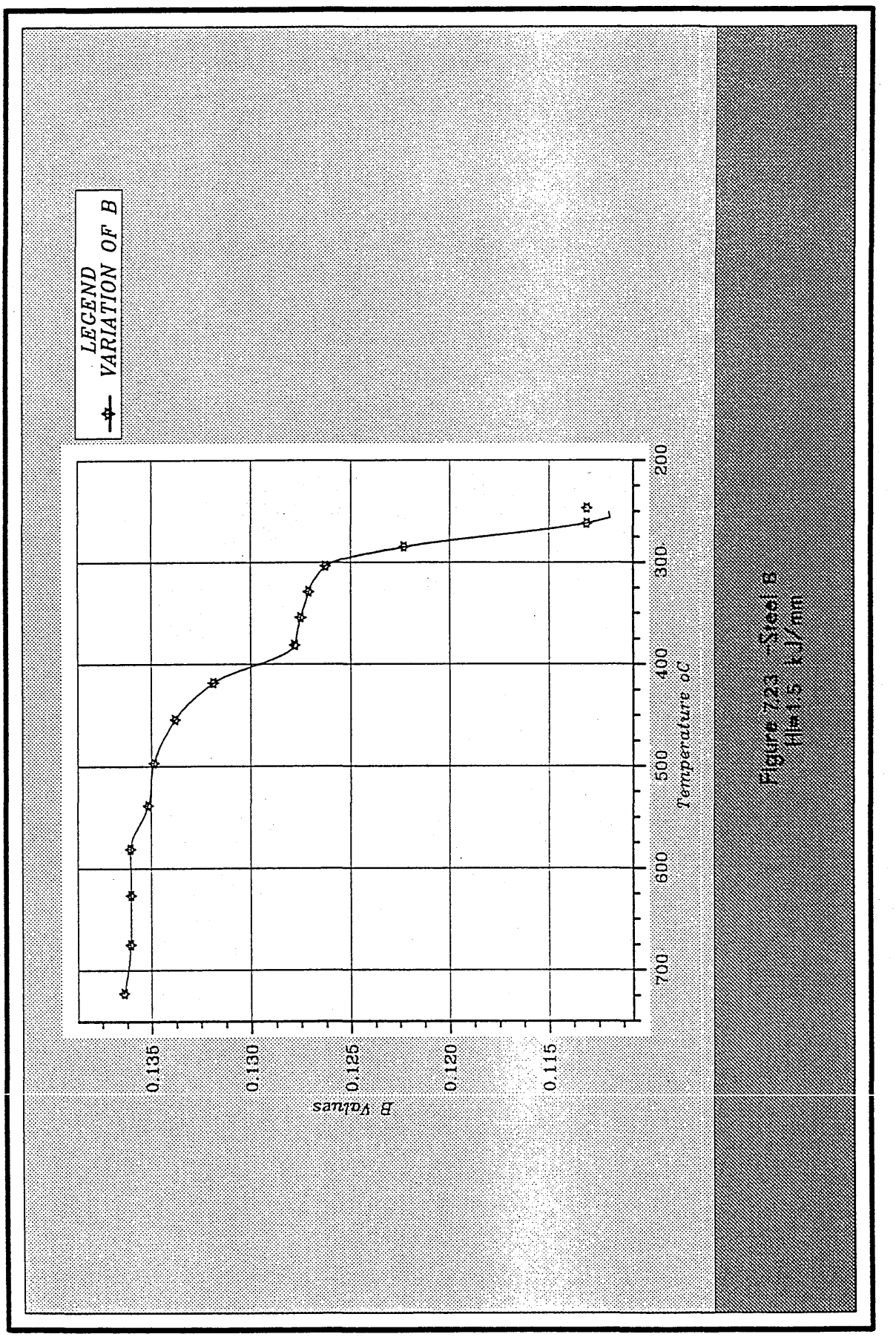

Figure 7.23 -Steel B
H=1.5 kJ/mm

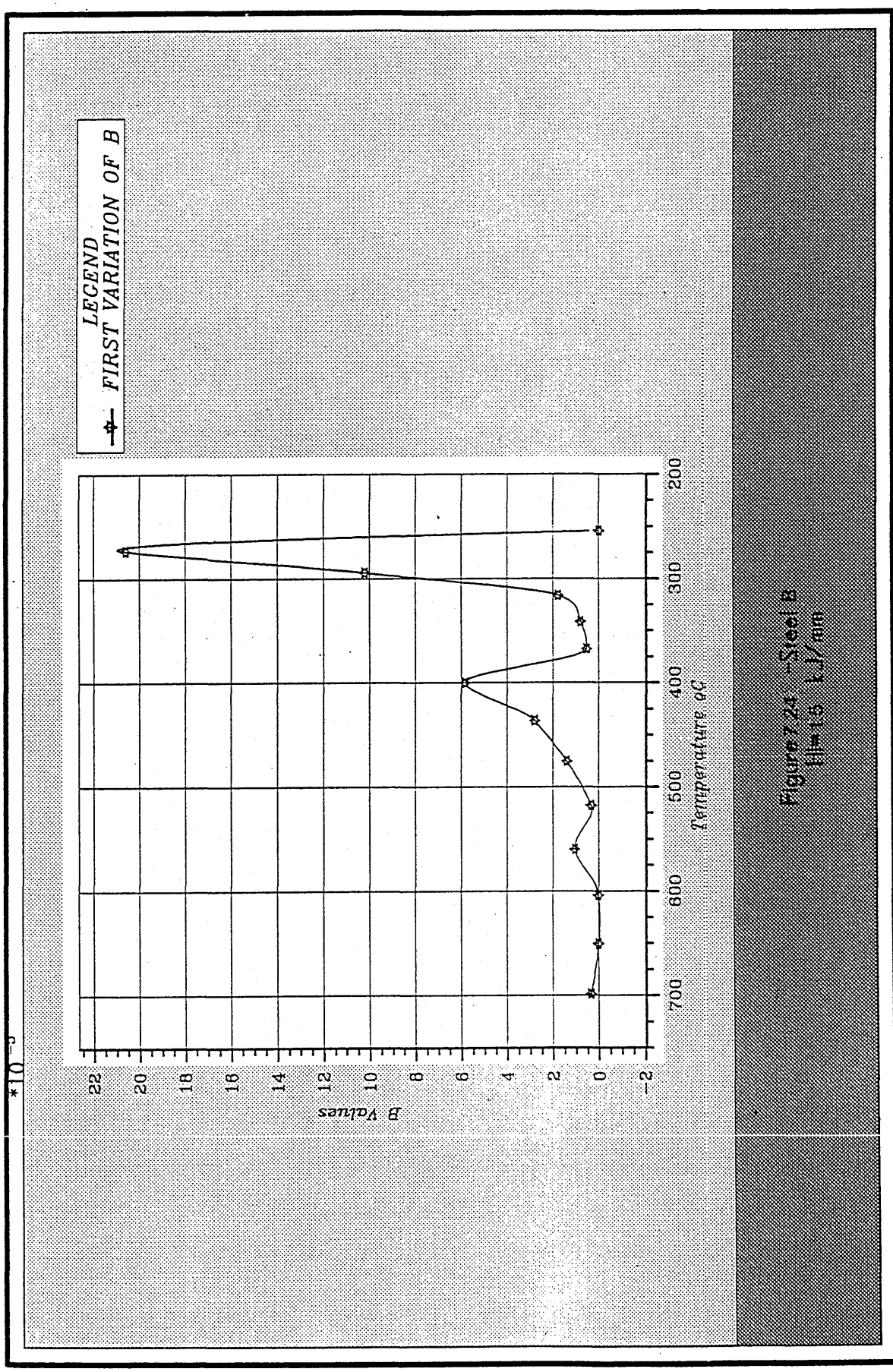

Figure 7.24 -Steel B
ll=15 1.7/cm

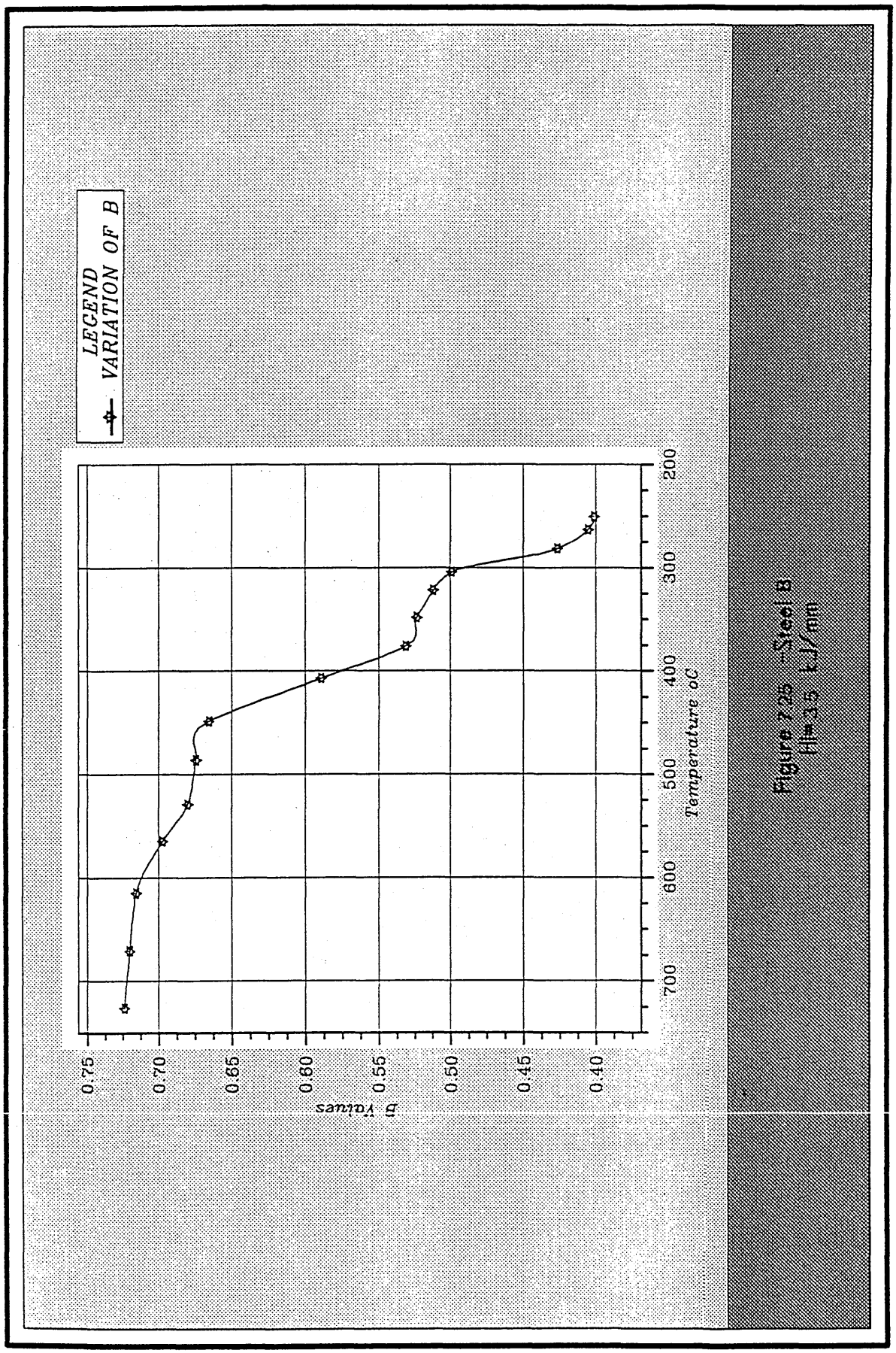

Figure 7.25 -Steel B
H= 35 kJ/mm

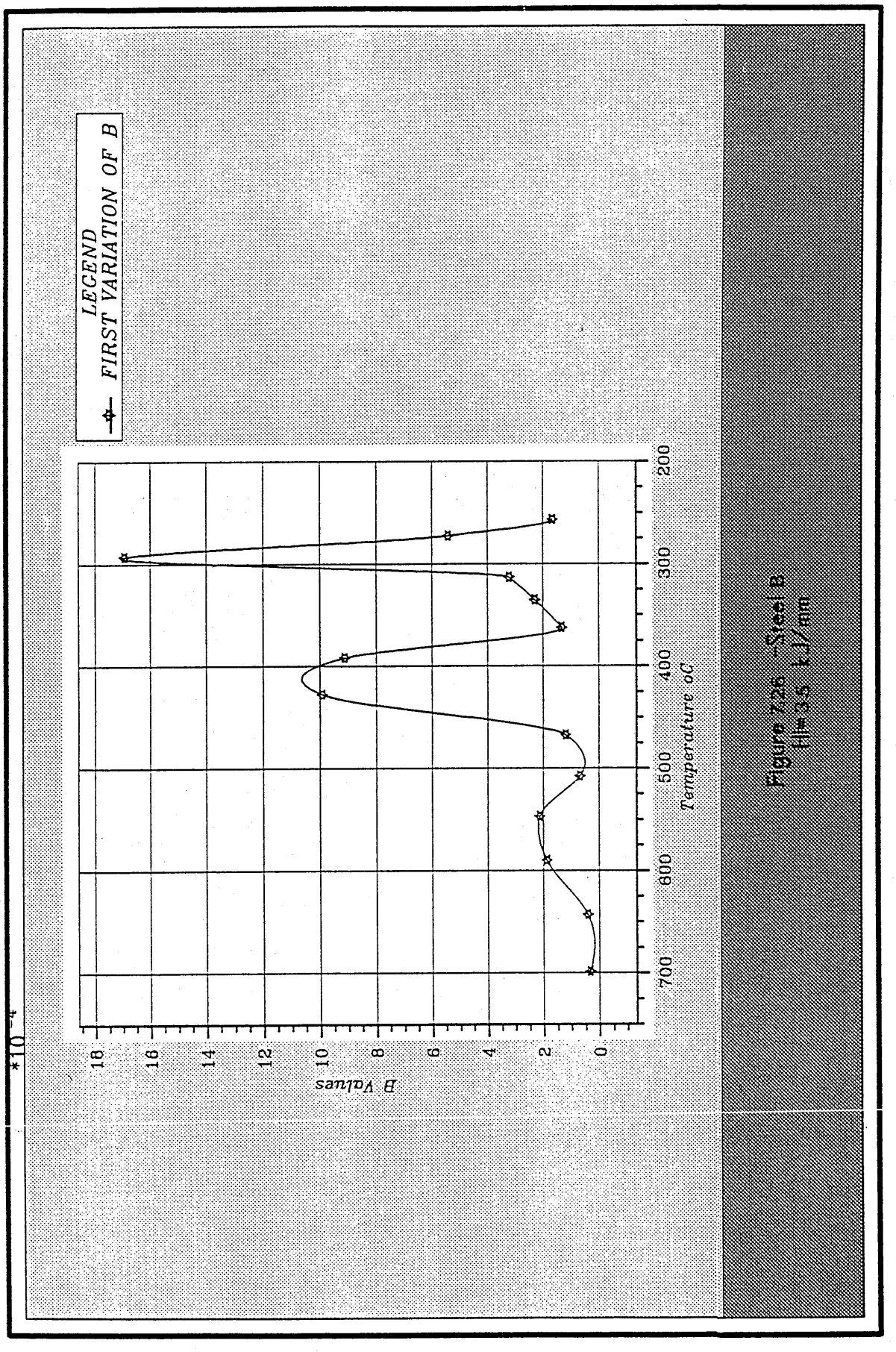

Figure 7.26 -Steel B
H=3.5 KJ/mm

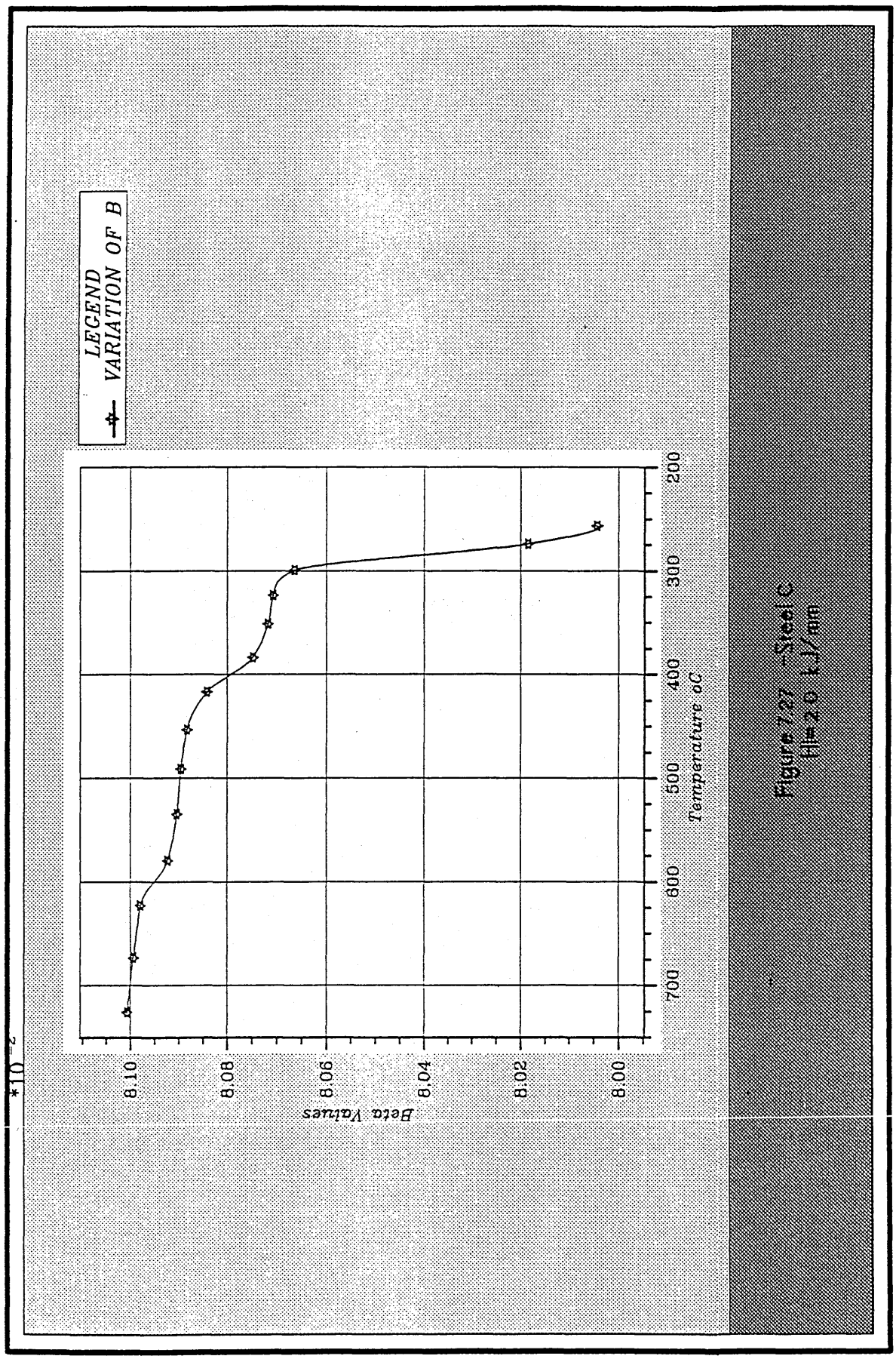

Figure 7.27 -Steel C
Hi=2.0 kJ/mm

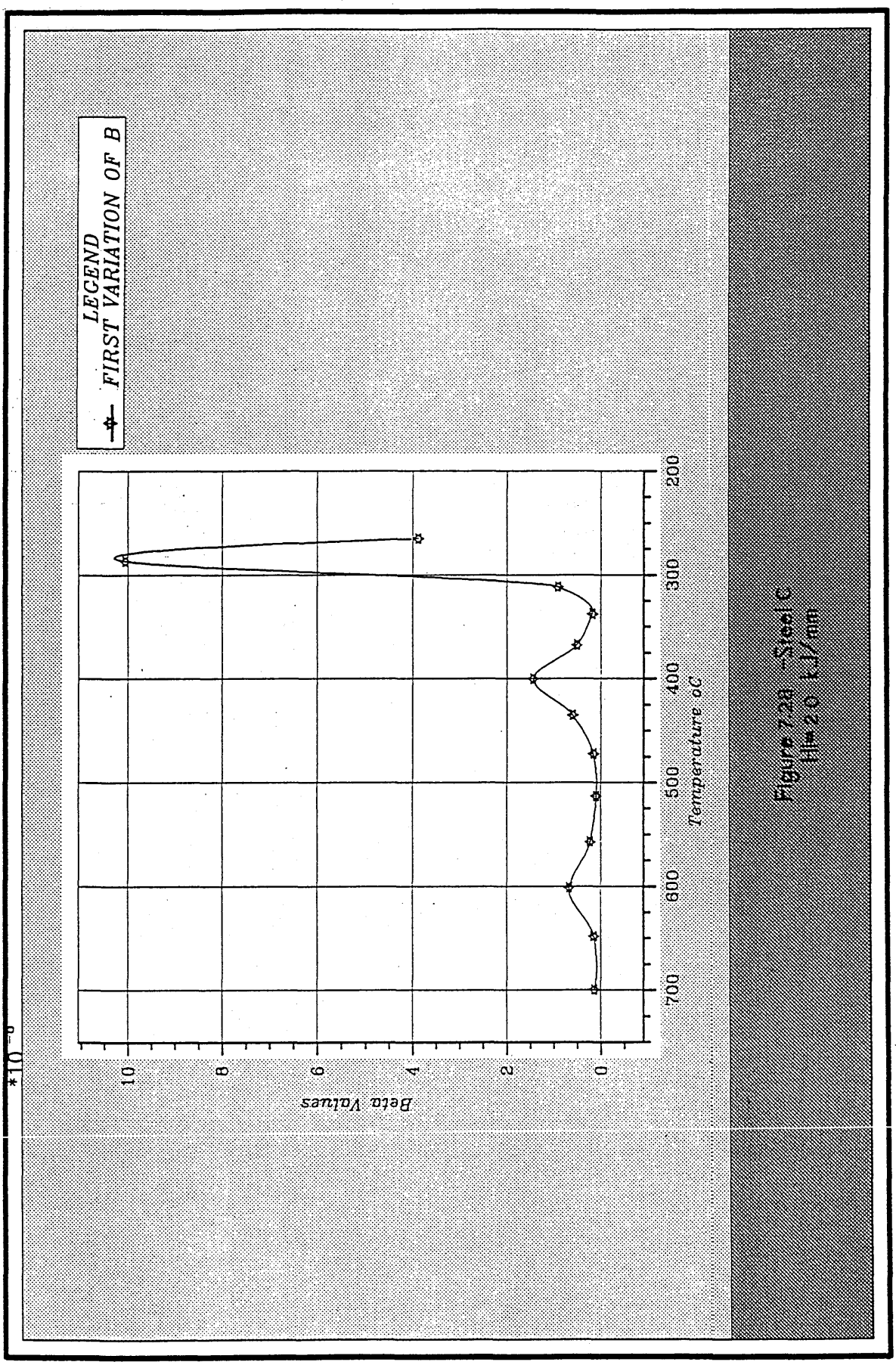

Figure 7.28 -Steel C
I/E= 2.0 kJ/mm

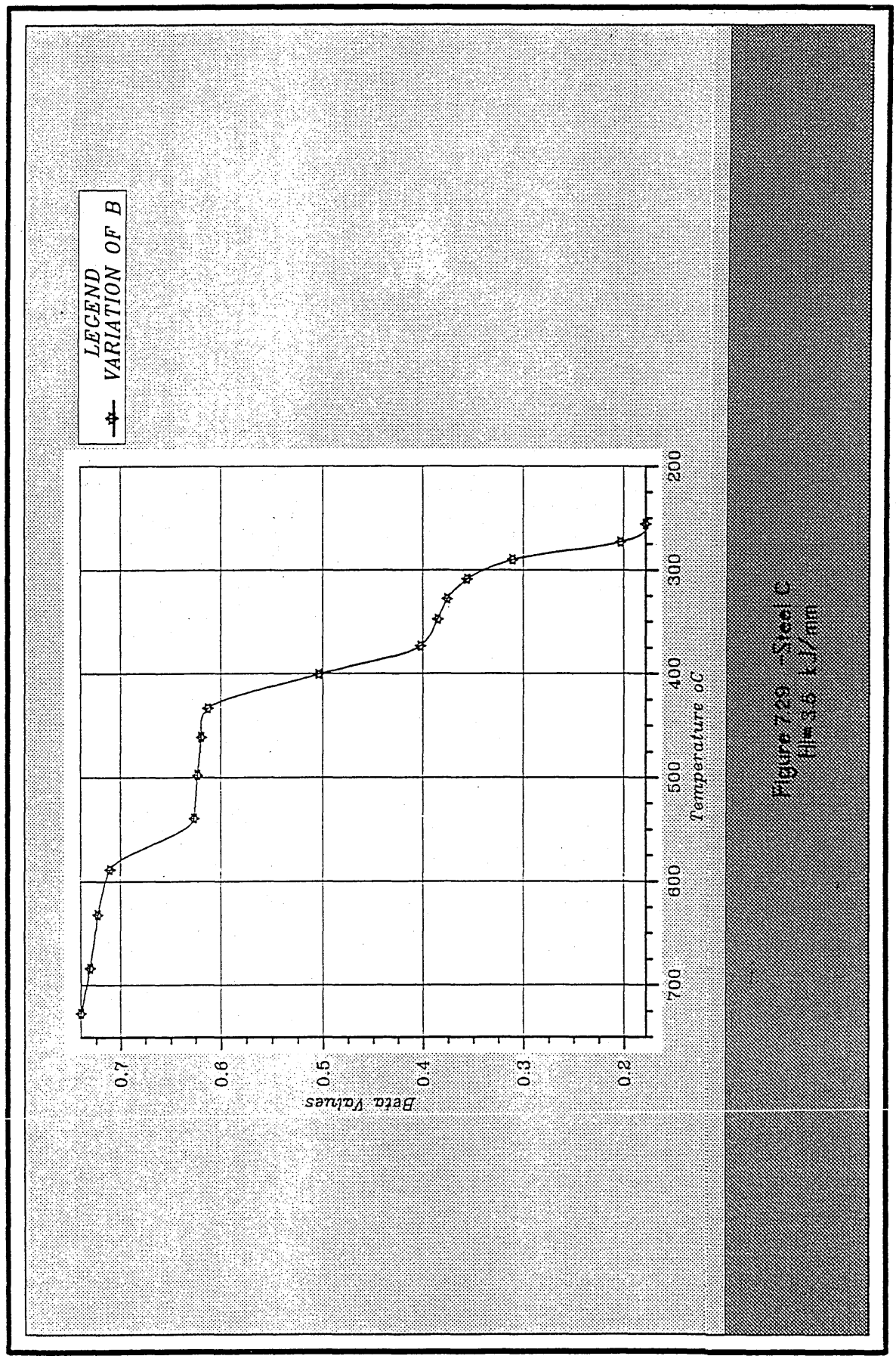

Figure 7.29 - Steel C
Hi=3.5 kJ/mm

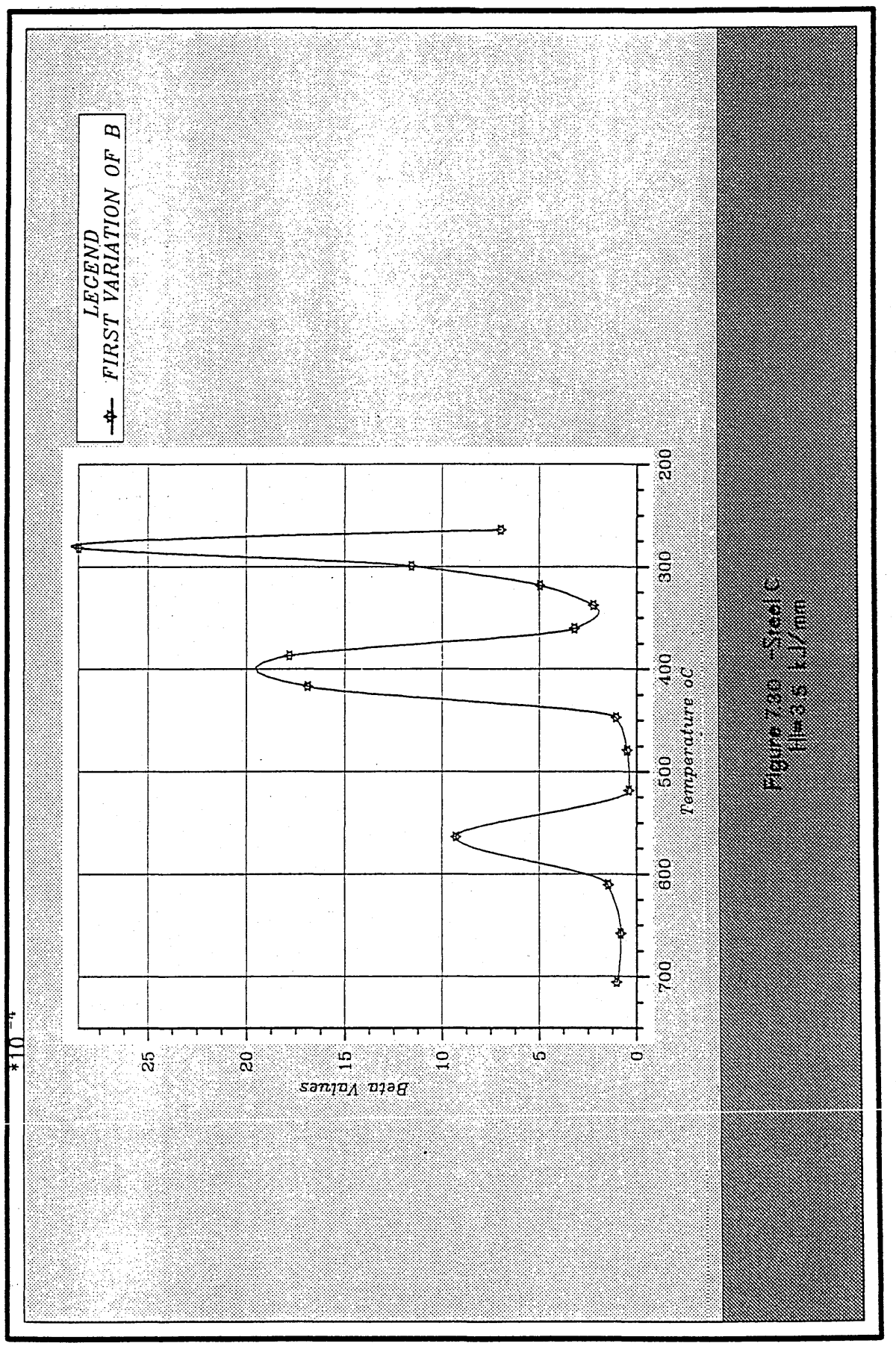

Figure 7.30 -Steel C
H=35 kJ/mm

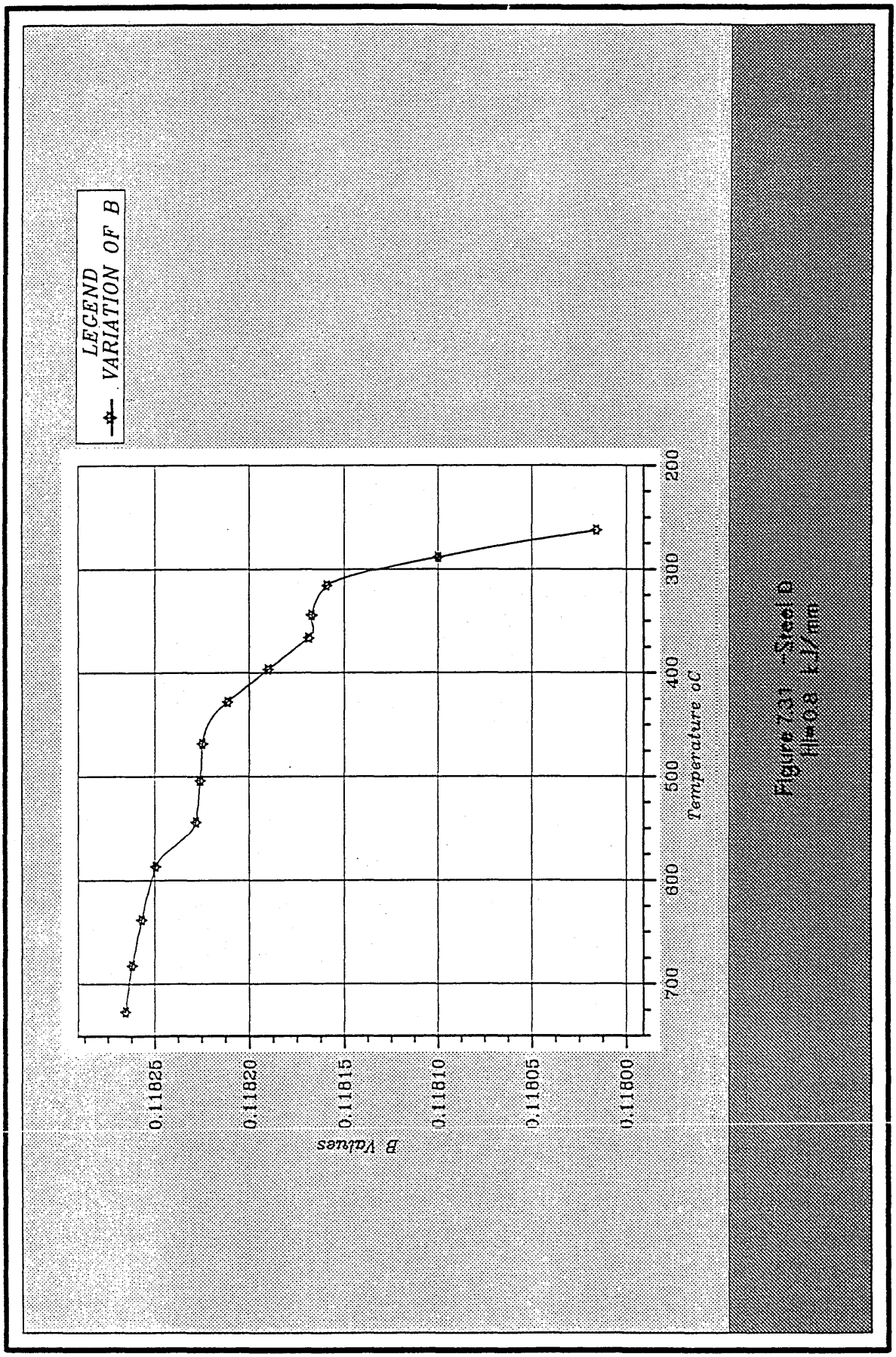

Figure 7.31 -Steel D
H=0.8 kJ/mm

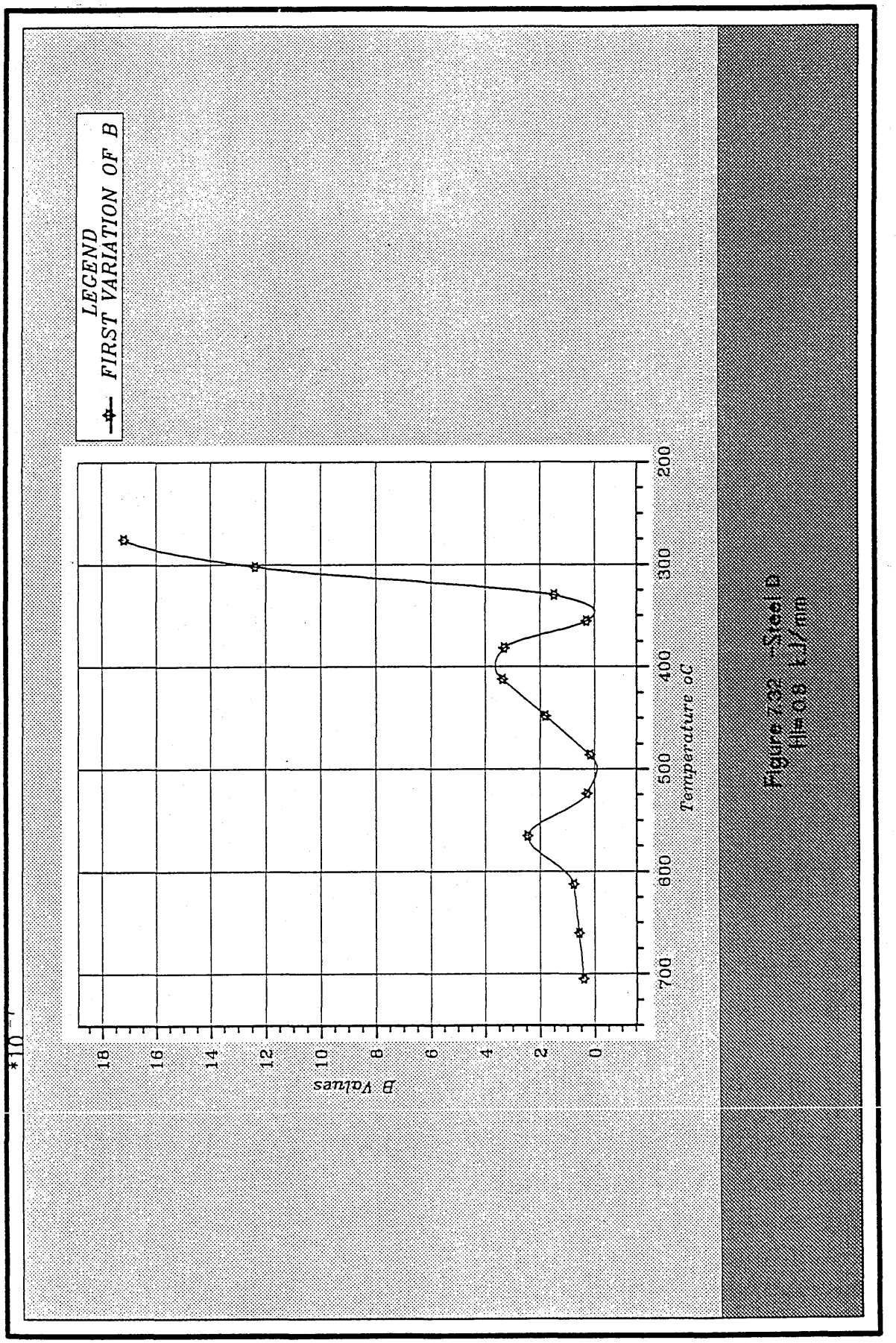

Figure 7.32 -Steel B
H= 0.8 kJ/mm

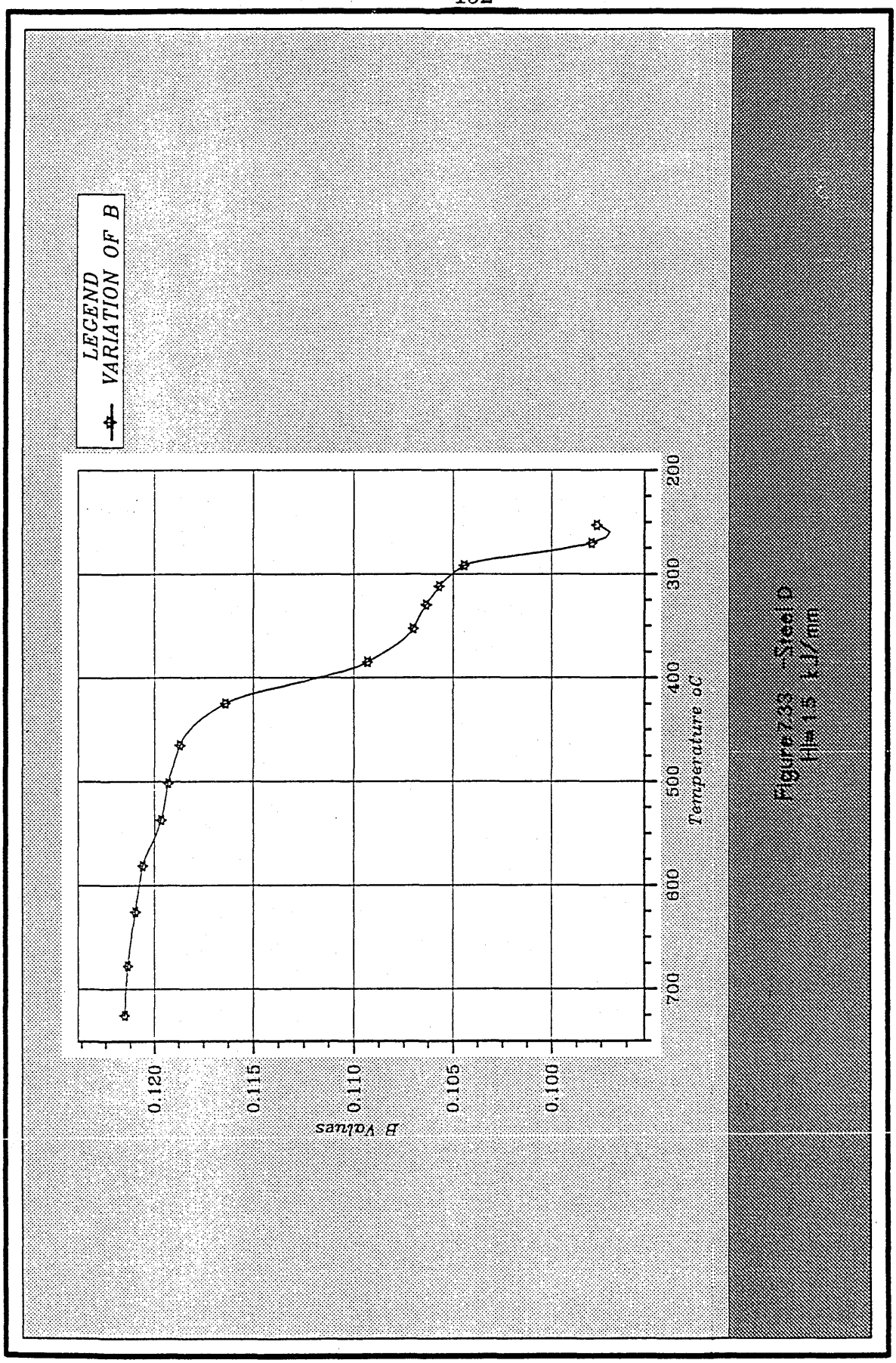

Figure 7.33 -Steel D
H= 1.5 kJ/mm

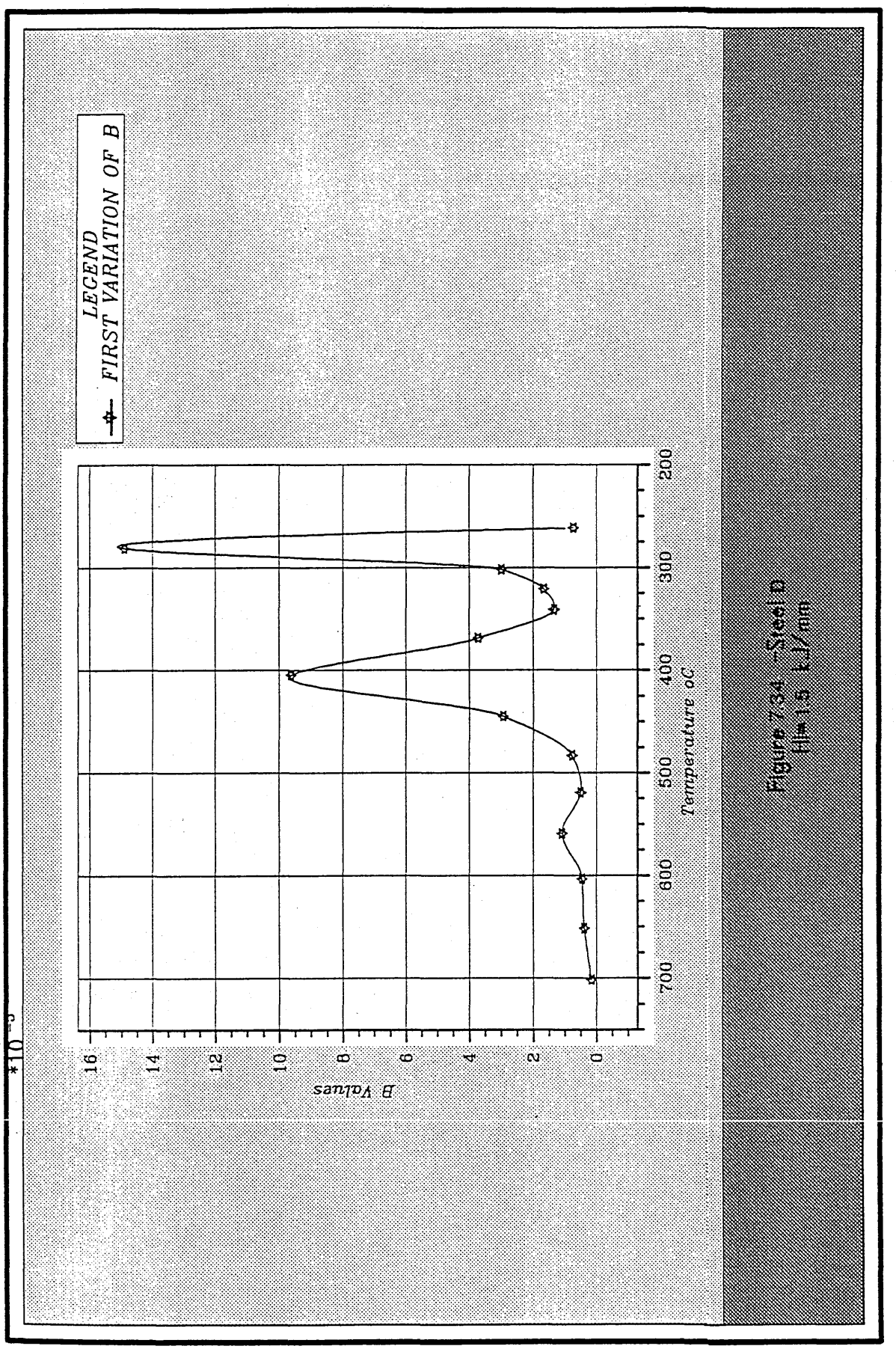

Figure 7.34 -Steel D
H= 1.5 kJ/mm

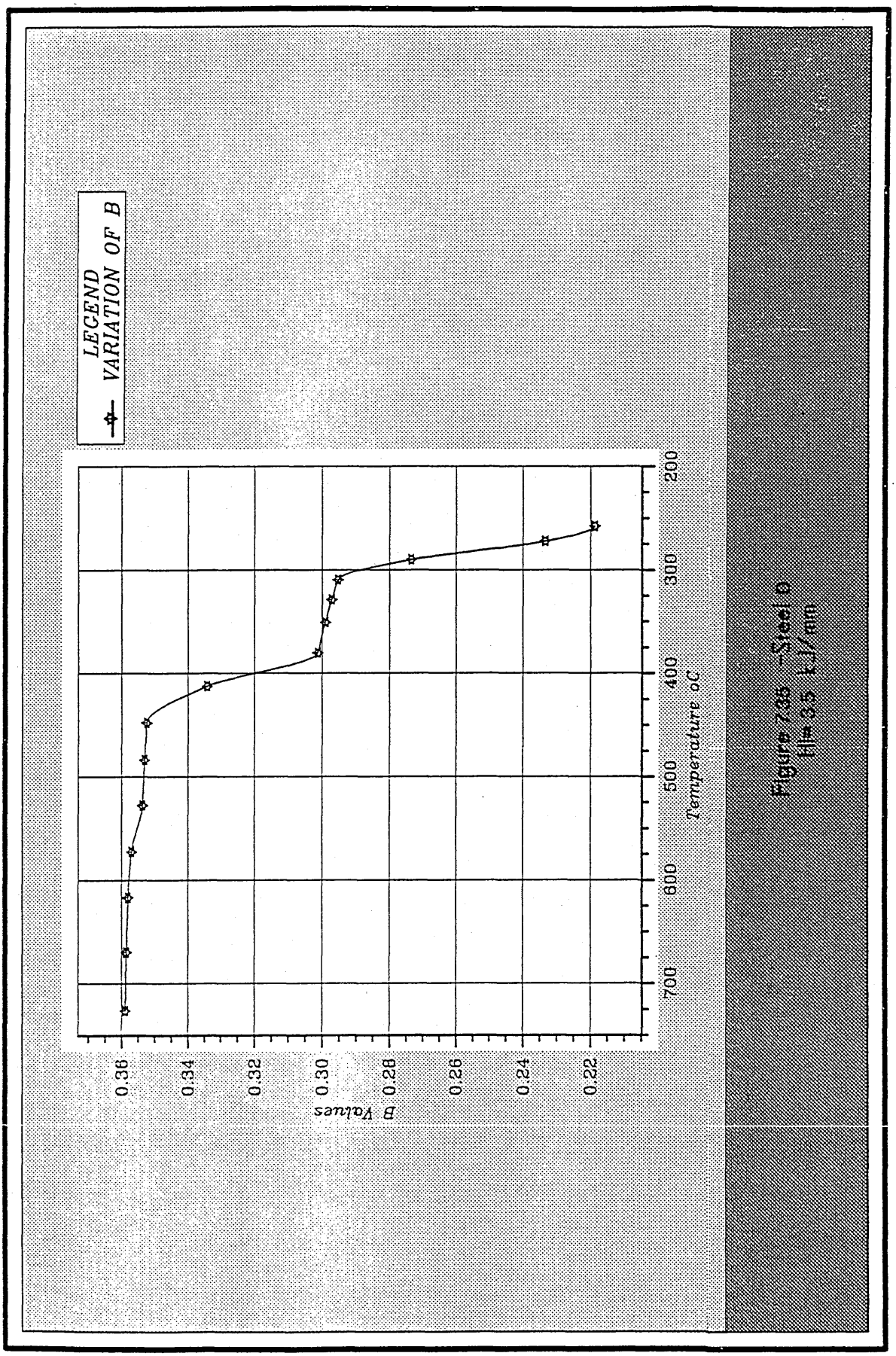

Figure 7.35 -Steel D
H= 3.5 kJ/mm

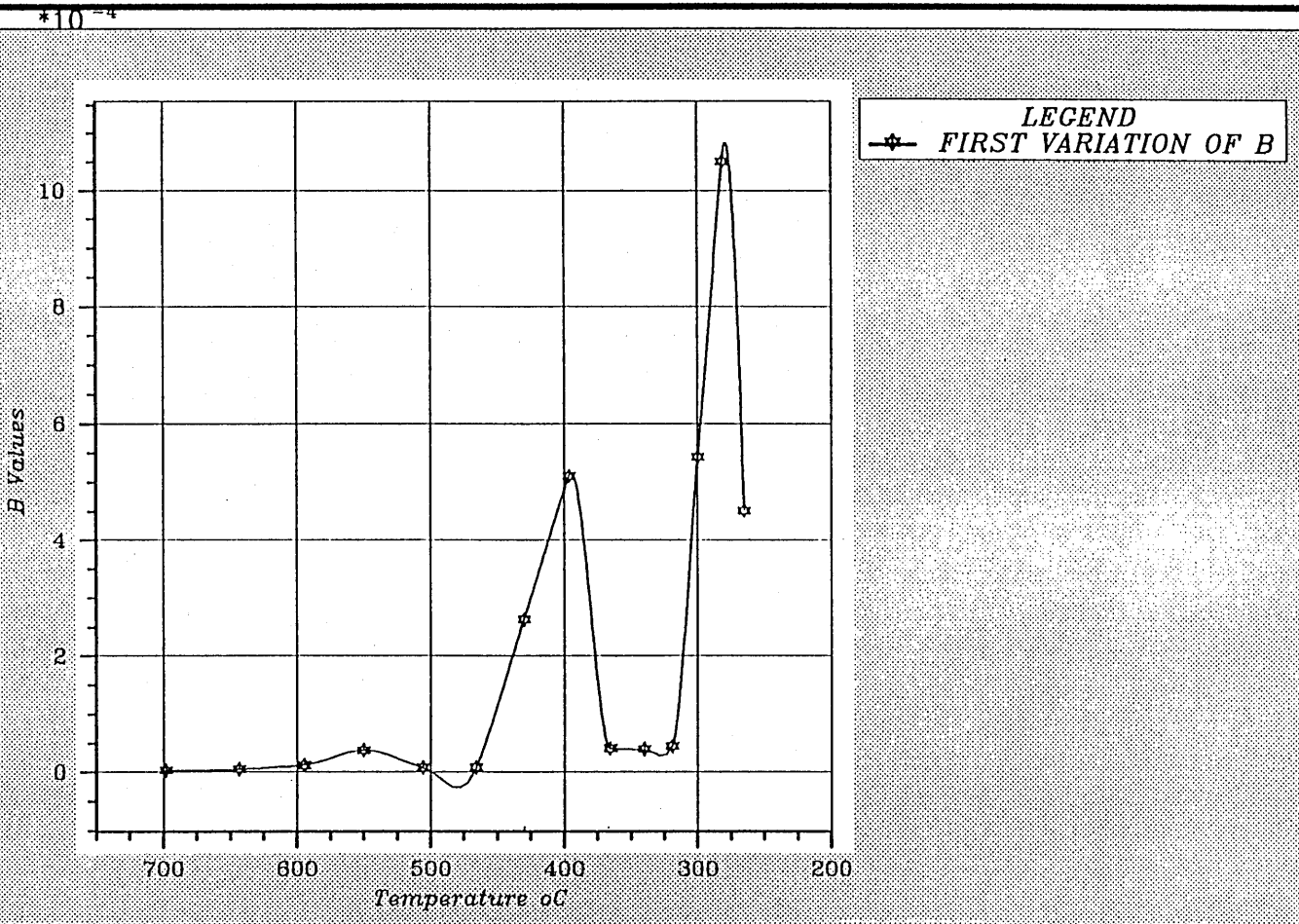

Figure 7.36 -Steel D
H= 3.5 kJ/mm

CHAPTER 8 MICROSTRUCTURAL EXAMINATION

8.1 Optical Metallography

8.1.1 Introduction

Optical metallography was employed to identify and quantify the microstructures produced in the coarse grained region of the HAZ's. The parent plates were also included. Microstructure examination had also an important role in substantiating the identification of the various ranges of transformation temperatures found by the statistical approach (refer Chapter 7).

8.1.2 Procedure

8.1.2.1 Sampling and Specimen Preparation

The longitudinal plane along the welding centreline, containing the thermocouples, was chosen to be examined. In this manner, it was expected to achieve consistency due to the HAZ along this plane being that along which the thermal cycles were measured. Moreover, the microstructures produced in this plane would have a very similar thermal history. From the practical aspect of the actual test, the location chosen facilitated the use of the fusion line as a reference; i.e. the longitudinal section presented roughly the fusion line as a straight line.

The preparation of the samples consisted of sectioning the specimens, and carefully grinding them until the holes containing the thermocouples were visible, as shown in Figure 5.21 (refer Chapter 5). This was followed by cutting (transversely to the longitudinal profile of the specimens) and mounting the samples, grinding and polishing to one micron standard and, finally, etching.

8.1.2.2 Qualitative and Quantitative Examination

The microstructures produced in the HAZ's were revealed by the etching agent Nital II(2% of nitric acid in alcohol).

In general the magnification employed for optical observations varied from 100 to 500 times according to microstructural definition required. In some cases, higher magnification was also applied in order to improve definition of a particular area or microstructural constituent.

The following five major constituents were selected to identify the various microconstituents produced in the HAZ's;

1) Primary Ferrite (**PF**);

2) Acicular Ferrite (**AF**);

3) Ferrite with Second Phase (**FS**);

4) Ferrite Carbide Aggregate (**FC**);

5) Martensite (**M**)

Although the above terminology was introduced by the IIW [1988] to identify microconstituents of ferritic weld metals, previous observations carried out by the author, revealed that the scheme proposed could be satisfactorily applied in the current work. It is worth mentioning that the same scheme for the identification of the microconstituintes was applied in quantitative metallography.

Quantitative metallography was by the point counting technique [Pickering, 1978]. The microstructures before the crossed lines on the microscope's eye piece, were identified and added by the Swift Point Counter. A total of 1000 points were counted for each sample, under a magnification of 400 times. Five counters were used representing each principal microstructure selected for examination. This selection was based on the guide for microscope examination proposed by IIW [IIW, 1988] as described previously. The scheme applied for classification of the microstructures can be seen in the figure 8.1. This was useful in order to distinguish some similar microconstituents during point counting.

8.1.3 Results

8.1.3.1 Introduction

In this section will be presented the results of the microstructural examinations carried out in the present work. In order to support the analysis of the various microstructures found during the investigation the results of hardness measurements (max-min/mean), although also presented in Section 8.2, accompany the presentation of each microstructure. In the HAZ's the heat input (HI) correspondent to each test weld will be also included.

8.1.3.2 Parent Plates

Figures 8.2 show that ferrite and pearlite are the microconstituents of the parent steels under investigation. Between the steels, 12 presents less evidence of rolling, i.e. the microstructure does not show marked banding. In this respect, the following increasing order was found regards to banding effect: 12, D, C and B. On the other hand, D presents less banding than B and C. The pearlite in steel 12 is not as well distributed as for the other steels. The same, to a less extent, is noted for steel D in comparison with B and C. The following increasing order is found for the ferrite grain size; D, C, B and 12, with 12 presenting a variable grain size and B slightly coarser than C. This is confirmed by the average parent plate ferrite grain size of 5.7, 9.2, 9.6 and 10.7μm measured by the mean linear intercept method [Pickering, 1976], for steels D, C, B and 12 respectively.

The pearlite in steels B and C is coarser than D and 12 (Figures 8.3). In this respect, D and 12 are very similar. In Figure 8.3(a), the steel 12 shows grey inclusions typical of sulphide [ASM, 1972] scattered in the matrix but associated with ferrite. These inclusions are short and less flattened, contrary to their usual long and thin shape. Segregation was found at approximately one third of the depth from a surface of the parent plates B, C and D, and inclusions of sulphides were associated with the segregation as shown in Figures 8.4. For steel D in particular this segregation was not as thin and long as is typical of sulphides. The analysis carried out by X-Ray non-dispersive analyzer coupled to the scanning electron microscope revealed that this segregation was of MnS. This can be seen from Figures 8.5 to 8.7.

8.1.3.3 Coarse Grained Region

Figure 8.8(a) shows a predominant martensitic microstructure (M) found in steel 12 welded at 0.8kJ/mm. As the heat input increased up to 2.5kJ/mm it became less martensitic (Figures 8.8(b), (c) and (d)) and ferrite with second phase (FS), primary ferrite (PF) and acicular ferrite (AF) started to be noted in higher proportions. For higher heat inputs these microconstituents were coarser and more scattered as shown in Figure 8.8(e) obtained in the test weld employing 3.0kJ/mm and in Figure 8.8(f) employing 3.5kJ/mm.

In steel B, martensite (M) could be found up to heat inputs of 2.5kJ/mm. It became less evident for heat inputs of 3.0 and 3.5kJ/mm. This can be seen from Figures 8.9(a) to (f). Figure 8.9(a) shows martensite as the major microconstituent in test weld with 0.8kJ/mm. Some coarse ferrite with second phase (FS) was found occasionally. This remained almost unchanged with heat input of 1.5kJ/mm as shown in Figure 8.9(b). At heat input of 2.0kJ/mm some softer microconstituents, primary ferrite (PF) and ferrite with second phase (FS) became more evident as presented in Figure 8.9(c). The unetched 'white area' marked with h was identified as FC. As the heat input increased the microstructure became coarsened and softer microconstituents became more evident. In Figure 8.9(d) is shown ferrite with second phase (FS), primary ferrite (PF), and occasionally martensite (M) and ferrite carbide aggregate (FC). In Figures 8.9(e) and 8.9(f) from test welds obtained with 3.0 and 3.5kJ/mm respectively, the microstructure was mainly formed by ferrite with second phase (FS), primary ferrite (PF), acicular ferrite (AF) and occasionally ferrite carbide aggregate (FC).

In resemblance to 12 and B, steel C presented martensitic microstructure with 0.8kJ/mm as shown in Figure 8.10(a). As is shown, the HAZ is less coarse than B and 12 welded with the same heat input. For 1.5kJ/mm in Figure 8.10(b) martensite is found in less proportion and softer microconstituent, primary ferrite (PF), ferrite with second phase (FS) and acicular ferrite (AF) started to be evident. Additionally, the coarse grained region seems to remain narrow despite the increase of heat input. This aspect began to change for heat input of 2.0kJ/mm as indicated by ferrite with second phase (FS) in Figure 8.10(c). For heat inputs of 2.5, 3.0 and 3.5kJ/mm ferrite with second phase (FS),

acicular ferrite (AF) and primary ferrite (PF) were the major microconstituents, see Figures 8.10 (d), (e) and (f) respectively. The coarsening aspect of the HAZ as a result of the increase of heat input, could only be well noted for heat inputs of 3.0 and 3.5kJ/mm. This was particularly demonstrated by the colonies of acicular ferrite (AF) surrounded by primary ferrite (PF) in the grain boundaries of the prior austenite.

Although the texture of the martensite in the HAZ of steel D at heat input of 0.8kJ/mm seems similar to steel C, this microconstituent was found in much less proportion and some coarse ferrite with second phase (FS) could be detected. This can be seem from Figure 8.11(a). It can be noted in Figure 8.11(b) that the HAZ coarsens more rapidly than for the other steels as the heat input increased to 1.5kJ/mm. In addition, martensite (M) became much less evident and ferrite with second phase (FS) and acicular ferrite (AF) (in lower proportion) can be detected. In Figure 8.11(c) softer microconstituents (ferrite with second phase (FS), primary ferrite (PF) and acicular ferrite (AF)) became more evident (heat input of 2.0kJ/mm). Unetched 'white area' marked with h, also found in steel B welded with 2.0kJ/mm and identified as ferrite with second phase, was quite often observed for heat inputs of 2.5, 3.0 and 3.5kJ/mm. This microconstituent coarsened as the heat input increased, as shown in Figures 8.11(d), (e) and (f) respectively.

The microconstituents described above in the coarse grained region of each test weld were quantified by point counting technique. The results are presented in Table 8.1. The proportion of non-determined microconstituents are identified as ND. The average cooling time for each experiment and the mean hardness are also included in this Table.

From the results gathered it can be noted that for each steel the proportion of softer microconstituents than Martensite (M) increased as the heat input increased; i.e the higher the cooling time through 800-500°C the more the coarse grained region tended to soften as a result of the decrease of Martensite (M). Figure 8.12 shows the variation of the proportion of Martensite (M) with respect to cooling time in the experimental work. It can be seen that in general, steels 12, C and D present a very similar trend with respect to the decrease of Martensite as the cooling time increases. Steel B retains quite a high proportion of Martensite (approximately 40%) up to a heat input of 2.0kJ/mm,

decreasing more slowly than in the other steels.

8.2 Hardness

8.2.1 Procedure

8.2.1.1 Method

Hardness measurements were carried out in both the parent plates and the coarse grained region of the HAZ's of the steels under study. Vickers hardness was chosen as it gave a good basis for comparison purposes considering that this is the most widely method employed in the field of welding. Although it can be time consuming, it is very flexible in application and offers a wide range of loads. In addition, no change of indentor or load is required over a wide range of hardness. This aspect clearly brought consistency to the tests considering the variation of microstructure found in the test welds.

8.2.1.2 Sampling

Most hardness measurements are taken on sections transverse to a weld direction. This implies the use of a number of transverse sections from one weld bead in order to make the test more representative. However, considerable variations are frequently observed and often promote discussion as to whether they are caused by real effects or operator inaccuracies [Brooks and Hart, 1977]. Kohno and Jones [1978] verified differences in weld thermal cycle measurement in the HAZ near to the fusion line due to the position of the thermocouple. In the current work, hardness tests were carried out by using the same samples used for the optical metallography on sections longitudinal to weld beads. In this manner, for each test weld the measurements were taken from a section which can be related to the same thermal cycle. In addition, a reasonable length of each weld bead (approximately 2cm) was examined which was considered satisfactorily representative of a test weld.

8.2.1.3 Surface Preparation

The surface preparation was by grinding and polishing to one

micron standard and, finally, etching using Nital II. Although the definition of the fusion line had already been obtained due to the contrast between the weld metal (Ni was used as a filler wire) and the HAZ, the surface preparation adopted proved to be useful for a clearer definition of the HAZ and a more precise assessment of the indentation sizes during the measurements.

8.2.1.4 Selection of Load

According to the document prepared by IIS/IIW Commission IX [1986] the loads of 5kgf and 10kgf seem to be most adequate for assessing the hardness in the HAZ in view of the dimensions generally encountered when using the arc welding processes. Initial examinations were carried out in order to evaluate the adequacy of those loads recommended. The Vickers method depends very much on obtaining a clear definition of the depression produced by the indentor on the surface of the material under analysis. In this respect, both loads were capable of producing satisfactory indents within the range of 0.8-3.5kJ/mm, i.e. range of heat input employed in the test welds. However, the load of 10kgf applied in test welds which employed lower heat input, i.e. 0.8 and 1.5kJ/mm, seemed less accurate with regards to location in only the coarse grained region of the HAZ. The load of 5kgf was more flexible and could easily be placed in the region of major interest. As a result, it was decided to use 5kgf throughout the hardness test.

8.2.1.5 Location of the Hardness Indents

At this stage, it was important to establish a criterion to locate the indents which could be applied to the 24 specimens under investigation. Observations of the profile of the longitudinal section of the weld beads of the specimens revealed that they presented an undulating penetration effect often observed in arc welds. It has been reported [Brooks and Hart, 1977 and Rönningen et al, 1973] that hardness measurements in these undulations had high peak-values in the shallower zones; conversely, the hardness was lower in more deeply penetrated zones. According to them, these variations in hardness were associated with the evolution of the thermal cycle as a function of the variations in the weld pool geometry. In this respect, it was decided to define a distance from the fusion line which would remain in the coarse grained region of

the HAZ but away from the undulation. This was accomplished by a series of trials in order to choose the most appropriate distance from the fusion line which could satisfy the various sizes of the coarse grained region. On this basis, it was found that a distance of approximately 0.05mm from the fusion line satisfactorily met the requirements. For each sample, a total of ten measurements was carried out and a distance of 1mm was kept between indentations.

8.2.2 Results

Table 8.2 presents the results of the hardness measurements for each test weld. In order to assist the understanding of the variations found in the hardness values, the respective average cooling time of each test weld has been included. The presentation of maximum, minimum and mean values gathered during the test was considered to be the most appropriate way to show the results for comparison with other results found in welding reports. Besides, it has become usual to adopt this type of presentation for hardness measurements of a similar nature.

In general, the hardness on the coarse grained region in the steels decreased as the cooling time increased. Steel B presented the hardest coarse grained region within the experiments followed by steel 12. Steel D presented slightly higher values than C as shown in Figure 8.13, where the maximum values of hardness was plotted with respect to the cooling time ($\Delta t_{8\text{-}5}$).

Table 8.1 - Proportion of microconstituents found in the coarse grained region of the HAZ's of the steels under study.

Test Weld	Cooling Time (s)	Microconstituents(%)						Mean Hardness (Hv)
		FS	AF	FC	PF	M	ND	
T12-1	3.3	28.1	6.0	3.0	6.9	53.0	3.0	359.6
T12-2	5.7	29.1	21.7	7.4	11.6	28.2	2.0	313.6
T12-3	7.9	35.3	25.9	9.9	15.4	10.3	3.2	276.2
T12-4	10.8	38.9	28.4	8.3	20.8	1.2	2.4	245.6
T12-5	13.3	42.2	22.2	6.5	27.2	0.3	1.6	221.1
T12-6	18.0	34.7	32.4	1.4	28.0	0.0	3.5	225.2
TB-1	3.0	16.8	9.6	7.4	2.1	62.0	2.1	395.3
TB-2	6.0	23.2	6.2	10.8	2.8	51.8	5.2	374.9
TB-3	8.2	24.8	8.6	16.6	8.0	37.6	4.4	326.5
TB-4	10.6	43.7	13.9	13.6	12.7	13.3	2.8	270.8
TB-5	12.0	42.5	20.5	11.0	15.7	8.1	2.2	262.5
TB-6	15.0	39.7	24.9	12.3	17.2	3.0	2.9	241.7

Table 8.1 - Cont'd

Test Weld	Cooling Time (s)	Microconstituents(%) FS	AF	FC	PF	M	ND	Mean Hardness (Hv)
TC-1	3.3	14.4	9.6	6.4	11.0	56.1	2.5	299.1
TC-2	5.6	30.1	16.2	12.0	18.8	21.5	1.4	264.1
TC-3	7.4	37.0	20.6	12.5	10.8	15.2	3.9	247.9
TC-4	9.8	33.5	26.5	15.6	17.1	4.2	3.1	232.2
TC-5	13.3	38.2	24.6	9.4	22.4	1.8	3.6	220.7
TC-6	17.1	30.4	34.6	8.0	23.9	0.4	2.7	211.4
TD-1	3.7	41.3	8.6	6.1	6.7	33.5	3.8	287
TD-2	6.0	44.6	16.2	10.1	15.5	11.1	2.5	259.4
TD-3	7.9	40.3	24.6	7.9	16.3	8.5	2.4	247.5
TD-4	10.8	37.9	32.5	5.1	18.7	2.2	3.6	236.2
TD-5	12.5	38.9	27.7	9.8	20.5	0.9	2.2	222.3
TD-6	15.2	37.2	23.8	7.0	30.7	0.0	1.3	217.8

Table 8.2- Hardness measurements in the experimental work.

Parent Plate	**Hardness Vickers (5kG) Max - Min / Mean**	
Steel 12	158 -151 / 155.8	
Test Weld		**Cooling Time (s)**
T12-1	371 - 336 / 359.6	3.3
T12-2	325 - 299 / 313.6	6.7
T12-3	296 - 268 / 276.2	7.9
T12-4	254 - 239 / 245.6	10.8
T12-5	227 - 214 / 221.1	14.7
T12-6	229 - 221 / 225.2	19.3
Steel B	168 - 161 / 164.6	
Test Weld		
TB-1	412 - 376 / 395.3	3.0
TB-2	386 - 358 / 374.9	6.0
TB-3	341 - 313 / 326.5	8.2
TB-4	286 - 260 / 270.8	10.6
TB-5	271 - 254 / 262.5	12.0
TB-6	254 - 234 / 241.7	15.0

Table 8.2 - Cont'd

Parent Plate	**Hardness Vickers (5kG) Max - Min / Mean**	
Steel C	171 - 157 / 163	
Test Weld		**Cooling Time (s)**
TC-1	313 - 268 / 299.1	3.3
TC-2	271 - 257 / 264.1	5.6
TC-3	265 - 232 / 247.9	7.4
TC-4	246 - 221 / 232.2	9.8
TC-5	225 - 212 / 220.7	13.3
TC-6	216 - 204 / 211.4	17.1
Steel D	158 - 153 / 156.2	
Test Weld		
TD-1	310 - 265 / 287	3.7
TD-2	280 - 234 / 259.4	6.0
TD-3	271 - 239 / 247.5	7.9
TD-4	244 - 232 / 236.2	10.8
TD-5	232 - 216 / 222.3	12.5
TD-6	227 - 210 / 217.8	15.2

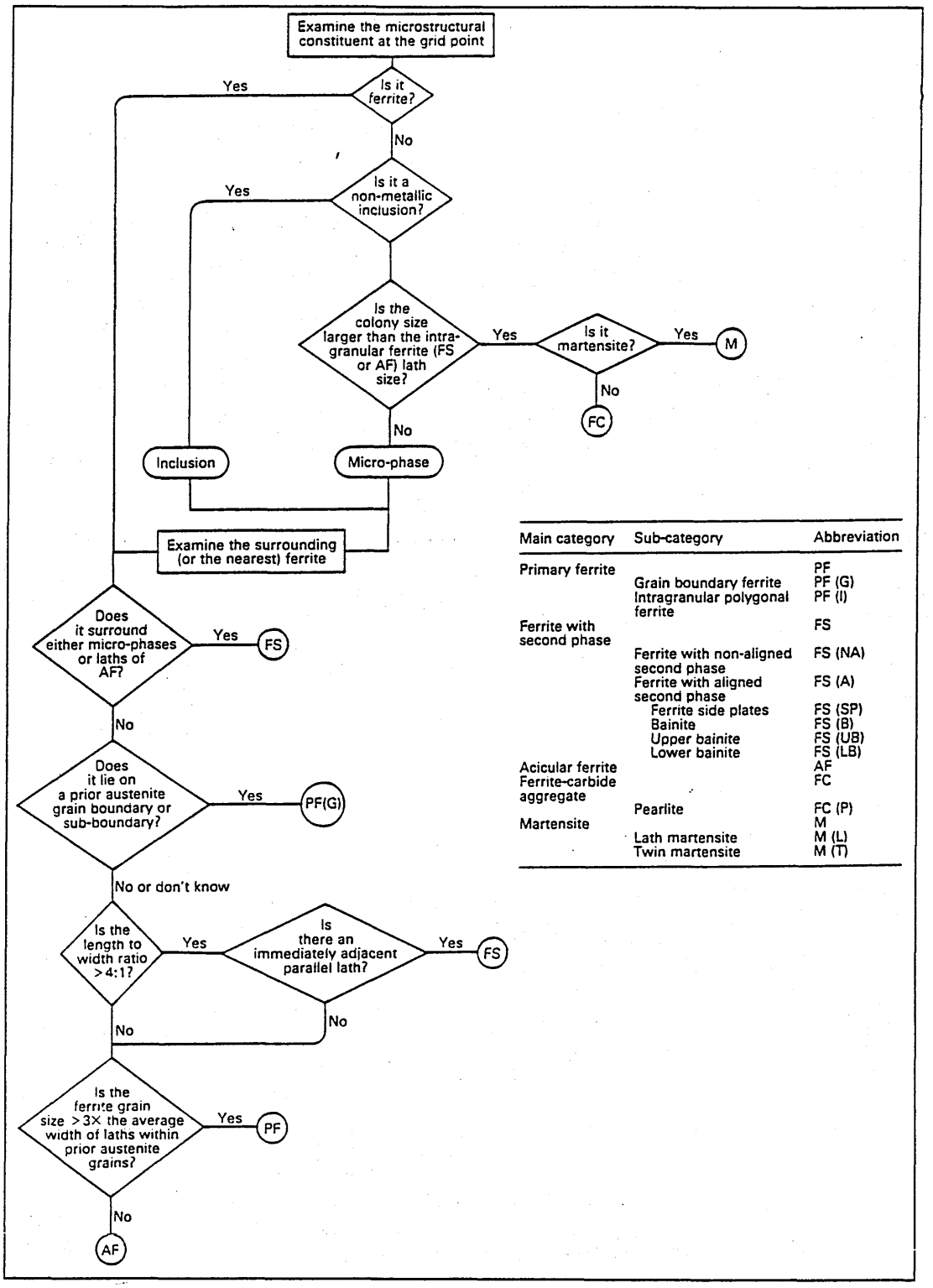

Main category	Sub-category	Abbreviation
Primary ferrite		PF
	Grain boundary ferrite	PF (G)
	Intragranular polygonal ferrite	PF (I)
Ferrite with second phase		FS
	Ferrite with non-aligned second phase	FS (NA)
	Ferrite with aligned second phase	FS (A)
	Ferrite side plates	FS (SP)
	Bainite	FS (B)
	Upper bainite	FS (UB)
	Lower bainite	FS (LB)
Acicular ferrite		AF
Ferrite-carbide aggregate		FC
	Pearlite	FC (P)
Martensite		M
	Lath martensite	M (L)
	Twin martensite	M (T)

Figure 8.1- Scheme for classification of microstructural constituents employed in optical metalography.

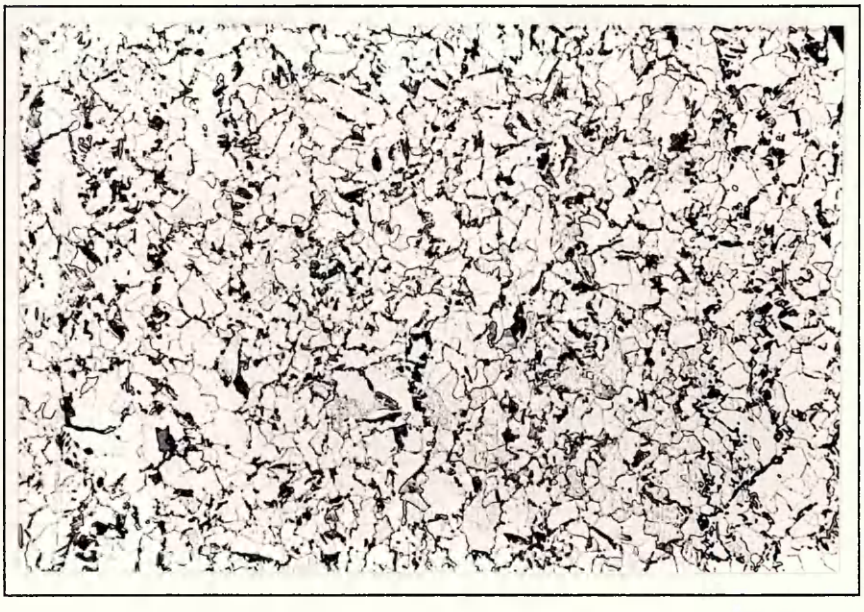

Fig. 8.2(a)
Steel 12
Parent Plate
240X

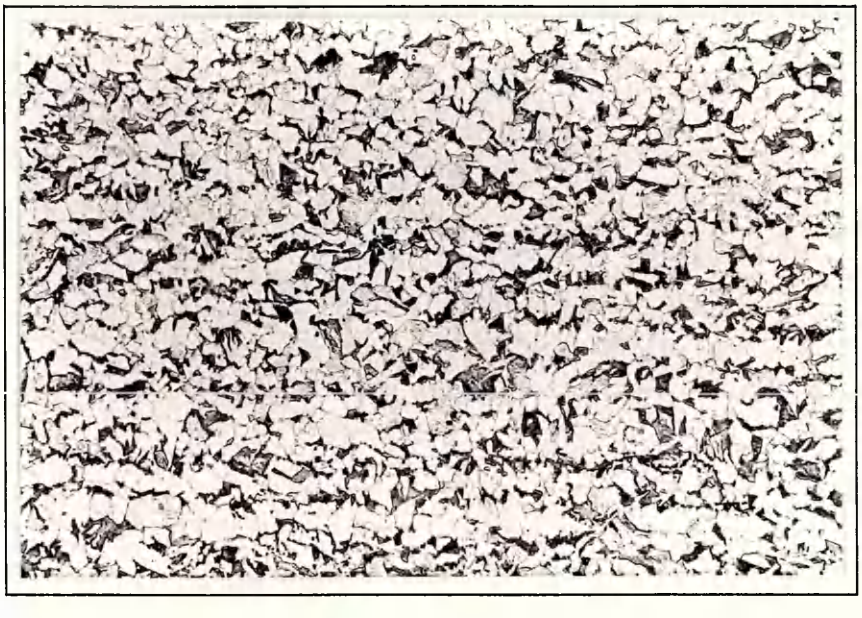

Fig. 8.2(b)
Steel B
Parent Plate
240X

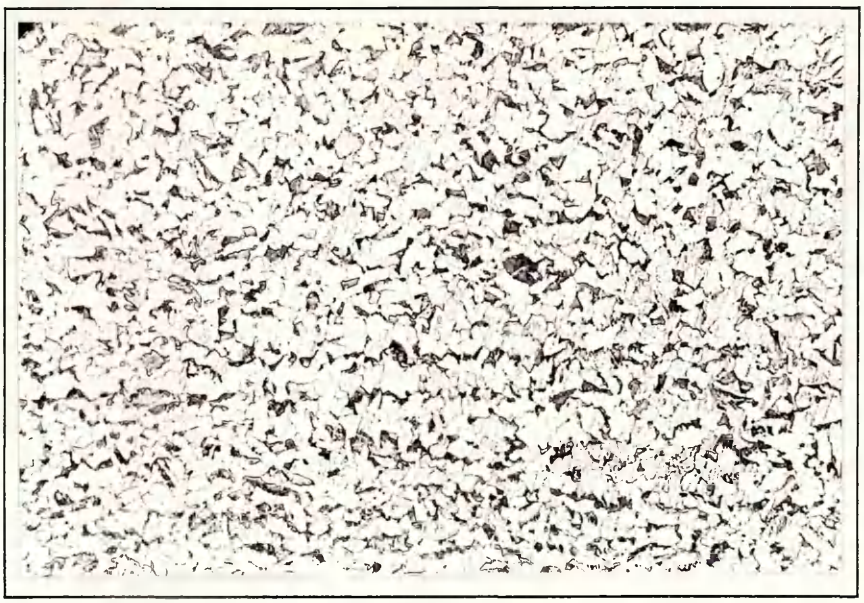

Fig. 8.2(c)
Steel C
Parent Plate
240X

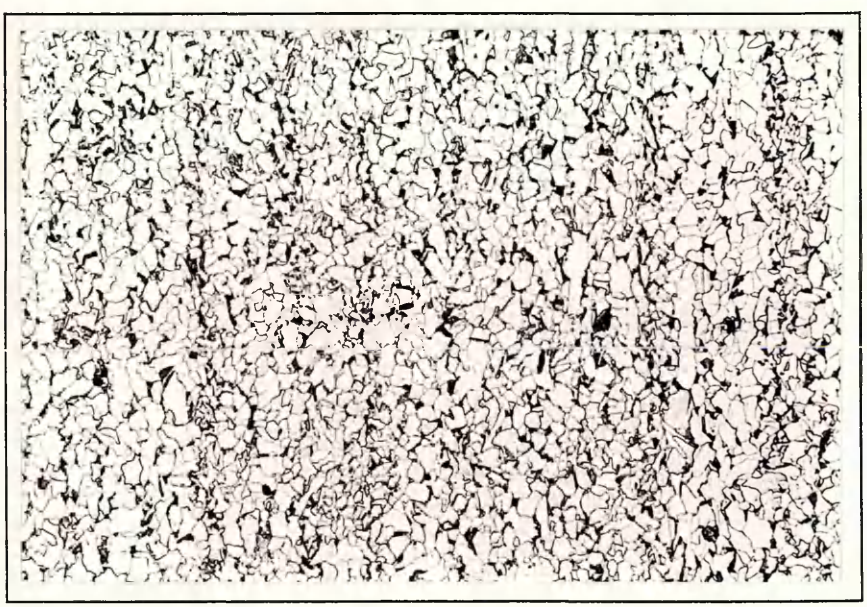

Fig. 8.2(d)
Steel D
Parent Plate
240X

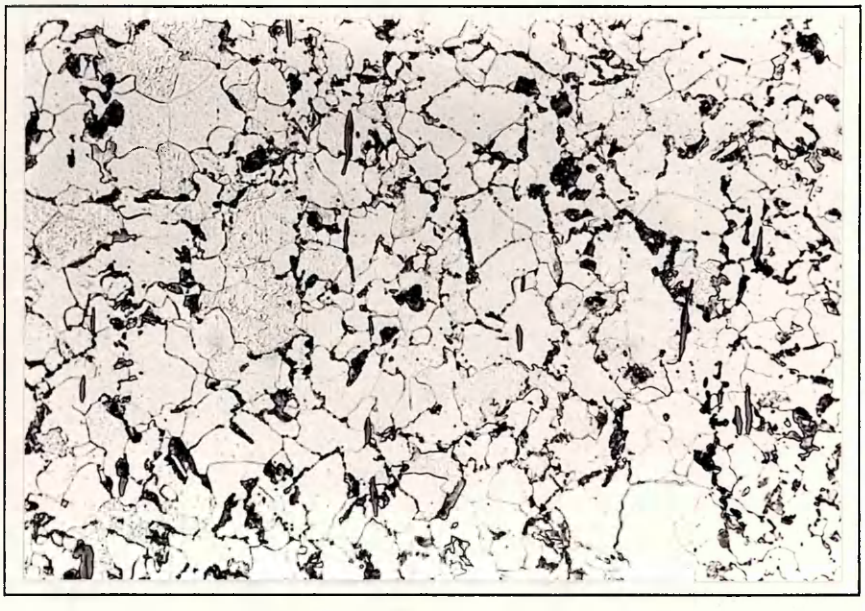

Fig. 8.3(a)
Steel 12
Parent Plate
480X

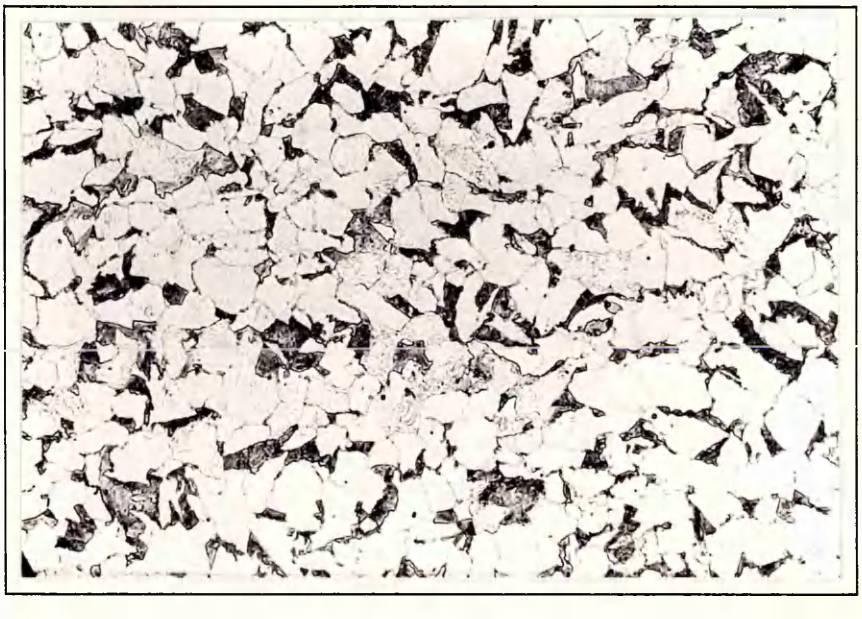

Fig. 8.3(b)
Steel B
Parent Plate
480X

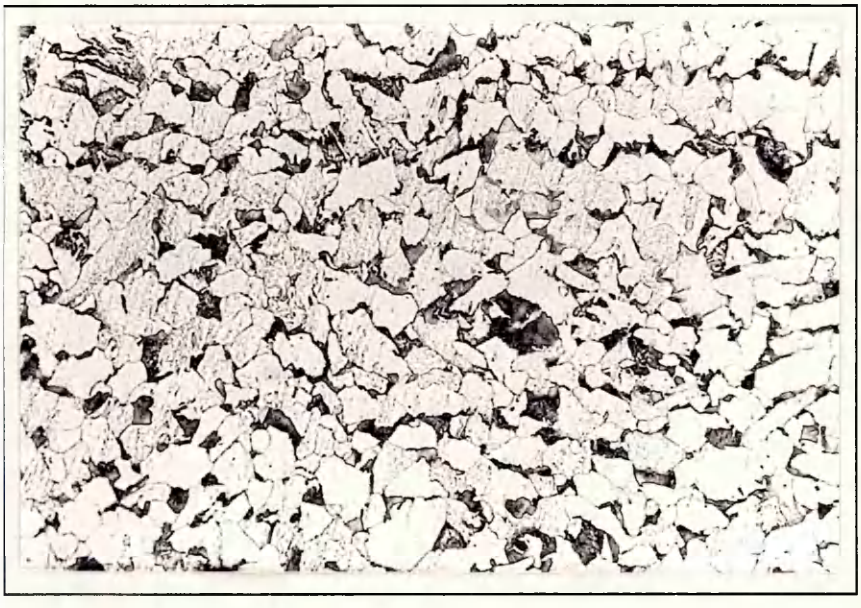

Fig. 8.3(c)
Steel C
Parent Plate
480X

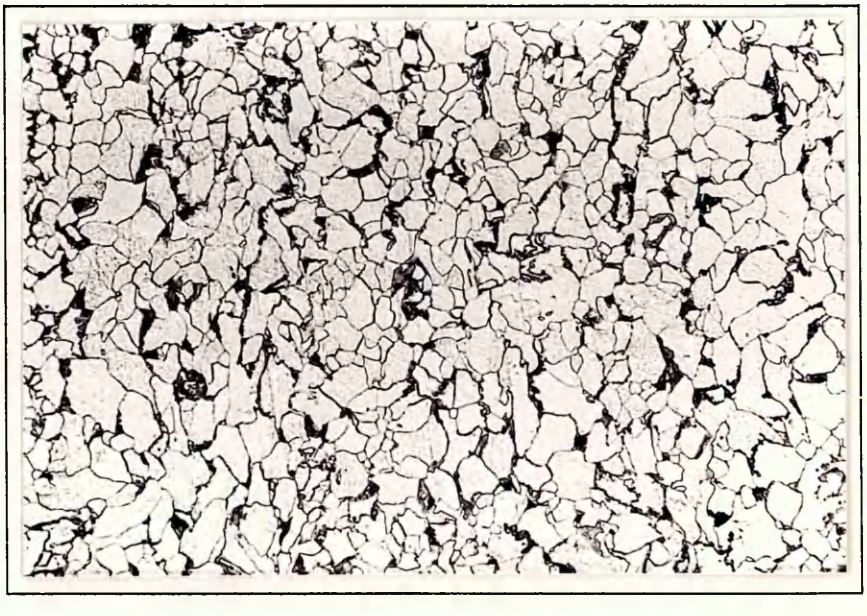

Fig. 8.3(d)
Steel D
Parent Plate
480X

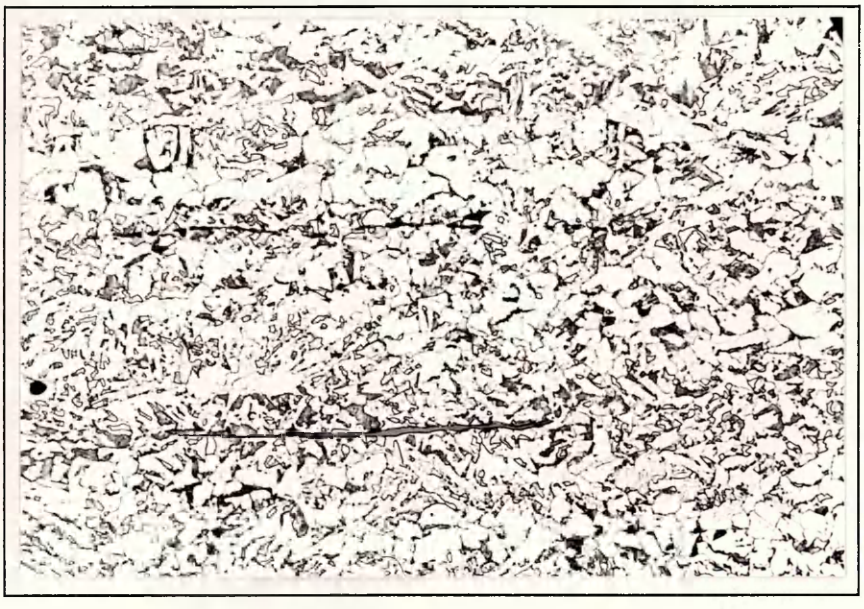

Fig. 8.4(a)
Steel B
Parent Plate
Inclusions
associated with
segregation
480X

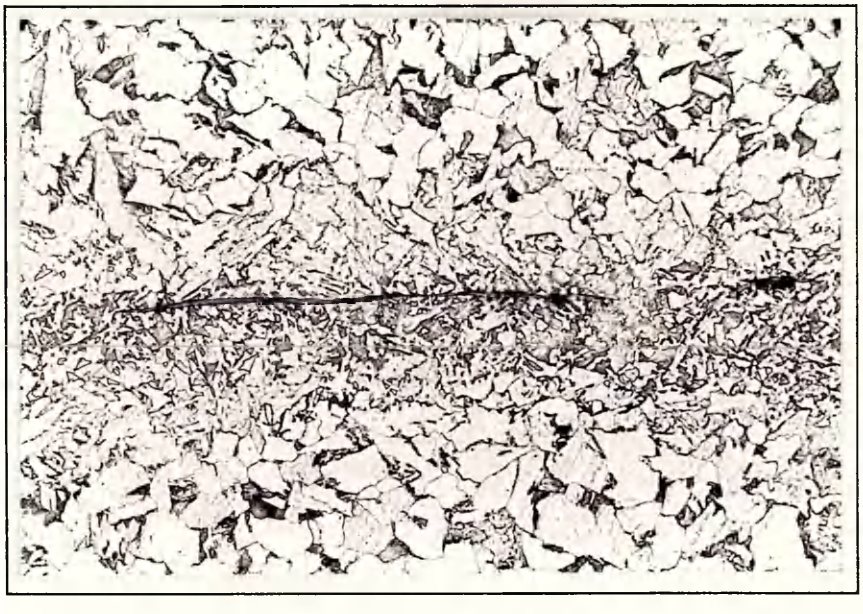

Fig. 8.4(b)
Steel C
Parent Plate
Inclusions
associated with
segregation
480X

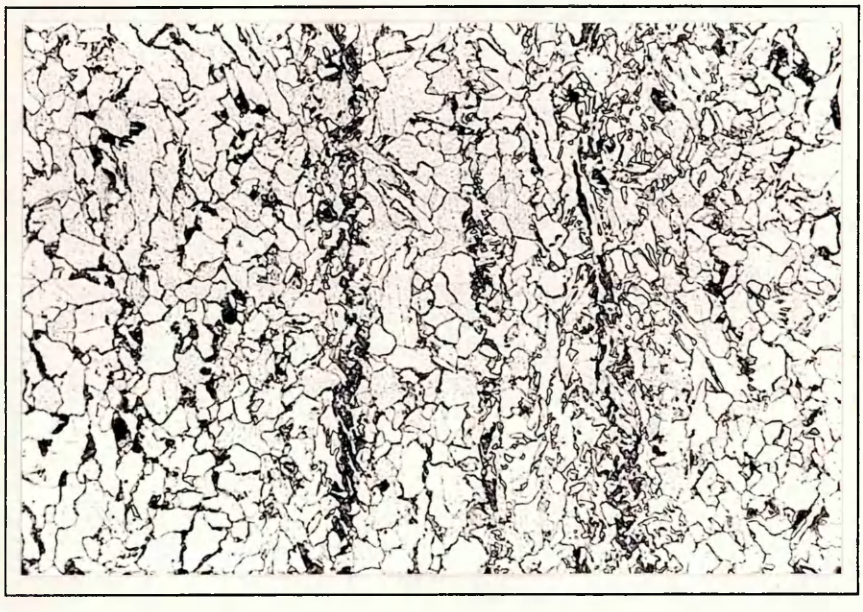

Fig. 8.4(c)- Steel D
Parent Plate
Inclusions associated with segregation
480X

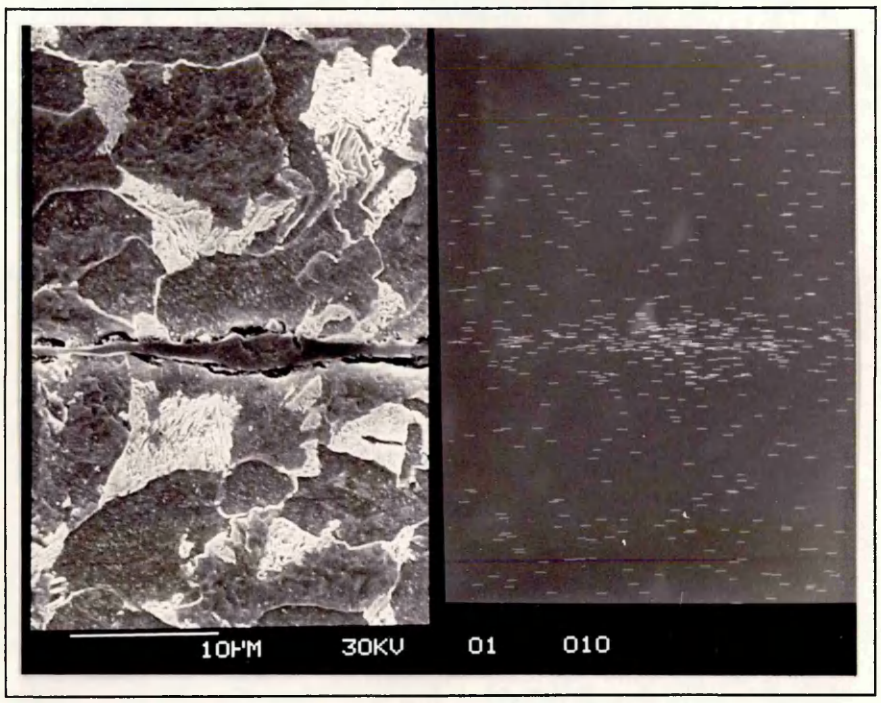

Fig. 8.5(a)- Analysis of Sulphur in segregation in Steel B.

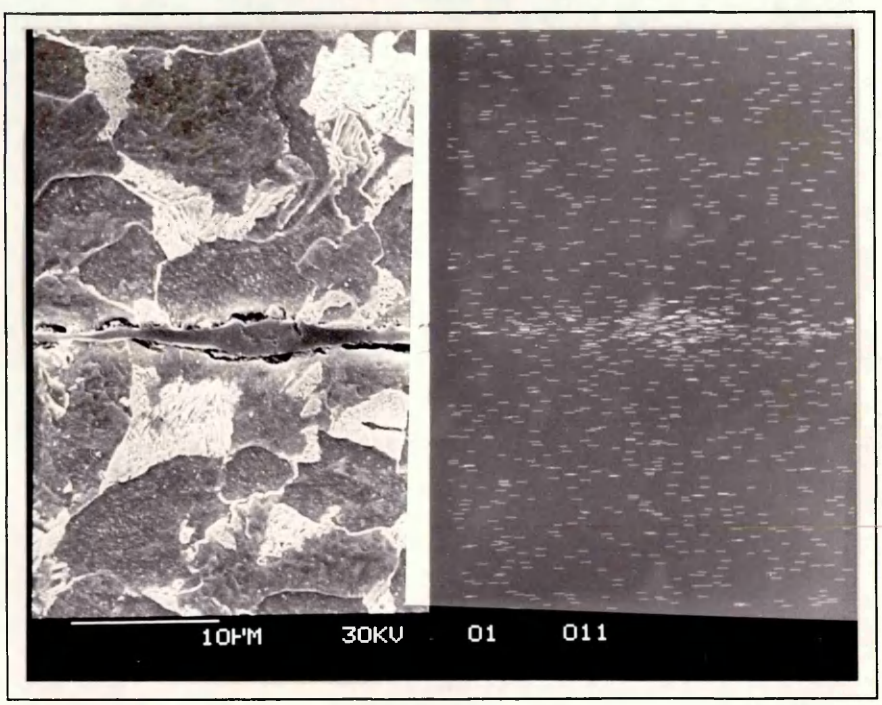

Fig. 8.5(b)- Analysis of Manganese in segregation in steel B

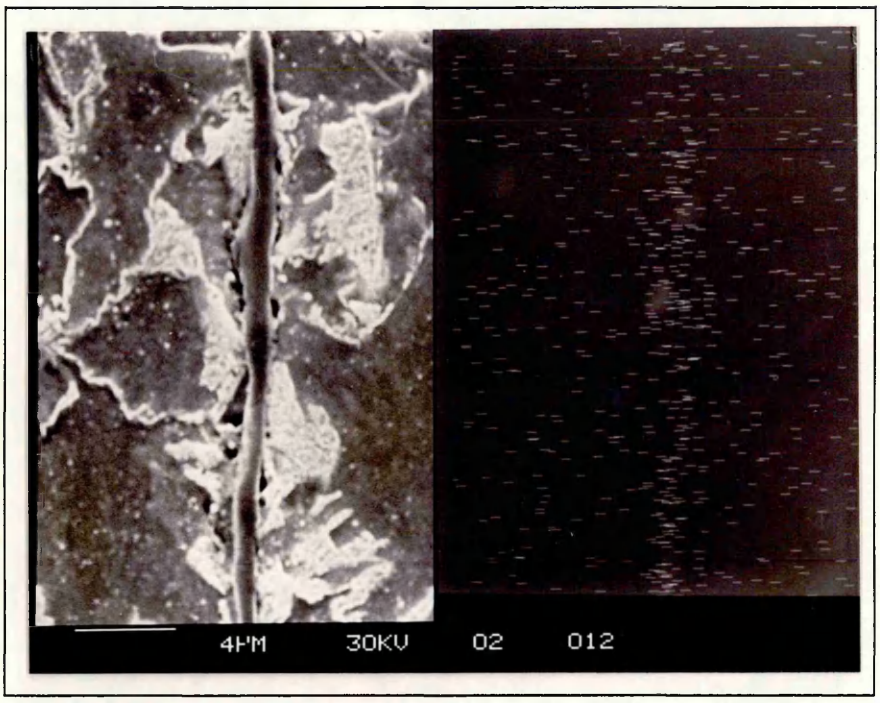

Fig. 8.6(a)- Analysis of sulphur in segregation in steel C

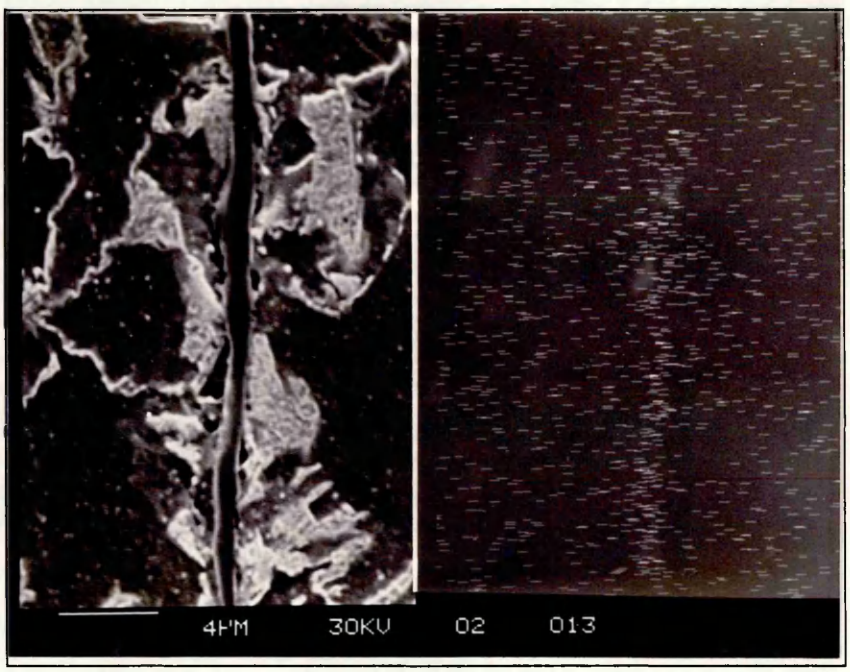

Fig. 8.6(b)- Analysis of Manganese in segregation in steel C

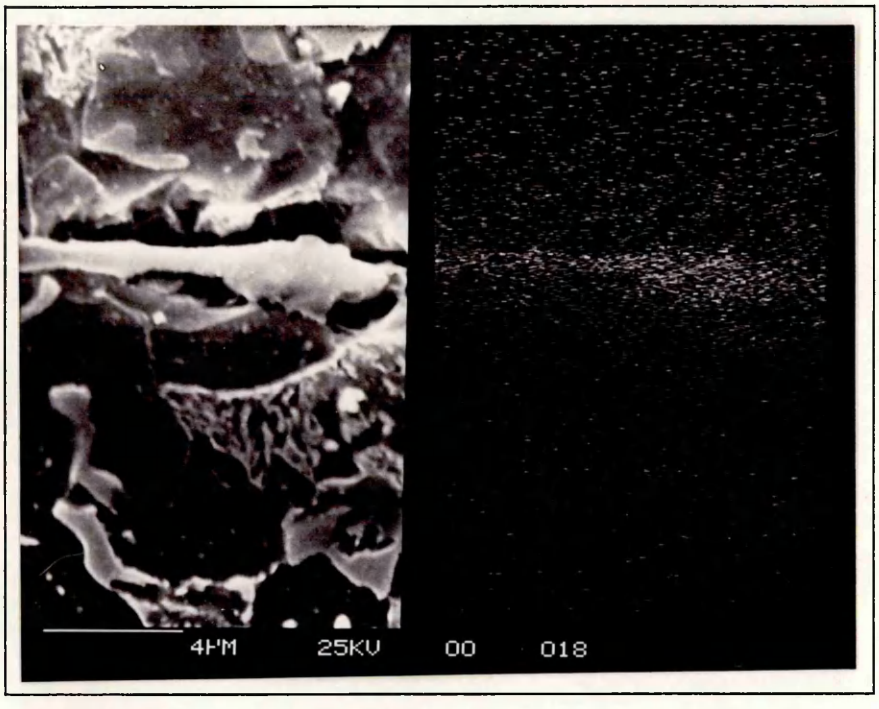

Fig. 8.7(a)- Analysis of sulphur in segregation in steel D

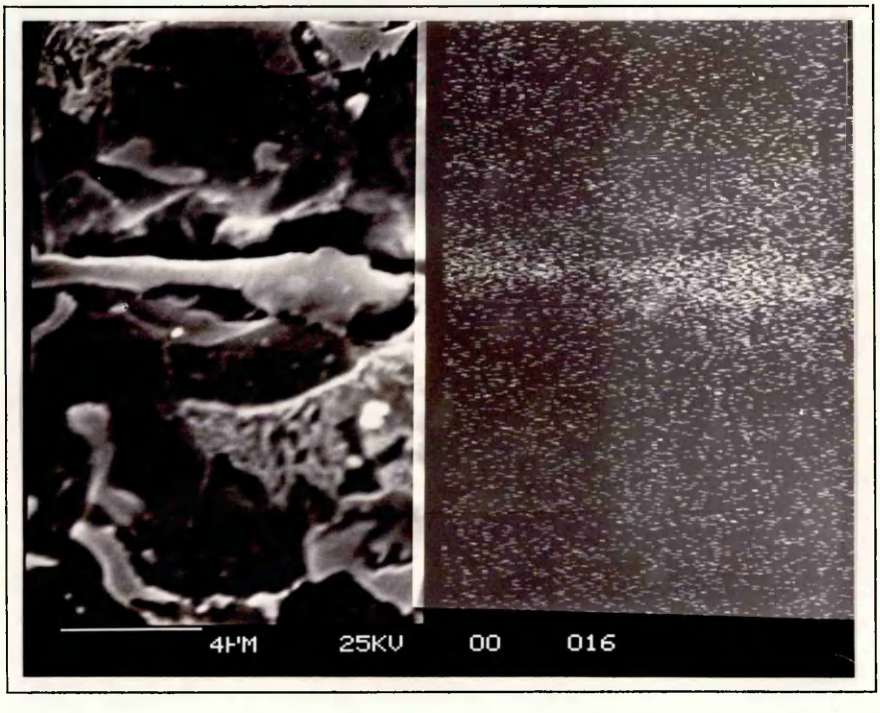

Fig. 8.7(b)- Analysis of manganese in segregation in steel D

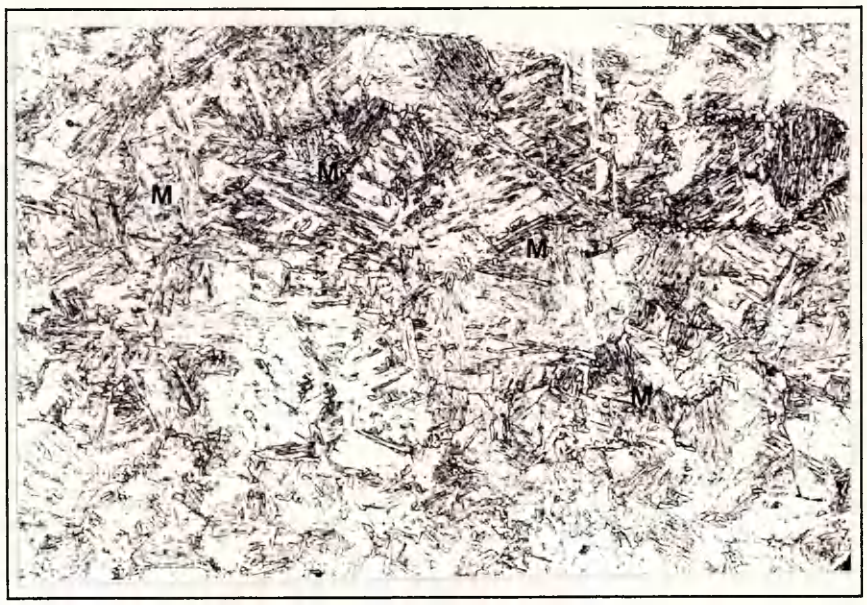

Fig. 8.8(a)
Steel 12
HI= 0.8kJ/mm
Hv=371-336
359.6
300X

Fig. 8.8(b)
Steel 12
HI=1.5kJ/mm
Hv=325-299
313.6
300X

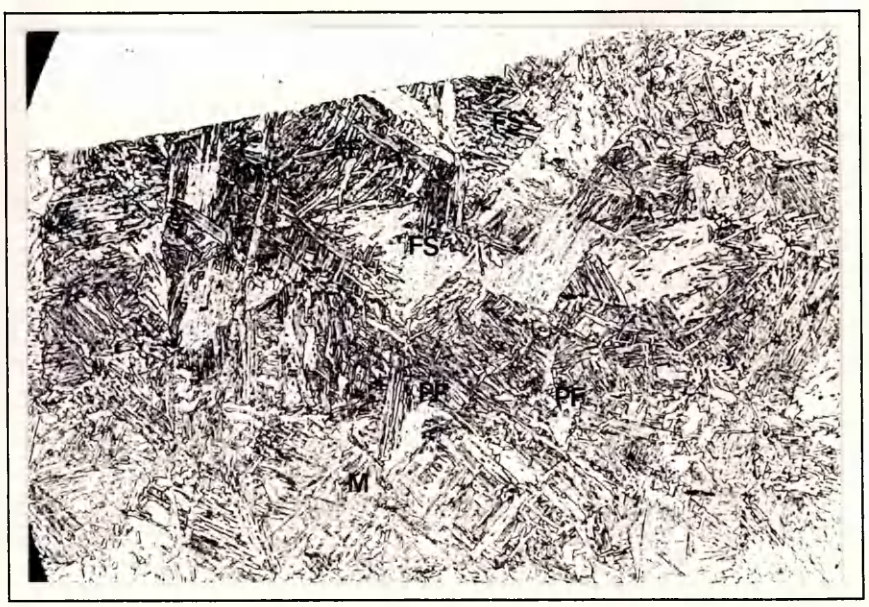

Fig. 8.8(c)
Steel 12
HI=2.0kJ/mm
Hv=296-268
276.2
300X

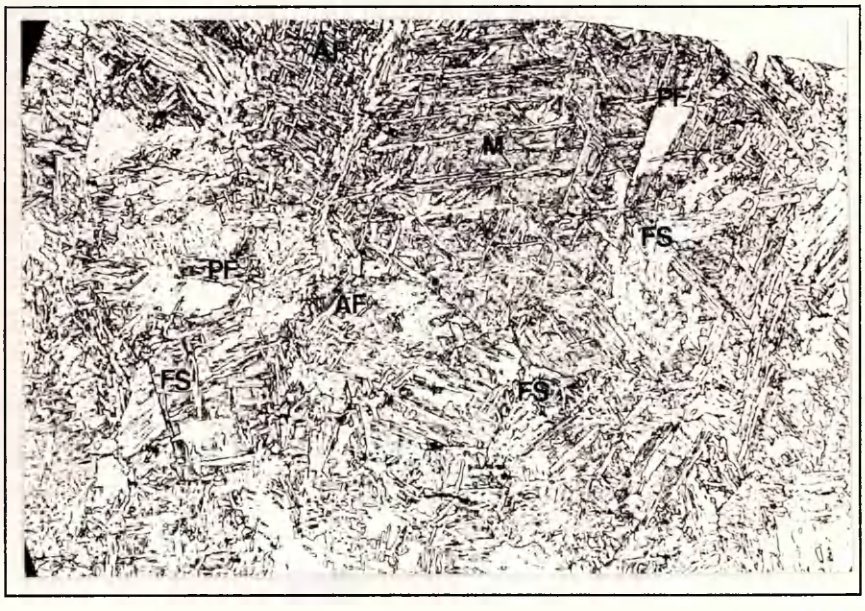

Fig. 8.8(d)
Steel 12
HI=2.5kJ/mm
Hv=254-239
245.6
300X

Fig. 8.8(e)
Steel 12
HI=3.0kJ/mm
Hv=227-214
221.1
300X

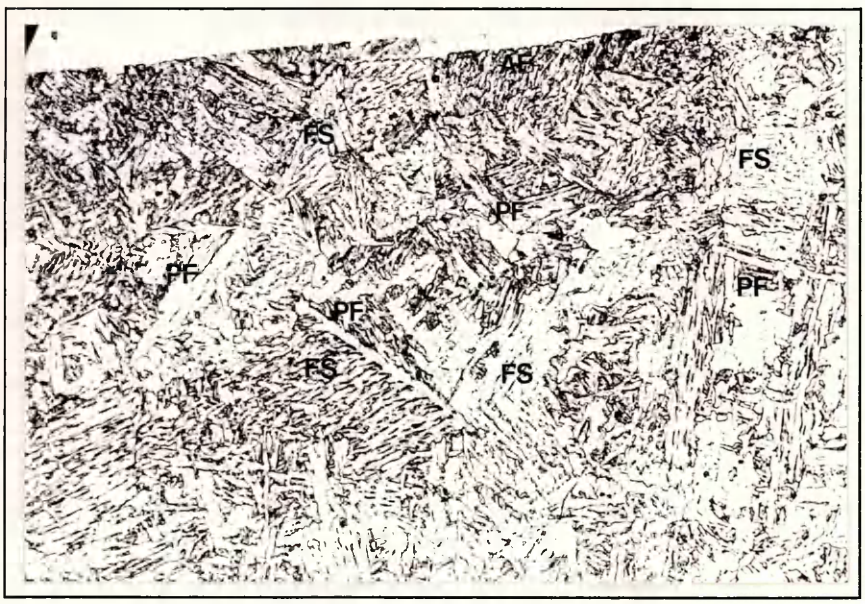

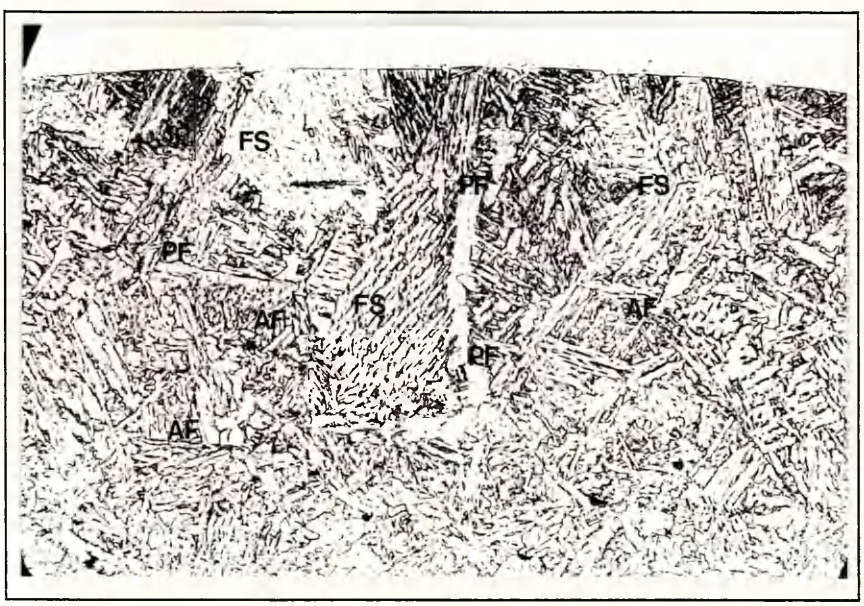

Fig. 8.8(f)
Steel 12
HI=3.5kJ/mm
Hv=229-221
225.2
300X

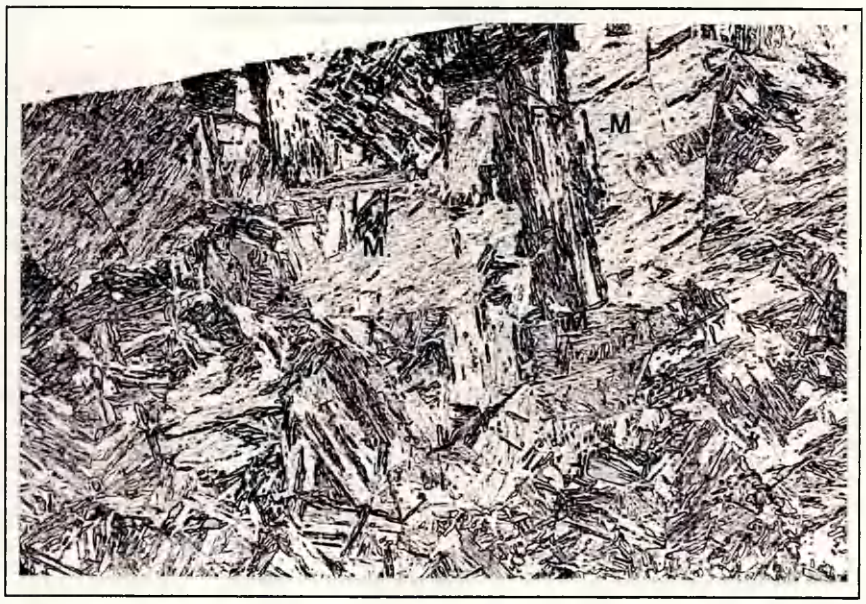

Fig. 8.9(a)
Steel B
HI=0.8kJ/mm
Hv=412-376
395.3
300X

Fig. 8.9(b)
Steel B
HI=1.5kJ/mm
Hv=386-358
374.9
300X

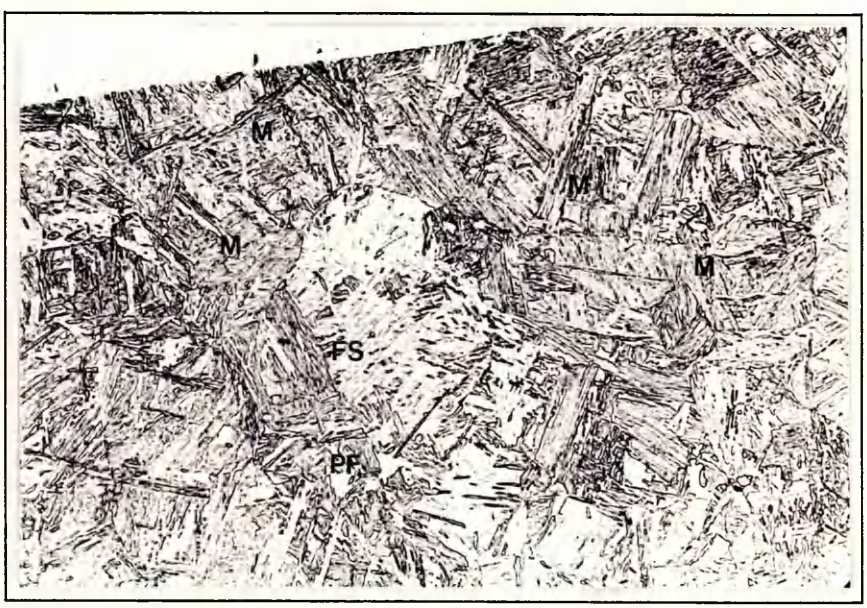

Fig. 8.9(c)
Steel B
HI=2.0kJ/mm
Hv=341-313
326.5
300X

Fig. 8.9(d)
Steel B
HI=2.5kJ/mm
Hv=286-260
270.8
300X

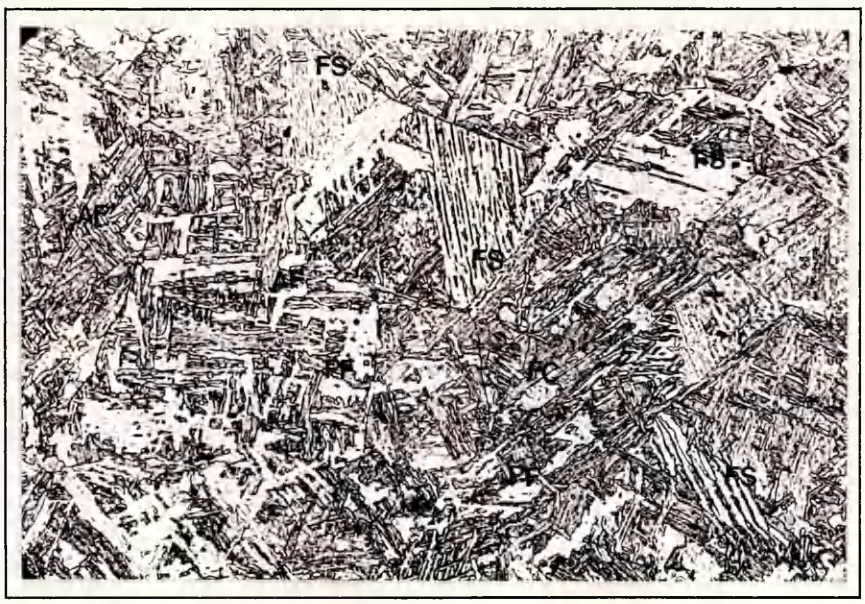

Fig. 8.9(e)
Steel B
HI=3.0kJ/mm
Hv=271-254
262.5
300X

Fig. 8.9(f)
Steel B
HI=3.5kJ/mm
Hv=254-234
241.7
300X

Fig. 8.10(a)
Steel C
HI=0.8kJ/mm
Hv=313-268
299.1
300X

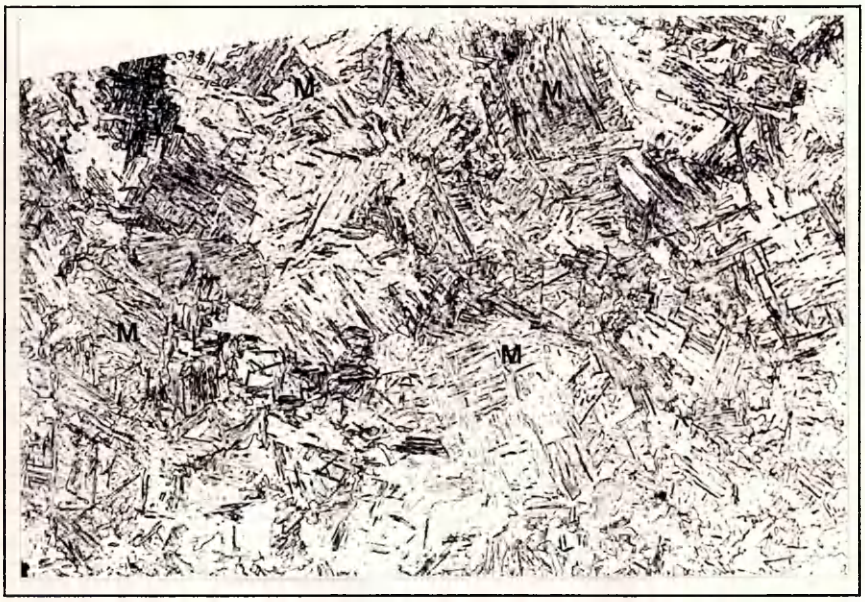

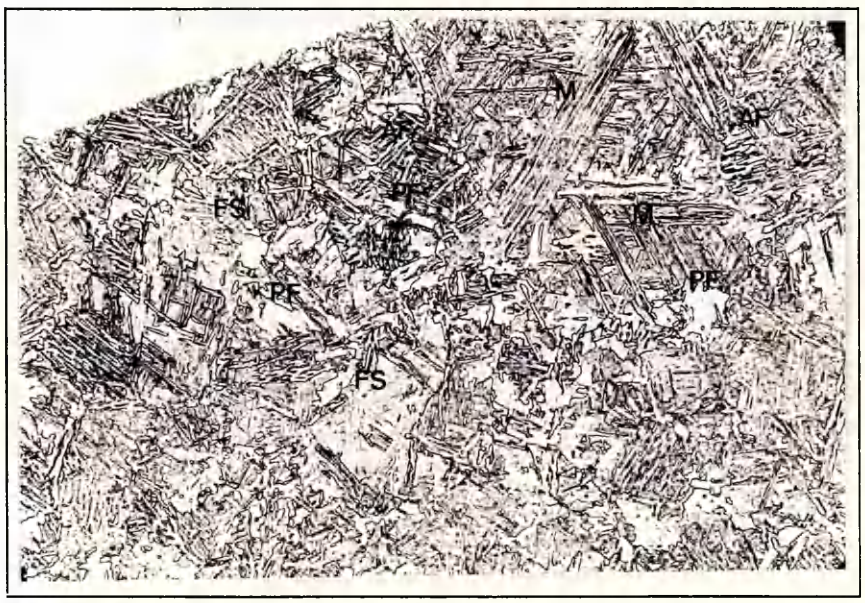

Fig. 8.10(b)
Steel C
HI=1.5kJ/mm
Hv=271-257
264.1
300X

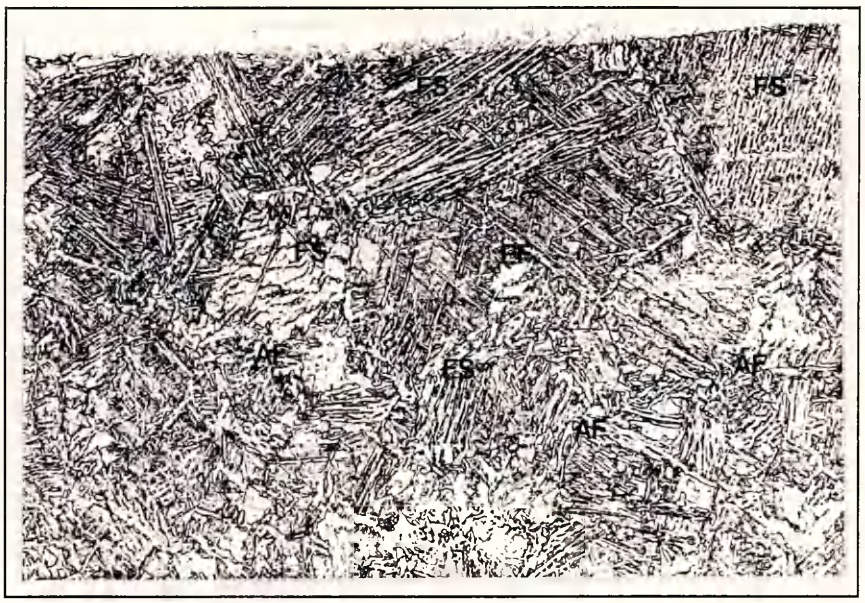

Fig. 8.10(c)
Steel C
HI=2.0kJ/mm
Hv=<u>265-232</u>
247.9
300X

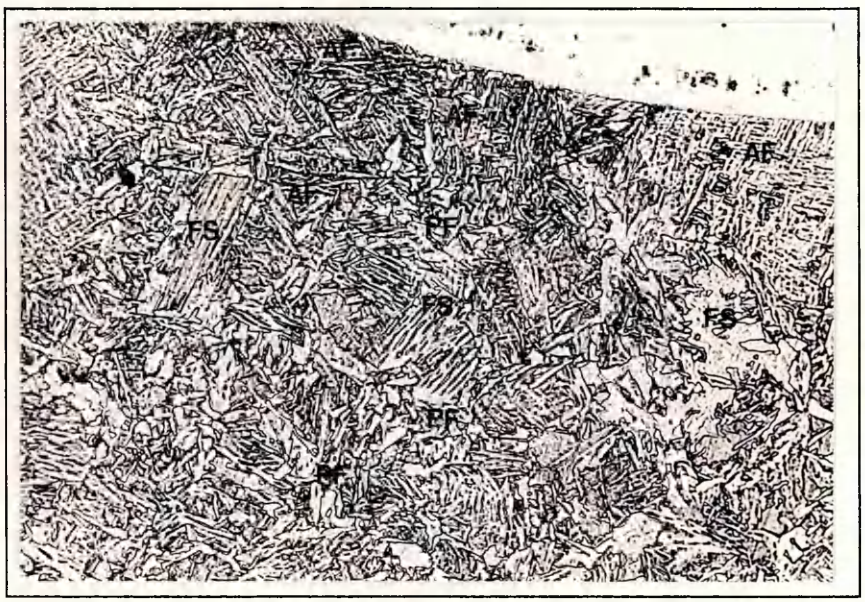

Fig. 8.10(d)
Steel C
HI=2.5kJ/mm
Hv=<u>246-221</u>
232.2
300X

Fig. 8.10(e)
Steel C
HI=3.0kJ/mm
Hv=225-212
220.7
300X

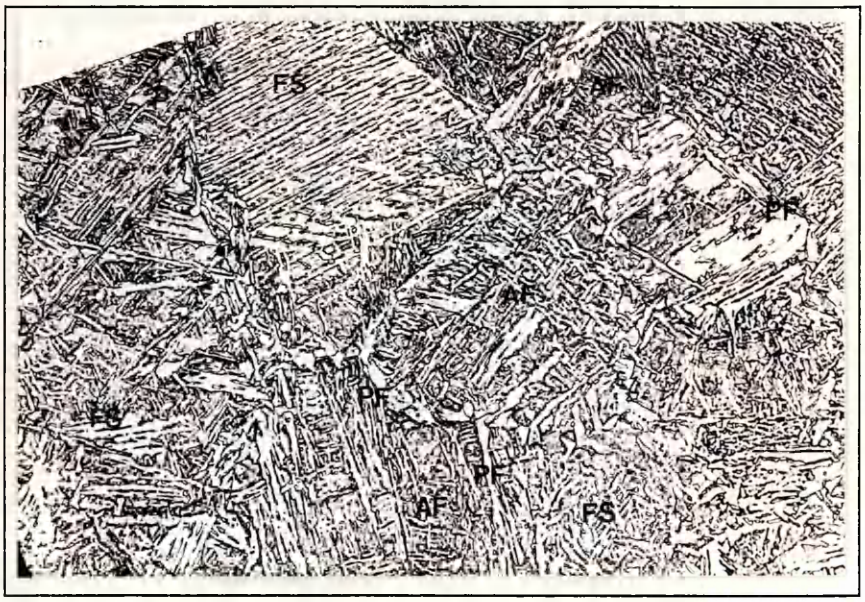

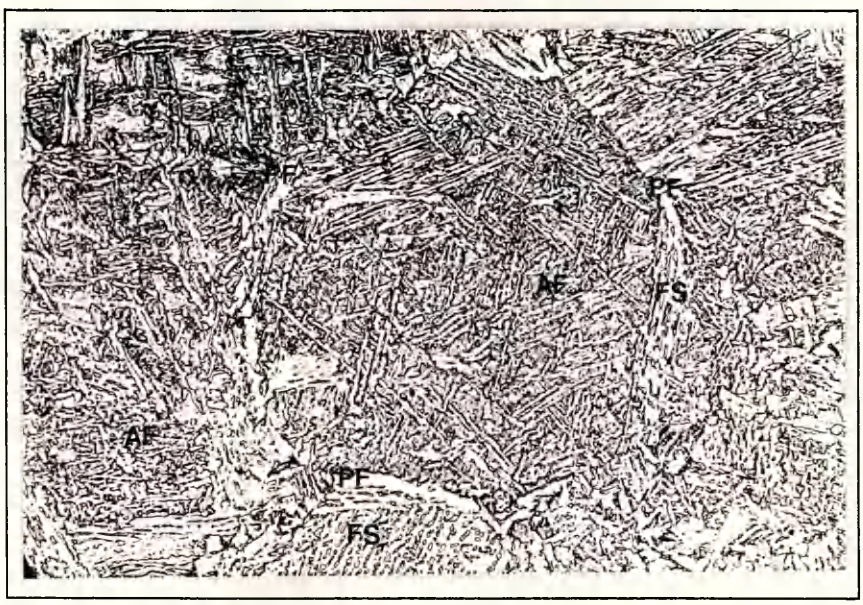

Fig. 8.10(f)
Steel C
HI=3.5kJ/mm
Hv=216-204
211.4
300X

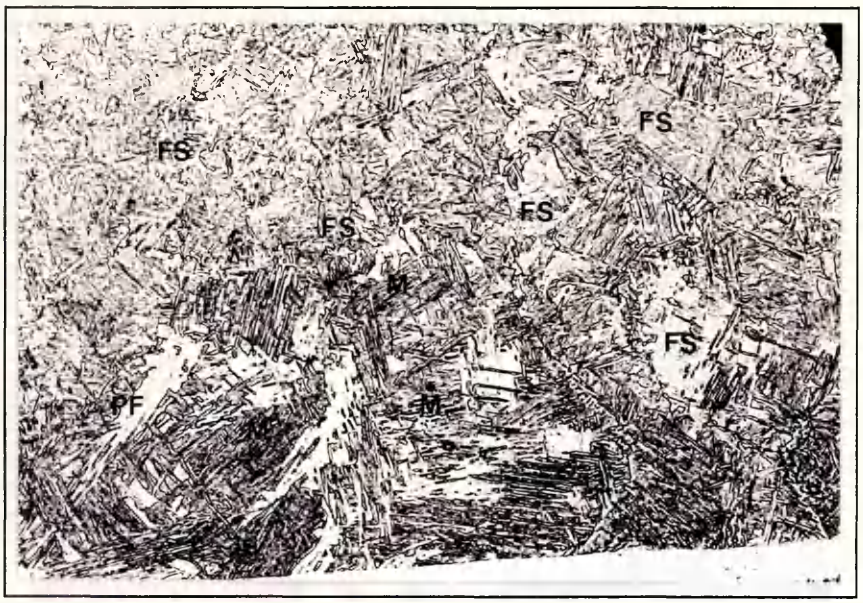

Fig. 8.11(a)
Steel D
HI=0.8kJ/mm
Hv=310-265
287
300X

Fig. 8.11(b)
Steel D
HI=1.5kJ/mm
Hv=280-234
259.4
300X

Fig. 8.11(c)
Steel D
HI=2.0kJ/mm
Hv=271-239
247.5
300X

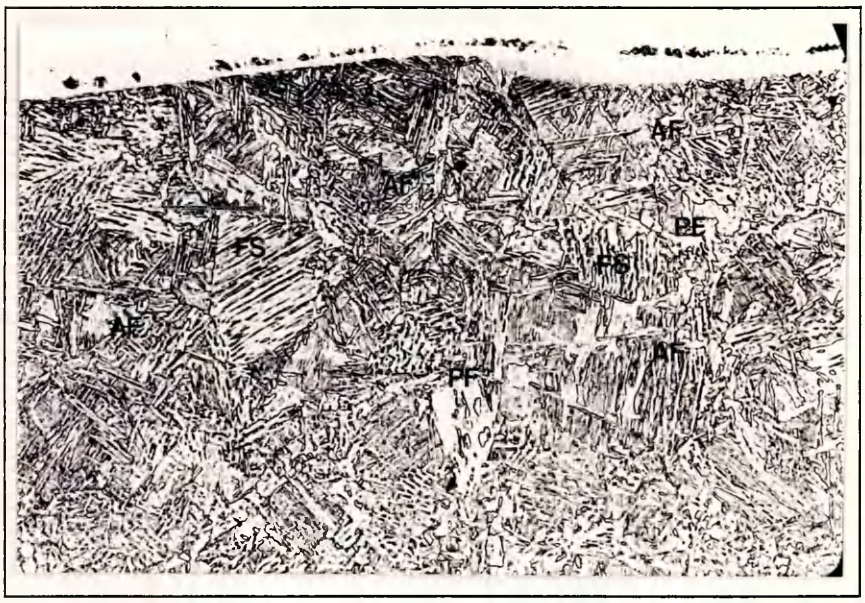

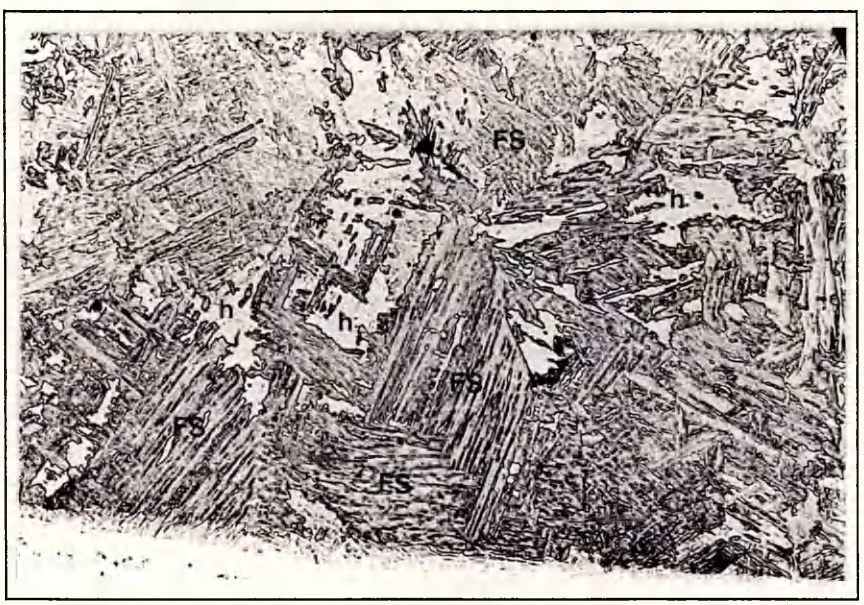

Fig. 8.11(d)
Steel D
HI=2.5kJ/mm
Hv=244-232
236.2
300X

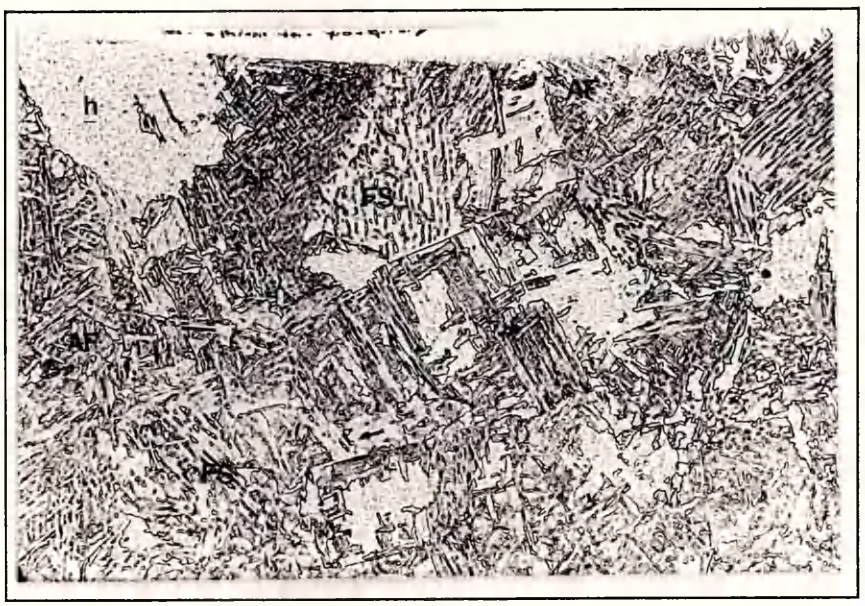

Fig. 8.11(e)
Steel D
HI=3.0kJ/mm
Hv=232-216
222.3
300X

Fig. 8.11(f)
Steel D
HI=3.5kJ/mm
Hv=227-210
217.8
300X

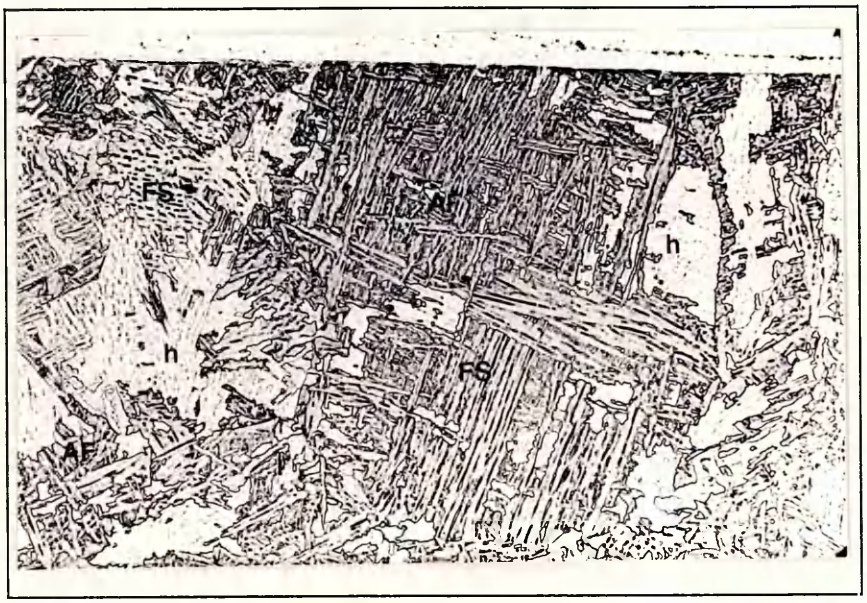

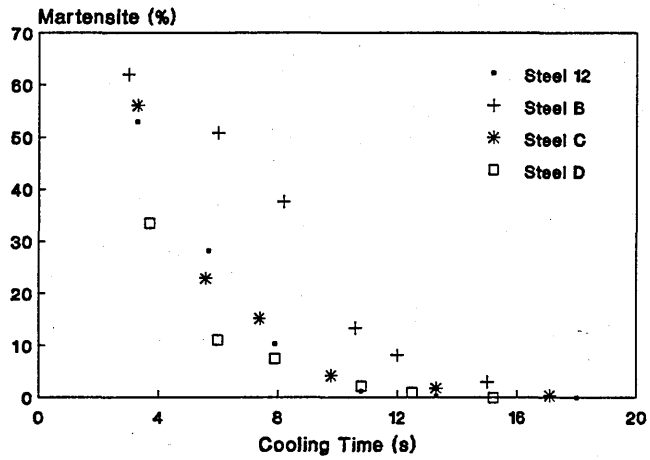

Figure 8.12- Variation of the amount of Martensite with respect to cooling time (Δt_{8-5}).

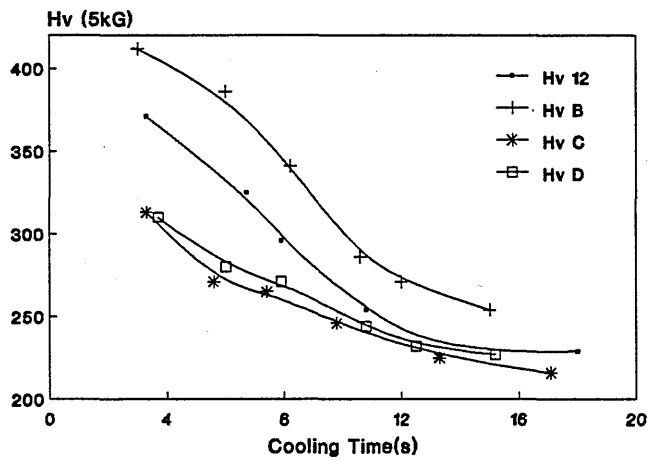

Figure 8.13- Variation of maximum hardness with respect to cooling time (Δt_{8-5}).

CHAPTER 9 DISCUSSION

9.1 Thermal Cycle Measurement

9.1.1 Introduction

The thermal cycle is a critical link in understanding the transformation from the parent microstructure to the **HAZ** structure and consequently to the changes in crack susceptibility and mechanical properties. Most previous work is considered to be unreliable with regard to the inaccuracy of its measurement of weld thermal cycles. The simplicity of much equipment employed in most previous work, although attractive from their operational and cost viewpoint, has resulted in it not being fast or sensitive enough to the extent required by real weld thermal cycle measurement. As a result, subsequent analysis and conclusions based upon this data must contain a significant element of doubt.

The purpose of the actual thermal cycle measurement in the current work was to generate thermal data which could be reliably employed in metallurgical analysis of the steels under investigation. This was achieved by developing a new approach in which the thermal data **as measured** was used in the thermal analysis of the microstructures produced in the coarse grained region of the HAZ's of the steels under study. This direct use of thermal data required greater accuracy in the measurement of thermal cycles than previously achieved and considerable effort was expended in improving recording techniques.

9.1.2 Technique

The technique adopted for measuring the weld thermal cycle in the coarse grained region of the HAZ (at the root of the bead) does not appear to have caused excessive disturbance of the heat flow due to the presence of the hole in the plate. This was confirmed by observations of longitudinal sections similar to Figure 5.21. The minimization of this effect was attributed to the holes being drilled perpendicular to the surface of the plate in a manner such that the thermocouple attached to the bottom of the hole would be normal to the fusion line [Kohno and Jones,1978 and Barlow, 1982a]. The procedure adopted for the

positioning and attaching the thermocouples was found to be successful. Although some losses occurred, not less than an average of three thermocouples out of four for each experiment were able to supply data for analysis. This technique is very time consuming and a great deal of care was required during the preparation of the experiment. However, no other alternative technique could be devised so that the method described was used throughout the work. Cleanliness of the holes, preparation of the thermocouple hot junction and a firm attachment of the thermocouples to the bottom of the holes are considered very important for successful measurement employing the drill hole technique. Although time consuming, the success of the technique in improving accuracy, reproducibility and general robustness did allow rapid processing of the experimental data such that much of the time spent in mounting thermocouples was more than recovered during later thermal analysis.

9.1.3 Welding Procedure

The welding consumables (nickel wire and an acid flux) gave adequate stability to the submerged arc welding process used. The choice of 300A and 30V with a range of welding speeds of 2.6-11.3mm/sec was suitable to achieve the range of heat inputs of 0.8-3.5kJ/mm without causing instability in the welding process which could compromise the success of the measurements. None of the thermal cycles measured showed any unexpected behaviour which could be accounted to the choice of the welding parameters.

9.1.4 Data Gathering System

Up to the present work, the data employed in thermal analysis have been gathered by recording instruments which are basically chart recorders. Although these instruments can give information with regards to the thermal history of a point under investigation, the data has to be converted to suitable format if thermal analysis of the microstructural transformations is to be undertaken using computers. This operation can be very time consuming and it is likely to be a source of error additional to any errors in actual temperature measurement.

In the current work a recording system was developed in which a modern data gathering unit was employed. This unit was an 8 bit A/D

converter with a resolution of less than 1% of the full scale and an accuracy of 6°C within the range of 200-1530°C chosen for the temperature measurements. In addition, it could be linked to any IBM compatible personal computer (PC) and the transference of the data could be immediately carried out after the experiment. This system provided a facility for storing the data on a floppy disk for future computer analysis. It is worth mentioning that the time spent between the welding operation and the graphical visualization of the thermal cycles for one experiment was achieved in less than 30 minutes, thus compensating for the time spent in mounting the thermocouples.

The reproducibility of the measurements will be discussed later in this section. However it is important to point out that the data gathering system developed in the current work proved to be reliable and flexible. A total of 83 thermal cycles were measured and very good agreement was achieved between test welds employing the same heat input. The interface amplifier built had an important role due to the very low output of the Pt/Pt-13%Rd thermocouples . By amplifying the output signals to the extent of the total scale available in the data logger unit used, it was possible to achieve a successfully graphical representation of the thermal cycles (Figures 5.9 to 5.20) with the same resolution of the recording unit, i.e. of the order of 1%. The possibility of dealing with the data **as they were gathered** brought a very high degree of accuracy to the information supplied by the software designed to produce the temperature-time diagrams, peak temperatures, heating and cooling times. It is important to point out that in most previous work, this information was obtained from plots which had been converted on the basis of calibration tables according to the type of thermocouple used. This procedure certainly gives insufficient accuracy and can lead to gross errors.

9.1.5 Thermal Cycles

9.1.5.1 Heating

The increase in heat input resulted in longer heating times (Table 5.3). This effect was also observed by Tecco [1985] and Andrade [1985] but no attempt was made to explain it. No other workers appear to have noted this effect, possibly due to insufficient accuracy in their technique. An explanation is found by establishing a parallel with the

decrease in bead penetration and fusion area as a consequence of the decrease in welding speed, verified by Allum and Quintino [1985]. According to them the heat transfer to the plate (as associated with plate melting) is small due to the arc acting on a cushion of deposited molten metal instead of directly on the plate. The molten metal tends to shield the action of the arc.In the present experiments carried out the increase of heat input was achieved by the decrease of welding speed. Therefore, similar influence can be expected because an increased amount of molten metal was obtained as the welding speed decreased and consequently more time was required for the heat to be conducted to the HAZ.

The majority of the peak temperatures recorded were within the range of 1300-1500°C (Table 5.3). This range conforms with the general pattern of results from accurately placed thermocouples in the coarse grained region of the HAZ. On the basis of observations of the longitudinal sections of the welded plates it was judged that for temperatures above 1400°C approximately, the thermocouples were positioned at the fusion line. Similar ranges of temperatures were found by other authors. Measurements carried out by Phillip [1983] found that at a distance of 0.38mm from the fusion line the peak temperature was 1300°C. Smith et al [1970] measuring thermal cycles in the HAZ found temperatures just below 1500°C at the fusion line. Kohno and Jones [1978] assumed that for peak temperatures above 1350°C the thermal cycles measured were related to the fusion line. In addition, the peak temperatures found in the current work may also serve to support the choice for temperatures higher than 1300°C as the basis for simulated thermal cycles. Abson et al [1978] suggested that transformation structures arising in coarse grained heat affected zone regions in carbon-manganese steels could be understood and predicted for austenitising temperatures ≥1300°C.

9.1.5.2 Cooling

Analysis of the cooling curves indicates that an inflexion was noted at temperatures between 1100 and 900°C in the cooling curve. This was even more noticeable as the heat input increased. This behaviour was also found by Apps and Coward [1967] within a similar range of temperatures. They suggested that it was caused by solidification progression in welding. Most of the latent heat of fusion is released at

the end of the welding pool and transfer of this heat could result in an inflection in the cooling curve. Tecco [1985] noted the same inflexion in the cooling curves. A similar explanation was given attributing this phenomenon to temperature fluctuations due to the solidification front within the pool. It is therefore considered that high temperature inflexion can be ignored in the thermal analysis to determine transformation temperatures.

The results obtained for cooling times through 800-500°C (Δt_{8-5}) (Table 5.3) and 800-300°C (Δt_{8-3}) (Figure 7.3) confirm a very good agreement between measurements in test welds at the same heat input. This observation also applies to steel 12 up to a heat input of 2.5kJ/mm. At heat inputs of 3.0 and 3.5kJ/mm in the experiments with steel 12 the cooling times were higher than those obtained for steels B, C and D. This is explained by the heat flow regime in the thinner plate (25mm), steel 12. At these heat inputs, the 2-D heat flow applies for steel 12 as shown in Table 5.4. Consequently, the heat sink efficiency is decreased resulting in longer cooling times. Although the same should have applied for 2.5kJ/mm, the results confirmed that the critical thickness calculated is irrelevant considering that is only slightly higher than 25mm. The other steels, B, C, and D, were thicker and 3D heat flow occurred at all heat inputs.

Up to a heat input of 2.0kJ/mm, Figure 5.23 shows a very good agreement between Δt_{8-5} theoretically predicted and measured in the test welds. For higher heat input, a clear tendency to longer cooling times than those predicted is demonstrated. These longer cooling times measured can be related to a decrease of the heat sink efficiency of the plates due to their dimensions.The theoretical predictions used [Barlow, 1982b] were for plates of infinite width. In his work examining the effect of the width, Barlow [1982b] verified that a bead-on-plate weld made at 3.2kJ/mm on a 50mm thick C-Mn steel plate would saturate through the thickness before the weld fusion line cooled below 300°C, increasing Δt_{8-3} by 25% over the value expected for true 3D cooling. By analyzing the distribution of various peak temperatures as a function of plate thickness and fusion line to plate edge distance with 3.2kJ/mm as shown in Figure 9.1, he estimated that if the test plate half width (from the fusion boundary to a plate edge) for a particular plate thickness is less than that in Figure 9.1 for a low peak edge temperature (e.g. 50°C), it is possible that thermal saturation will occur in the plate

before the weld has cooled sufficiently. This influence was also examined by Kohno and Jones [1978].According to this investigation, 400mm was the necessary width of 25mm thick plate such that 100°C would be the maximum edge temperature for heat inputs of up to 6.0kJ/mm. The uniform tendency verified in all experiments for heat inputs higher than 2.0kJ/mm can be attributed to heat reflections due to the dimensions of the test plates. Their design was such that each weld bead was distanced 40mm to one edge and 110mm to the other (refer Figure 5.2). By applying the results in Figure 9.1 to the test welds with 3.0kJ/mm the further edge from the bead might have achieved approximately 100°C, whereas the edge at 40mm reached over 150°C.

9.2 Thermal Analysis Technique

The use of data loggers in actual thermal cycle measurements had been reported before [Barlow, 1982a]. However, no attempt was made to analyze the microstructural transformations in HAZ employing the thermal data gathered.

The novelty of the present work lies in the successful employment of actual thermal data in thermal analysis of the transformation temperatures. In addition, this work has the quality of showing the drawbacks which can be found in the use of this technique and some methods to overcome them.

The software routine written to assist the thermal analysis could not completely fulfil the objective of identifying the transformation temperatures. Electrical background noise gathered from the arc or even from the power supply seemed to be the main drawback. Another possible problem which has been raised is the influence of the nature of the data collected during the measurements. The data logger employed was of an analog/digital (A/D) converter type and the main characteristic of these data acquisition equipment is that the recording is done in steps. This implies that there is an interval of time during the measurements in which the analog information (output from the thermocouple) is converted into digital and stored on the memory. By applying the 'In Situ' thermal analysis using the software routine it was verified that both the electrical background noise and the interval between recordings had been amplified (refer Figure 6.1) to an extent that originated interferences which prevented **a direct detection** of the

transformation temperatures.

One approach which attempted to minimise both of these discontinuities was the introduction of a filtering routine to the programme. In fact this brought a significant improvement to the thermal analysis and indications of transformation started appearing in the curves generated by 'In Situ' thermal analysis. However, this could not be extended to all experiments. Furthermore, during the analysis of the various thermal cycles employing the filtering routine, no systematic number of points could be defined to be filtered. That had to be done by means of increasing progressively the filter factor until a satisfactory shape of curve was achieved. This proved to be very time consuming and a possible source of error. That is, a more uniform curve could be obtained by increasing the filter factor but indications of transformation temperatures could be suppressed as a consequence of strong filtering (refer Chapter 6). The possibility of eliminating indications of transformation due to strong filtering has also been found by Wang [Wang,1990] in thermal analysis of weld metal.

The changes introduced in the temperature/temperature method (refer Chapter 6) as previously developed by Tecco [1985] did, in fact, prove to be advantageous. The reference temperatures generated by the regression analysis of an actual cooling curve could be readily obtained and were used in place of the temperatures measured by Tecco in untransformed steel. In addition, the differentiation of the curve resultant from the temperature/temperature method proved to be a useful supplement to the differentiation (dT/dt) of the temperature/time curve.

By submitting the data generated by the 'In Situ' thermal analysis to statistical calculations it became evident (by the graphs presented in Chapter 7) that the discontinuities such as noise and time intervals discussed above, did not appear to have caused undue interference in the thermal analysis. Certain ranges of transformation temperatures which were not clearly shown by the first technique employed could be detected with a satisfactory accuracy. Its development has been extensively discussed in Chapter 7 and the transformation temperatures obtained in the test welds will be discussed later in this chapter.

The 'In Situ' thermal analysis as originally developed by Granjon

and Gaillard [1966], modified by Phillip [1983], and improved by Tecco [1985] has been shown to be a very powerful technique in analysis of microstructural transformations using real weld thermal cycles. The use of a modern data gathering system combined with computer software routines employed in the current work, has taken one further step towards the full use of the potential capability of the 'In Situ' thermal analysis. However, it became clear in the development of the thermal analysis that most difficulties were associated with the limitations found with regards to the technical characteristics of the data logger unit employed. Although the data gathering unit was shown to be satisfactory in measuring the thermal cycles - and the discussion about the reproducibility of the measurements has proved so- it did not fully satisfy the need for more accurate measurements in the 'In Situ' thermal analysis. A 12 bits unit with faster recording speed and consequently higher memory capacity would be of greater adequacy in thermal analysis using real thermal cycles.

9.3 Microstructural Examination

9.3.1 Parent Plates

The steel making process had an important role in the size and distribution of the microstructures in the steels under investigation. The accelerated cooling process (OLAC), to which steels B, C and D were submitted, was very effective in decreasing uniformly the ferrite grain size. Between them, the smallest grain size, found for steel D, could be accounted for by the higher Ni and Mn contents. It is well known that the addition of these elements depresses the γ to α phase transformation to lower temperatures, i.e. both A_{r3} (start of the decomposition of austenite) and A_{r1} (end of the decomposition of austenite) are lowered. On the other hand, the result of the conventional normalizing heat treatment for steel 12 was less efficient in providing smaller and more uniform ferrite but gave a better distribution of the pearlite. The pearlite was also finer than that found for steels B and C. This variation in ferrite grain size might have been caused by the fact that the time spent in the region where recrystallization occurs, which is about 100°C above Ac_3 [Honeycombe, 1987], was not sufficient to achieve the homogenous austenite grain size required for uniform ferrite. Apart from fine ferrite, it has been reported [Youn, 1987] that the second phase in the accelerated cooled steels is

more likely to be bainite as opposed to the pearlite usually found in normalized steels. Kozasu [1983] described the microstructure of accelerated cooled steels as consisting of refined ferrite grains with some substructures, and a fine and uniform dispersion of bainite in place of banded pearlite. Morikawa [1985] verified that when a pearlite colony was small, a lamellar structure developed perfectly as usually observed in steels cooled slowly from austenite. In the case of relatively large pearlite colonies he observed what he called 'pseudo-pearlite' and this would appear with less cementite inside a colony. In the optical metallography carried out in the present project all steels had pearlite as second phase. The coarser pearlite found in B and C could explain the slightly higher hardnesses obtained for these steels in comparison with D and 12 (see Figures from 8.3(a) to 8.3(d) in Chapter 8).

One of the features of the OLAC-processed plates is to suppress separation or splitting as it is also known, which generates 'hook cracks' during forming. This is due to the disappearance of banded microstructure [Arikata, 1985]. According to this author the banding effect appears in controlled rolling at finishing rolling temperatures below A_{r3} because of the development of crystallographic texture. In OLAC steels, because the controlled rolling stops just above A_{r3} at which point accelerated cooling starts the banding effect hardly appears.In the present steels this was not effective in steel B and to a lesser extent in C (refer Figures 8.2(b) and 8.2(c)). This leads to the possibility that the accelerated cooling started when the temperature of the plate had cooled below A_{r3}. In addition, it indicates the importance of controlling the finishing rolling temperature above A_{r3} for each steel in order to avoid banded microstructures.

Steels B, C and D show segregation, probably due to continuous casting. Internal quality has been reported [Walker,1988] as a potential problem in the continuous casting process. The presence of the segregation seems to disrupt the general pattern of the microstructure found in the plates. Smaller ferrite grains seem to be associated with the segregation. Higher concentrations of pearlite aligned with the segregation was also found (refer Figures 8.4). The presence of segregation is very undesirable because it gives preferential sites for initiation of brittle fracture. Consequently, it decreases the through-thickness ductility which is claimed [Nippon Kokan, 1983] to be one of the achievements of the OLAC steels. The segregated regions also had

very thin non-metallic inclusions. These were identified by SEM analysis as sulphides (predominantly MnS) despite the low general S level in these steels. For steel 12 the non-metallic inclusions were again identified as MnS were more uniformly distributed in the matrix which was less banded. The inclusions were also less elongated indicating less severe reductions during the rolling process.

9.3.2 Coarse Grained Region

9.3.2.1 Microstructural Identification

The establishment of an adequate scheme for the identification of the various microstructures in ferritic weld metal has been a matter of discussion for several years. The IIW first pronounced on this matter through its Document II-A-389-76 [IIW, 1976]. However, the same systematic approach has not been reported for the HAZ and in particular, for the coarse grained region. In this respect, a consultation with the Welding Institute [Bailey, 1989] was made and it was suggested that the use of the terminology which had recently been published by the IIW [1988] for weld metal could be used. In this document, although descriptions and microphotographs were given for the five main microconstituents (namely, primary ferrite, acicular ferrite, ferrite with second phase, ferrite carbide aggregate, and martensite) and their sub-categories, it was found that there was a lack of a similar presentation for the bainite and martensite microstructures. Difficulties in adopting the suggested terminology were envisaged in the initial observations of the samples due to the considerable proportion of bainitic microstructures found, in all specimens within the range of heat inputs used and the percent of martensite found in most samples at heat inputs of up to 2.5kJ/mm . At this stage, the author thought of applying a different scheme able to cover more broadly the microstructures found in the present work. This was accompanied by an extensive survey which showed that most work on HAZ's presented a **very general description** of the microstructures and **very seldom** was this accompanied by a clear identification on the micrographs. Two other important aspects were noted during the survey. First, the investigations on heat affected zone were very much concentrated on HSLA type of steels, developed during the 70's, in which carbon is around 0.17-0.22% and the microalloying elements are often Nb and/or V, and/or Ti [Watkinson, 1967; Dolby, 1970; Smith, 1970; Perdigao, 1978

and Andrade, 1985]. Secondly, in the majority of these studies the microstructural analysis was conducted on the basis of simulation or dilatometry. As presented in Section 2.2.1 (Chapter 2), the validation of using some of the conclusions found by simulation to predict microstructures and properties of real weld heat affected zones remains a highly debated matter. The thermal history of an actual thermal cycle cannot be thoroughly reproduced by those equipments employed in simulation. Uncertainties with regard to the most adequate peak temperature to reproduce the austenite grain size of an actual HAZ also seems to exist. Some other recent work which dealt with steels of a lower carbon content (C≤ 0.14%) was also found but the microstructures were from simulated specimens [Koso et al, 1981; Thaulow et al, 1987 and Mckeown, 1983].

In respect of bainitic transformations, some extensive studies [Habraken et al and Pickering, 1967] have been carried out in order to understand the morphology, crystallography and mechanical properties of certain features of the bainite reaction, in particular the two major forms, namely upper and lower bainite . Habraken et al [1967] pointed out the difficulty in distinguishing between lower bainite and self-tempered martensite (or autotempered martensite) in lower carbon alloy steels. They also claimed that self-tempered martensite presents higher toughness than bainitic microstructures. Pickering [1967] investigated the effect of carbon content in bainitic transformation and found that the temperature at which upper bainite is replaced by lower bainite is about 450°C in steels containing 0.1% C. He also suggested that upper bainite has a generally higher impact transition temperature despite its lower strength, than does lower bainite.

The decision to apply the terminology suggested, i. e. IIW [1988], was taken therefore, because there is no alternative terminology for microstructures in the coarse grained region of the HAZ. The limited number of examples found in the literature did not provide sufficient information for the introduction of a more informative classification system. It is important to point out that the terminology adopted by the IIW [1988] for weld metal is based on microstructural features not on properties of the microconstituents. That is, for instance, upper bainite and lower bainite can be identified as ferrite with aligned second phase (FS) but this does not imply that they have similar properties. In the present work no distinction could be made between lower bainite and

self-tempered martensite. Consequently, lower temperature transformation products have been identified as martensite. It is suggested that the introduction of a classification system for HAZ is a matter of some urgency. However, such a classification would require IIW approval or international acceptance.

9.3.2.2 Microstructural Examination

As expected, increase in heat input resulted in a decrease in martensite in the coarse grained HAZ's of all steels and a resultant decrease in measured hardness. This is clearly shown in Table 8.1. The variation of the martensite showed a very close relation with the cooling times (Figure 8.12). Similarly, the maximum hardness measured in each test weld HAZ was related to cooling time and content of martensite (Figure 8.13). The type of martensite found in the heat affected zones seems to be lath martensite. This type of martensite, as opposed to twinned martensite, is associated with a content of carbon lower than approximately 0.25% [Porter et al and Honeycombe, 1987].

Steel B had the highest proportion of martensite (with 13% at a heat input as high as 2.5kJ/mm) and the laths presented were very coarse. From the hardness measurements, B presented the hardest HAZ in the range of heat input employed (0.8-3.5kJ/mm). At the lowest heat input the maximum hardness value was 412Hv and the mean was approximately 395Hv. These values drop markedly to values around 280Hv (13%M) at heat input of 2.5kJ/mm. As the heat input increases hardness decreases reaching a mean value of approximately 240Hv at 3.5kJ/mm. For steel 12 the martensite present was less coarse than B. The highest hardness value measured at 0.8kJ/mm was of approximately 370Hv and the mean was of 360Hv. Similarly to B, the drop in hardness to values not much higher than 280Hv was verified at a heat input of 2.0kJ/mm with martensite content of approximately 10%. For higher heat inputs (3.0-3.5kJ/mm) hardnesses as low as 220Hv were found. Unlike steels B and 12, steel C presented a less steep variation in hardness as the heat input increased within the range of 0.8-2.5kJ/mm. Although the proportion of martensite was similar to that presented by 12 in the range of heat input of 0.8-2.0kJ/mm the heat affected zone was not as hard. The martensite found presented less coarse than that in the HAZ of steel 12. Maximum values of hardness were registered that were not much higher than 300Hv at 0.8kJ/mm.

Steel D followed the pattern of C with mean hardnesses having very little difference, possibly within the experimental error. The martensite laths were fine and similar to C. In respect to martensite content, it was lower than that obtained in C, being as low as approximately 10% at heat input of 1.5kJ/mm.

A criteria had to be laid down to identify the transformation temperatures of the martensite detected by the 'In Situ' thermal analysis. This was established on the basis of changes in hardness as a result of increase in heat input and, consequently, decrease in martensite content. By examining the marked changes in hardness it can be verified that the maximum drop in hardness obtained for steel 12 was at a heat input of 2.0kJ/mm (10.3%M) and in B was at 2.5kJ/mm (13.3%M) (refer Figure 8.13). Although this change was not as marked as that for C and D owing to the low maximum hardness profile presented by these steels, the maximum hardness of C became similar to D when the percent of martensite was lower than 15% at 2.0kJ/mm. In D the proportion of 11.1% was achieved at heat input of 1.5kJ/mm. Thus, it appears that martensite above 10% influenced the steel heat affected zones by increasing the hardness. For martensite content lower than 10%, softer microconstituents had a greater influence and, consequently a decrease in hardness was obtained. In this manner, the transformation temperatures associated with martensite were calculated as an average of the lower ranges of temperatures as shown in Table 7.2 up to martensite of 10%. On this basis, the average range of transformation temperatures of the martensitic areas found in the HAZ of the steels B, 12, C and D was 433-359°C; 440-368°C; 442-353°C and 450-345°C respectively. The lower carbon content of D (0.08%) seems to have contributed to the slightly higher Ms compared to the other the steels. By applying the same analysis the increasing order presented for the Ms followed the decreasing order of carbon content in B, 12 and C, i.e 0.13, 0.12 and 0.11% respectively. Finally, the lower range of transformation temperatures found for the test welds other than those associated with martensite could be related to lower bainite as discussed below.

The difficulty in distinguishing between tempered martensite and lower bainite in the steels examined has already been mentioned. Unfortunately the literature is of little help in steels of these compositions so that the problems of interpretation are obviously

widespread. Hardness is often used to distinguish martensite and this does offer some help. For steel B, the hardness level of 400Hv measured in the HAZ produced at a heat input of 0.8kJ/mm is a clear demonstration of the presence of martensite. For the other steels, where macrohardnesses did not exceed 350Hv, the proof is less conclusive. However the fact that the microstructures of all the steel HAZ's produced at low heat inputs were very similar offers clear evidence that some martensite was present. Unfortunately, insufficient time was available to use electron microscopy which would have given a clearer distinction between the low temperature transformation products.

Transformation temperatures associated with martensite in the HAZ were quite high, 450-345°C. However the temperature of the start of martensite (Ms) within this range is frequently quoted for lower carbon steels. Figure 9.2, taken from Porter and Easterling [1987] shows that martensite transformation temperatures (Ms and Mf) are closely related to carbon content. Ms and Mf increase as the carbon content decreases. Rothwell et al [1980] investigating steels with carbon within 0.06-0.08% associated the range of 480-420°C with autotempered martensite (low carbon martensite that forms at a high enough temperature for tempering to occur on further cooling). On the other hand, for intermediate carbon steels (carbon of approximately 0.14%), a similar range accounted for lower bainite. They also found that relatively high toughness was related to both lower bainite and autotempered martensite structures as opposed to the low toughness caused by the presence of upper bainite. Boniszewski [1984] studying heat affected zone of some modern low carbon (0.14%C) low sulphur (0.009%S) steels found autotempered martensite from electron microscope examinations associated with a maximum of 397Hv2.5 down to 322Hv2.5. On the basis of carbon content in the steels it could be expected that all martensite would be autotempered. However, the amount of autotempering is dependent on the cooling time. For fast cooling time (e.g. at a heat input of 0.8kJ/mm) the autotempering would not be too effective and high hardness could be expected. This was evident for steels B and 12 and to a lesser extent for C and D. As the cooling time became longer a clear decrease in hardness was obtained for all steels.

The range of 610-460°C was associated with the transformation temperatures of austenite to ferrite with second phase (FS) in most test welds. For steel 12 at heat inputs of 3.0 and 3.5kJ/mm this range was

higher (630-548°C) owing to the slower cooling rates achieved. With respect to these ranges of transformation temperatures of FS microstructures, no comparison with previous results could be made due to the lack of information in the literature regarding thermal analysis employing measurements of real weld thermal cycles. Comparisons with results obtained from simulation process or dilatometric analysis would be too speculative because correlations of microstructures with transformation temperatures are very limited and microturctures bear little resemblance to real HAZ microstructures. Identification of individual microstructural features and phases is virtually non-existent.

From the results obtained in the microstructural examination, it could be noted that carbon content had an important role in changing the width of the laths of the martensite as observed for all steels, in particular for steels B and 12. In this respect, the laths of martensite in B were thicker, with consequences in higher hardness. For these steels, the increase in heat input provoked a decrease in the amount of martensite, reflected by a decrease in hardness. With steel 12 this was even more marked (due to lower cooling rates) for heat inputs above 2.5kJ/mm. The influence on the coarsening of softer microstructures seems to be preponderant at this stage in steel 12. Steels C and D behaved similarly for heat inputs higher than 1.5kJ/mm. The slightly higher mean hardness for C in test welds at 0.8 and 1.5kJ/mm could be associated to the higher carbon content found in this steel. For higher heat inputs the similar proportion of softer microconstituent brought them to a similar mean hardness level.

9.3.2.3 Hardenability

HAZ hardness depends on the hardenability of the steel, on the cooling rate and, to a lesser degree, on the prior austenite grain size. The hardenability of a steel may be generally correlated with the carbon equivalent (Ceq). Because carbon equivalent formulae are empirical, the influence of various alloying elements may differ with total alloy content or carbon content. Thus many different research workers have produced Ceq formulae which can vary markedly. The most widely used Ceq formula is that adopted by IIW [1967] and is represented by IIWCE:

$$IIWCE = C+Mn/6+(Cr+Mo+V)/5+(Ni+Cu)/15$$

In this respect a modification by Dolby (1972) is also popular:

Ceq= IIWCE+Si/6

These formulae seem to be most suitable for conventional structural steels (e.g. %C 0.13-0.23, %Mn 1.0-1.5). The Ito and Bessyo (1969) formula is also widely used and can be represented by P_{cm}:

P_{cm}= C+Si/30+Mn/20+Cu/20+Ni/60+Cr/20+Mo/15+V/10

This formula is claimed to be suitable for steels with a wide range of C (0.07-0.22%) and alloy elements and also includes a term for diffusible hydrogen in the weld metal.

In a carbon equivalent formula, the hardenability effect of each alloying element is divided by a factor that gives the carbon equivalent of that element, i.e. the effect of the percentage of element on the steel expressed in the terms of an equivalent percentage of carbon. Thus a carbon equivalent formula is a convenient, but empirical, way of expressing hardenability in a single figure. In this respect, taking only into account the carbon content of the steels under study, the following decreasing order **B** (C=0.13%), **12** (C=0.12%), **C** (C=0.11%) and **D** (C=0.08%) is obtained for the degree of hardenability. The contribution of Mn is usually considered in the calculations of Ceq and its content is divided by the factor 6 as first proposed by Dearden et al [1940] and adopted by the IIW [1967]. In this respect, **B** and **C** have similar hardenability (Ceq=0.35) followed by **D** (Ceq=0.34) and **12** (Ceq=0.33). According to the formula of carbon equivalent adopted by the IIW [1967] (see Table 4.1 for Ceq*) the highest Ceq was of **D** followed by **12**, with **B** and **C** presenting similar carbon equivalent . By adding Si/6 to the IIW formula as suggested by Dolby et al [1972] the deceasing order of carbon equivalent is **D** and **12** (Ceq=0.44), **C** (Ceq=0.42) and **B** (Ceq=0.41). The formula adopted by the Japanese Welding Engineering Society (see Table 4.1 for Ceq**), which was due to Ito and Bessyo [1969] was also calculated and the results shows **12** more hardenable than **B** followed by **C** and **D**. Only carbon content gives a true picture of the hardenability rating of the steels determined experimentally.

Thus the concept of carbon equivalent seems to be flawed when applied to modern structural steels produced by the OLAC route.

Additionally, the concept of carbon equivalent is very limited because it may only apply to a fixed welding conditions and, consequently it does not depict the softening trend verified in steels under study as cooling time increases owing to higher heat inputs.

More recent formulae pursue the determination of the maximum hardness by linking the carbon equivalent to the cooling time through 800-500°C (Δt_{8-5}) as described in Chapter 2. On this basis, a survey was carried out in order to select the best fit predictions for maximum hardness in the HAZ's of the steels used in the present work. This can be seen from Figure 9.3. As is shown, only that of Yurioka and his co-workers [1987] correlates satisfactory with steels C and D, and partially with 12 for heat inputs in the range of 0.8-2.0kJ/mm. Poor correlation was obtained for both 12 (for heat inputs higher than 2.0kJ/mm) and B. Nevertheless, B seems to be best predicted by Yurioka [1981] and Suzuki [1983].

On the basis of the poor predictions found for steels C, D and 12 the following new formula was developed by employing statistical analysis (multiple regression) and adopting the carbon equivalent proposed by Yurioka [1981] to the chemical composition of the steels in the present work.

$$H_{max} = 251.7(C) + 101.7\ Ceq_I + 159.7 - [228.7(C) - 92.4\ Ceq_I + 62] \arctan K \qquad ...[1]$$

where

$$K = \frac{\log \Delta t_{8-5} - 2.822\ Ceq_{II} + 0.262}{0.526 - 0.195\ Ceq_{II}}$$

$$Ceq_I = C + \frac{Si}{24} + \frac{Mn}{6} + \frac{Cu}{15} + \frac{Ni}{40} + \frac{Cr}{6} + \frac{Mo}{4}$$

$$Ceq_{II} = C - \frac{Si}{30} + \frac{Mn}{5} + \frac{Cu}{5} + \frac{Ni}{20} + \frac{Cr}{4} + \frac{Mo}{6}$$

Figure 9.4 shows a very good correlation (correlation coefficient r=0.94) obtained by the new formula developed to predict maximum hardness for the steels C, D and 12. However steel B results do not fit the predictions of this equation any better than the earlier predictions shown in Figure 9.3. In the formula developed, Ceq_I is related to the hardness for a long cooling time, and Ceq_{II} corresponds to the critical cooling time when a ferrite structure begins to form in a 100% martensite structure [Yurioka, 1981].

The complex carbon equivalent formulae employed in the development of hardness prediction formula indicates the changes needed in the rather more conventional ones in the analysis of hardenability of modern low carbon steels. Although the variation of hardness is better expressed by the formula developed than those found in the literature, it seems that it is only suitable to the steels studied. A more general application of it would require further investigation on the basis of a wider range of steels. In fact it seems unlikely that any metallurgical principles can be attributed to the formula

The greater hardness of the heat affected zone of steel B might find an explanation by comparing the differences in chemical composition and mechanical properties of the parent plate with those of the other steels. These steels were produced by the OLAC process and are typically 500MPa grade steels. Steel D has the lowest carbon and the highest manganese. It has also additions of Ni and Cu. This seems to compensate for its low carbon content resulting in tensile properties and toughness as high as those obtained for C (refer Table 4.2). The high properties of C was achieved with slightly higher carbon and silicon but lower manganese than D. On the other hand, B has higher carbon, lower manganese and silicon than C and D. On the basis of this description it seems that a good balance in chemical composition was achieved between C and D but the same does not apply to B. For steel B tensile properties were found similar to C and D but higher carbon might have influenced the decreased toughness despite the reduction in manganese and silicon. One hypothesis could be that the decrease in manganese and silicon to compensate higher carbon content and therefore, to keep toughness at the same level found for C and D was not sufficient. That is, the carbon content of 0.13% found in steel B seems to overrule any balance which could be achieved by reducing Mn and Si with benefits in toughness as found for steel C. In spite of the

fine ferrite grain size found for steel B (9.6μm) - and carbon is an effective element to promote the refinement of ferrite grains by lowering A_{r3}- again an unbalanced alloy combination in steel B resulted in lower toughness. With regards to steel 12, too low manganese could account for lower toughness compared to B, C and D. Although the impact test carried out with 12 was at lower temperature (-40°C) than that for those steels (-20°) it could be expected that the result at similar temperature would not be as high as for those steels.

In the formulation adopted for the chemical composition of the OLAC steels, carbon content is kept low and not much higher than 0.1% . Thus, the additions of elements such as Mn, Si, Ni and Cu combined with accelerated cooling process can give the mechanical properties desired without markedly affecting hardenability [Kozasu, 1983]. Although carbon can be efficient in the OLAC process by decreasing A_{r3} and, consequently achieving microstructure with very fine grain (as found in B), this element is the most critical in terms of hardenability. The carbon content of 0.13% seems to have caused the increase in hardness with possible consequences of higher cracking susceptibility compared to its counterpart C and D.

9.4 Implications

This present work has provided evidence that the OLAC steels employed have microstructures with a more uniform and finer grain size than steel produced by a more conventional method (normalizing heat treatment). In most steels, the microstructure produced in the coarse grained region of the HAZ was found to be martensitic for heat inputs in the range of 0.8-2.0kJ/mm. For the steel with lower carbon, higher Mn and Ni, HAZ martensite was clearly identified only up to heat input of 1.5kJ/mm. The type of martensite found was of the autotempered type consistent with the high range of transformation temperatures determined for this microconstituent. For high heat inputs, bainitic microstructures were found to be the major microconstituents.

Difficulties were found during the identification of the various microconstituents. Although hardness measurements followed the variation of martensite content, the degree of difficulty in differentiating this microconstituent from bainitic structures seemed to increase as the heat input increased. Microhardness can be very useful in differentiating

microconstituents and, consequently can give indications of their contribution to the overall hardness. However, the time scale available for this project did not allow these tests to be carried out. Microhardness tests can be time consuming and the risk of no conclusive results was considered very high due to the limited information on the type of steels studied. Future work, using microhardness for the identification of the various microconstituents in the HAZ would obviously be worthwhile.

One of the major applications of the steels studied is in fabrication of offshore structures. In this respect, some integrity requirements are made which are related to metallurgical aspects of welding. For instance, avoidance of HAZ hydrogen cracking is always required since it can initiate fracture in service. This is normally controlled by a limit in maximum hardness in the HAZ. A maximum hardness to protect the structures from environmental stress corrosion cracking (SCC) is also sometimes required. Considering the discrepancies found in the literature regarding to hardness criteria for these two metallurgical aspects mentioned above, it is considered worthwhile for the author to present a brief review on these matters.

The use of a value for maximum hardness in the HAZ was reported as early as to 1939 [Bailey, 1990]. Reeve [Bailey, 1990] (whose cracking test was the forerunner of the CTS test) whilst not knowing the role played by hydrogen concluded that cracking would almost certainly take place immediately after welding if the joint was restrained and if the local Vickers hardness at the weld boundary exceeded 400Hv. Reeve also suggested that there was apparently no danger of cracking if the maximum hardness was below 350 Vickers. Since then, requirements with regards to maximum hardness in the HAZ to avoid hydrogen HAZ cracking have been varying around these values. These different requirements are sometimes also related to the loads with which the maximum hardness criterion is established and this is usually in the range of 2.5 to 10kg. For instance, Dolby [1984] reported that a common requirement is 325Hv5 maximum in as-welded procedure qualification tests. Nevertheless, he announced that tests carried out at laboratories in the UK and elsewhere had suggested that HAZ hydrogen cracking was likely in C-Mn steels when hardness exceeded 350-375Hv2.5, depending upon the levels of hydrogen and restraint. In his conclusions, he suggested that the limit to avoid hydrogen-induced HAZ cracking

could be safely raised to nearer 350Hv5, provided preheating is used to ensure low hydrogen levels. Coe [1973] suggested, as preliminary guide, 350Hv maximum allowable hardness for welding processes giving weld metal hydrogen levels in excess of about 20ml/100g, 375Hv for medium hydrogen processes and 400Hv for low hydrogen processes. A 450Hv limit was also applicable for very low hydrogen systems (such as argon or CO_2 shielded solid wire processes using clean wires and the TIG process).

Boniszewski and Keeler [1984] did not share any of the above views for maximum hardness. They believed, for instance, that the criterion of 350Hv10 as the maximum allowable hardness was no longer true in controlling hydrogen-induced HAZ cracking. According to them, that value was arrived at over a quarter of century before when even so-called 'low hydrogen' electrodes gave customarily 15ml H_2/100g or more. At the time of writing there were electrodes which, after drying at 250-300°C gave less than 5ml H_2/100g consistently, with typical values being 2.5-3ml H_2/100g. Furthermore, they stressed their point by stating that there is no 'magic' HAZ hardness criterion for the avoidance of cracking. In their views some steelmakers still mistakenly belabour this point , whilst neglecting to pursue the HAZ hardness problem in the SCC context, and to develop steels with consistent and predicable HAZ hardenability.

With regards to the avoidance of SCC, some criteria are also found and they vary from 200-350Hv for the maximum hardness to be avoided in the HAZ, either with 10 or 5kg load indentations. Tandberg [1983] who reported a range of 200-260Hv as given in various specifications, believed that these figures are based on attempts to convert the classic 22HRC (248Hv) by Nace, rather than a critical assessment of actual conditions in each case. According to him, conversions as such are not to be recommended as the Nace criterion was based on steels of higher strength than normally employed in welded steelwork, for instance for offshore structures. Furthermore, the cited author supported moving towards 350Hv as a realistic maximum requirement, which was also supported by Gooch [1982]. However some scepticism was shown by him in view of the wide range of environments which can cause SCC, which are unlikely to be covered by a single hardness. Recommended, levels down to 280Hv are also common as a means of avoiding HAZ SCC [Dolby, 1984]. However, to avoid HAZ SCC the specifications of Hv

maximum values less than 325Hv5 is unrealistic and unnecessary except in full sour conditions, in his view, provided a maximum C content is specified on steel purchase.

From the review presented it appears that although a hardness criterion for HAZ hydrogen cracking is widely debated, a compromise hardness level could be reached at 350Hv. Similar value may be appropriate for SCC. In the results of maximum hardness shown in Figure 8.13 it appears that no need for preheating would be required for steels C and D since at the lowest heat input the maximum hardness measured was not much higher than 300Hv5. On the hand, some degree of care should be considered for steels B and 12. Steel B had maximum hardness exceeding 350Hv5 in the range of heat input of 0.8-1.5kJ/mm and at 2.0kJ/mm maximum hardness was just below this value. For 12, 350Hv5 was only exceeded at 0.8kJ/mm. This analysis may indicate a low risk of hydrogen cracking by the steels studied in particular with C and D. Nevertheless, it appears that these steels require further investigation in which cracking tests would be of a greater indication of the susceptibility of the HAZ hydrogen cracking.

Apart from the hardenability property another aspect that has been a matter of concern in the offshore industry lately is the HAZ fracture toughness. In the past, the vast majority of HAZ toughness data consisted of Charpy impact tests. Most of these data showed adequate to highly satisfactory HAZ toughness. Occasional low values were observed in HAZ tests on some steels, but even these tests did not show very low toughness, and they were usually reconciled by conventional Charpy re-testing provisions [Pisarski and Pargeter, 1983 and Royer, 1987]. Consequently, early HAZ toughness investigations based on Charpy impact testing usually concluded that HAZ toughness was acceptable. According to Pisarski and Pargeter [1983], although a certain amount of information on the variation in the HAZ toughness can be obtained by such test, its primary aim is to ensure that a certain quality workmanship is maintained; the nature of the tests, in particular with respect to the often arbitrary position from which the specimens are taken, prevents the Charpy test from being much more. In their view, for instance, since most specimens are taken from a weld containing an inclined bevel, the fusion line is not parallel to the notch, so that along the length of the notch a mixture of different microstructures will be sampled. In multipass welds deposited at low energies the HAZ will be

narrow and the specimens sampling regions other than the fusion line will sample predominantly parent plate or weld metal. Therefore, the toughness values may be unrepresentative of the HAZ . They concluded that since the Charpy test measures the energy required for crack initiation and propagation over the whole crack front, the presence of any localised brittle zones may be masked by the surrounding high toughness material. Nevertheless, the occasional low values may be a genuine indication of a local brittle zone which has been missed by the other specimens. The term 'local brittle zones' (**LBZ**) has been used to describe a discontinuous coarse grained region HAZ found in multipass welding that exhibits low fracture toughness. In this respect, it is a general view that Charpy tests can not assess the significance of the toughness values measured with respect to the brittle fracture resistance of a structure containing LBZ's.

Fracture mechanics tests based on K_{IC} /CTOD have become widely used to evaluate the toughness of the HAZ [Haze and Aihara, 1988]. Unlike the Charpy V test the results from fracture mechanics tests provide a fracture characterising parameter to which enables a structure's fracture resistance to be assessed. However, similar difficulty found in Charpy V test regards positioning of the notch in the HAZ has been found for fracture tests with respect to the correct positioning of the fatigue crack tip in the HAZ needed for the conduction of these tests. It appears that the single bevel or the K-shaped weld bevel have been stipulated in order to obtain a straight HAZ perpendicular to the plate surface [Lessells, 1984].

The LBZ's in the HAZ of a multipass welded joint are usually characterized by grain coarsened zones without reheating thermal cycle or with low temperature reheating, and grain coarsened zones reheated between A_{r1} and A_{r3}. Local toughness of these zones have been mentioned [Haze and Aihara, 1988] to be influenced by metallurgical factors such as hardness, amount of high carbon martensitic islands and grain size. Research programmes have been carried out in order to evaluate the extent of these factors regarding modern steels such as the ones used in the present work. The results appear to have not been conclusive. For instance, Dolby [1984] discussing current problems associated with the specification and fabrication of steels for offshore structures concluded that it was not known, at that time, whether recent trends in steels chemistry (he was referring to low carbon low

sulphur modern steels) have altered HAZ toughness significantly. He added that fracture toughness tests on HAZ regions are recommended in an initial assessment of any new steel type. Until more data are generated by steels suppliers and other organisations these steels also need to be subjected to selected welding procedure qualification tests before production welding is carried out. Harneshaug and Valland [1988] examining the fracture toughness of local brittle zones concluded that controlled cooled steel under certain circumstances may exhibit local zones of reduced fracture toughness. The coarse grained part of the HAZ and the intercritical part of the HAZ may show reduced fracture toughness.According to them, this reduced fracture toughness in the intercritical part of the HAZ was due to the presence of high carbon martensite. Nevertheless, by comparing the accelerated cooled steels fracture toughness results to normalized steels, they found that the former ones, on the whole, presented better results.

The influence of the steel making process and the chemical composition of the new modern steels again appeared very debatable with regards to fracture toughness in particular to local brittle zones found in multipass welding. The apparent high hardenability presented by these steels and its influence on fracture toughness has not in fact been fully understood and can be a matter of further investigation.

The evidences brought about in the present work shows that the situation regarding the significance of microstructure and its associated hardness in the weld HAZ of modern structural steels is clearly unsatisfactory. Much more work is required on typical HAZ's in a wide range of steels in order to clarify the microconstituents, their proportions present and their influence on hardness. Equally, carbon equivalent formulae leave a lot to be desired: at the best they give a useful guide, at worst they are totally misleading. Practically however, there is ample evidence that HAZ hardness is an excellent empirical criterion for the prediction of susceptibility to HICC, SCC and low fracture toughness, provided it is used with common sense.

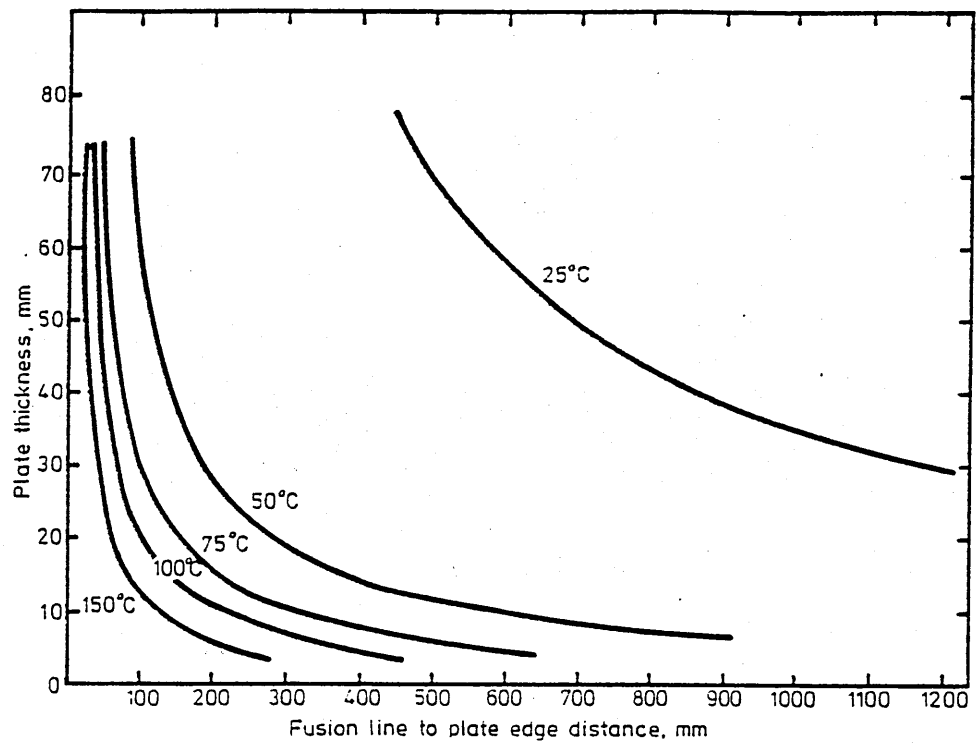

Figure 9.1- Theoretical effect of plate dimensions for different peak edge temperatures at a heat input of 3.2kJ/mm.

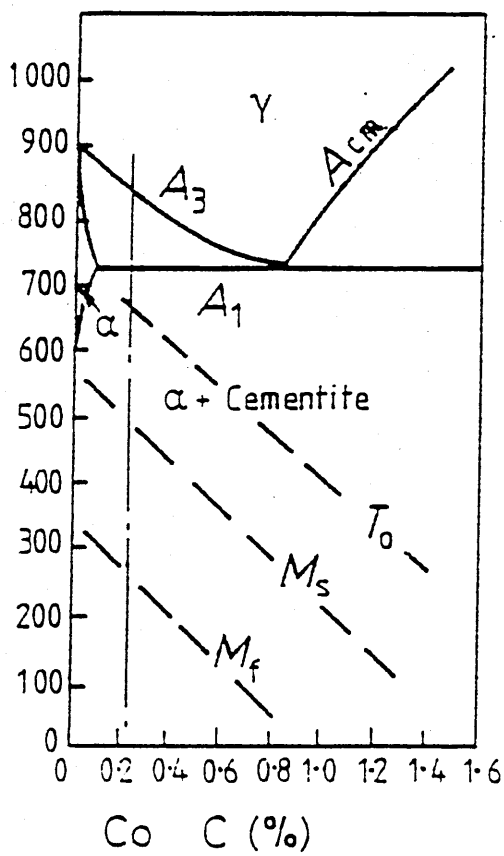

Figure 9.2- The Ms and Mf temperatures as a function of carbon content [Easterling, 1985].

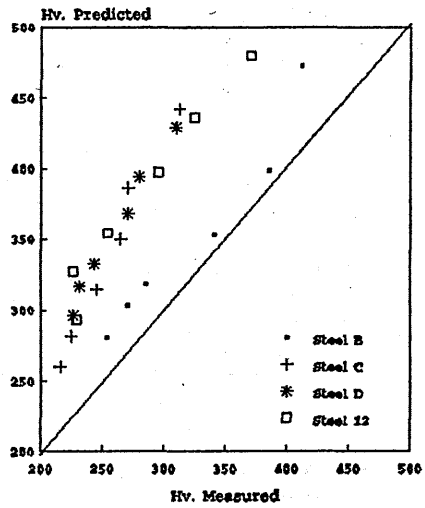

(a)

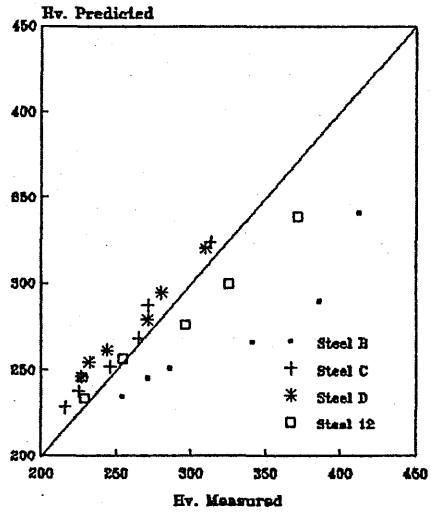

(b)

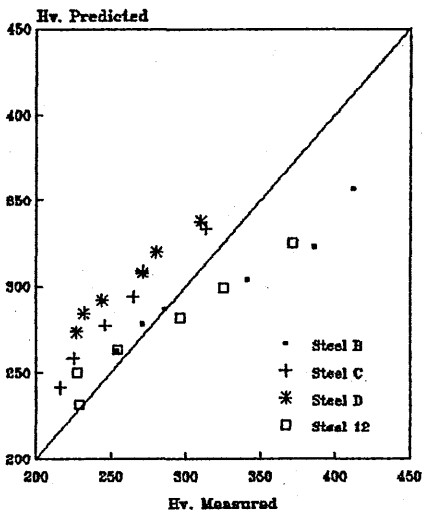

(c)

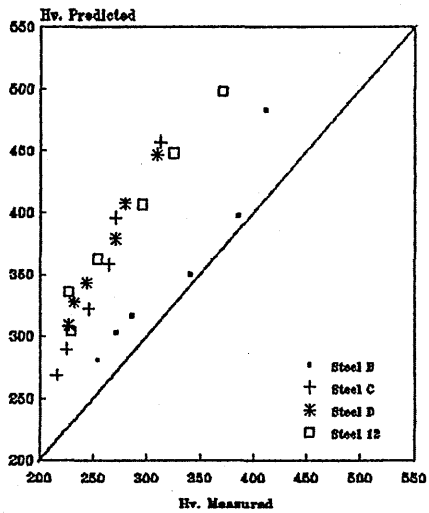

(d)

Figure 9.3- Hardenability of the experimental steels according to some authors.

(a) Yurioka [1981]

(b) Yurioka et al [1987]

(c) Cottrell [1984]

(d) Suzuki [1983]

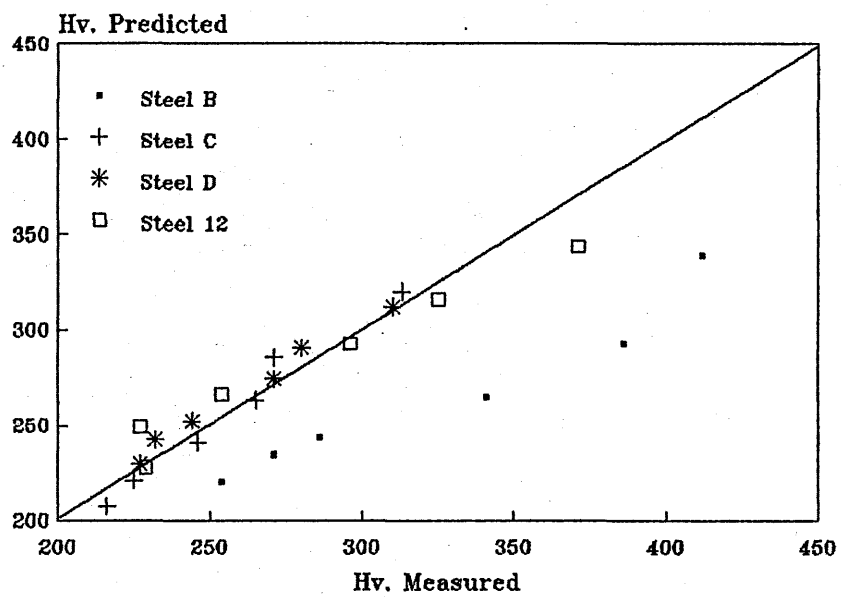

Figure 9.4- Hardenability of the steels B, C, D and 12 according to the formula developed.

CHAPTER 10 CONCLUSIONS

1. The drilled hole technique proved to be suitable for measuring actual thermal cycles in weld heat affected zones. No undue disturbance of the heat flow occurred which could compromise the reliability of the measurements. Thermocouple attachment was reasonably robust resulting in data obtained from 75% of all thermocouples.

2. The data gathering system developed for measuring the thermal cycles proved to be reliable and flexible. Very good reproducibility was achieved between test welds employing the same heat input adding confidence to the overall system.

3. The interface amplifier built for the data gathering system brought an improvement in the resolution of the measurements. This made it possible to use the total scale of the recording unit to obtain the graphical representation of the thermal cycle, despite the low output signal of the thermocouples used.

4. The software programme designed to assist the analysis of the thermal data was capable of giving relevant and accurate information regarding peak temperatures, cooling and heating times. Two difficulties were found which prevented the use of the initial software routine designed to be employed in 'In Situ' thermal analysis. First, was the electrical background noise. Secondly, was the interval of time between each data item gathered. These were solved by statistical calculations applied to the data generated by 'In Situ' thermal analysis. This proved to be satisfactory and transformation temperatures of the various microconstituents in the heat affected zone were determined.

5. The use of actual thermal data in the 'In Situ' thermal analysis is the most suitable for determining the transformation temperatures in weld heat affected zones.

6. Autotempered martensite was identified in the heat affected zone of the all low carbon structural steels under investigation. Low hardness values confirmed that the martensite present was of the autotempered type.

7. The range of martensite transformation temperatures determined was within 450-345°C. The bainitic transformation was 610-460°C.

8. Soft microconstituents such as primary ferrite, acicular ferrite and ferrite with second phase were found in all low carbon steels investigated. Two of the accelerated cooled steels had these microconstituents in considerable proportion at heat inputs as low as 1.5kJ/mm.

9. It was found that the introduction of a classification system for HAZ is a matter of some urgency. However, such a classification would need IIW approval or international acceptance.

10. No existing carbon equivalent formulae were adequate for predicting the hardenability of all the steels studied. Only carbon gave a true indication of the hardenability rating of the steels.

11. A formula was developed which was capable of predicting satisfactorily the variation of hardness with respect to cooling time through 800-500°C for three of the four steels studied.

REFERENCES

Abson, D.J.and Dolby,R.E. (1978).'Microstructural Transformation in Steel Weld Metals- A Reappraisal'. The Welding Institute Research Bulletin,Jul, pp.202-207.

Adams, C. M. (1958), 'Cooling Rates and Peak Temperatures in Fusion Welding'. Welding Journal- Welding Research Supplement pp.210s-215s.

Akselsen, O. M. and Simonsen, T. (1987), 'Techniques for Examining Transformation Behaviour in Weld Metal and HAZ- A State of the Art Review'. Welding in the World, vol..25, No.1/2 pp.26-34.

Allum, C. J. and Quintino, L (1985), 'Control Fusion Characteristics in Pulsed Current GMAW'. Part I - Fusion Characteristics, Metal Construction, Apr.

Andrade, A. M. V. Pia De (1985), 'A Study of Coarse Grained Heat Affected Zones in Ferritic Steels'. PhD Thesis, Feb., Cranfield Institute of Technology, pp.1-267.

Apps, R. L. and Coward, M. D. (1967), 'Measurement of Thermal Cycles in the Weld Heat Affected Zone of Mild Steel'. The College of Aeronautics, Department of Materials, Cranfield Institute of Technology, Sep., pp.1-7.

Apps, R. L. and Milner, D. R. (1963), 'A Note on the Behaviour of Liquid Metal under the Arc'. British Welding Journal, Jul., pp.348-350.

Apps, R. L. and Milner, D. R. (1955), 'Heat Flow in Argon Welding'. British Welding Journal, 2(10) pp.475-485.

Araujo, C. L. D. et al (1989), 'The Measurement and Analysis of Weld Thermal Cycles Using Microprocessor Based Equipment'. Proceedings of The International Conference on the Joining of Materials pp.320-325.

Arikata, K. et al (1985), 'Applications of On-Line Accelerated Cooling to Steel Plates for Shipbuilding and Offshore Structures'. Proc. of SEAISI Japan Conference, Mar.,

Aronson, A. H. (1966), 'The Weldability of Columbium- Bearing High Strength Low Alloy Steel'. Welding Journal- Welding Research Supplement, Jun., pp.266s-271s.

ASM, (1972), 'Atlas of Microstructure Alloy'. Metal Handbook, Vol. 7, 8th edition.

Bailey, N. (1990), 'The Development and Use of Carbon Equivalent in Britain'. Proc. of Select Conference, Hardenability of Steels, Publ. by The Welding Institute, May, pp.25-40.

Barlow, J. A. (1982b), 'The Effect of Plate Size on the Submerged Arc Weld Thermal Cycle'. The Welding Institute Research Bulletim, Mar., pp.77-82.

Barlow, J. A. (1982a), 'Measurement and Analysis of the Thermal Cycles in Submerged Arc Welding'. The Welding Institute Research Bulletim, Jan., pp.5-8.

Bayley, N. (1989), The Welding Institute, Private Communication. Boniszewski, T. and Keeler, T. (1984). 'HAZ Hardness Contol in C-Mn Microalloyed Structural Steels'. Metal Construction, Oct., pp.608-617.

Boniszewski, T. and Moreton, J (1967), 'Effect of Micro-Voids and Manganese Sulphide Inclusios in Steel on Hydrogen Evolution and Embrittlement'. British Welding Journal, Jun., pp.321-336.

Boothby, P.J. and Rodgerson, P. (1984), 'Offshore Structural Steels: Weldability and Hardenability'. Proc. of the Conference Towards Rational and Economic Fabrication of Offshore Structures-Overcoming the Obstacles,
Nov., London, UK, pp.97-103.

Brooks, T. L. and Hart, P. H. M. (1977), 'Do Hardness Measurements Impress You?'. The Welding Research Bulletim, Mar., pp.69-72.

Calex, (1987), 'Temperature and Infrared Thermometry Handbook'. Fourth Edtion.

Chatfield, C (1983), 'Statistics for Technology'. Published by Chapman and Hall, Third Edition

Christensen, N et al (1965), 'Distribution of Temperature in Arc Welding'. British Welding Journal, Feb. pp.54-75.

Cline, H. E. and Anthony, T. R. (1977), 'Heat Treating and Melting Material with a Scaning Laser or Electron Beam'. Journal of Applied Phisics, 48(9), Sept., pp.3895-3900.

Coe, F. R. (1973), 'Welding Steels without Hydrogen Cracking'. Published by The Welding Institute, pp.19-23.

Cohen, M and Hansen, S. S. (1985), 'On the Fundamentals of HSLA Steels'. Proc. International Conference on HSLA Steels' 85, Beijing, China, Nov., Published by ASM International, pp.61-71.

Constant, A. and Murry, G. (1963), Soudage et Technique Conexes, vol. 17, p.405.

Cottrell, C. L. M. (1984), 'Hardness Equivalent May Lead to a More Critical Measure of Weldability'. Metal Construction, Dec., pp.740-744.

Dearden, J. and O'Neil, H. (1940), 'A Guide to the Selection and Welding of Low Alloy Structural Steels'. The Institute of Welding, Vol.3, No.4, Oct., pp.203-214.

Doc. IIS/IIW-382-71 (ex doc.1X-646-69) Commission IX (1971), Guide to the Welding and Weldability of C-Mn Steels and C-Mn Microalloyed Steels.

Dolby, R. E. (1979), 'HAZ Toughness of Structural and Pressure Vessel Steels- Improvement and Prediction'. Welding Research Supplement, Aug., pp.225s-238s.

Dolby, R. E. and Saunders, G. G. (1972), 'Metallurgical Factors

Controling the Heat Affected Zone Tpughness of Carbon: Manganese and Low Alloy Steels'. The Welding Institute Research Report, Jun, pp.1-14.

Dolby, R. E. and Widgery, D. J. (1970), 'The Simulation of HAZ'. The Welding Institute Research Report, M/52/70, Jul, pp.1-15.

Dolby, R.E. (1984), 'Steels for Offshore Construction'. Proc. of the Conference Towards Rational and Economic Fabrication of Offshore Structures-Overcoming the Obstacles, Nov., London, UK, pp.65-73.

Duren, C. F. (1990), 'Prediction of the Hardness in the HAZ of HSLA Steels by means of the C-equivalent'. Proceedings of Select Conference, Hardenabilityof Steels, Publ. by The Welding Institute, May, pp.51-62.

Easterling, K. (1985), 'Introduction to the Physical Metallurgy of Welding'. Published by Butterworths & Co

Gooch, T. G. (1982), 'Hardness and Stress Corrosion Cracking of Ferritic Steel'. The Welding Institute Research Bulletin, Aug., pp.241-246.

Granjon, H and Gaillard, R. (1967a), 'Possibilites Offertes par L'Analyse Thermique << In Situ>> pour L'Etude des Transformations de L'Acier au Cours
du Soudage'. Memoires Scientifiques Rev. Metallurg., LXIV, No. 4, Oct, pp.335-343.

Granjon, H. (1969), 'The 'Implants' Method for Studying the Weldability of High Strength Steels'. Metal Construction and British WeldingJournal, Nov., pp.509-515.

Granjon, H. (1967b), 'Aspects Thermiques et Metallurgiques du Soudage et du Decoupage des Aciers'. Revue de la Soudure, 23, pp.1-9.

Granjon, H. and Gaillard, R. (1966), 'Application de L'Analyse Thermic'. Journee des Aciers Speciaux, Saint-Etienne, May, pp.145-166.

Habraken, L. J. and Economopoulos, M (1967), 'Bainitic Microstructures in Low-Carbon Alloy Steels and Their Mechanical

Properties'. Proc. Transformation and Hardenability in Steels, Symposium Sponsered by Climax
Molybdenum Company of Michigan, pp.69-108.

Harneshaug, I. S. et al (1988), 'HAZ Fracture Toghness in Low Carbon, Controlled Rolled and Accelerated Cooled Steel Used in Nothe Sea Offshore Platforms Structures'. Proc. Seventh International Conference on Offshore
Mechanics and Arctic Engineering, Feb., pp.181-189.

Hart, P. H. M. (1978), 'Low Sulphur Levels in CMn Steels and their Effect on HAZ Hardenability and Hydrogen Cracking'. International Conference Trends in Steels and Consumables for Welding, London, 13- 16 Nov., pp.21-53.

Hart, P.H.M. (1985), 'The Influence of Steel Cleanliness on HAZ Hydrogen Cracking: The Present Position'. Welding in the World, No.9/10 23, pp.230-238.

Haze, T. and Aihara, S. (1988), 'Influence of Toughness and Size of Local Brittle Zone on HAZ Toughness of HSLA Steels,. Seventh International Conference on Offshore Mechanics and Arctic Engineering, Houston, Texas,
Feb., pp.515-523.

Hess, W. F., Merrill, L. L. and Nippes, E. F. (1943), 'The Measurement of Cooling Rates Associated with Arc Welding and their Application to the Selection Optimum Welding Conditions'. Welding Journal, vol. 22, Sep.,
pp.377s-422s.

Hewitt, J. and Murray, J. D. (1968), 'Effect of Sulphur on the Production and Fabrication of Carbon-Manganese Steel Forgings'. British Welding Journal, Apr., pp.151-158.

Hofmann, W. and Burat, F. (1962), 'Immediate Recording of Continuos TTT- diagrams during Welding and Studies on Cold Cracking'. Doc. IIW IX-318-62

Honeycombe, R. W. K. (1987), 'Steels Microstructures and

Properties'. Published by Edward Arnold Ltd., ISBN 0 7131 2793 7, pp.76-165.

Humphries, C. (1971), 'Use of the Thermocouple for Temperature Control and Measurement, Part 1- Choice of thermocople materials'. Welding Research Bulletim, Apr., pp.101-103.

International Institute of Welding (IIW) (1986), 'Hardness Testing in the Heat Affected Zone of Steel Welds'. Welding in the World, Vol.25, No.1/2, 1987, pp.2-10.

International Institute of Welding (IIW) (1976), 'A Technique for the Characterization of Weld Metal Microstructure'. Do. IIW/IIS II-A-389-76

International Institute of Welding (IIW) (1988), 'Guide to the Light Microscope Examination of Ferritic Steel Weld Metal'. IIW Doc.No.IX-1533-88, Jun, pp.1-5.

International Institute of Welding (IIW) (1967), 'Technical Report'. Doc. IX-535-67, IXG-13067,

Ito, Y. and Bessyo, K. (1969), 'Weldability Formula of High Strength Steels Related to Heat-Affected Zone Cracking'. The Sumitomo Search No.1, May, pp-59-70.

Jones, L. and Chin, A. F. (1983), 'Electronic Instruments and Measurements'. Published by John Wiley & Sons, Inc. pp.153-165.

Kirkwood, P.R. (1987), 'A Viewpoint on the Weldability of Modern Structural Steels'. Proc. Inter. Symp. on Welding Metallurgy of Structural Steels, Annual Meeting of the Metallurgy Society, Denver, Colorado, Feb.,
pp.21-32.

Kohno, R. and Jones, S. B. (1978), 'An Initial Study of Arc Energy and Thermal Cycles in the Submerged Arc Welding of Steel'. Research Report of The Welding Institute 81/1978/PE, Dec. pp.1-20.

Korchynsky, M. (1985), 'Development of 'Controlled Cooling'

Practice'. Proc. of Symposium Sponsored by the Ferrous Metallurgy, Soc.of AIME, Pitsburg, Pennsylvania, Aug., pp.3-13.

Koso, M., Miura, M. and Ohmori, Y. (1981), 'Microstructure and Toughness of Weld Heat Affected Zone in 785MNm-2 HSLA Steel'. Metal Technology, Dec., pp.482-487.

Kou, S. (1987), 'Welding Metallurgy'. Published by John Wiley & Sons, Inc. pp.36-47.

Kou, S. and Lee, Y. (1983), 'Three-Dimensional Heat Flow and Solidification During Autogenous GTA Welding of Aluminium'. Metall. Trans. A, 16A, pp.2245-2253.

Kovitya, P. et al (1986), 'Theoretical Prediction of Weld Pool and Weld Bead Shapes'. Aust. Welding Journal, Dec., pp.94-98.

Kozasu, I (1987), 'Thermomechanically Processed Steels with Improved Weldability'. Proc. Inter. Symp. on Welding Metallurgy of Structural Steels, Annual Meeting of the Metallurgical Society, Inc., in Denver, Colorado, Feb., pp.63-77.

Kozasu, I. (1983), 'Metallurgical Design and Properties of Structural Steels for Arctic Use'. CANMET/PMRL, Ottawa, Oct., pp.1-35.

Kozasu, I. (1985), 'Overview of Accelerated Cooling of Plate'. Proc. of Symp. Accelerated Cooling of Steel, Sponsored by the Ferrous Metallurgy, Soc. of AIME, Pitsburg, Pennsylvania, Aug., pp.15-31.

Lancaster, J. F. (1987), 'Metallurgy of Welding'. Published by Allen & Unwin Ltd, Fourth Edition

Lessels, J. (1984), 'Discussion Session II of the Paper Offshore Structural Steels: Weldability and Hardneability'. Proc. of the Conference Towards Rational and Economic Fabrication of Offshore Structures Overcoming the Obstacles, London, UK, Nov., pp.97-110.

Mat. No.69, M.Sc. Handout (1986), 'Metallurgy, Defects, Cracking'. 2.

McKeown, D. et al. **(1983)**, 'The Weldability of Low Sulphur Steels'. Metal Construction, Nov., pp.667-673.

Modenese, P. J. **(1990)**, 'Statistical Modelling of th Narrow Gap Gas Metal Arc Welding Process'. Ph.D, Cranfield Institute of Technology, Apr.

Moore, J. E. et al **(1985)**, 'A Comparison of the Point Source and Finite Element Schemes for Computing Weld Cooling'. Weld Research: The Sate of the Art, Weld. Inst. of Canada, pp.1-9.

Morikawa, H. and Hasegawa, T. **(1985)**, 'Microstructures and Strengthening Factors of Accelerated Cooled Steels'. Proc. The Ferrous Metallurgy, AIME, Pitsburg, Pennsylvania, Aug., pp.83-96.

Nippes, E. F. and Savage, W. F. **(1949)**, 'Development of Specimen Simulating Weld Heat-Affected Zones'. Welding Journal-Welding Research Supplement, Nov., pp.534s-546s.

Nippon Kokan **(1982)**, 'Development of an On-Line Accelerated Cooling Method for the Production of Steel Plate'. Research and Development in Japan Awarded the Okochi Memorial Prize (Gran Production Prize. Publ. by Okochi Memorial Fundation, pp.14-20.

Nippon Kokan Technical Report Overseas No.39 **(1983)**, 'Development of Class 50kgf/mm2 Steel for Offshore Structures and Vessels in the Arctic'. pp.1-11.

Nunes, A. C. **(1983)**, 'An Extended Rosenthal Weld Model'. Welding Journal- Welding Research Supplement, Jun., pp.165s-170s.

Ouchi, C, et al. **(1979)**, 'Optimization of Processing, and Service Performance through Microstructural Control'. ASTM STP 672,pp.105-125.

Ouchi, C., Sampei, T., and Kozasu, I. **(1982)**, Trans. Iron and Steel Inst. Japan, 22, pp.214-222.

Pedder, C. **(1973)**, 'Harpoon Thermocouples'. W.I.Res.Bull., 14 (11), pp.333-334.

Perdigao, S. C. (1980), 'A Study of the Weld Heat Affected Zone of Carbon Microalloyed Steel'. PhD Thesis, The Univ. of Aston in Birmingham, Jun., pp.1-358.

Phillips, R. H. (1983), 'In Situ' Determination of Transformation Temperatures in the Weld Heat-Affected Zone'. Welding Research Supplement, Jan., pp.12s-18s.

Phillips, R. H. (1968), 'Improved Techniques for Determining Transformation Temperatures during Simulated Welding Conditions',. British Welding Journal, Nov., pp.547-552.

Pickering, F B. (1967), 'The Structure and Properties of Bainite in Steels'. Transformation and Hardenability in Steels, Symposium Sponsored by Climax Molybdenum Company of Michigan and the Univ. of Michigan pp.109-129.

Pisarski, H. G. and Pargeter, R. J. (1983), 'Fracture Toghness of Weld Heat Affected Zones (HAZs) in Steels Used in Constructing Offshore Platforms'. International Conference Welding in Energy Related Projects, Toronto, Canada, Sept, pp.415-427.

Porter, D. A. and Easterling, K. E. (1987). 'Phase Transformations in Metals and Alloys'. Published by Van Nostrand Reinhold (International) Co. Ltd, pp.382-401.

Preston, R.R. (1976), 'A Review of High Strength, Low Alloy Steel Metallurgy in Europe'. Proceedings of Conference on Welding of HSLA (Microalloyed) StructuralSteels, Rome, Nov.,ASM.

Pumphrey, W. I. et al. (1983), 'The Weldability of Low Sulphur Steels'. Metal Construction, Nov., p.667.

Rodrigues, P. E. L. B. (1978), 'The Relationship between the Welding Conditions Thermal Cycles, Microstructures and Toughness of Weld Metal in C-Mn Steels'. PhD Thesis, Feb., Cranfield Institute of Technology, pp.1-106.

Ronningen, J. A. et al (1973), 'On the Assessment of the HAZ

Microstructures in C-Mn Steels'. Scandinavian Journal of Metallurgy, Vol. 2, pp.87-90.

Rosenthal, D (1941), 'Mathematical Theory of Heat Distribution during Welding and Cutting'. Welding Journal- Welding Research Supplement, May pp.220s-234s.

Rosenthal, D. (1946), 'The Theory of Moving Sources of Heat and Its Application to Metal Treatments'. Transactions of the A.S.M.E., Nov., pp.849-866.

Rosenthal, D. and Schmerber, R. (1938), 'Thermal Study of an Arc Welding- Experimental Verification of Theoretical Formulae'. Welding Journal, vol.17, Apr., pp.2-8.

Rothwell, A. B. and Bonomo, F. (1980), 'Weldability of HSLA Steels in Relation to Pipeline Field Welding'. International Document, CBMM pp.118-146.

Royer, C. P. (1987), 'A User's Perspective on Heat-Affected Zone Toghness'. Proc. of International Symposium on Welding Metallurgy of Structural Steels, Metallurgical Society, Inc., AIME, Denver, Colorado, Feb.' pp.255-262.

Smith, E., Coward, M. D. and Apps, R. L. (1970). 'Weld Heat-Affected Zone Structure and Properties of Two Mild Steels'. Welding and Metal FAbrication, Jun., pp.242-251.

Smith, N. and Bagnall, B. I. (1968), 'The Influence of Sulphur on Heat-Affected Zone Cracking of Carbon Manganese Steel Welds'. British Welding Journal, Feb., pp.63-69.

SPSS^x,(1983), User's Guide. Software Produced by SPSS Inc.

Stuart, H. (1985), 'The Microalloying Industry-A Perspective'. Proc. of an International Conference on HSLA Steels' 85, Nov., Beijing, China, pp.45-57.

Suzuki, H. (1983), 'Root Cracking and Maximum Hardness in High-Strength Steels Welds'. IIW Doc IX-1280-83 pp.1-22.

Tandberg, S. (1983), 'Offshore Structures for the North Sea HAZ Hardness Requirements and Practical Implications'. WIC?ISC Int. Conf. Welding in Energy Related Projects, Toronto, Canada, Sep., pp.279-287.

Tecco, D. G. (1985), 'Thermal Cycles and HAZ Characteistic of Single Pass Welds in HSLA Steels'. PhD Thesis, Cranfield Institute of Technology, Dec., pp.1-163.

Tekriwal, P. and Mazumder, J. (1986), 'Finite Element Modeling of Arc Welding Processes'. Advances in Welding Science and Technology, ASM, pp.71-80.

Thomas, J. A. (1973). 'Chart Recorders' Instrumentation, Published by The Open University Press pp.94-100.

Ushio, M. et al (1977), 'Theoretical Calculation on Shape of Fusion Boundary and Temperature Distribution Around Moving Heat Source (Report 1)'. Trans. JWRI, 6(1), pp.1-6.

Walker, E. F. (1988), 'Steel Quality, Weldability and Toughness'. Seventh International Conference on Offshore Mechanics and Artic Engineering, Houston, Texas, Feb., pp.49-69.

Wang, D. (1990), 'Hydrogen Cracking in Multi-Pass Steel Weld Metals'. Ph.D Thesis, Cranfield Institute of Technology, Jun.

Watkinson, F. and Baker, R. G. (1967), 'Welding of Steel to BS. 968: 1962'. British Welding Journal, Nov., pp.603-613.

Wells, A. A. (1952), 'Heat Flow in Welding'. Welding Journal-Welding Research Supplement, May, pp.263s-267s.

Youn, J. G. and Kim, J. (1987), 'Characteristics of TMCP Steel and Its Softening'. Proc. International Symposium on Welding Metallurigy of Structural Steels, Metallurgical Society, Inc., Denver, Colorado, Feb.' pp.157-262.

Yurioka, N. (1990), 'Carbon Equivalents for Hardenability and Cold Cracking Susceptibility of Steels'. Proceedings of Select Conference,

Hardenability of Steels, Publ. by The Welding Institute, May, pp.41-50.

Yurioka, N. et al (1981), 'Study on Carbon Equivalents to Assess Cold Cracking Tendency and Hardness in Steel Welding'. Proceedings of Pipeline Welding in the 80's, Australian Welding Research Association, Paper 1.c, pp.1-18.

Yurioka, N. et al (1987), 'Prediction of HAZ Hardness of Transformable Steels'. Metal Construction, Apr., pp.217r-223r.

APPENDIX I

```
C     ******************************************************
C          THERMIC PROGRAMME
C     THIS PROGRAMME ANALYSES WELDING THERMAL CYCLES RECORDED
C     BY THE BOX DATA LOGGER.
C     By C. L. ARAUJO & P. J. Modenesi (1989)

C     ******************************************************

C        MAIN VARIABLES USED BY PROGRAM

C            VARIABLE NAME      TYPE        DEFINITION

C         NOME    ---------  CHAR  ---- DATA FILE SPEC.
C         VOLT(200) -------  REAL  ---- THERMOCOUPLE TABLE
C         TEMP(200) -------  REAL  ----      "          "
C         Y(6,5460) -------  REAL  ---- NOFILTERED DATA
C         Y(6,5460) -------  REAL  ---- FILTERED DATA
C         SCAMAX(6) -------  REAL  ---- MAX. VALUE FOR EACH CHANNEL
C         SCAMIN(6) -------  REAL  ---- MIN.   "    "    "      "
C         NB(6) -----------  INT   ---- NUMBER OF FILTERED POINTS
C         NP(6) -----------  INT   ---- TOTAL NB OF POINTS
C         IMIN(6) ---------  INT   ---- FIRST AVAILABLE POINT
C         DT(6) -----------  REAL  ---- TIME BETWEEN POINTS
C         NCHAN -----------  INT   ---- NUMBER OF CHANNELS
C         IDEV ------------  INT   ---- SELECT DEVICE(PLOTTING)
C         IFILTER ---------  INT   ---- DATA FILTERING LEVEL

C     ******************************************************

      CHARACTER*30 NOME,TABLE_NAME,A*1
      DIMENSION VOLT(200),TEMP(200)
      DIMENSION Y(6,5460),YF(6,5460),SCAMAX(6),SCAMIN(6)
     1          ,NB(6),IMIN(6),NP(6)

      EXTERNAL DISP,GRAFV,INTRO,CMVTOT
      COMMON /DATT/YF,Y
      COMMON /PARAM/NB,IMIN,DT,NCHAN,NP
      COMMON /COEFT/SCAMAX,SCAMIN
      COMMON /THERM/VOLT,TEMP,V_MAX,T_MAX
      COMMON /DEV/IDEV
      DT=-1
      IDEV=0

C     ******************************************
C     READ THERMCOUPLE TABLE

      TABLE_NAME='PLATINUM.DAT'
      CALL READ_TABLE(TABLE_NAME)

C     OPEN REPORT FILE AND PRESENT MAIN MENU

      OPEN(UNIT=25,FILE='OJUARA.DAT',STATUS='NEW')

10    PRINT*,' ***************************************'
      PRINT*,'                  MENU'
      PRINT*,' ***************************************'
      PRINT*,' '
      PRINT*,'   (0) CHANGE DEFAULT THERMCOUPLE'
      PRINT*,'   (1) INPUT DATA FILE'
      PRINT*,'   (2) DISPLAY DATA'
      PRINT*,'   (3) PLOT DATA(GRAPHIC TERMINAL)'
```

```
      PRINT*,'   (4) FILTER SIGNAL(TRIANGLE ROUTINE)'
      PRINT*,'   (5) CALCULATE CYCLE CHARACTERISTICS'
      PRINT*,'   (6) CREATE AVERAGE THERMOCYCLE'
      PRINT*,' '
      PRINT*,'  YOUR CHOICE'
      READ(*,*) IC
      PRINT*,' '
      IF((IC.LT.0).OR.(IC.GT.6)) GO TO 30

      IF(IC.EQ.0) THEN
         PRINT*,' INPUT NEW THERMCOUPLE TABLE NAME'
         READ(*,'(A)') TABLE_NAME
         CALL READ_TABLE(TABLE_NAME)
         PRINT*,' '
      END IF

      IF((IC.NE.1).AND.(DT.LE.0)) GO TO 10

C     READ DATA FILE
      IF(IC.EQ.1) THEN
         CALL INTRO(NOME,IFILTER)
      END IF

C     DISPLAY DATA ON SCREEN OR SAVE DATA ON FILE
      IF(IC.EQ.2) CALL DISP(IFILTER)

C     PLOTTING ROUTINE
      IF(IC.EQ.3) CALL GRAFV

C     DATA FILTERING ROUTINE
      IF(IC.EQ.4) CALL FILTTT(IFILTER)

C     THERMAL CYCLE ANALYSIS
      IF(IC.EQ.5) CALL THERMPAR(IFILTER)

C     AVERAGED THERMOCYCLE
      IF(IC.EQ.6) CALL MEAN_CYCLE

5     PRINT*,' '
      PRINT*,' CONTINUE(C/c) OR STOP(S)?'
      READ(*,'(1A)') A
      IF(A.NE.'S') THEN
           IF(A.NE.'s') GO TO 10
      END IF
30    CLOSE(25)
      STOP
      END


C     ***************************************

C     SUBROUTINE READ_TABLE(TABLE_NAME)
C     THIS ROUTINE READS A THERMOCOUPLE TABLE
C     IN THE FILE "TABLE_NAME".
C     ***************************************

      DIMENSION VOLT(200),TEMP(200),NB(6),IMIN(6)
      CHARACTER*30 TABLE_NAME

      COMMON /PARAM/NB,IMIN,DT
      COMMON /THERM/VOLT,TEMP,V_MAX,T_MAX
```

```
      OPEN(UNIT=15,FILE=TABLE_NAME,STATUS='OLD')
      READ(15,*) J
      READ(15,*) (TEMP(I),VOLT(I),I=1,J)
      CLOSE(15)
      V_MAX=VOLT(J)
      T_MAX=TEMP(J)
      PRINT*,' '
      WRITE(*,100) TABLE_NAME
      PRINT*,' '
      DT=-1
100   FORMAT(' THERMCOUPLE TABLE: ',30A)
      RETURN
      END

C       ************************************

            SUBROUTINE GRAFV

C       ************************************

C     MAIN VARIABLES OF ROUTINE:

C       TLABEL(2) -------  CHAR -----  AXIS LABELS
C       TEXT ------------  CHAR -----  TEXT LINE
C       VMIN(2) ---------  REAL -----  AXIS STARTING VALUES
C       VMAX(2) ---------  REAL -----  AXIS FINNISHING VALUES
C       X(5460) ---------  REAL -----  X COORDINATES
C       Y(5460) ---------  REAL -----  Y COORDINATES
C       FTEX ------------  REAL -----  TEXT POSITION FACTOR
C       FX0,FY0 ---------  REAL -----  GRAPHIC ORIGEN POS. FACTOR
C       WL --------------  REAL -----  PLOT LINE THICKNESS
C       IBACK -----------  INT  -----  BACKGROUND COLOUR
C       ILINE -----------  INT  -----  LINE COLOUR
C       FLABEL ----------  REAL -----  CHARACTER SIZE FACTOR
C       FDX,FDY ---------  REAL -----  AXIS LENGTH FACTORS
C       HT --------------  REAL -----  CHARACTER HEIGHT
C       X0,Y0 -----------  REAL -----  PLOT ORIGEN COORDINATES
C       DX,DY -----------  REAL -----  PLOT AXIS LENGTHS
C       XDEV,YDEV -------  REAL -----  DEVICE DIMENSIONS
C       YTEX ------------  REAL -----  TEXT LINE POSITION(Y DIRECT.)

C     ************************************************************

      CHARACTER*20 TLABEL(2),CHYNAME,CHXNAME
      CHARACTER*100 TEXT,PROMPT*50

      DIMENSION VMIN(2),VMAX(2),X(5460),Y(5460),TMAX(6),
     1          TMIN(6),TEMP(6,5460),NB(6),IMIN(6)
      DATA FTEX/0.45/,FX0,FY0/1.79,1.57/,ISYN/5460/,
     1     YLASER/195.1/,WL/-2/,VS/0.0/
      DATA IBACK,ILINE/7,4/
      DATA YMIN,YMAX/100.,1000./

      COMMON /DATT/TEMP
      COMMON /PARAM/NB,IMIN,DT,NCHAN
      COMMON /COEFT/TMAX,TMIN
      COMMON /DEV/IDEV

      FLABEL=3.0/YLASER
      TLABEL(2)='Temperature(C)$'
      PRINT*,' '
```

```
      IF(IDEV.NE.0) GO TO 10
      PRINT*,'************************************'
      PRINT*,' '
      PRINT*,'  SELECT TERMINAL: (1) LT4109'
      PRINT*,'                   (2) VT4014'
      PRINT*,'                   (3) DUMMY DRIVER'
      PRINT*,'                   (4) VAXSTATION'
      PRINT*,'                   (5) RETURN'
      READ(*,*)IDEV
      IF((IDEV.LT.1).OR.(IDEV.GT.4)) THEN
            IDEV=0
            RETURN
      END IF

10    PRINT*,' '
      PRINT*,'************************************'
      PRINT*,' '
      PRINT*,'  PLOT OPTIONS: (1) T-t CURVE'
      PRINT*,'                (2) T-T CURVE'
      PRINT*,'                (3) T-T CURVE(SINTHETIC REFERENCE)'
      READ(*,*) IPLOT
      IF((IPLOT.GT.3).OR.(IPLOT.LT.1)) RETURN

C     DEFINE PLOT PARAMETERS
      IF(IPLOT.EQ.1) THEN
          TLABEL(1)='Time(s)$'
          FDX=0.90
          FDY=0.60
      ELSE
          TLABEL(1)='Temperature(C)$'
          FDX=0.70
          FDY=FDX
      END IF

      NPOINT=0
90    PRINT*,' '
C     SYNTHETIC THERMAL CYCLE
      IF(IPLOT.EQ.3) THEN
          PRINT*,'INPUT WELDING ENERGY(KJ/MM)'
          READ(*,*) ER
          PRINT*,' '
            IF((ER.LE.0).OR.(ER.GT.100)) GO TO 10
          PRINT*,'CREATING SYNTHETIC THERMAL CYCLE'
          PRINT*,' '
          CALL SYNT(Y,ISYN,DT,ER,YMAX,YMIN,IYMAX)
            PRINT*,'STARTING POINT= ',IYMAX
          PRINT*,' '
          IPOINT=ISYN
          PRINT*,'INPUT SECOND CHANNEL NUMBER'
          READ(*,*) ICHX
          CHXNAME=' *SECOND CHANNEL*'
          ISTART=1
          GO TO 105
      END IF

      IF(IPLOT.EQ.1) THEN
          PRINT*,'INPUT CHANNEL NUMBER'
          READ(*,*) ICHY
          CHYNAME=' '
      ELSE
          PRINT*,'INPUT REFERENCE CHANNEL NUMBER'
          READ(*,*) ICHY
```

```
      CHYNAME=' *REFERENCE CHANNEL*'
      PRINT*,'INPUT SECOND CHANNEL NUMBER'
      READ(*,*) ICHX
      CHXNAME=' *SECOND CHANNEL*'
    END IF

    IF((ICHX.GT.NCHAN).OR.(ICHY.GT.NCHAN)) GO TO 90
    PRINT*,' '

100 WRITE(*,'(20A)') CHYNAME
    WRITE(*,200) IMIN(ICHY)
    READ(*,*) ISTART
    IF((ISTART.LT.IMIN(ICHY)).OR.(ISTART.GE.NB(ICHY)))
    1                                          GO TO 100
    IPOINT=NB(ICHY)-ISTART+1

105 IF(IPLOT.NE.1) THEN
       J=NB(ICHX)-IMIN(ICHX)+1
       IF(J.LT.IPOINT) IPOINT=J
    END IF

    WRITE(*,210) IPOINT
    READ(*,*) NP
    IF((NP.LE.0).OR.(NP.GT.IPOINT)) GO TO 100
    IF(IPLOT.NE.1) THEN
      PRINT*,' '
      WRITE(*,'(20A)') CHXNAME
      I=NB(ICHX)-NP+1
      WRITE(*,220) IMIN(ICHX),I
      READ(*,*) IISTART
      PRINT*,' '
      IF((IISTART.LT.IMIN(ICHX)).OR.(IISTART.GE.I))
    1                                        GO TO 90
    END IF
    IFLAG=0

125 DT0=-DT
    J=ISTART-1
    K=IISTART-1
    IF(IPLOT.EQ.1) THEN
      DO I=1,NP
        Y(I)=TEMP(ICHY,J+I)
        X(I)=DT0
        DT0=DT0+DT
      END DO
      TY_MAX=TMAX(ICHY)
      TY_MIN=TMIN(ICHY)
      PROMPT='MEAS. TEMPERATURE'
      CALL TA_BOM(TY_MAX,TY_MIN,PROMPT)
      VMAX(1)=X(NP)
      VMAX(2)=TY_MAX
      VMIN(1)=X(1)
      VMIN(2)=TY_MIN
    END IF

    IF(IPLOT.EQ.2) THEN
      DO I=1,NP
        Y(I)=TEMP(ICHY,J+I)
        X(I)=TEMP(ICHX,K+I)
      END DO
      TY_MAX=TMAX(ICHY)
      TY_MIN=TMIN(ICHY)
```

```
          PROMPT='REFERENCE'
          CALL TA_BOM(TY_MAX,TY_MIN,PROMPT)
          VMAX(2)=TY_MAX
          VMIN(2)=TY_MIN
          TY_MAX=TMAX(ICHX)
          TY_MIN=TMIN(ICHX)
          PROMPT='MEAS. TEMPERATURE'
          CALL TA_BOM(TY_MAX,TY_MIN,PROMPT)
          VMAX(1)=TY_MAX
          VMIN(1)=TY_MIN
      END IF

      IF(IPLOT.EQ.3) THEN
          DO I=1,NP
            X(I)=TEMP(ICHX,K+I)
          END DO
          TY_MAX=TMAX(ICHX)
          TY_MIN=TMIN(ICHX)
          PROMPT='MEAS. TEMPERATURE'
          CALL TA_BOM(TY_MAX,TY_MIN,PROMPT)
          VMAX(1)=TY_MAX
          VMIN(1)=TY_MIN
          VMAX(2)=YMAX
          VMIN(2)=YMIN
      END IF

      X1=VMIN(1)
      X2=VMAX(1)
      Y1=VMIN(2)
      Y2=VMAX(2)

      IF(IFLAG.GT.0) GO TO 80
C     SELECT DEVICE
      IF(IDEV.EQ.1) THEN
            CALL GROUTE('SEL LT4109;EX')
      ELSE IF(IDEV.EQ.4) THEN
            CALL GROUTE('SEL MGPX;EX')
      ELSE IF(IDEV.EQ.2) THEN
            CALL GROUTE('SEL VT4014;EX')
      ELSE IF(IDEV.EQ.3) THEN
            CALL GROUTE('SEL MDUMDR;EX')
      END IF

C     START UNIRAS
80    CALL GOPEN
      CALL GRPSIZ(XDEV,YDEV)

C     DEFINE PLOT DIMENSIONS
      HT=FLABEL*YDEV
      DX=FDX*YDEV
      DY=FDY*YDEV
      X0=(XDEV-DX)/FX0
      Y0=(YDEV-DY)/FY0
      YTEX=FTEX*Y0
      CALL BGRAF(X0,Y0,DX,DY)
      IF(((IDEV.EQ.1).OR.(IDEV.EQ.4)).AND.(IFLAG.EQ.0))
      1                                    CALL BGRAFB(IBACK)
      CALL GCHARF('SOFT')
      CALL GCHARF('ITAL')

C     DEFINE AND DRAW AXES
      DO I=1,2
```

```
      CALL BAXLAB(HT,HT,999,999)
      CALL BTICKM(4)
      CALL BAXIS(I,VMIN(I),VS,VMAX(I),TLABEL(I))
      IF(I.EQ.1) THEN
        CALL BAXORI(X0,Y0+DY)
      ELSE
        CALL BAXORI(X0+DX,Y0)
      END IF
      CALL BAXLAB(0.,0.,999,999)
      CALL BAXIS(-I,VMIN(I),VS,VMAX(I),'$')
    END DO

C   DRAW DATA POINTS
    CALL GLIMIT(X1,X2,Y1,Y2,0.,0.)
    CALL GVPORT(X0,Y0,DX,DY)
    CALL GWBOX(DX,DY,0.)
    CALL GSCALE
    IF(((IDEV.EQ.1).OR.(IDEV.EQ.4)).AND.(IFLAG.EQ.0))
    1                                  CALL GWICOL(-1,ILINE)
    IF(IFLAG.GT.0) THEN
        CALL GWICOL(WL,1)
    END IF
    CALL GVECT(X,Y,NP)

C   WRITE TEXT
    CALL GSCAMM
    IF(IFLAG.GT.0) THEN
      XJUS=XDEV/2
      CALL GCHARF('TRIP')
      CALL GCHARJ(1)
      CALL GCHART(1)
      CALL GCHAR(TEXT,XJUS,YTEX,HT)
      CALL GSEGCL(IFLAG)
    END IF

C   TERMINATE UNIRAS
    CALL GCLOSE

    PRINT*,'  DEVICE PLOT AREA LENGTHS(MM)'
    PRINT*,'  X= ',XDEV,' Y= ',YDEV
    IF(IFLAG.GT.0) RETURN

    PRINT*,' '
    PRINT*,'************************************'
    PRINT*,' '
    PRINT*,'  SELECT OPTION: (1) MODIFY PLOT'
    PRINT*,'                 (2) NEW PLOT OPTION'
    PRINT*,'                 (3) HARDCOPY'
    PRINT*,'                 (4) RETURN'
    READ(*,*)I
    IF((I.EQ.1).AND.(IPLOT.EQ.3)) THEN
      CALL SYNT(Y,ISYN,DT,ER,YMAX,YMIN,IYMAX)
      GO TO 105
    END IF

    IF(I.EQ.1) GO TO 100
    IF(I.EQ.2) GO TO 10

C   HARDCOPY
    IF(I.EQ.3) THEN
      PRINT*,' '
      PRINT*,' INPUT SEGMENT NUMBER(1-99)'
```

```
      READ(*,*) IFLAG
      PRINT*,' '
      PRINT*,' INPUT TEXT(MAX. 100 CHAR.)'
      READ(*,'(100A)') TEXT
      CALL CONCAT(TEXT,100)
      CALL GROUTE('SEL HPOSTA4L;EX')
      CALL GSEGCR(IFLAG)
      IF(IPLOT.EQ.3) CALL SYNT(Y,ISYN,DT,ER,
     1                                YMAX,YMIN,IYMAX)
      GO TO 125
    END IF

200 FORMAT('  INPUT STARTING POINT( >',I4,')')
210 FORMAT('  INPUT NUMBER OF POINTS( <',I4,')')
220 FORMAT('  INPUT STARTING POINT(>',I4,' , <',I5,')')
    RETURN
    END

C   ***********************************************

      SUBROUTINE TA_BOM(TY_MAX,TY_MIN,PROMPT)

C   ***********************************************

    CHARACTER*50 PROMPT,DEC*1
    PRINT*,' '
    WRITE (*,100) PROMPT,TY_MAX,TY_MIN
100 FORMAT(' MAXIMUN AND MINIMUN FOR ',A,/,'       MAX: ',
    1   F7.1,'      MIN: ',F7.1,//,'  DO YOU WANT TO CHANGE?[N] ')
    READ(*,'(A)')DEC
    IF((DEC.EQ.'Y').OR.(DEC.EQ.'y')) THEN
10     PRINT*,' '
       WRITE(*,'(A)')' INPUT MAX'
       READ(*,*)Y_MAX
       WRITE(*,'(A)')' INPUT MIN'
       READ(*,*) Y_MIN
       IF(Y_MIN.GE.Y_MAX) GO TO 10
       TY_MAX=Y_MAX
       TY_MIN=Y_MIN
    END IF
    RETURN
    END


C   ***********************************************

            SUBROUTINE FILTTT(IFILTER)
C         WEIGHTED MEAN FILTERING ROUTINE

C   ***********************************************

    DIMENSION YF(6,5460),Y(6,5460),COX(50),
    1         NB(6),NPOINT(6),IMIN(6)
    COMMON /DATT/YF,Y
    COMMON /PARAM/NB,IMIN,DT,NCHAN,NPOINT

    PRINT*,' '
    PRINT*,' INPUT CHANNEL NUMBER(0=ALL)'
    READ(*,*) ICHAN
    IF((ICHAN.LT.0).OR.(ICHAN.GT.NCHAN)) RETURN
    PRINT*,' '
    PRINT*,' INPUT FILTER FACTOR(0-50)'
```

```
      READ(*,*) IFILTER
      IF((IFILTER.LE.0).OR.(IFILTER.GT.50)) THEN
         DO I=1,NCHAN
            IMIN(I)=1
            NB(I)=NPOINT(I)
            DO J=IMIN(I),NB(I)
                YF(I,J)=Y(I,J)
            END DO
         END DO
         RETURN
      END IF
      CO0=1./(1.+IFILTER)
      DO I=1,IFILTER
         COX(I)=(1.+IFILTER-I)/(1.+IFILTER)**2
      END DO

      IF(ICHAN.EQ.0) THEN
         DO J=1,NCHAN
            NB(J)=NPOINT(J)-IFILTER
            IMIN(J)=IFILTER+1
            DO I=IMIN(J),NB(J)-1
               YF(J,I)=Y(J,I)*CO0
               DO JJ=1,IFILTER
                 YF(J,I)=YF(J,I)+(Y(J,I-JJ)+Y(J,I+JJ))*
     1                    COX(JJ)
               END DO
            END DO
         END DO
      ELSE
         IMIN(ICHAN)=IFILTER+1
         NB(ICHAN)=NPOINT(ICHAN)-IFILTER
         DO I=IMIN(ICHAN),NB(ICHAN)-1
             YF(ICHAN,I)=Y(ICHAN,I)*CO0
             DO JJ=1,IFILTER
               YF(ICHAN,I)=YF(ICHAN,I)+(Y(ICHAN,I-JJ)+Y(ICHAN
     1                     ,I+JJ))*COX(JJ)
             END DO
         END DO
      END IF
      RETURN
      END


C     ***********************************************

                SUBROUTINE INTRO(NAME,IFIL)
C                  READ DATA FILE
C     ***********************************************

      CHARACTER*30 NAME
      DIMENSION DATF(6,5460),DAT(6,5460),CALIB(6),CALIB0(6),
      1          NPOINT(6),IMIN(6),NB(6),Y_MIN(6),Y_MAX(6)
      COMMON /DATT/DATF,DAT
      COMMON /PARAM/NB,IMIN,DT,NCHAN,NPOINT
      COMMON /COEFT/CALIB,CALIB0
      COMMON /THERM/VOLT,TEMP,V_MAX,T_MAX

      DO I=1,6
         Y_MAX(I)=0.
         Y_MIN(I)=T_MAX
      END DO
      PRINT*,' '
```

```
      PRINT*,' INPUT FILENAME'
      READ(*,'(A)') NAME
      OPEN(UNIT=20,FILE=NAME,STATUS='OLD')
      READ(20,*) NCHAN,DT
      DO I=1,NCHAN
         READ(20,*) K,NPOINT(I),CALIB(I),CALIB0(I)
      END DO
      DO I=1,NCHAN
         READ(20,*) K
        READ(20,*) (DAT(I,J),J=1,NPOINT(I))
      END DO
      CLOSE(20)

      WRITE(*,100) NCHAN,DT
      WRITE(*,110)
      DO I=1,NCHAN
         WRITE(*,120) I,NPOINT(I),CALIB(I),CALIB0(I)
      END DO

      DO I=1,NCHAN
         DO J=1,NPOINT(I)
            DAT(I,J)=CALIB0(I)+CALIB(I)*DAT(I,J)
            DAT(I,J)=CMVTOT(DAT(I,J))
            DATF(I,J)=DAT(I,J)
            IF(DAT(I,J).LT.Y_MIN(I)) Y_MIN(I)=DAT(I,J)
            IF(DAT(I,J).GT.Y_MAX(I)) Y_MAX(I)=DAT(I,J)
         END DO
         NB(I)=NPOINT(I)
         IMIN(I)=1
      END DO
      IFIL=0

      DO I=1,NCHAN
         J=Y_MIN(I)/100
         K=Y_MAX(I)/100
         CALIB(I)=100*K + 100.
         CALIB0(I)=100*J
      END DO

      WRITE(25,200)NAME
      RETURN
100   FORMAT(//,' NUMBER OF CHANNELS:',I4,/,' TIME INTERVAL(S):',
     1       F8.5,///)
110   FORMAT(' CHANNEL No',8X,'POINTS',14X,'SLOPE',12X,'INTERCEPT')
120   FORMAT(I6,10X,I8,10X,F10.5,10X,F10.3)
200   FORMAT(//,20X,'*******************************************
     1*********************',/,20X,' DATA FILE: ',30A,/)
      END

C     ***********************************************

                    FUNCTION CMVTOT(X)
C             CONVERT BYTE PATTERN INTO mV
C     ***********************************************

      DIMENSION V(200),T(200)
      COMMON /THERM/ V,T,V_MAX,T_MAX

      IF(X.LE.0) THEN
        CMVTOT=0
        RETURN
      END IF
```

```
      IF(X.GE.V_MAX) THEN
        CMVTOT=T_MAX
        RETURN
      END IF
      I=2
      DO WHILE(X.GT.V(I))
         I=I+1
      END DO
      CMVTOT=T(I-1)+(T(I)-T(I-1))/(V(I)-V(I-1))*(X-V(I-1))

      RETURN
      END

C     ***********************************************

                     SUBROUTINE DISP(IFILT)
C     DISPLAY (OR SAVE) DATA POINTS ON SCREEN OR FILE
C     ***********************************************

      DIMENSION NB(6),Y(6,5460),IMIN(6),CALIB(6),CALIB0(6)
      CHARACTER*1 DECISION,NAME*30
      COMMON /PARAM/NB,IMIN,DT,NCHAN
      COMMON /COEFT/CALIB,CALIB0
      COMMON /DATT/Y

      PRINT*,' '
      PRINT*,' SELECT CHANNEL NUMBER'
      READ(*,*) ICH
      IF((ICH.LT.1).OR.(ICH.GT.NCHAN)) RETURN
      PRINT*,' FIRST AVAILABLE POINT:',IMIN(ICH)
      PRINT*,' LAST  AVAILABLE POINT:',NB(ICH)
10    PRINT*,' '
      PRINT*,' INPUT LOWER LIMIT'
      READ(*,*) ILOW
      IF((ILOW.LT.IMIN(ICH)).OR.(ILOW.GT.NB(ICH))) GO TO 10
20    PRINT*,'       UPPER LIMIT'
      READ(*,*) IUP
      IF((IUP.LT.ILOW).OR.(IUP.GT.NB(ICH))) GO TO 20
      PRINT*,' '
      PRINT*,' SELECT DISPLAY OUTPUT: SCREEN  --- S'
      PRINT*,'                        OJUARA  --- J'
      PRINT*,'                        NEW FILE -- F'
      READ(*,'(A)') DECISION
      PRINT*,' '

      IF((DECISION.EQ.'S').OR.(DECISION.EQ.'s')) THEN
         WRITE(*,100) (Y(ICH,I),I=ILOW,IUP)
      ELSE IF((DECISION.EQ.'J').OR.(DECISION.EQ.'j')) THEN
         WRITE(25,110) ICH,IFILT,ILOW,IUP
         WRITE(25,120) (Y(ICH,I),I=ILOW,IUP)
         WRITE(25,130)
         PRINT*,' INFO: DATA SAVED IN OJUARA.DAT'
         PRINT*,' '
      ELSE IF((DECISION.EQ.'F').OR.(DECISION.EQ.'f')) THEN
         PRINT*,' INPUT FILENAME'
         READ(*,'(30A)') NAME
         OPEN(UNIT=35,FILE=NAME,STATUS='NEW')
         WRITE(35,*) ICH,IFILT,ILOW,IUP
         WRITE(35,*) DT
         WRITE(35,*) CALIB(ICH),CALIB0(ICH)
         DO I=ILOW,IUP
            WRITE(35,100) (I-ILOW)*DT,Y(ICH,I)
```

```
      END DO
      WRITE(*,140) NAME
      CLOSE(35)
    END IF
100 FORMAT(F10.3,3X,F10.1)
110 FORMAT(////,20X,'CHANNEL NUMBER:',I3,/,20X,'FILTER FACTOR:'
    1      ,I4,/,20X,'LOWER LIMIT:',I6,10X,'UPPER LIMIT:',
    2       I6,//)
120 FORMAT(10X,8F10.1)
130 FORMAT(///)
140 FORMAT(' DATA SAVED IN ',30A//)

    RETURN
    END

C   ************************************************************

                  SUBROUTINE THERMPAR(IFILTER)
C           CALCULATE THERMAL CYCLE CHARACTERISTICS
C   ************************************************************
C   MAIN VARIABLES:

C   Tdiv ---------------------- Temperature intervals(x100)
C   Htime --------------------- Heating times
C   Ctime --------------------- Cooling times
C   Tpeak --------------------- Peak temperature
C   Ipeak --------------------- Point where T = Tpeak
C   Ist ----------------------- Thermal cycle starting point
C   Iend ---------------------    "      "   finishing point
C   DER ----------------------- Derivative buffer

    CHARACTER*20 XAXIS,YAXIS,FILE_NAME*40
    DIMENSION Tdiv(15),Htime(15),Ctime(15),TEMP(6,5460),NB(6)
    DIMENSION IMIN(6),YY(2000),DER(2000)
    COMMON /PARAM/NB,IMIN,DT,NCHAN
    COMMON /DATT/ TEMP

    YREF=900
    PRINT*,' '
    PRINT*,' SELECT CHANNEL NUMBER'
    READ(*,*) ICHAN
    IF((ICHAN.LT.1).OR.(ICHAN.GT.NCHAN)) RETURN

    CALL CALC_TH(ICHAN,Ist,Ipeak,Tpeak,Ilast,Icool,Iend,Tdiv,
    1            Htime,Ctime,YREF,IREF)
    WRITE(25,190) ICHAN,IFILTER
    WRITE(25,200) Tpeak,Ist,Ipeak
    WRITE(25,210)
    PRINT*,' '
    PRINT*,' THERMAL CYCLE CHARACTERISTICS'
    WRITE(*,100) Tpeak,Ist,Ipeak
    WRITE(*,110)
    DO i=Ilast,Icool
          WRITE(25,220) Tdiv(i),Htime(i),Ctime(i)
          WRITE(*,120) Tdiv(i),Htime(i),Ctime(i)
    END DO
    PRINT*,' '
10  IF(Tpeak.GT.1000) THEN
     PRINT*,' SELECT OPTION: (1) PLOT dT/dt'
     PRINT*,'                (2) PLOT dT/dTref'
     PRINT*,'                (3) CREATE dT/dt file'
     PRINT*,'                (4) CREATE dT/dTref file'
```

```
      PRINT*,'                    (5) RETURN'
      READ(*,*) IDEC
      PRINT*,' '
      IF((IDEC.GE.1).AND.(IDEC.LE.4)) THEN
         XAXIS='Temperature(C)$'
         XMAX=1000.
         XMIN=200.
         IIN=Iend-IREF+1
C           *** dT/dt ***
         IF((IDEC.EQ.1).OR.(IDEC.EQ.3)) THEN
            YAXIS='Cooling rate(C/s)$'
            J=0
            DO I=IREF,Iend
              J=J+1
              YY(J)=TEMP(ICHAN,I)
               END DO
            CALL DERIV(YY,2000,IIN,DT,DER,IOUT)

            YMAX=DER(1)
               YMIN=DER(1)
            DO I=2,IOUT
              IF(DER(I).GT.YMAX) YMAX=DER(I)
              IF(DER(I).LT.YMIN) YMIN=DER(I)
            END DO
            IF(YMIN.GT.0) YMIN=0
         END IF
C           *** dT/dTref ***
         IF((IDEC.EQ .2).OR.(IDEC.EQ.4)) THEN
             YAXI S='dT/dTref$'
             J=0
             DO I=IREF,Iend
               J=J+1
               YY(J)=TEMP(ICHAN,I)
                END DO
             PRINT*,'INPUT WELDING ENERGY(KJ/MM)'
             READ(*,*) ER
             PRINT*,' '
             PRINT*,'CREATING SYNTHETIC THERMAL CYCLE'
             PRINT*,' '
             CALL SYNT(DER,2000,DT,ER,YREF,0,IYMAX)
             DO I=1,2000-IYMAX
                DER(I)=DER(I+IYMAX)
             END DO
             CALL DERIV(YY,2000,IIN,0,DER,IOUT)
             YMAX=DER(1)
                YMIN=DER(1)
             DO I=2,IOUT
               IF(DER(I).GT.YMAX) YMAX=DER(I)
               IF(DER(I).LT.YMIN) YMIN=DER(I)
             END DO
             IF(YMIN.GT.0) YMIN=0
         END IF
         IF((IDEC.EQ.1).OR.(IDEC.EQ.2)) THEN
           CALL PLOTDEV(IOUT,XMIN,XMAX,YMIN,YMAX,YY,DER,XAXIS,YAXIS)
         END IF
C      ************** CREATE DEV FILE **************
         IF((IDEC.EQ.3).OR.(IDEC.EQ.4)) THEN
                PRINT*,' INPUT FILE NAME:'
                READ(*,'(A)') FILE_NAME
                OPEN(UNIT=16,FILE=FILE_NAME,STATUS='NEW')
                DO I=1,IOUT
                   WRITE(16,*) YY(I),DER(I)
```

```
                END DO
                CLOSE(16)
            END IF
C       ********************************************

            GO TO 10
         END IF

      END IF
100   FORMAT(/,' PEAK TEMPERATURE(C) :',F9.3,/,
     1       ' THERMAL CYCLE STARTING POINT:',I5,/,
     2       ' PEAK POINT:                  ',I5//)
110   FORMAT(/36X,'HEATING',23X,'COOLING',/,' TEMPERATURE',24X,
     1         'TIME(s)',23X,'TIME(s)'/)
120   FORMAT(F10.0,2(20X,F10.1))
190   FORMAT(//,60X,'*************',//,
     1          20X,' CHANNEL NUMBER: ',I3,/,20X,' FILTER FACTOR: '
     2          ,I4,/)
200   FORMAT(/,20X,' PEAK TEMPERATURE(C) :',F9.3,/,20X,
     1       ' THERMAL CYCLE STARTING POINT:',I5,/,20X,
     2       ' PEAK POINT:                  ',I5//)
210   FORMAT(/56X,'HEATING',23X,'COOLING',/,20X,' TEMPERATURE',24X,
     1     'TIME(s)',23X,'TIME(s)'/)
220   FORMAT(20X,F10.0,2(20X,F10.1))
250   FORMAT(' CHANNEL:',I2,'$')

      RETURN
      END


C     ***************************************************************

          SUBROUTINE SYNT(Y,ID,DT,ENERGY,YMAX,YMIN,IYMAX)
C                 CREATE SYNTHETIC THERMAL CYCLE

C         Y(ID) -------- SYNTHETIC THERMAL CYCLE VECTOR
C         DT ----------- TIME INTERVAL
C         ENERGY ------- WELDING ENERGY(KJ/MM)
C         YMAX --------- MAX. TEMPERATURE
C         YMIN --------- MIN. TEMPERATURE
C         IYMAX -------- POINT FROM WHERE Y < YMAX

C     ***************************************************************

      DIMENSION Y(ID)
      DATA A,B/0.001,1.3424E-4/
      IYMAX=1
      C=B/ENERGY

      DO I=1,ID
         T=(I-1)*DT
         Y(I)=1/(A+C*T)
         IF(Y(I).GT.YMAX) THEN
            Y(I)=YMAX
            IYMAX=I+1
         END IF
         IF(Y(I).LT.YMIN) Y(I)=YMIN
      END DO

      RETURN
      END
```

```
C     ********************************************************

          SUBROUTINE DERIV(Y,IDIM,NIN,DT,DXY,NOUT)
C                 CALCULATE DERIVATIVES

C        Y(IDIM) ---------- Y VECTOR
C        NIN -------------- NUMBER OF DATA POINTS(INPUT)
C        DT --------------- TIME INTERVAL
C        DXY -------------- OUTPUT: DERIVATIVE
C                                   DT>0 --> dy/dt
C                                   DT<=0--> dy/dx
C                           INPUT(DT<0): X VECTOR
c        NOUT ------------- NUMBER OF DATA POINTS(OUTPUT)
C                           YVECTOR IS ALTERED BY ROUTINE

C     ********************************************************

      DIMENSION DXY(IDIM),Y(IDIM)

      IDELTA=0
      IDEL=0
      NOUT=NIN-2
      IF(DT.LE.0) THEN
        DO I=1,NOUT
          DELTA=DXY(I)-DXY(I+2)
          IF(DELTA.EQ.0) THEN
            DELTA=-999.999
                IDELTA=IDELTA+1
          END IF
          DXY(I)=(Y(I)-Y(I+2))/DELTA
        END DO
        IF(IDELTA.NE.IDEL) THEN
           PRINT*,' *** ',IDELTA,' DIVISIONS BY ZERO***'
           IDEL=IDELTA
        END IF
      ELSE
        DELTA=2*DT
        DO I=1,NOUT
           DXY(I)=(Y(I)-Y(I+2))/DELTA
        END DO
      END IF
      DO I=1,NOUT
         Y(I)=Y(I+1)
      END DO
      RETURN
      END

C     ************************************************************

      SUBROUTINE PLOTDEV(NB,XMIN,XMAX,YMIN,YMAX,TEMP,CRATE,
      1                       XLABEL,YLABEL)
C                   PLOT DERIVATIVES

C          NB ----------------- NB OF POINTS
C          XMIN,YMIN ---------- MIN. VALS FOR X AND Y
C          XMAX,YMAX ---------- MAX. VALS FOR X AND Y
C          TEMP(I) ------------ X AXIS VECTOR
C          CRATE(I) ----------- Y AXIS VECTOR
C          XLABEL,YLABEL------- AXIS LABELS

C     ************************************************************
```

```
      CHARACTER*30 TLABEL(2),XLABEL,YLABEL,TEXT*100

      DIMENSION VMIN(2),VMAX(2),X(2000),Y(2000),TEMP(2000),
     1          CRATE(2000)
      DATA FDX,FDY,FTEX/0.75,0.51,0.57/,FX0,FY0/1.79,1.57/,MCODE/5/,
     1     YLASER/195.08/,WL/-2./
      DATA IBACK,IMARK,ILINE/7,2,4/,FACTOR/0.43/,CMIN,CMAX/0.,600./
      COMMON /DEV/IDEV

      FLABEL=3.0/YLASER
      IMIN=1

      IF(IDEV.EQ.0)THEN
        PRINT*,' '
        PRINT*,'***************************'
        PRINT*,'SELECT TERMINAL: (1)LT4109'
        PRINT*,'                 (2)VT4014'
        PRINT*,'                 (3)DUMMY DRIVER'
        PRINT*,'                 (4)VAXSTATION'
        PRINT*,'                 (5)RETURN'
        READ(*,*)IDEV
        IF((IDEV.LT.1).OR.(IDEV.GT.4)) THEN
              IDEV=0
            RETURN
        END IF
      END IF

      TLABEL(1)=XLABEL
      TLABEL(2)=YLABEL
      VMIN(1)=XMIN
      VMIN(2)=YMIN
      VMAX(1)=XMAX
      VMAX(2)=YMAX

10    WRITE(*,200) IMIN
      READ(*,*) ISTART
      IF((ISTART.LT.IMIN).OR.(ISTART.GE.NB)) GO TO 10
11    WRITE(*,210) NB-ISTART+1
      READ(*,*) NP
      IF((NP.LE.0).OR.(NP.GT.NB-ISTART+1)) GO TO 11
      PRINT*,' DO YOU WANT GRID? (1)YES'
      PRINT*,'                   (2)NO'
      READ(*,*) IGRID

      IFLAG=0
125   J=ISTART-1
      DO I=1,NP
        Y(I)=CRATE(J+I)
        X(I)=TEMP(J+I)
      END DO

      IF(IFLAG.EQ.0) THEN
        IF(IDEV.EQ.1) THEN
           CALL GROUTE('SEL LT4109;EX')
        ELSE IF(IDEV.EQ.2) THEN
           CALL GROUTE('SEL VT4014;EX')
        ELSE IF(IDEV.EQ.3) THEN
           CALL GROUTE('SEL MDUMDR;EX')
        ELSE IF(IDEV.EQ.4) THEN
           CALL GROUTE('SEL MGPX;EX')
        END IF
      END IF
```

```
      CALL GOPEN
      CALL GRPSIZ(XDEV,YDEV)

      HT=FLABEL*YDEV
      DX=FDX*XDEV
      DY=FDY*YDEV
      X0=(XDEV-DX)/FX0
      Y0=(YDEV-DY)/FY0
      YTEX=FTEX*Y0
      X1=VMIN(1)
      X2=VMAX(1)
      Y1=VMIN(2)
      Y2=VMAX(2)

      CALL BGRAF(X0,Y0,DX,DY)
      IF(((IDEV.EQ.1).OR.(IDEV.EQ.4)).AND.(IFLAG.EQ.0))
     1                                    CALL BGRAFB(IBACK)
      CALL GCHARF('SOFT')
      CALL GCHARF('ITAL')

      DO 30 I=1,2
      CALL BAXLAB(HT,HT,999,999)
      CALL BTICKM(4)
      CALL BAXIS(I,VMIN(I),VS,VMAX(I),TLABEL(I))
      IF(I.EQ.1) THEN
        CALL BAXORI(X0,Y0+DY)
      ELSE
        CALL BAXORI(X0+DX,Y0)
      END IF
      CALL BAXLAB(0.,0.,999,999)
30    CALL BAXIS(-I,VMIN(I),VS,VMAX(I),'$')

      IF(IGRID.EQ.1) CALL BGRID(1,1)
      CALL GLIMIT(X1,X2,Y1,Y2,0.,0.)
      CALL GVPORT(X0,Y0,DX,DY)
      CALL GWBOX(DX,DY,0.)
      CALL GSCALE
      IF(((IDEV.EQ.1).OR.(IDEV.EQ.4)).AND.(IFLAG.EQ.0))
     1                                   CALL GWICOL(-1,ILINE)
      IF(IFLAG.GT.0) CALL GWICOL(WL,1)
      CALL GVECT(X,Y,NP)

      CALL GSCAMM
      IF(IFLAG.GT.0) THEN
        XJUS=XDEV/2
        CALL GCHARF('TRIP')
        CALL GCHARJ(1)
        CALL GCHART(1)
        CALL GCHAR(TEXT,XJUS,YTEX,HT)
        CALL GSEGCL(IFLAG)
      END IF
      CALL GCLOSE

      PRINT*,'  DEVICE PLOT AREA LENGTHS(MM)'
      PRINT*,'X= ',XDEV,' Y= ',YDEV

130   PRINT*,' '
      PRINT*,'       SELECT OPTION:'
      PRINT*,'                  (1)MODIFY PLOT'
      PRINT*,'                  (2)HARDCOPY'
      PRINT*,'                  (3)RETURN'
```

```
      READ(*,*)I
      IF(I.EQ.1) GO TO 10
      IF(I.EQ.2) THEN
        PRINT*,' '
        PRINT*,' INPUT SEGMENT NUMBER(1-99)'
        READ(*,*) IFLAG
        PRINT*,' '
        IF((IFLAG.LT.1).OR.(IFLAG.GT.99)) GO TO 130
        PRINT*,' INPUT TEXT(MAX. 100 CHAR.)'
        READ(*,'(100A)') TEXT
        CALL CONCAT(TEXT,100)
        CALL GROUTE('SEL HPOSTA4L;EX')
        CALL GSEGCR(IFLAG)
        GO TO 125
      END IF
200   FORMAT('  INPUT STARTING POINT( >',I4,')')
210   FORMAT('  INPUT NUMBER OF POINTS( <',I4,')')
      RETURN
      END

C     ********************************************************

                    SUBROUTINE CONCAT(XIN,N)

C     ********************************************************

      CHARACTER*100 XIN,XOUT
      I=N+1
10    I=I-1
      IF(I.EQ.0)THEN
        I=1
      ELSE
        IF(XIN(I:I).EQ.' ')GOTO 10
      END IF
      XOUT=XIN(:I)//'$'
      XIN=XOUT
      RETURN
      END


C     ********************************************************

      SUBROUTINE CALC_TH(ICHAN,Ist,Ipeak,Tpeak,Ilast,Icool,Iend,
      1                   Tdiv,Htime,Ctime,TCRIT,ICRIT)

C         ICHAN  ------------------- Channel number
C         Ist    ------------------- First TC point
C         Ipeak  ------------------- Peak T point
C         Tpeak  ------------------- Peak temperature
C         Ilast
C         Icool
C         Iend   ------------------- Last point
C         Tdiv
C         Htime
C         Ctime
C         TCRIT
C         ICRIT

C     ********************************************************

      DIMENSION Tdiv(15),Htime(15),Ctime(15),TEMP(6,5460),NB(6)
      DIMENSION IMIN(6)
```

```
      COMMON /PARAM/NB,IMIN,DT,NCHAN
      COMMON /DATT/ TEMP

      DO i=1,15
          Tdiv(i)=100.*(i+1)
          Htime(i)=0
          Ctime(i)=0
      END DO
      Tbase=250.
      Tbasf=Tbase-10.
      Iflag=0
      Tpeak=0

      DO i=IMIN(ICHAN),NB(ICHAN)
         X=TEMP(ICHAN,i)
         IF((X.GE.Tbase).AND.(Iflag.EQ.0)) THEN
            Ist=i-1
            Iflag=1
            Tstart=X
         END IF
         IF(Tpeak.LT.X) THEN
            Tpeak=X
            Ipeak=i
         END IF
         IF((X.LT.Tbasf).AND.(Iflag.EQ.1)) THEN
            Iend=i+1
            Tend=X
            GO TO 5
         END IF
      END DO

5     IF(Ist.LT.IMIN(ICHAN)) Ist=IMIN(ICHAN)
      IF(Iend.GT.NB(ICHAN)) Iend=NB(ICHAN)
      Iheat=Tstart/100
      Icool=Tpeak/100-1
      Ilast=Tend/100
      IF(Ilast.GT.Iheat) Ilast=Iheat
      IF(Ilast.LT.1) Ilast=1

      k=Iheat
      DO I=Ist,Ipeak
         X=TEMP(ICHAN,I)
         IF(X.GE.Tdiv(k)) THEN
            Htime(k)=(Ipeak-I)*DT
            k=k+1
         END IF
      END DO

      K=Icool
      DO I=IpeaK,Iend
         X=TEMP(ICHAN,I)
         IF(X.LE.Tdiv(K)) THEN
            Ctime(k)=(I-IpeaK)*DT
            IF(Tdiv(K).EQ.TCRIT) ICRIT=I
            K=K-1
         END IF
      END DO
      RETURN
      END

C     ******************************************************
```

```
                SUBROUTINE MEAN_CYCLE

C     ********************************************************

      CHARACTER*1 DEC(6)
      DIMENSION Tdiv(15),Htime(15),Ctime(15),TEMP(6,5460),NB(6)
      DIMENSION IMIN(6),ICT(6,15)
      DIMENSION IORIG(6),I_min(6),I_max(6)
      COMMON /PARAM/NB,IMIN,DT,NCHAN
      COMMON /DATT/ TEMP

      PRINT*,' SELECT CHANNELS TO AVERAGE:'
      NSEL=0
      TTMAX=2000
      DO I=1,NCHAN
         PRINT*,'        CHANNEL ',I,' (Y/N)?'
         READ(*,'(A)') DEC(I)
         IF((DEC(I).EQ.'Y').OR.(DEC(I).EQ.'y')) THEN
           DEC(I)='Y'
           NSEL=NSEL+1
           CALL CALC_TH(I,Istart,Ipeaktemp,Tempeak,Ilastp,Icoolp,Iend
     1                                  ,Tdiv,Htime,Ctime,900,ICRIT)
C          Ist(I)=Istart
C          Ipeak(I)=Ipeaktemp
c          Tpeak(I)=Tempeak
           IF(Tempeak.LT.TTMAX) TTMAX=Tempeak
C          Iend(I)=Iend
C          Icool(I)=Icoolp
           DO J=1,15
              ICT(I,J)=Ctime(J)/DT+Ipeaktemp
           END DO
         END IF
      END DO
      IF(NSEL.LE.1) RETURN
5     PRINT*,' WHICH CHANNEL WILL BE OVERWRITTEN?'
      READ(*,*) IOVER
      IF((IOVER.LE.0).OR.(IOVER.GT.NCHAN).OR.(DEC(IOVER).NE.'Y'))
     1                                                    GO TO 5
      PRINT*,' SELECT REFERENCE TEMPERATURE'
10    READ(*,*) ITREF
      IIREF=ITREF/100
      ITREF=IIREF*100
      IF((ITREF.GT.1000).OR.(ITREF.LT.300)) THEN
        PRINT*,' REFERENCE TEMPERATURE OUT OF RANGE(300-1000)'
        IF(ITREF.GT.TTMAX) PRINT*,' PEAK TEMPERATURE BELOW REFERENCE!'
           GO TO 10
         END IF
      PRINT*,' '
      PRINT*,' REF. TEMPERATURE: ',ITREF
      I_neg=6000
      I_pos=6000
      DO I=1,NCHAN
          PRINT*,I
          IF(DEC(I).EQ.'Y') THEN
             IF(I_neg.GT.(ICT(I,IIREF)-IMIN(I)))
     1                          I_neg=ICT(I,IIREF)-IMIN(I)
             IF(I_pos.GT.(NB(I)-ICT(I,IIREF)-1))
     1                          I_pos=NB(I)-ICT(I,IIREF)-1
          END IF
      END DO
         DO J=0,I_neg+I_pos
         DO I=1,NCHAN
```

```
      IF((DEC(I).EQ.'Y').AND.(I.NE.IOVER)) THEN
         TEMP(IOVER,ICT(IOVER,IIREF)-I_neg+J)=
1                   TEMP(IOVER,ICT(IOVER,IIREF)-I_neg+J)+
2                   TEMP(I,ICT(I,IIREF)-I_neg+J)
      END IF
   END DO
   TEMP(IOVER,ICT(IOVER,IIREF)-I_neg+J)=
1        TEMP(IOVER,ICT(IOVER,IIREF)-I_neg+J)/NSEL
END DO
PRINT*,' ****************************************'
PRINT*,' *   ORIGINAL DATA WILL BE RESTORED IF    *'
PRINT*,' *         CHANNEL IS FILTERED!           *'
PRINT*,' ****************************************'

RETURN
END
```

APPENDIX II

```
C       ***********************************************
C       *                                             *
C       *          link as: UNILINK myprogram         *
C       *  Program written by C.L.Araujo & S.C.A.Alfaro *
C       *                                             *
C       ***********************************************


      CHARACTER NES*1,W*1,WA*2,WB*2,WC*1
      CHARACTER*20 NAME
      CHARACTER*21 NNAME
      CHARACTER*20 TEAM(150)
      CHARACTER NBETA*25,PD*25,SD*25,NAME01*25
      CHARACTER*25 TLABEL(2),TLEGEND(6)
      CHARACTER*80 TEXT1,TEXT2,TEXT3,TEXT4
      DIMENSION X(2000),Y(2000),YY(100),XX(100)
      DIMENSION BETA(100),BETAA(100),TI(100),TF(100),TI10(100),
     1 TF10(100),A(100),B(100)
      DIMENSION PVB(100),PVBA(100),SVB(100),TMB(100),TMSB(100)
      DIMENSION U(100,5),V(100,5),MCODE(5),NP(5),ICLIN(5),
     1 IDLIN(5)
      DIMENSION VMIN(2),VMAX(2),XP(100),YP(100),IAXIS(2)
      INTEGER EN,TR,T10,T7,T5,T3,N7,N5,N3,NF,MD,SF,DD,
     1 VEC(150),CLOCK
      REAL TLS,TLI,MIN,MAX,MINB,MAXB,MINSB,MAXSB,TM(100),
     1 ASOMX,ASOMY,CC,CCP,SCB,SC1B,SC2B
      DATA NF,MD,SF,DD/1,1,0,1/
      DATA TLS,TLI/750.0,200.0/
      DATA FD,FTEX,HTX/0.51,0.57,3.0/,FX0,FY0/2.30,1.57/,VS/0.0/,
     1 YLASER/195.08/,WLX,WL,WLL,WML/-12.,-3.,-1.,-6./,
     2 MCODE/15,18,4,21,12/
      DATA IBACK/5/,ICLIN/2,4,3,5,6/,IDLIN/0,2,4,7,10/
      INTEGER *4 STATUS,LIB$INIT_TIMER
      STATUS=LIB$INIT_TIMER()
      CALL LIB$SIGNAL(%VAL(STATUS))
      XLASER=270.94
      FLABEL=2.0/YLASER


      OPEN(UNIT=9,FILE='CATALOG.DAT',STATUS='OLD')
      PRINT*,'NUMBER OF PLOTS TO BE READ'
      READ(*,*)NPP
      CALL LIB$ERASE_PAGE (1,1)
      DO 5 I=1,NPP
      READ(9,*)VEC(I),TEAM(I)
      PRINT*,VEC(I),'  ',TEAM(I)
5     CONTINUE
      PRINT*,'                                                  '
      PRINT*,'FROM WHICH NUMBER TO ANOTHER DO YOU WANT TO PLOT'
      READ(*,*)IN,JN
      CALL LIB$ERASE_PAGE (1,1)
      PRINT*,'                                                  '
      PRINT*,'Choose num. elem. and temp. range between 700-500 oC'
      READ(*,*)N7,T7
      PRINT*,'                                                  '
      PRINT*,'                                                  '
      PRINT*,'Choose num. elem. and temp. range between 500-350 oC'
      READ(*,*)N5,T5
      PRINT*,'                                                  '
      PRINT*,'                                                  '
      PRINT*,'Choose num. elem. and temp. range between 350-200 oC'
```

```
READ(*,*)N3,T3
PRINT*,'                                                    '
PRINT*,'                                                    '
PRINT*,'Do you want to expand the scale ? if (yes) <type Y>'
PRINT*,'                                        if (no)  <R>'
READ(*,'(A)')NES
IF(NES.EQ.'Y'.OR.NES.EQ.'y')THEN
PRINT*,'                                                    '
PRINT*,'                                                    '
PRINT*,'What is the expanded value scale in percentage value ?'
READ(*,*)CCP
CC=CCP/100.
ELSE
END IF

CALL LIB$ERASE_PAGE (1,1)

PRINT*,CHAR(27)//'[7m'
PRINT*,'*****************************************************'
PRINT*,'                                                     '
PRINT*,'                PROGRAM IN PROGRESS                  '
PRINT*,'                                                     '
PRINT*,'*****************************************************'
PRINT*,CHAR(27)//'[m'

CLOCK=0
DO 7 K=IN,JN
IKK=0
IC=0
ICB=0
CLOSE(UNIT=9)


NAME=TEAM(K)
OPEN (UNIT=10,FILE=NAME,STATUS='OLD')
T10=45
TV=TR
MIN=0
MAX=0
MINB=0
MINSB=0
MAXB=0
MAXSB=0
DO 15 I=1,1500
READ(10,*)Y(I),X(I)
IF(Y(I).GT.TLS)GO TO 15
IC=IC+1
YY(IC)=Y(I)
XX(IC)=X(I)
IF(Y(I).LE.TLS.AND.Y(I).GE.700.OR.NFF.EQ.1)THEN
TI10(IC)=YY(1)
TF10(IC)=YY(IC)
TV10=TI10(IC)-TF10(IC)
TR=T10
IF(TV10.LT.T10)THEN
EN=IC+1
TV=TR
NFF=1
ELSE
EN=IC
NFF=0
END IF
```

```
      GO TO 81
      END IF
      IF(Y(I).LT.700.AND.Y(I).GE.500)THEN
      TR=T7
      EN=N7
      ELSE
         IF(Y(I).LT.500.AND.Y(I).GE.350)THEN
         TR=T5
         EN=N5
         ELSE
        IF(Y(I).LT.350.AND.Y(I).GE.200)THEN
         TR=T3
         EN=N3
        ELSE
        END IF
         END IF
      END IF
81    IF((IC.LE.EN).OR.(Y(I).LT.250.).OR.(TV.LT.TR))THEN
        SOMX=SOMX+X(I)
        SOMY=SOMY+Y(I)
        IF(IC.EQ.EN.OR.Y(I).LT.250.OR.TV.LT.TR)THEN
          ASOMX=SOMX/IC
          ASOMY=SOMY/IC
          DO 16 IJ=1,IC
          A(IJ)=YY(IJ)-ASOMY
          B(IJ)=XX(IJ)-ASOMX
          TSOM=TSOM+A(IJ)*B(IJ)
          TTSOM=TTSOM+B(IJ)**2
16        CONTINUE
          ICB=ICB+1
          BETA(ICB)=TSOM/TTSOM
          TI(ICB)=YY(1)
          TF(ICB)=YY(IC)
          TM(ICB)=(TI(ICB)+TF(ICB))/2.
          TV=TI(ICB)-TF(ICB)
          IF(Y(I).LT.250.)GO TO 40
          IF(TV.LT.TR)THEN
            ICB=ICB-1
            GO TO 15
          ELSE
          END IF
          IC=0
          SOMX=0
          SOMY=0
        ELSE
        END IF
      ELSE
      END IF
15    CONTINUE
40    CLOSE(UNIT=10)


      W='B'
      WA='1B'
      WB='2B'
      WC='$'
      NBETA=W//NAME
      PD=WA//NAME
      SD=WB//NAME


      DO 500 J=1,ICB
```

```
      BETAA(J)=ABS(BETA(J))
500   CONTINUE
      MIN=BETAA(1)
      MAX=BETAA(1)
      DO 98 J=1,ICB
          IF(BETAA(J).GE.MAX)THEN
            MAX=BETAA(J)
          ELSE
            IF(BETAA(J).LT.MIN)MIN=BETAA(J)
          END IF
98    CONTINUE
      OPEN(UNIT=99,FILE=NBETA,STATUS='NEW')
      WRITE(99,97)NF,MD,SF
97    FORMAT(1X,3(I3,2X))
      IF(NES.EQ.'Y'.OR.NES.EQ.'y')THEN
      SCB=MAX-MIN
      MAX=MAX+(SCB*CC)
      MIN=MIN-(SCB*CC)
      ELSE
      END IF
      WRITE(99,95)TLS,TLI,MIN,MAX
95    FORMAT(1X,2(F5.1,4X),2(F16.9,4X))
      WRITE(99,94)DD,DD
94    FORMAT(1X,2I3)
      WRITE(99,93)NF,ICB
93    FORMAT(1X,2I4)
      DO 502 J=1,ICB
502   WRITE(99,91)J,TM(J),BETAA(J)
91    FORMAT(1X,I5,3X,F5.1,3X,F16.9)
      WRITE(99,*)'Temperature oC$'
      WRITE(99,*)'B Values$'
      WRITE(99,*)'Figure      -Steel    $'
      NNAME=NAME//WC
      WRITE(99,*)'HI=     kJ/mm$'
      WRITE(99,*)' $'
      WRITE(99,*)'LEGEND$'
      WRITE(99,*)'VARIATION OF B$'
      CLOSE(UNIT=99)



      ICBM=ICB-1
      NM=0
      DO 50 J=1,ICBM
      PVB(J)=(BETA(J+1)-BETA(J))/(TF(J+1)-TI(J))
      PVBA(J)=ABS(PVB(J))
      NM=NM+1
      IF(NM.EQ.1)THEN
      MINB=PVBA(1)
      MAXB=PVBA(1)
      ELSE
      END IF
      TMB(J)=(TM(J+1)+TM(J))/2
          IF(PVBA(J).GT.MAXB)THEN
            MAXB=PVBA(J)
          ELSE
            IF(PVBA(J).LT.MINB)MINB=PVBA(J)
          END IF
50    CONTINUE
      OPEN(UNIT=11,FILE=PD,STATUS='NEW')
      WRITE(11,*)NF,MD,SF
21    FORMAT(1X,3(I3,2X))
```

```
      IF(NES.EQ.'Y'.OR.NES.EQ.'y')THEN
      SC1B=MAXB-MINB
      MAXB=MAXB+(SC1B*CC)
      MINB=MINB-(SC1B*CC)
      ELSE
      END IF
      WRITE(11,22)TLS,TLI,MINB,MAXB
22    FORMAT(1X,2(F5.1,4X),2(F16.9,4X))
      WRITE(11,23)DD,DD
23    FORMAT(1X,2I3)
      WRITE(11,24)NF,ICBM
24    FORMAT(1X,2I4)
      DO 17 J=1,ICBM
17    WRITE(11,25)J,TMB(J),PVBA(J)
25    FORMAT(1X,I5,3X,F5.1,3X,F16.9)
      WRITE(11,*)'Temperature oC$'
      WRITE(11,*)'B Values$'
      WRITE(11,*)'Figure      -Steel    $'
      NNAME=NAME//WC
      WRITE(11,*)'HI=     kJ/mm$'
      WRITE(11,*)' $'
      WRITE(11,*)'LEGEND$'
      WRITE(11,*)'FIRST VARIATION OF B$'
      CLOSE(UNIT=11)


      ICBMM=ICB-2
      NMS=0
      DO 51 J=1,ICBMM
      SVB(J)=(PVBA(J+1)-PVBA(J))/(TF(J+2)-TI(J))
      NMS=NMS+1
      IF(NMS.EQ.1)THEN
      MINSB=SVB(1)
      MAXSB=SVB(1)
      ELSE
      END IF
      TMSB(J)=(TMB(J+1)+TMB(J))/2.
          IF(SVB(J).GT.MAXSB)THEN
            MAXSB=SVB(J)
          ELSE
            IF(SVB(J).LT.MINSB)MINSB=SVB(J)
          END IF
51    CONTINUE
      OPEN(UNIT=12,FILE=SD,STATUS='NEW')
      WRITE(12,26)NF,MD,SF
26    FORMAT(1X,3(I3,2X))
      IF(NES.EQ.'Y'.OR.NES.EQ.'y')THEN
      SC2B=MAXSB-MINSB
      MAXSB=MAXSB+(SC2B*CC)
      MINSB=MINSB-(SC2B*CC)
      ELSE
      END IF
      WRITE(12,27)TLS,TLI,MINSB,MAXSB
27    FORMAT(1X,2(F5.1,4X),2(F16.9,4X))
      WRITE(12,28)DD,DD
28    FORMAT(1X,2I3)
      WRITE(12,24)NF,ICBMM
29    FORMAT(1X,2I4)
      DO 18 J=1,ICBMM
18    WRITE(12,30)J,TMSB(J),SVB(J)
30    FORMAT(1X,I5,3X,F5.1,3X,F16.9)
      WRITE(12,*)'Temperature oC$'
```

```
      WRITE(12,*)'B Values$'
      WRITE(12,*)'Figure      -Steel    $'
      NNAME=NAME//WC
      WRITE(12,*)'HI=     kJ/mm$'
      WRITE(12,*)' $'
      WRITE(12,*)'LEGEND$'
      WRITE(12,*)'SECOND VARIATION OF B$'
      CLOSE(UNIT=12)


      DO 84 IKK=1,3
      CLOCK=CLOCK+(33.3/(JN-IN+1))
      IF(IKK.EQ.1)THEN
      NAME01=NBETA
      ELSE
       IF(IKK.EQ.2)THEN
        NAME01=PD
        ELSE
        NAME01=SD
        END IF
      END IF
      OPEN(UNIT=60,FILE=NAME01,STATUS='OLD')
      READ(60,*)NF,MD,SF

C           NF --- NUMBER OF FIGURES
C           MD --- MARKER FREQUENCY(MD<0 NO LINE IS DRAWN)
C                                  (MD=0 NO POINT IS DRAWN)
C                                  (MD>0 EACH MDth POINT IS DRAWN)
C           SF --- LINE SMOOTHING FACTOR(0-9)

      NLEG=NF+1
      READ(60,*)(VMIN(I),VMAX(I),I=1,2)
      READ(60,*)(IAXIS(I),I=1,2)
C              NP --- NUMBER OF POINTS
      DO 61 J=1,NF
      READ(60,*) N,NP(J)
      DO 61 I=1,NP(J)
61    READ(60,*) N,U(I,J),V(I,J)
      DO 62 I=1,2
62    READ(60,'(25A)')TLABEL(I)
      READ(60,'(80A)')TEXT1
      READ(60,'(80A)')TEXT2
      READ(60,'(80A)')TEXT3
      DO 63 I=1,NLEG
63    READ(60,'(25A)') TLEGEND(I)
      CLOSE(60)

      IFLAG=IFLAG+1
      IF(IFLAG.GE.100)STOP
      CALL GLN03A

      CALL GOPEN
      CALL GSEGWK(0)
      IF(IFLAG.GT.0) CALL GSEGCR(IFLAG)
      CALL GRPSIZ(XDEV,YDEV)
      XXY=YDEV
      XXX=XDEV

      HT=FLABEL*XXY
      DX=FD*XXY
      DY=DX
      X0=(XXX-DX)/FX0
```

```
      Y0=(XXY-DY)/FY0
      XDX=X0+DX
         YDY=Y0+DY
      XR1=X0-52.0
      YR1=Y0-15.0
      XR2=XDX+77.0
      XR3=X0-3.0
      XR4=XDX+3.0
      YR2=YDY+10.0
      YR3=YDY+3.0
      YR4=Y0-3.0
      CALL RRECT(XR1,YR3,XR2,YR2,7,4)
      CALL RRECT(XR1,YR1,XR3,YR3,7,4)
      CALL RRECT(XR3,YR1,XR2,YR4,7,4)
      CALL RRECT(XR4,YR4,XR2,YR3,7,4)
         YT1=YR1-25.0
      CALL RRECT(XR1,YT1,XR2,YR1,30,4)
      YTEX=FTEX*Y0
      YLEG=Y0+DY-2*NLEG*HT
      XLEG=X0+DX+2*HT

      CALL BGRAF(X0,Y0,DX,DY)
      CALL GCHARF('SOFT')
      CALL GCHARF('ITAL')

      DO 67 I=1,2
      CALL BAXLAB(HT,HT,999,999)
      CALL BTICKM(4)
67    CALL BAXIS(I,VMIN(I),VS,VMAX(I),TLABEL(I))
      CALL GVECT(X0,YDY,0)
      CALL GWICOL(WLL,1)
      CALL GVECT(XDX,YDY,1)
      CALL GVECT(XDX,Y0,1)
      CALL GVECT(XR1,YT1,0)
      CALL GWICOL(WL,1)
      CALL GVECT(XR1,YR2,1)
      CALL GVECT(XR2,YR2,1)
      CALL GVECT(XR2,YT1,1)
      CALL GVECT(XR1,YT1,1)
      XR5=XR1-3.0
      YR5=YT1-3.0
      YR6=YR2+3.0
      XR6=XR2+3.0
      CALL GVECT(XR5,YR5,0)
      CALL GWICOL(WLX,1)
      CALL GVECT(XR5,YR6,1)
      CALL GVECT(XR6,YR6,1)
      CALL GVECT(XR6,YR5,1)
      CALL GVECT(XR5,YR5,1)
      CALL GVECT(XR1,YR1,0)
      CALL GWICOL(2,1)
      CALL GVECT(XR2,YR1,1)
      CALL BGRID(1,1)

      DO 80 J=1,NF
      DO 70 KK=1,NP(J)
      XP(KK)=U(KK,J)
70    YP(KK)=V(KK,J)
      IF(MD.NE.0)THEN
        CALL BMARK(MCODE(J),MD)
        CALL BMARKH(HT)
      END IF
```

```
      IF(MD.GE.0) CALL BSMTH(ISMO)
      CALL BLIWDH(WL)
      CALL BDASH(IDLIN(J))
80    CALL BLINE(XP,YP,NP(J))
      CALL BLEGND(XLEG,YLEG,TLEGEND,25,NLEG,1.5*HT)

      XJUS=XDEV/2
      CALL GCHARF('SHA1')
      CALL GCHARJ(1)
      CALL GCHAR(TEXT1,XJUS,YTEX,HTX)
      YTEX=YTEX-1.5*HTX
      CALL GCHAR(TEXT2,XJUS,YTEX,HTX)
      YTEX=YTEX-1.5*HTX
      CALL GCHAR(TEXT3,XJUS,YTEX,HTX)
      IF(IFLAG.GT.0) CALL GSEGCL(IFLAG)
      CALL GCLOSE


      CALL LIB$ERASE_PAGE (1,1)

      PRINT*,CHAR(27)//'[7m'
      PRINT*,'*************************************************'
      PRINT*,'*                                               *'
      PRINT*,'*                                               *'
      PRINT*,'*Please wait programme in progress',CLOCK,'% Done*'
      PRINT*,'*                                               *'
      PRINT*,'*                                               *'
      PRINT*,'*************************************************'
      PRINT*,CHAR(27)//'[m'


84    CONTINUE


7     CONTINUE
      CALL LIB$SHOW_TIMER()
C     PRINT*,CHAR(27)//'[m'
      STOP
      END
```